

Design and Study of Highly Luminescent Pyrrole-Based Near-IR Dyes

Yaroslav Zems



Department of Chemistry
McGill University
Montreal, Quebec,
Canada

*Presented in Partial Fulfilment of the Requirements for
the degree of Master of Science*

© Yaroslav Zems April 2019

Abstract

Near-infrared (NIR) emissive dyes are in high demand within the fields of biomedical science, military technology and materials science. Luminescent dyes invariably experience a precipitous drop in photoluminescence as their operational wavelengths extend to the red. This thesis describes the synthesis and functionalization of novel pyrrole and isoindole-based dyes with a focus on mitigating loss of NIR emissivity to non-radiative decay. Specifically, highly soluble platinum (II) tetraaryltetrabenzoporphyrins (PtAr₄TBIP, Ar = Ph, Ph-d₅) and π -extended benzo-annulated BODIPYs were prepared and characterized. Structure-property relationships were gleaned from their photophysical study. The effects of discrete structural differences in a photophysical context are discussed for each class of dye.

Résumé

Les colorants émissifs proche infrarouge (PIR) sont très demandés dans les domaines de la science biomédicale, la technologie militaire et la science des matériaux. Les colorants luminescents subissent invariablement une baisse abrupte de leur photoluminescence lorsque leurs longueurs d'onde opérationnelles s'étendent vers le rouge. Cette thèse détaille la synthèse et la modification de nouveaux matériaux à base de pyrrole et isoindole en mettant l'accent sur l'atténuation de la perte de l'émissivité PIR. Plus précisément, une famille de tétraaryltétrabenzoporphyrines de platine (II) de haute solubilité (PtAr₄TBIP, Ar = Ph, Ph-d₅, C₆F₅) et de BODIPY benzo-annulées/ π -étendues ont été préparées. Les relations structure-propriété ont été glanées à partir de leur études en photophysique. Les résultats de la modification structurelle discrète sont discutés dans un contexte photophysique pour chaque classe de matériel.

Acknowledgements

Above all, I would like to express my sincerest appreciation and gratitude to both my supervisors, Prof. Dmitrii Perepichka and Prof. Neil Robertson, without whom this work would not be possible.

I'm forever grateful to Prof. Perepichka for introducing me to materials chemistry research and feeding my passion for it during my time at McGill. The large degree of creative control I had over my projects under his supervision fuelled my development as independent scientist. His counsel and direction have proven invaluable over the years; it was his encouragement to pursue this joint Ph.D program that led to a level of personal and intellectual growth I would not have achieved otherwise.

I'm indebted to Prof. Neil Robertson for taking me on as a postgraduate student and guiding me through the transitional period. His vigilant supervision and invaluable advice have kept me from spinning my wheels on more than several occasions. During my stay in Edinburgh, I was able to benefit from his large pool of knowledge during out meetings which were integral in shaping my progression and this thesis.

A debt of gratitude is owed to Andrey Moiseev, who supervised my day-to-day undergraduate work and mentored me through the tar-filled pits of porphyrin chemistry. Even under endless bombardment with questions from all members of the research group, he remained unflinching and eager to teach where others would have surely lost patience.

Working in two separate labs, I've had the privilege of meeting many students and research fellows of different backgrounds, with whom I've shared much needed moments of repose. I wish to thank all members of the Perepichka and Robertson groups.

At McGill University, I'm appreciative for the technical support provided from Fred Morin at the NMR lab, Nadim Saadé and Alexander Wahba at the mass spectrometry lab as well as Francine Bélanger-Gariépy at the University of Montréal for X-ray crystallographic analysis.

At the University of Edinburgh, I would like to thank Jochen Arlt from the physics department (COSMIC) for our attempts at lifetime measurements, Stuart Johnstone for his masterful glassblowing, Lorna Murray for her assistance with the NMR facilities, Gary Nichol for X-ray crystallographic analysis as well as Logan McKay for assistance with mass spectrometry. Additionally, I would like to thank Renato Neiva Sampaio from Gerald Meyer's group at UNC-Chapel Hill and Sofia Garakyaraghi from Felix Castellano's group at NCSU for their photophysical measurement of my materials.

A thank you to all the support and technical staff of both departments whose behind-the-scenes work keeps the departments running and is often underappreciated.

Last but not least, I thank my family for their unconditional support, patience and understanding, particularly during my years in Edinburgh spent away from home.

Preface

Molecules that absorb and emit light are classified as luminescent dyes. In recent years, there has been a push to develop dyes capable of bright NIR emission. They are of strong interest to materials scientists for a number of applications such as organic light-emitting diodes (OLEDs), non-linear optics, telecommunications, solar energy conversion, photon upconversion/downconversion and security inks. Biomedical sciences have also come to rely on the benefits of working with NIR light. Chiefly, being able to operate in the biological window (650 nm – 1450 nm) has appreciably lowered limits of detection for analytical instrumentation. NIR dyes have enabled breakthroughs in fluorescence-guided surgery, cancer theranostics and biomedical imaging/sensing (*i.e.* contrast agents).

While optical properties of dyes can be accurately predicted, there remain significant challenges to overcome before design of materials with precise photophysical properties becomes routine. As a dye's HOMO-LUMO gap narrows, there is a concomitant and precipitous decline in photoluminescence quantum yield (PLQY), as predicted by the Energy Gap law. Bright emission is arguably a dye's most important quality which is why a large number of spectroscopists and chemists have dedicated their efforts to the study of this problem. To this day, researchers rely on empirical guidelines such as increasing molecular rigidity, reducing aggregation in solution and eliminating strong IR-active vibrational modes to achieve high PLQY. The motivation for the work presented in this thesis is to explore and study the effects such strategies in novel NIR dyes and in doing so, contribute knowledge to the expanding field of NIR-luminescent materials.

The chapters outlined below report the work done to prepare and characterize novel pyrrolic dyes. Particular emphasis was placed on correlating structure to photophysical properties.

Chapter 1 introduces the necessary photophysical concepts for the study of emissive dyes in solution and surveys current literature involving NIR-emissive materials. Pyrrole is introduced as a heterocyclic building block for dipyrrens, BODIPYs and porphyrins, all of which are also introduced in terms of their structure, synthesis and optical properties.

Chapter 2 details the synthesis, characterization and photophysical study of a series of tetraaryltetra-benz[c]annulated platinum (II) porphyrins (PtAr₄TBIP). Specifically, the

identity of *meso*-aryl substituents is varied (Ph, Ph-*d*₅ and C₆F₅) with the hopes of modulating photophysical properties.

Chapter 3 explores benz[*c*]annulated BODIPY dyes as an organic extension of the work done for Chapter 2. These dyes exhibited unusually high fluorescence in the red (unity PLQY in a few cases) and remained emissive ($\Phi_F > 0.1$) in the NIR ($\lambda_{em} = 780$ nm) after functionalization at the 3,5-positions.

Chapter 4 presents the concluding remarks from the thesis.

Appendix contains work that was not completed due to time constraints.

Contribution of Authors

Dr. Andrey Moiseev synthesized platinum (II) tetrabenzoporphyrin as a photochemical standard for porphyrin quantum yield measurements as well as supervising and performing exploratory synthesis of the unsubstituted pyrrole precursor used in this work.

X-ray analysis was performed by Dr. Gary Nichol at the University of Edinburgh and by Francine Bélanger at the University of Montreal.

Transient absorption spectroscopy (TAS) and photophysical characterization was carried out by Renato Neiva Sampaio from Gerald Meyer's group at UNC-Chapel Hill and Sofia Garakyaraghi from Felix Castellano's group at NCSU.

Yaroslav Zems is the principle author of this thesis and has performed synthesis/characterization of the compounds presented in this thesis unless otherwise indicated.

Abbreviations

1,2,4-TCB	1,2,4-trichlorobenzene
2-EH	2-ethylhexyl
AcOH	acetic acid
AgCl	silver (I) chloride
AgOAc	silver (I) acetate
B3LYP	hybrid exchange-correlation functional (Becke, three parameter, Lee-Yang-Parr)
BF ₃ OEt ₂	boron trifluoroetherate
Bu ₂ O	dibutyl ether
Bu ₄ NCl	tetrabutylammonium chloride
CCl ₄	carbon tetrachloride
Cs ₂ CO ₃	caesium carbonate
CuI	copper (I) iodide
DBU	1,8-diazabicyclo[5.4.0]undec-7-ene
DCM	dichloromethane
DDQ	2,3-dichloro-5,6-dicyano-1,4-benzoquinone
Def2SVPP	Ahlrichs and co-workers' basis set (single valence polarized)
DMSO	dimethylsulfoxide
DIPA	diisopropylamine
DIPEA	di(isopropyl)ethylamine
DSSC	dye-sensitized solar cell
DR-NIR	deep-red/near-infrared
Et ₂ O	diethyl ether
EWG	electron-withdrawing groups
FR	far red
H ₂ O	water
HBr	hydrobromic acid
HCl	hydrochloric acid
H ₂ O ₂	hydrogen peroxide
HRMS	high-resolution mass spectrometry
ISC	intersystem crossing
<i>m</i> -CBA	<i>m</i> -chlorobenzoic acid

<i>m</i> -CPBA	<i>m</i> -chloroperoxybenzoic acid
MOM	metallo-organic material
MeOH	methanol
MTBE	methyl tert-butyl ether
Na ₂ SO ₄	sodium sulfate
NCS	<i>N</i> -chlorosuccinimide
NEt ₃	triethylamine
NIR	near infra-red
NIST	National Institute of Standards and Technology
NSD	normal-coordinate structure decomposition
Pd(PPh ₃) ₄	palladium (0) tetrakis(triphenylphosphine)
PES	potential energy surface
PhCN	benzonitrile
PhLi	phenyllithium
PhSH	thiophenol
PPh ₃	triphenylphosphine
Pt/C	platinum metal supported on carbon
PtAr ₄ TBIP	platinum (II) tetraaryltetrabenzo[2,3]imide porphyrin
PtOEP	platinum octaethylporphyrin
PtTPTBP	platinum (II) tetraphenyltetrabenzo porphyrin
PtTPTBIP	platinum (II) tetraphenyltetrabenzo[2,3]imide porphyrin
Pt(OAc) ₂	platinum (II) acetate
pyr	pyridine
RBF	round bottom flask
RMS	root-mean-squared
RTP	room temperature phosphorescence
SO ₂	sulfur dioxide
TAS	transient absorption spectroscopy
TFA	trifluoroacetic acid
THF	tetrahydrofuran
TTF	tetrathiafulvalene
ZnPh ₄ P	zinc tetraphenylporphyrin
Zn(OAc) ₂	zinc (II) acetate

Contents

Abstract	ii
Résumé	iii
Acknowledgements	iv-v
Preface	vi-vii
Contribution of Authors	viii
Abbreviations	ix-x
1 An Introduction to Near-Infrared Photoluminescent Dyes	1
1.1 Introduction to Molecular Photophysics	1
1.1.1 Experimental PLQY measurement	4
1.2 NIR Emissive Materials	4
1.2.1 Synopsis of Frontier Dyes	6
1.2.1.1 Organics	7
1.2.1.2 Inorganics.....	8
1.2.2 Challenges	8
1.2.2.1 Mitigating Photoluminescence Losses.....	9
1.2.3 Red-shifting strategies	10
1.3 Pyrrole: nature's heterocycle.....	11
1.3.1 Heterocycle Assembly and Reactivity	12
1.3.2 Stability and Related Heterocycles	14
1.4 BODIPY & Dipyrrin	14
1.4.1 Nomenclature and Synthesis	15
1.4.2 Post-synthetic Modification	16
1.5 Porphyrin.....	17
1.5.1 Structure and Nomenclature.....	17
1.5.2 Synthetic Methodology	18
1.5.3 Electronic properties.....	20
1.6 Conclusions	20
1.7 References	21
2 Tuning Photophysics via Modular Aryl Moiety in a Family of Novel PtAr₄TBIP Dyes	30
2.1 Introduction to π -Extended Porphyrins	30

2.1.1	Applications	33
2.1.2	Synthetic Methodology	34
2.2	Synthesis of <i>meso</i> -Aryl Tetrabenzoporphyrins	36
2.2.1	Synthesis of 4,5,6,7-Tetrahydroisoindole Precursor	36
2.2.2	Synthesis of Pt(II)Ar ₄ TBIPs	38
2.3	Solubility and Stability Studies	40
2.4	Crystal Structures	42
2.5	Electronic and Photophysical Properties	44
2.5.1	Effect of Deuteration	46
2.5.1.1	Literature Precedents	46
2.5.1.2	Photophysical Effects of Deuteration	48
2.5.2	Excitation Wavelength Dependence of Φ_P	51
2.6	Conclusions	53
2.7	Experimental	54
2.8	References	63
3	Remarkably Bright NIR Emission in Novel π-extended BODIPYs	84
3.1	Introduction to π -Extended BODIPYs	84
3.2	Synthesis of Bz ₂ -Annulated BODIPYs	87
3.3	Physical properties	92
3.3.1	Crystal Structures	92
3.3.2	Photophysical Properties.....	93
3.5	Conclusions	95
3.6	Experimental	95
3.7	References	101
4	Concluding Remarks	114
A	Appendix	116
A.1	Synthesis of Carboxylated Ar ₄ TBPs/Molecular Tectonics	117
A.2	Inducing Severe Distortion via Quadruple <i>meso</i> , β -Fusion	133

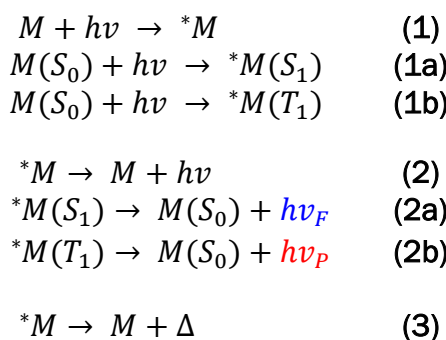
Chapter 1

An Introduction to Near-Infrared Photoluminescent Dyes

This chapter introduces photophysical concepts necessary for the study of fluorescent and phosphorescent materials in solution. A literature survey of cutting-edge organic and inorganic dyes, along with applications and challenges, is presented. Finally, pyrrole will be introduced as a heterocyclic building block for the synthesis of dipyrroles/BODIPYs and porphyrins, which constitute the foundation of the work described in this dissertation and will be used as a springboard into NIR-emissive materials.

1.1 Introduction to Molecular Photophysics

Molecular photophysics concerns itself with the study of molecular dynamics and structures resulting from interactions between molecules (physical matter) and light. Such interactions include diffraction, refraction, reflection, scattering, transmission and absorption of the incoming photon. The latter is of particular importance in the study of



Scheme 1.1 Overview of basic photophysical processes: (1) absorption, (2) emission and (3) internal conversion/thermal emission.

photophysical processes occurring in solution. At the basest level (scheme 1.1), the absorption (1) of light ($h\nu$) by a molecule (M) produces an electronically excited state (*M) which can subsequently undergo a radiative (2) transition by emitting a photon or internal conversion (3) by releasing heat (Δ) into its surroundings. A more detailed account of these photophysical processes specifies the type of transition undergone upon absorption and the type of emission (fluorescence $h\nu_F$ shown in 2a and phosphorescence $h\nu_P$ shown in 2b). Fluorescence is defined as the radiative transition between the lowest excited state S_1 and the ground state S_0 while phosphorescence undergoes the same transition but from the lowest excited triplet state T_1 . It should be noted that under normal circumstances, (1b) does not occur because it is a spin forbidden transition which violates the rule of conservation of angular momentum. The Jablonski diagram in Figure 1.1 summarizes and illustrates these photophysical processes. It is also a very useful tool to visually represent different electronic states (S_0 , S_1 , S_2 , T_1 , T_2 , etc) with their vibrational sublevels and what role they play in internal conversion (IC), intersystem crossing (ISC) and internal vibrational relaxation (IVR).

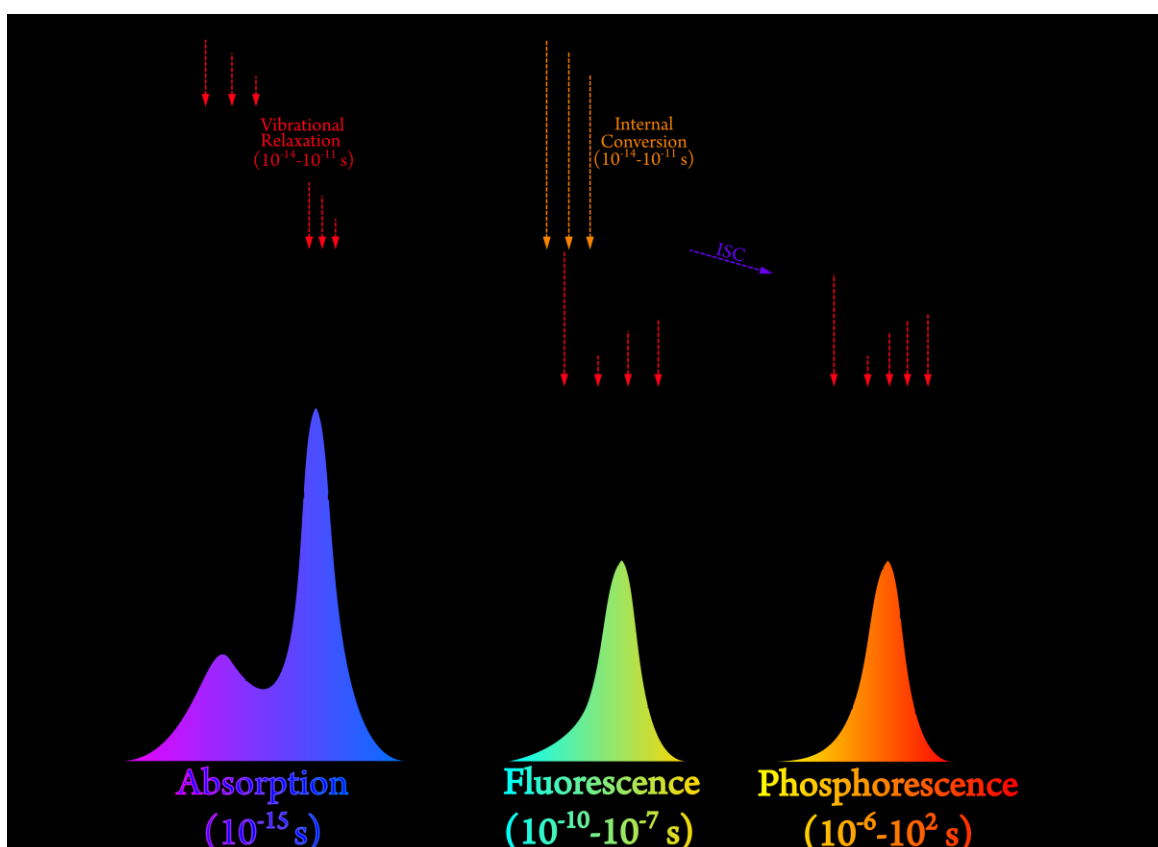


Figure 1.1 Jablonski energy diagram summarizing major photophysical processes and correlation of transitions to different vibrational sublevels to spectral shape.

The tendency for a particular molecule to undergo radiative transition (also termed emission) instead of a non-radiative transition is a measure of how bright a luminescent molecule is. The efficiency of this process is an important experimental parameter called photoluminescence quantum yield (PLQY or Φ) and is defined in (4) as a ratio of emitted photons (η_e) versus absorbed photons (η_a). For instance, a material with a PLQY of 0.5 re-emits exactly half of the photons it absorbs whereas a material that re-emits every photon it absorbs would have a PLQY of 1 (unity). It can also be defined as the ratio of radiative rate (k_r) versus the sum of radiative and non-radiative (k_{nr}) or as the product of k_r and experimentally determined emission lifetime (τ_e).

$$\Phi = \frac{\eta_e}{\eta_a} = \frac{k_r}{k_r + k_{nr}} = k_r \tau_e \quad (4)$$

It is important to keep in mind Kasha's rule, which states that fluorescence/phosphorescence will only be observed experimentally from the lowest to the thermally equilibrated S_1 and T_1 states, respectively. In other words, if absorption of high energy light leads to a higher excited state ($S_0 \rightarrow S_2$), the system will have had a chance to undergo IC/IVR to the lowest-vibrational state of S_1 on a timescale orders of magnitude faster than before radiative transition occurs. Vavilov's rule, a corollary to Kasha's rule, states that fluorescence or phosphorescence PLQY is independent of initial excitation energy. The rate of ISC (k_{ISC}) for $S_1 \rightarrow T_1$ is largely affected by molecular structure, particularly by the presence or absence of heavy atoms such as halogens, transition metals or heteroatoms. The effect is particularly pronounced when the chromophore already had inherently low k_{nr} and k_{ISC} prior to introduction of the heavy atom(s).

The effect of molecular structure on photophysical properties (PLQY, lifetime) is discussed later on in this chapter, in particular how stretching and twisting of molecular structure leads to non-radiative decay of the excited state. Additionally, the concept of promoter and acceptor vibrational modes will be introduced with specific examples that relate structure and observed PLQY. Finally, the Energy Gap law for internal conversion ($S_0 \rightarrow S_1$) and its particular relevance to low bandgap NIR-emitting materials will be presented along with a discussion of how deuteration can be used to improve photophysical properties in these dyes.

1.1.1 Experimental PLQY Measurement

Accurate determination of relative PLQYs¹ has always been an area of contention and controversy for spectroscopists and materials chemists alike. Accuracy of published values are affected by a multitude of factors² including variations in equipment calibration, analyst technique, excitation wavelength, temperature, failure to correct emission spectra,³ and inadequate choice/purity of the photoluminescence standard.⁴ The increased availability of integrating spheres has enabled routine determination of absolute PLQY, which is not however without its own challenges⁵ (*i.e.* reabsorption effects, reproducibility of sample positioning, wavelength reflectivity on sphere walls). A detailed, comparative study of relative and absolute PLQY measurements using traceable equipment was carried out to quantify contributions from specific sources of uncertainty. Nevertheless, relative PLQY measurements remain the standard in most research labs. Literature PLQY values are commonly reported with a 10% error margin yet this number should be a conservative estimate at best. This is chiefly relevant to FR-NIR emitters, as spectral responsivity tails off non-linearly in this region (requiring careful calibration and correction) and reliability of PLQY values in emission standards (particularly phosphorescent ones) is inadequate, having been identified as the major contributor to systematic variation.⁶ Dye self-quenching and oxygen effects on phosphorescence measurements pose additional considerations for solution PLQY measurements. In cases where dissolved oxygen is suspected to interfere with accurate PLQY determination, samples should be thoroughly degassed and isolated from ambient atmosphere with sealed cuvettes. Viscosity of the measurement medium has also been shown to have an effect on Φ_F measurements.⁷ Advances have been made with claims of improved measurement accuracy^{8,9} as well as using chain NIST-traceable transfer standard dyes (starting from quinine sulfate) to map out a series of red and NIR emission standards up to 1000 nm.¹⁰ While affected to a much lesser extent by experimental uncertainty, lifetime measurements of dilute dye solutions could also benefit from comparison to known lifetime standards, due to differences in excitation wavelength and fluorimeter setup.¹¹

1.2 NIR Emissive Materials

NIR materials are defined as being materials whose optoelectronic properties operate in the region of 700 nm – 2500 nm. Since William Herschel discovered IR radiation in 1800,¹² research into NIR-emitting materials has remained largely stagnant

until recent years with the advent of more available and sensitive spectroscopic equipment capable of NIR-detection. Infrared technology has benefited from the large bloom in applied research, being driven in large part by civilian and military needs. These include night vision, surveillance, remote temperature sensing, weather forecasting, wireless communication and spectroscopy. Such practical applications have emerged as a result of fervent pursuit of NIR dyes and tailoring of their properties in different fields such as materials science, biomedical imaging and sensing,¹³ fluorescence guided surgery,¹² cancer theranostics,¹⁴ telecommunications, optical signal processing and solar energy conversion (Figure 1.2). For example, strides have been realized in biological and medical fields by taking advantage of the enhanced optical sensitivity in the biological window¹⁶ (650 nm – 1450 nm) where light scattering and auto-fluorescent interference from endogenous biomolecules are minimized (Figure 1.3). Lower-energy nature of NIR light also minimizes photodamage to biological samples. In the purview of materials science, there is great interest in developing NIR materials transparent to the visible region with applications in NIR-photon harvesting luminescent solar concentrators¹⁷ and high-efficiency NIR OLEDs.^{15,18}

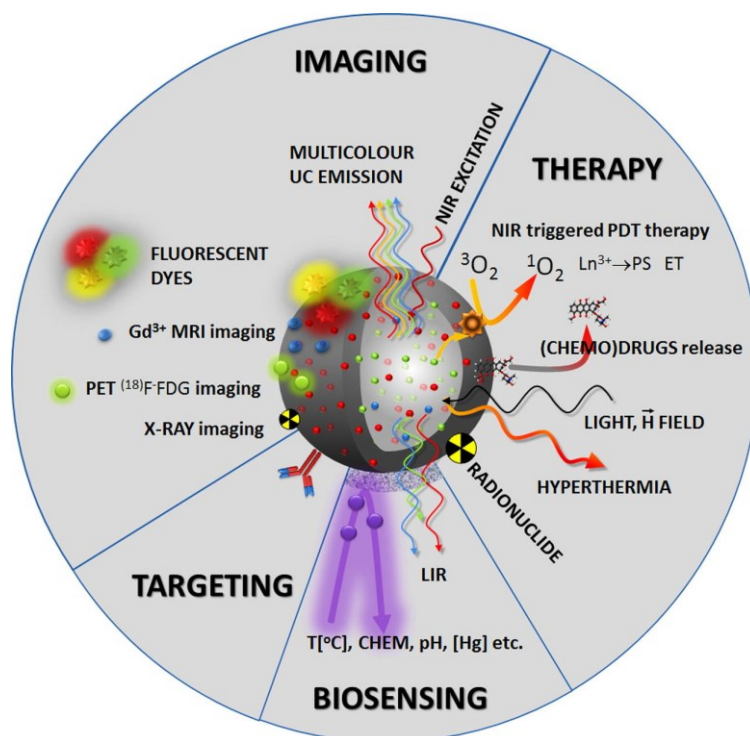


Figure 1.2 Non-exhaustive overview of applications for NIR materials. Reproduced with permission from [20] Copyright 2017 Elsevier.

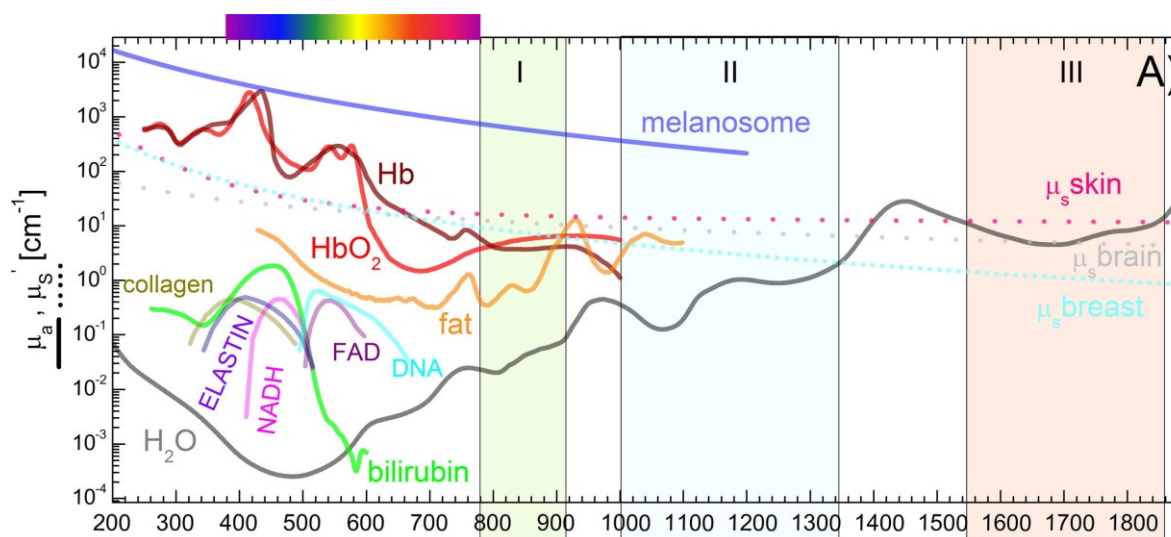


Figure 1.3 Absorption (μ_a) and reduced scattering (μ_s') coefficients of major tissue components/representative tissues with fluorescence spectra of major tissue components. Reproduced with permission from [14] Copyright 2017 Elsevier.

NIR-emitting materials can be divided into two distinct classes, each with their own distinct properties and challenges. Inorganics (*i.e.* QDs, Ln nanoparticles) have the advantage of being significantly more resistant to photo bleaching yet struggle with preparations at scale and reproducibility.¹⁹ Recent concerns over *in vivo* cytotoxicity of inorganic materials and their components is a primary reasons for the observed resurgence of NIR fluorophore research. Organics (*i.e.* cyanines, squaraines, phthalocyanines, porphyrins, BODIPY and perylene) benefit from more focused tuning of optical properties by virtue of a more versatile synthetic toolbox and potentially cheaper large-scale production of materials. Materials such as carbon nanotubes do not fall in either category, yet possess desirable photophysical properties. A thorough and comprehensive review²⁰ of all known NIR emitting dyes (incl. commercial dyes) used in biological imaging recently analysed structure-property relationships within each class of material.

1.2.1 Synopsis of Frontier Dyes

Chemical literature is replete with examples of both organic and inorganic materials emitting in the NIR region. This section provides an overview of the leading, cutting-edge dyes (determined by factors such as solubility, photostability, brightness, etc.) along with brief description of their intended applications. Very thorough and comprehensive reviews

on NIR phosphorescent materials²¹, long-wavelength optical materials²² and a synopsis²⁰ of NIR dyes and their photophysical properties provide an exhaustive discussion of NIR materials if required.

1.2.1.1 Organic Luminophores

NIR-emissive dyes are often complex, extended structures which require multiple synthetic steps to prepare. Therefore, ease of preparation and synthetic accessibility are of primary importance when designing organic materials. Such qualities have been incorporated into the water-soluble seminaphthofluorones²³ and photostable ECX dyes²⁴ which show true NIR properties ($\lambda_{\max} = 880$ nm, $\lambda_{\text{em}} = 920$ nm, $\Phi_{\text{F}} = 0.133$) while being essentially transparent to the visible region. Structural modification of traditional dyes has resulted in novel NIR-active cyanines²⁵ and red-light indigo photoswitches.²⁶ Nevertheless, facile preparation of the dye is not always possible when more specialized properties are required. For example, Pt(II) complexes of core-fused chlorins have proven themselves to be effective oxygen-sensing NIR phosphors.²⁷ Their superior persistence and selective accumulation²⁸ in cancerous tissue make porphyrins *par excellence* dyes for sensitization of singlet oxygen (*i.e.* PDT). These properties make them effective NIR agents in photoacoustic imaging.²⁹ Additional examples include *in vivo* thiol and reactive oxygen

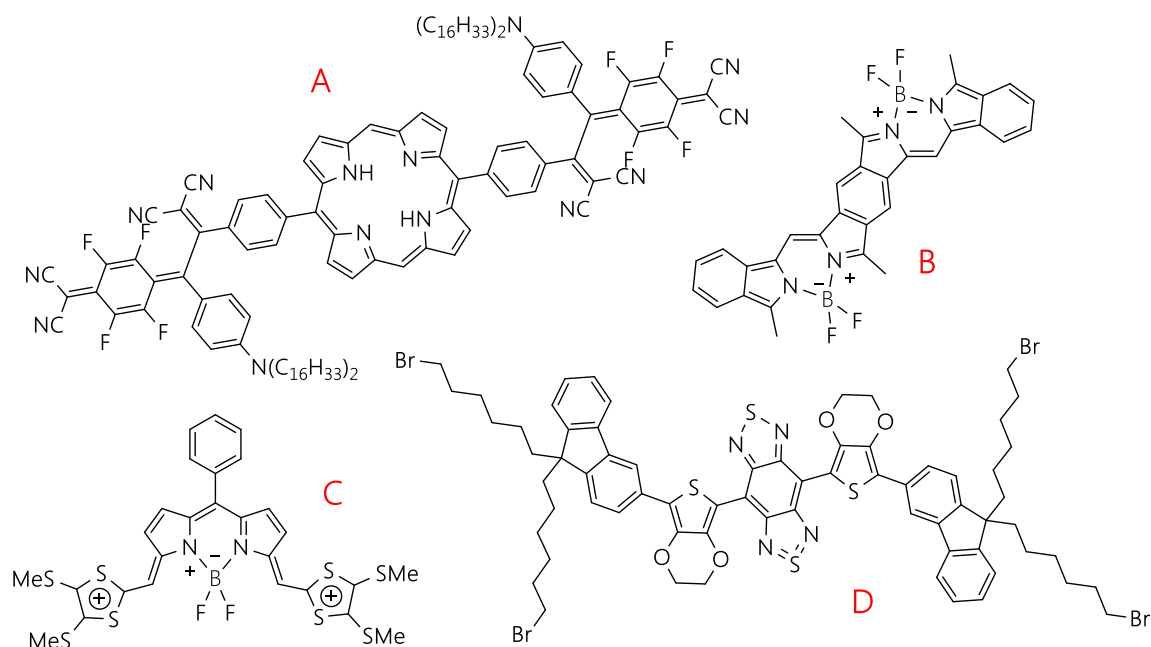


Figure 1.4 Representative “state-of-the-art” NIR organic dyes. A) R33 from Ref. [29]. B) *anti*-9 from Ref. [31]. C) ex-TTF-BODIPY 1²⁺ from Ref. [34]. D) IR-FE from Ref. [42].

sensing (ROS) by functionalized coumarin derivatives.³⁰ More exotic substitution patterns are found in π -extended bis-fused,³¹ azaBODIPYs,³² thien[2,3-b]annulation³³ as well as hybrid systems such as TTF-BODIPY³⁴ which displays redox-switchable “on-off-on” emission that extends well into the NIR region ($\lambda_{em} = 1185$ nm, $\Phi_{F,estim.} = 0.00048$), making it the most red-emitting BODIPY known to date.

Only a handful of organic dyes have crossed the 1000 nm barrier while remaining adequately emissive: IR-E1³⁵ ($\lambda_{em} = 1071$, $\Phi_F = 0.007$), SCH1100³⁶ ($\lambda_{em} = 1100$ nm, $\Phi_F = 0.002$) and CH1055-PEG³⁷ ($\lambda_{em} = 1055$ nm, $\Phi_F = 0.003$). The latter benefited from rapid systemic elimination (~90% excretion through the kidneys in 24 hours), making it superior to all other NIR developed so far in terms of *in vivo* biocompatibility. However, IR-FE and IR-FEP exhibit PLQYs of 0.31 (PhMe) and 0.02 in (H₂O) in a similar emission range ($\lambda_{em} \sim 1100$ nm) and hold the current record for brightest NIR-emission from an organic material reported to date.³⁸ New supramolecular and photophysical strategies currently being explored are redefining expectations of what properties can be achieved inorganic materials. For example, organic small-molecule NPs³⁹ and aggregation-induced FR-NIR emission from organic nanoprobables⁴⁰ is being developed for imaging applications.

1.2.1.2 Inorganic Luminophores

An unfortunate consequence of photophysical interaction is inevitable photobleaching of the material. Inorganic materials have the advantage of greatly enhanced photostability over their organic counterparts, who are particularly susceptible due to their enhanced reactivity and extended π -electron systems. Recently, Martinić and co-workers developed highly photostable Zn²⁺/Ln³⁺ metallacrowns⁴¹ capable of differentiating the chronic cells from living cells in the first reported case of NIR-emission from a single Ln(III) cation being applied to bio-imaging. Photostable and ultra-bright Nd³⁺ doped BiVO₄ nanocrystals showed great promise for use as deep-tissue contrast agents.⁴² “Egyptian blue” (CaCuSi₄O₁₀) is known as the first synthetic pigment in human history and was ubiquitous in ancient Egypt, Mesopotamia and Greece. Its renowned photostability and NIR emission ($\lambda_{em} = 910$ nm, PLQY = 0.105) observed in the bulk material are retained when exfoliated to a 2D nanosheet. Its compatibility with inkjet printing makes it an attractive material for applications in IR telecommunications and security ink. Inorganics also lend themselves well to interdisciplinary study. For instance, DNA origami-directed

self-assembly of CdPb QDs displayed NIR-emission and remarkable stability in aqueous high-salt concentration conditions.⁴⁵

1.2.2 Challenges

Despite to their advantageous applications in the red and NIR regions, these materials are still plagued with shortcomings that need to be addressed. They range from niche concerns such as low biocompatibility to more general deficiencies. Photostability and solubility are major issues of contention for NIR materials, given their extended π -systems and often planar structures which lend themselves to aggregation, though this is not always an issue (*i.e.* in the solid state). However, such extended structures often lead to flexible substitution patterns and high rotational/vibrational degrees of freedom within the molecule. As a result of excessive functionalization, lowering of photoluminescence quantum yield (PLQY) could render these materials too inefficient and restrict real-world application. Therefore, a significant portion of NIR literature deals in PLQY improvement methods and strategies.

1.2.2.1 Mitigating Photoluminescence Losses

Highly flexible dyes or dyes incorporating highly rotating substituents often end up with a very low Φ_F and Φ_P . These characteristics provide effective funnels to the ground state via non-radiative relaxation of the excited state to the ground state. Therefore, the fundamental hurdle in uncovering the full potential of any NIR-emissive material lies in suppression of non-radiative decay (k_{nr}) rates. By virtue of their narrow HOMO-LUMO gap, NIR dyes prove to be consistently weaker emitters compared to their UV-Vis counterparts. This relationship is expressed by a basic statement⁴⁶⁻⁴⁸ of the Energy Gap law:

$$k_{nr} \propto \exp(-\gamma\Delta E/v_M) \quad (5)$$

where ΔE is the energy gap between potential minima of the states involved, v_M is the dominant vibrational frequency in the system and γ is an empirically fitted constant. Red-shifting of spectral properties is ultimately achieved at the expense of PLQY. Theoretical and spectroscopic study of underlying photophysical processes helped established general strategies⁴⁹ to be applied towards preserving and improving PLQY in NIR materials. Empirically, these include increasing chromophore rigidity and planarity, reducing self-aggregation via steric substitution as well as removing intrinsic contributors⁵⁰ to k_{nr}

through isotopic substitution and fluorination.^{51,52} The latter has proven itself a powerful tool for PLQY enhancement, a result particularly well documented⁵³ for Ln complexes. However, fluorine's electronegative nature effects significant change in dipole/ k_r , often leading to unexpected modification of photophysical properties. Notably, *p*-fluorination of *meso*-Ph rings in PtTPTBP resulted in ~20% relative enhancement of Φ_P while further fluorination drastically reduces PLQY and lifetime.⁵⁴ Conversely, isotopic substitution (*i.e.* deuteration) does not modulate electronic properties and is a very attractive option for tuning photophysics while preserving molecular geometry and spectral characteristics.

Structural rigidity and molecular aggregation play a large role in determining how emissive a material can be. Conformational restriction of BODIPY dimers has been shown to dramatically enhance Φ_F due to a more rigid structure.⁵⁵ benzo[b]fused BODIPY monomer ($\lambda_{em} = 690$, $\Phi_F < 0.01$) and dimer ($\lambda_{em} = 940$, $\Phi_F < 0.01$) achieve an impressive red shifting of optical properties due to decreased LUMO levels, but at the cost of reduced PLQY.⁵⁶ The authors cite restricted area while rotation on the BODIPY skeleton as one of the reasons for low emission. In contrast, the annulated aromatic ring in highly emissive benzo[c]fused BODIPYs is ideally positioned to provide steric bulk, which prevents free-rotation of *meso*-aryl rings. Interestingly, a 15-fold enhancement in NIR emission ($\lambda_{em} = 748$ nm) was observed when an emissive film of gel-immobilized π -extended BODIPY was mechanically sheared.⁵⁷ The authors cite differences in chromophore packing introduced by mechanical stress of the film as the reason for amplified PLQY.

Because of their slow radiative rates, lanthanide complexes are particularly prone to excited state deactivation⁵⁸ through vibronic coupling to X-H oscillators in proximity to the metal center. A longstanding strategy to minimize k_{nr} in such systems involves perdeuteration/fluorination⁵⁹ of ligands. There is also something to be said for avoiding specific non-radiative relaxation pathways entirely. NIR to green light upconversion was achieved by doping a GaEr complex with long-lived Cr(III) to access new upconversion pathways, avoiding the efficient non-radiative relaxation pathways in the original material.⁶⁰

As mentioned previously, increasing the number of vibrational degrees of freedom in a material can have detrimental effects on PLQY. "Promoter" vibrational modes induce significant nuclear displacement, accessing geometries which facilitate conical intersections for non-radiative $T_1/S_1 \rightarrow S_0$ surface crossings.⁶¹ Low-energy (< 800 cm⁻¹) aromatic C=C and C-H distortion modes (*i.e.* C=C twisting, C-H out-of-plane bending) have been identified as some of the most efficient promoters of non-radiative decay.

Comparable low-energy modes were shown to account for the majority (>50%) of reorganizational energy in model aromatic systems. Non-radiative decay is commonly ascribed to high-frequency vibrations (*i.e.* C-H stretching); however, these “acceptor” modes are not to blame as they involve minimal nuclear displacement and serve almost exclusively as spectating energy sinks for vibronic quanta.

1.2.3 Red-shifting strategies

Given the variety of chemical structures, each with their own set of properties and photophysical behaviour, it would be prudent not to ascribe the rigid set of guidelines in the design of NIR materials. Therefore, compound-specific strategies will be discussed in the relevant experimental chapter while this section is meant to provide a brief, general overview of available methods. Bathochromic shifting of optical properties in organic molecules is achieved by a narrowing of the HOMO-LUMO gap, which can be done in a number of ways. Extending π -conjugation,⁶² including fusion of aromatic rings, red-shifts optical properties to an extent. There is a diminishing return effect upon every successive extension of the π -system. Nevertheless, literature is replete with examples of π -extension leading to red-shifted properties.^{21,24,38,66} Destabilizing the HOMO level by incorporation of heterocycles and heteroatoms into the structure has also been shown to achieve the same result. Transition metals⁶⁸ have been shown to promote ISC and subsequent phosphorescence from the lower-lying triplet state in organic dyes. Donor-acceptor systems⁶⁹⁻⁷¹ have been used to successfully shift optical properties but in the majority of cases led to a precipitous decline in PLQY, likely due to non-radiative charge transfer. There are exceptions however, as a push-pull system was recently used to achieve redder emission in a family of azaBODIPY dyes⁷² with only modest losses in PLQY. Substituent effects are usually not considered in the context of optoelectronics since they offer limited control over optical properties. Incorporating pyrrole in the design of NIR materials is a convenient way that takes advantage of all of the aforementioned strategies. As an aromatic heterocycle, it is effective at extending length of the π -system through conjugation and has a rich pool of organic chemistry to fine-tune optoelectronic properties. Additionally, several classes of pyrrolic compounds are known to form very stable and luminescent metal complexes.

1.3 Pyrrole: Nature's Heterocycle

Pyrrole was first detected as a component of coal tar distillate by Runge in 1834 and named it from the Greek *pyrrhos* and *elaion* (meaning “red” and “oil”, respectively) likely due to the reddening of pyrrole-containing tar fractions upon treatment with acid. It is one of nature's most abundant heterocycles by virtue of being the main building block in a myriad of natural products, coenzymes and pigments. A non-exhaustive list of examples (some are shown in Figure 1.4) include the heme family and its breakdown products biliverdin and bilirubin, chlorophyll, ageliferin, ryanodine, PQQ, prodigiosin, vitamin B₁₂ and haemin, for which Hans Fisher received the Nobel Prize in 1930. The heme family of compounds is responsible for the color of our erythrocytes while chlorophyll is a key component in the photosynthetic chain to which all foliage ascribes its green colour. Prodigiosin exemplifies the tripyrrolic prodiginines, a class of red alkaloids receiving increased attention as potential antibacterial and anticancer agents. Interestingly, atorvastatin (brand name Lipitor) ranks as the top-selling pharmaceutical drug in history and is a fully-substituted pyrrole.

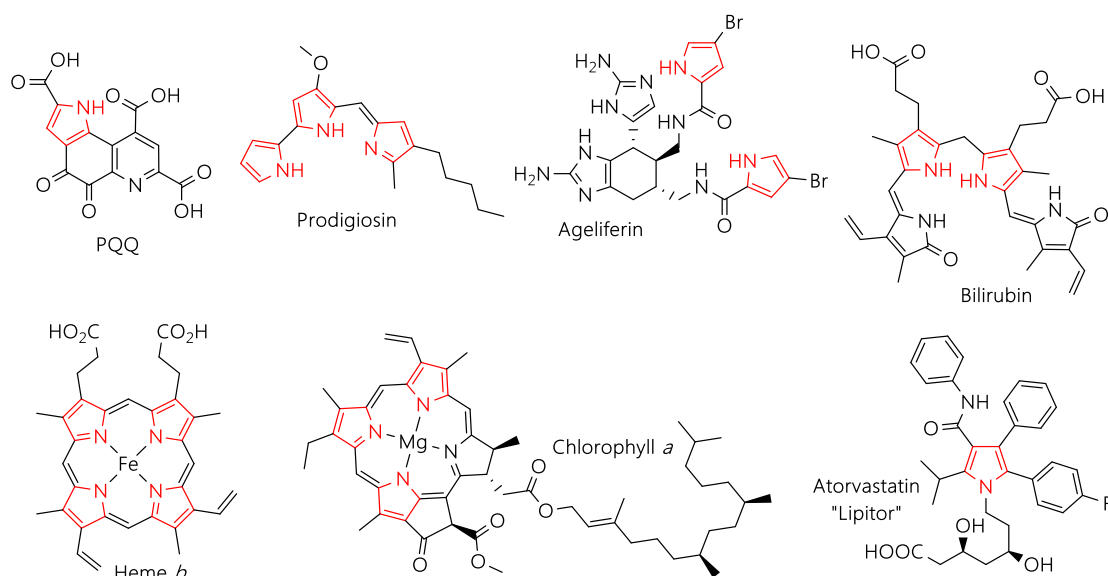
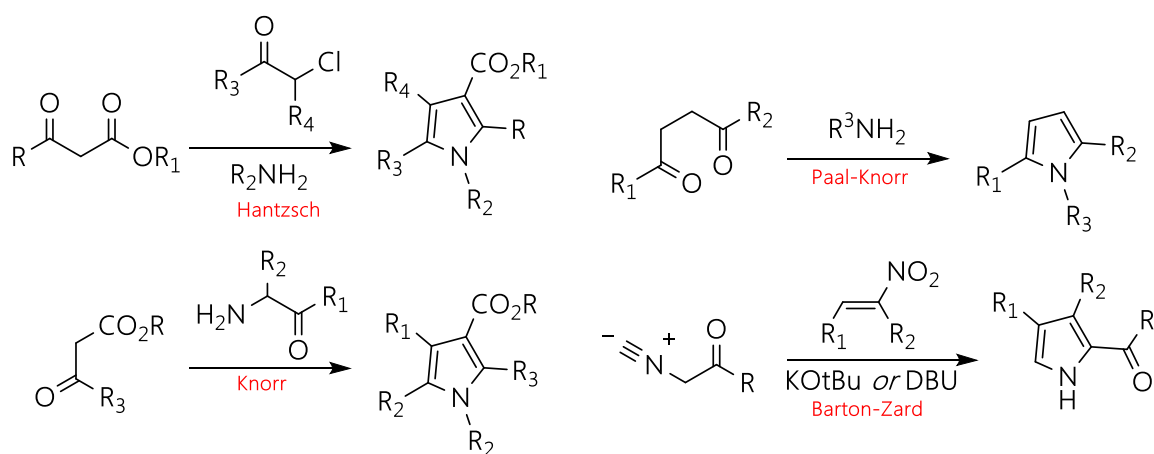


Figure 1.5 Various chemical structures of pyrrole-containing natural products.

1.3.1 Heterocycle Assembly and Reactivity

The synthetic chemistry of pyrrole has been reviewed extensively.⁷⁶⁻⁷⁹ The most relevant and important methodologies (Scheme 1.1) are outlined below with accompanying examples. The widely-used Paal-Knorr synthesis⁸⁰ generates the pyrrole heterocycle via acid-catalyzed condensation of 1,4-dicarbonyls and alkylamines. As an alternative to the classical procedures requiring prolonged heating, microwave-assisted reactions offer much higher yields and shorter reaction times.⁸¹ A variety of “masked” 1,4-dicarbonyl starting materials may also be used such as 2,5-Ometetrahydrofuran⁸² and α -nitroketones.⁸³ The Knorr pyrrole synthesis⁸⁴ involves the condensation of an α -amino- β -ketoester or an α -aminoketone with an activated methylene compound. Higher selectivity in the reaction was achieved with sterically hindered β -ketones.^{85 85 86} Pd-catalyzed oxidation and cyclization of β -hydroxyenamines readily obtained from condensation of β -aminoalcohols and 1,3-diketones also yields substituted pyrrole in good yields. Ionic liquids have been used as reaction media for the Paal-Knorr synthesis. The Hantzsch pyrrole synthesis proceeds through β -ketoesters and α -haloketones in the presence of primary amines.⁸⁸⁻⁹¹ The Barton-Zard condensation has found widespread application in the field of materials science, in particular for the preparation of optoelectronic materials precursors. Due to its versatility, it is also routinely employed in total syntheses of complex natural products. Barton and Zard demonstrated condensation of nitroolefins with α -isocyanoacetate esters, with resulting pyrrole substitution patterns being very fortuitous for fields of porphyrin and polypyrrole synthesis. Alternatively, α,β -unsaturated sulfones⁹⁹ have successfully been used in place of nitroolefins. An elegant example of applied Barton-Zard chemistry is the preparation of 2-(SnMe₃)pyrroles via



Scheme 1.1 Generalized representations of the most widely applied pyrrole synthesis methodologies.

condensation of *in situ*-stannylated isocyanide,¹⁰⁰ which were cross-coupled with aryl bromides. Other miscellaneous methodologies include the Zav'yalov pyrrole synthesis,^{101,102} Dieckmann-type condensation of enamines and McMurry coupling of enamines and masked 1,3-dicarbonyl compounds. Atom-economical multi-component and microwave-assisted⁷⁸ syntheses of pyrrole are a current area of interest due to a push towards greener methods in modern heterocyclic chemistry. To that end, an incredibly expansive range of transition metal-mediated syntheses have been developed for pyrrole.⁷⁶ Exemplifying this is the elegant example where sustainable iridium-catalyzed reaction of secondary alcohols and amino alcohols under mild conditions produces pyrroles with only hydrogen gas as a by-product.¹¹³

Electrophiles generally react with pyrrole at the activated α -position (2,5-positions), unless these positions are already functionalized or the pyrrole is N-substituted. Pyrroles readily react with halogenating, nitrating, sulfonating and acylating agents. Formylation at the 2-position can be achieved through the Vilsmeier-Haack reaction. *tert*-Butyl 2-pyrrole carboxylate readily undergoes de-esterification/decarboxylation in one step in neat TFA or other strong acids. Given moderate acidity of the NH proton, it readily undergoes deprotonation when treated with strong bases (i.e. alkylolithiums, NaH) to produce the corresponding pyrrolide which acts as a strong nucleophile. The scope of pyrrole reactivity, much like its synthesis, has been reviewed extensively in literature.^{114,115}

1.3.2 Stability and Related Heterocycles

While pyrrole itself readily undergoes oxidation upon exposure to air and light, pyrroles substituted at the 2,5-positions and the *N*-position with EWGs in particular show improved benchtop stability over their unsubstituted counterpart which usually need to be distilled before use. 2-Halopyrroles, while potentially very useful precursors, are notoriously unstable decomposing at room temperature within seconds.¹¹⁶ Isoindole, of particular interest in materials science, is too unstable¹¹⁷ to be handled by itself. Usually, “masked” isoindoles or tetrahydropyrrole precursors are employed instead of isoindole itself.

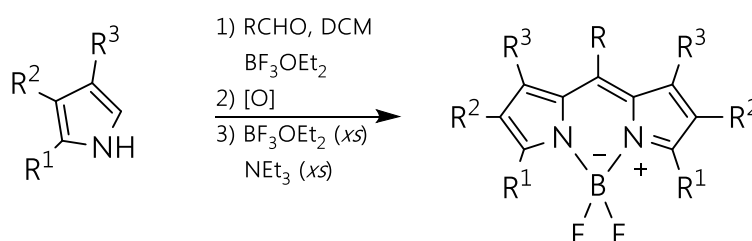
1.4 BODIPY & Dipyrin

Near-infrared (NIR) radiation has taken on a more primary role in advanced materials and bio-medical research in recent years. The advent of more accessible⁷¹ NIR

sources and detectors has proven to be a considerable boon for experimental science and demand for more photostable and brighter NIR fluorophores has grown in tandem. Difluoro-boraindacene dyes (widely known as BODIPY dyes) have emerged in recent years as biological dyes *par excellence* and are one of the most investigated organic chromophores. They are encountered everywhere from telecommunications¹¹⁸, organic photovoltaics¹¹⁹, ion sensors, and DSSCs¹²¹ to bio-medical imaging¹²² and photodynamic therapy^{123,124}. First prepared in 1968¹²⁵, BODIPY dyes have become prized for their intense absorption profile ($\epsilon > 90000 \text{ M}^{-1}\text{cm}^{-1}$) and high PLQY ($\Phi > 0.50$) expressed via narrow Gaussian-shaped peaks. These spectroscopic features¹²⁶ are largely insensitive to changes in solvent polarity and dyes themselves are highly soluble in most organic solvents. Facile synthesis and versatile substitution patterns of the BODIPY framework make them readily accessible and versatile tools for specialized applications.¹²⁷ Their excellent photostability is enhanced by negligible excited triplet state formation in both solution and solid-state.¹²⁸ These desirable features serve collectively as an ideal foundation for development of effective NIR fluorophores. Similar to fluorescein and rhodamine dyes, non-functionalized BODIPY dyes are limited in operation between 470-530 nm. Recent efforts¹²⁹ to red-shift spectral properties were aimed at efficient fluorescence in the biological window¹³⁰ (650-900 nm).

1.4.1 Nomenclature and Synthesis

BODIPYs are simply $-\text{BF}_2$ complexes of dipyrins (Figure 1.5) and while their stability and optical properties may be dramatically different, their synthetic chemistry can be interchangeably applied to either of them with minor modifications. A more detailed introduction to dipyrin-specific chemistry will be presented in chapter 4. Synthesis of the BODIPY core usually goes through acid-catalyzed oxidative condensation (Scheme 1.2) of



Scheme 1.2 General representation of an acid-catalyzed oxidative condensation between substituted pyrrole and aldehyde.

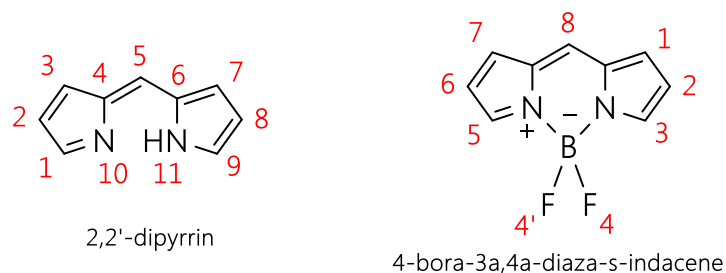


Figure 1.6 structures and IUPAC-recommended numbering systems for (left) dipyrrens and (right) BODIPYs.

pyrroles with an electrophilic carbonyl compound (i.e. aldehydes, acyl chlorides) followed by treatment with an excess of BF_3OEt_2 in the presence of a base. While some published syntheses will deviate in one aspect or another, oxidative condensation (see section 1.5.2) is ubiquitous in dipyrren and BODIPY chemistry. Typically, R^1 is substituted to prevent unwanted polycondensation of the pyrrole during synthesis. If a 3,5-unsubstituted BODIPY is desired, a large excess of pyrrole in relation to the aldehyde must be used. In any case, the other R groups can take on the role of conceivably any substituent, the sheer number of which is a testament to the versatility of BODIPY chemistry (Figure 1.6).

1.4.2 Post-synthetic modification

BODIPYs react with a variety of electrophilic reagents (i.e. NCS, NBS, Br_2) in the following order: at the 2,6-positions, 1,7-positions and finally 3,5-position. The BODIPY chromophore can be chlorinated, brominated and iodinated and even a few instances where sulfonation and nitration was achieved at the 2,6-positions.¹³² Chloro- moieties can be incorporated into the least reactive positions (3,5-) by functionalization of the dipyrromethane precursor prior to complexation with BF_2 . All halogenated BODIPYs are known to participate in Pd-catalyzed C-C coupling reactions, which has enabled access to a vast library of derivatives. Additionally, 3,5-halogenated derivatives undergo nucleophilic attack at the same positions by alkoxides, thioalkoxides and amines.¹³²⁻¹³⁴ For additional information on BODIPY syntheses and their post-synthetic functionalization, comprehensive and well-written reviews by Burgess¹²⁶ and Bessette¹¹⁹ are recommended for further reading.

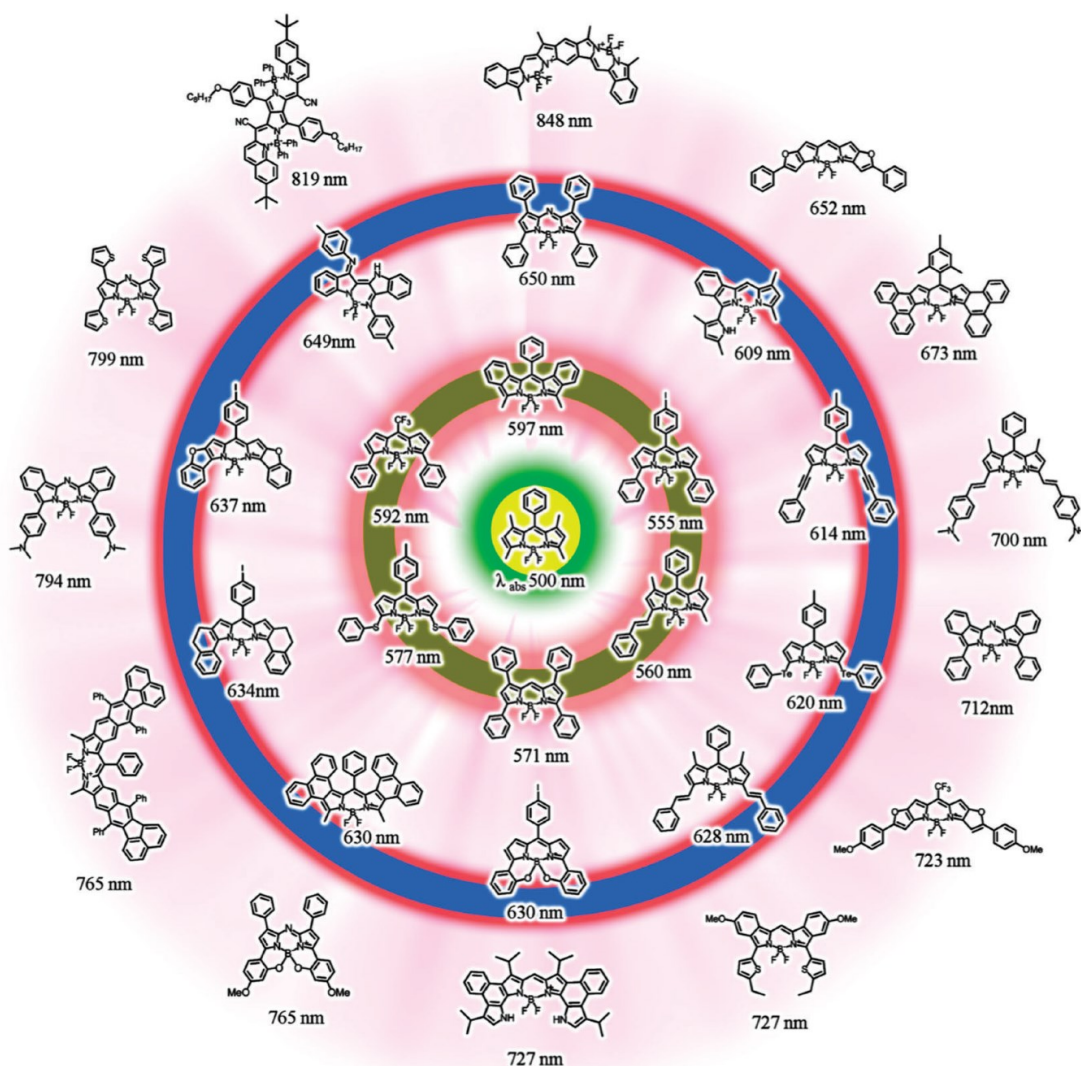


Figure 1.7 A representative sample of BODIPY dyes spanning the entire visible-NIR region. Reproduced with permission [124] Copyright 2014 Royal Society of Chemistry.

1.5 Porphyrins

1.5.1 Structure and Nomenclature

Porphyrins are the most abundantly occurring class of heterocyclic macrocycles, both in nature and in material sciences. Their name is derived from the Greek word “*porphyra*”, translated *purple*. Indeed, many porphyrins exhibit lavish purple and greenish-blue colours in solution as well as solid-state due to their intense absorption bands in the visible region. A famous example is heme *b*, an iron-porphyrin complex (Figure 1.7) found in haemoglobin that facilitates oxygen transport in blood. Another important example is

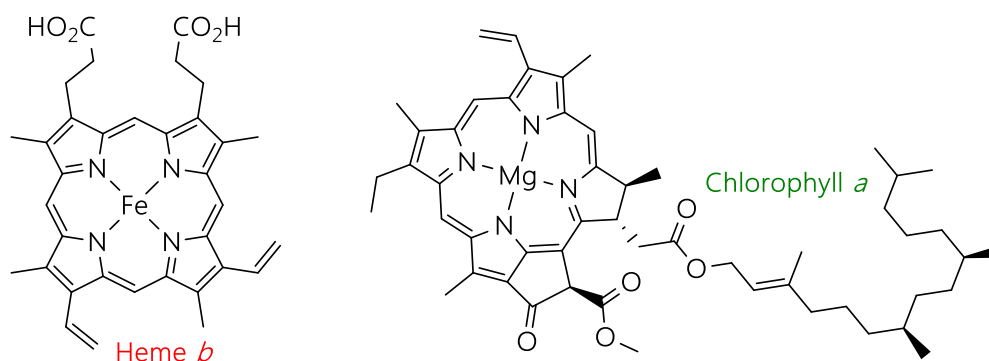


Figure 1.8 Structures of heme *b* (porphyrin) and chlorophyll *a* (chlorin).

chlorophyll, the green pigment vital to photosynthesis found in most plants and cyanobacteria. Structurally, it is considered a chlorin which is a porphyrin with one reduced olefinic bond. Porphyrin macrocycles are comprised of four pyrrole units connected via methine (=CH-) bridges. Taking the simplest example, unsubstituted parent porphyrin (porphine) contains four nitrogen atoms and twenty carbon atoms. Obeying Hückel's rule, ($4n+2 \pi$ electrons, with $n = 4$) porphyrins are planar and highly conjugated systems with two delocalization pathways across the macrocycle shown in (Figure 1.7). Hans Fisher was the first to introduce nomenclature¹³⁵ for the porphyrin system where every pyrrole was labelled A-D, carbons adjacent to the nitrogen were called “ α -carbons” and the methine carbons were labelled with lower-case Greek letters $\alpha - \delta$. These methine carbons were also called *meso*-carbons, a naming convention that endured even after the systematic and more complete IUPAC nomenclature was introduced (Figure 1.8).

1.5.2 Synthetic Methodology

Many more 5,10,15,20-aryl substituted porphyrins have been prepared and studied than their *meso*-unsubstituted counterparts, due to their significantly improved solubility and synthetic versatility. Of these, tetraphenylporphyrin (TPP) has the most basic structure and is the most commonly encountered *meso*-aryl porphyrin dye. The first reported synthesis¹³⁶ of TPP was by Rothmund more than 80 years ago where pyrrole and benzaldehyde were reacted in a sealed bomb with pyridine at 150° for 24 hours. These harsh conditions have resulted mostly in tarry mixtures in addition to limiting the scope of substituted benzaldehyde starting materials. Adler and Longo improved¹³⁷ upon the low-yielding Rothmund conditions by refluxing the starting materials in propionic acid and using atmospheric oxygen as an oxidant. Crystalline TPPs were obtained in yields of up to 15% and this procedure was employed on a multigram preparative scale for a

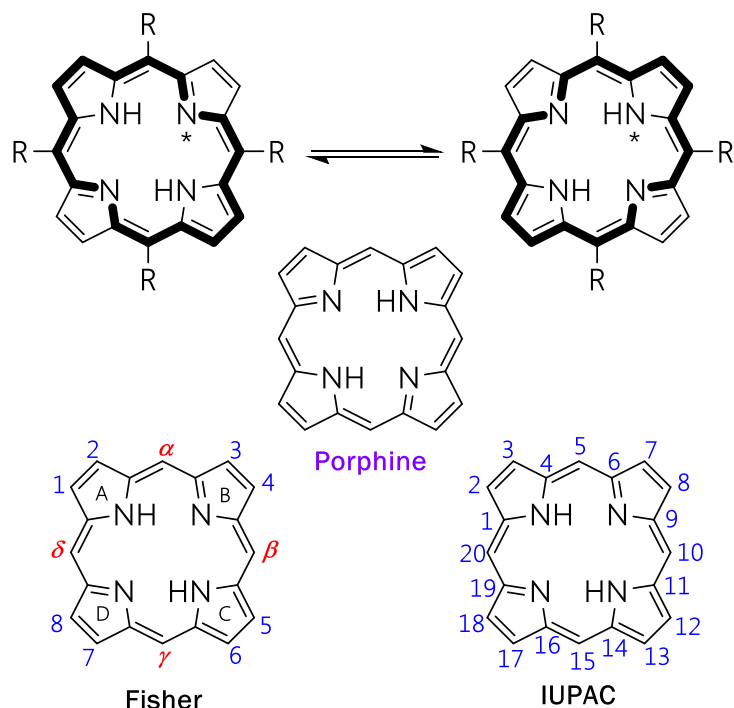
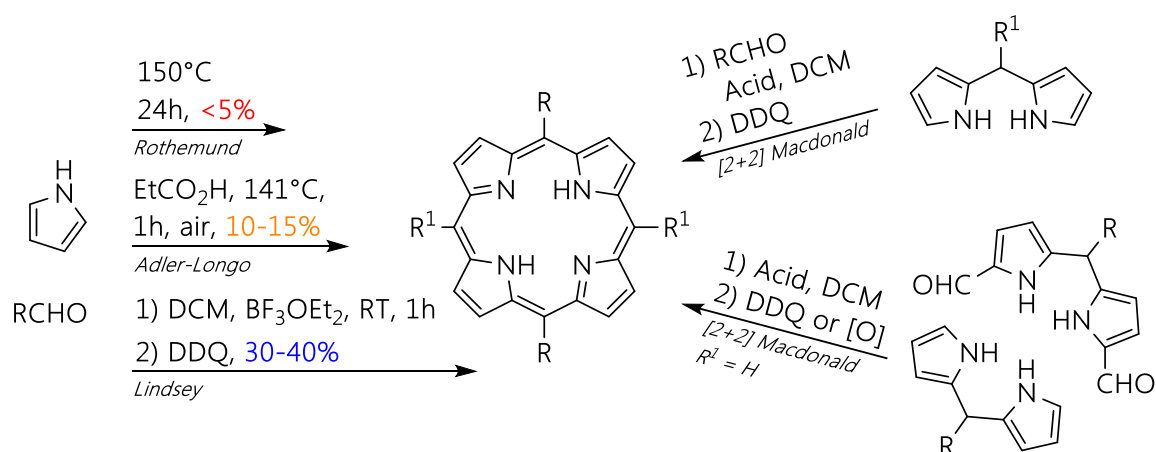


Figure 1.9 (Top) Tautomerization of substituted porphyrin. (Bottom) Fischer and IUPAC nomenclature conventions of the porphyrin macrocycle.

number of porphyrins. Nevertheless, this methodology has been plagued with poor reproducibility, intolerance of sensitive functional groups and purification issues resulting from the tarry mixtures with porphyrins that do not easily crystallize out. Excluding special cases of exceedingly unreactive or sterically hindered aldehydes, the majority of modern porphyrin syntheses use an iteration of the Lindsey method.¹³⁸ The desired pyrrole and



Scheme 1.3 Synthetic methodologies for (left) symmetrical porphyrins and (right) asymmetric and 5,15-unsubstituted porphyrins.

aldehyde are condensed in high dilution conditions with Lewis acid catalysis followed by oxidative aromatization with a hydrogen transfer reagent (*i.e.* DDQ, chloranil). Of all methods described so far, (Scheme 1.3) the Lindsey method is the mildest, highest yielding synthesis with the widest functional group tolerance available to this day. However, the Lindsey method struggles with oxidative condensation of sterically-hindered *o*-substituted aldehydes (mesitaldehyde, *o*-alkoxyaldehyde); BF₃OEt₂-EtOH co-catalysis¹³⁹ was found to be necessary to achieve porphyrin yields. Access to *meso*-asymmetric porphyrins is achieved through the [2+2] Macdonald oxidative condensation with corresponding dipyrromethanes. In the case where 5,5'-diformyldipyrromethanes condensed with unsubstituted dipyrromethane, atmospheric oxygen can serve as the oxidant. With one notable exception, all porphyrins in this dissertation were prepared by the Lindsey method. While this short survey is by no means exhaustive, it is a general highlight of the most widely used methods and porphyrin chemistry. If more information is required, the reader is referred to recently-published exhaustive reviews of porphyrin chemistry their post-synthetic modification.¹⁴¹

1.5.3 Properties and Applications

Similar to BODIPYs, porphyrins show high chemical- and photostability and possess a highly conjugated, rigid and planar macrocyclic core. In fact, the latter imparts desirable crystallization properties onto porphyrins, in some cases allowing direct crystallization of bright purple porphyrin crystals out of complex tarry mixtures in acetic/propionic acid. They owe their exceptionally strong light absorption ($\epsilon > 150000 \text{ M}^{-1} \text{ cm}^{-1}$) and other optoelectronic properties to an extended π -electron system. This has led to widespread application¹⁴² of porphyrins as photonic and optoelectronic materials. This includes optical limiters, nonlinear optics and dye-sensitized solar cells^{146,147} (DSSCs) as well as bioimaging^{148,149} and photodynamic therapy¹⁵⁰ with emerging applications in photon upconversion via triplet-triplet annihilation¹⁵¹ (TTA) and 2-photon absorption. Their optical, electric, and even magnetic properties can be widely tuned by modification of the pyrrole and aldehyde moieties and via coordination to different metals.¹⁵³ Their group 4 metal complexes exhibit bright fluorescence ($\Phi_F > 0.3$) while group 5-6 metal complexes tend to phosphoresce. Noteworthy are Pd(II)/Pt(II) complexes which show efficient ISC rates and low triplet energies making them important phosphorescent dyes.¹⁵⁴ In fact, platinum

octaethylporphyrin (PtOEP) was the first material used in phosphorescent light-emitting diodes.^{155,156}

1.6 Conclusion

The ever-increasing sophistication of spectroscopic equipment and elegant synthetic methodologies being devised, preparation and study of FR-NIR dyes is bound to attract many researchers and inspire innovation in multiple fields. Porphyrins and BODIPYs benefit from a synergistic pool of synthetic methodology built up over the last century, which permits facile preparation and study of these dyes. Their attractive optoelectronic properties (sharp and intense absorption bands, high PLQY) as well as rigid and highly stable structures make them desirable springboards for accessing bright, π -extended FR-NIR materials.

1.7 References

- (1) Crosby, G. A.; Demas, J. N. Measurement of photoluminescence quantum yields. Review *J. Phys. Chem.* **1971**, *75*, 991.
- (2) Resch-Genger, U.; Hoffmann, K.; Nietfeld, W.; Engel, A.; Neukammer, J.; Nitschke, R.; Ebert, B.; Macdonald, R. How to Improve Quality Assurance in Fluorometry: Fluorescence-Inherent Sources of Error and Suited Fluorescence Standards *J. Fluoresc.* **2005**, *15*, 337.
- (3) Velapoldi, R. A.; Tønnesen, H. H. Corrected Emission Spectra and Quantum Yields for a Series of Fluorescent Compounds in the Visible Spectral Region *J. Fluoresc.* **2004**, *14*, 465.
- (4) Resch-Genger, U.; Hoffmann, K.; Pfeifer, D. In *Simple Calibration and Validation Standards for Fluorometry*; Springer New York: New York, NY, **2009**, p 1.
- (5) Wuerth, C.; Resch-Genger, U. Determination of photoluminescence quantum yields of scattering media with an integrating sphere: direct and indirect illumination *Appl. Spectrosc.* **2015**, *69*, 749.
- (6) Wurth, C.; Grabolle, M.; Pauli, J.; Spieles, M.; Resch-Genger, U. Comparison of methods and achievable uncertainties for the relative and absolute measurement of photoluminescence quantum yields *Anal. Chem.* **2011**, *83*, 3431.
- (7) Sharafy, S.; Muszkat, K. A. Viscosity dependence of fluorescence quantum yields *J. Am. Chem. Soc.* **1971**, *93*, 4119.
- (8) Nawara, K.; Waluk, J. Improved Method of Fluorescence Quantum Yield Determination *Anal. Chem.* **2017**, *89*, 8650.
- (9) Kempe, D.; Schöne, A.; Fitter, J.; Gabba, M. Accurate Fluorescence Quantum Yield Determination by Fluorescence Correlation Spectroscopy *J. Phys. Chem. B.* **2015**, *119*, 4668.
- (10) Rurack, K.; Spieles, M. Fluorescence Quantum Yields of a Series of Red and Near-Infrared Dyes Emitting at 600–1000 nm *Anal. Chem.* **2011**, *83*, 1232.

- (11) Boens, N.; Qin, W.; Basarić, N.; Hofkens, J.; Ameloot, M.; Pouget, J.; Lefèvre, J.-P.; Valeur, B.; Gratton, E.; vandeVen, M.; Silva, N. D.; Engelborghs, Y.; Willaert, K.; Sillen, A.; Rumbles, G.; Phillips, D.; Visser, A. J. W. G.; van Hoek, A.; Lakowicz, J. R.; Malak, H.; Gryczynski, I.; Szabo, A. G.; Krajcarski, D. T.; Tamai, N.; Miura, A. Fluorescence Lifetime Standards for Time and Frequency Domain Fluorescence Spectroscopy *Anal. Chem.* **2007**, *79*, 2137.
- (12) Haque, A.; Faizi, M. S. H.; Rather, J. A.; Khan, M. S. Next generation NIR fluorophores for tumor imaging and fluorescence-guided surgery: A review *Biorg. Med. Chem.* **2017**, *25*, 2017.
- (13) Reineck, P.; Gibson, B. C. Near-Infrared Fluorescent Nanomaterials for Bioimaging and Sensing *Adv. Opt. Mater.* **2017**, *5*, 1600446.
- (14) Liu, T.-M.; Conde, J.; Lipiński, T.; Bednarkiewicz, A.; Huang, C.-C. Smart NIR linear and nonlinear optical nanomaterials for cancer theranostics: Prospects in photomedicine *Prog. Mater. Sci.* **2017**, *88*, 89.
- (15) Stender, B.; Völker, S. F.; Lambert, C.; Pflaum, J. Optoelectronic Processes in Squaraine Dye-Doped OLEDs for Emission in the Near-Infrared *Adv. Mater.* **2013**, *25*, 2943.
- (16) Smith, A. M.; Mancini, M. C.; Nie, S. Second window for in vivo imaging *Nat. Nanotechnol.* **2009**, *4*, 710.
- (17) Zhao, Y.; Meek, G. A.; Levine, B. G.; Lunt, R. R. Near-Infrared Harvesting Transparent Luminescent Solar Concentrators *Adv. Opt. Mater.* **2014**, *2*, 606.
- (18) Tuong Ly, K.; Chen-Cheng, R.-W.; Lin, H.-W.; Shiau, Y.-J.; Liu, S.-H.; Chou, P.-T.; Tsao, C.-S.; Huang, Y.-C.; Chi, Y. Near-infrared organic light-emitting diodes with very high external quantum efficiency and radiance *Nat. Photon.* **2017**, *11*, 63.
- (19) Resch-Genger, U.; Grabolle, M.; Cavaliere-Jaricot, S.; Nitschke, R.; Nann, T. Quantum dots versus organic dyes as fluorescent labels *Nat. Meth.* **2008**, *5*, 763.
- (20) Martinić, I.; Eliseeva, S. V.; Petoud, S. Near-infrared emitting probes for biological imaging: Organic fluorophores, quantum dots, fluorescent proteins, lanthanide(III) complexes and nanomaterials *J. Lumin.* **2017**, *189*, 19.
- (21) Xiang, H.; Cheng, J.; Ma, X.; Zhou, X.; Chruma, J. J. Near-infrared phosphorescence: materials and applications *Chem. Soc. Rev.* **2013**, *42*, 6128.
- (22) Pansare, V.; Hejazi, S.; Faenza, W.; Prud'homme, R. K. Review of Long-Wavelength Optical and NIR Imaging Materials: Contrast Agents, Fluorophores and Multifunctional Nano Carriers *Chem. Mater.* **2012**, *24*, 812.
- (23) Yang, Y.; Lowry, M.; Xu, X.; Escobedo, J. O.; Sibrian-Vazquez, M.; Wong, L.; Schowalter, C. M.; Jensen, T. J.; Fronczek, F. R.; Warner, I. M.; Strongin, R. M. Seminaphthofluorones are a family of water-soluble, low molecular weight, NIR-emitting fluorophores *P. Natl. Acad. Sci.* **2008**, *105*, 8829.
- (24) Lei, Z.; Li, X.; Luo, X.; He, H.; Zheng, J.; Qian, X.; Yang, Y. Bright, Stable, and Biocompatible Organic Fluorophores Absorbing/Emitting in the Deep Near-Infrared Spectral Region *Angew. Chem. Int. Ed.* **2017**, *56*, 2979.
- (25) Gorka, A. P.; Nani, R. R.; Schnermann, M. J. Cyanine polyene reactivity: scope and biomedical applications *Org. Biomol. Chem.* **2015**, *13*, 7584.
- (26) Huang, C.-Y.; Bonasera, A.; Hristov, L.; Garmshausen, Y.; Schmidt, B. M.; Jacquemin, D.; Hecht, S. N,N'-Disubstituted Indigos as Readily Available Red-Light Photoswitches with Tunable Thermal Half-Lives *J. Am. Chem. Soc.* **2017**, *139*, 15205.
- (27) Pereira, N. A. M.; Laranjo, M.; Casalta-Lopes, J.; Serra, A. C.; Piñeiro, M.; Pina, J.; Seixas de Melo, J. S.; Senge, M. O.; Botelho, M. F.; Martelo, L.; Burrows, H. D.; Pinho e Melo, T. M. V. D. Platinum(II) Ring-Fused Chlorins as Near-Infrared Emitting Oxygen Sensors and Photodynamic Agents *ACS Med. Chem. Lett.* **2017**, *8*, 310.

- (28) MacDonald, T. D.; Liu, T. W.; Zheng, G. An MRI-Sensitive, Non-Photobleachable Porphysome Photothermal Agent *Angew. Chem.* **2014**, *126*, 7076.
- (29) Li, L.; Wang, D.; Wang, L.; Ramella, D.; Wang, H.; Gao, H.; Zhang, J.; Xing, Y.; Li, B.; Yang, Z.; Cao, H.; He, W. The photoacoustic effect of near-infrared absorbing porphyrin derivatives prepared via click chemistry *Dyes Pigm.* **2018**, *148*, 501.
- (30) Yuan, L.; Lin, W.; Zhao, S.; Gao, W.; Chen, B.; He, L.; Zhu, S. A Unique Approach to Development of Near-Infrared Fluorescent Sensors for in Vivo Imaging *J. Am. Chem. Soc.* **2012**, *134*, 13510.
- (31) Nakamura, M.; Tahara, H.; Takahashi, K.; Nagata, T.; Uoyama, H.; Kuzuhara, D.; Mori, S.; Okujima, T.; Yamada, H.; Uno, H. [small pi]-Fused bis-BODIPY as a candidate for NIR dyes *Org. Biomol. Chem.* **2012**, *10*, 6840.
- (32) Sheng, W.; Cui, J.; Ruan, Z.; Yan, L.; Wu, Q.; Yu, C.; Wei, Y.; Hao, E.; Jiao, L. [a]-Phenanthrene-Fused BF₂ Azadipyromethene (AzaBODIPY) Dyes as Bright Near-Infrared Fluorophores *J. Org. Chem.* **2017**, *82*, 10341.
- (33) Wang, J.; Li, J.; Chen, N.; Wu, Y.; Hao, E.; Wei, Y.; Mu, X.; Jiao, L. Synthesis, structure and properties of thiophene-fused BODIPYs and azaBODIPYs as near-infrared agents *New J. Chem.* **2016**, *40*, 5966.
- (34) Bill, N. L.; Lim, J. M.; Davis, C. M.; Bahring, S.; Jeppesen, J. O.; Kim, D.; Sessler, J. L. [small pi]-Extended tetrathiafulvalene BODIPY (ex-TTF-BODIPY): a redox switched "on-off-on" electrochromic system with two near-infrared fluorescent outputs *Chem. Commun.* **2014**, *50*, 6758.
- (35) Zhang, X.-D.; Wang, H.; Antaris, A. L.; Li, L.; Diao, S.; Ma, R.; Nguyen, A.; Hong, G.; Ma, Z.; Wang, J.; Zhu, S.; Castellano, J. M.; Wyss-Coray, T.; Liang, Y.; Luo, J.; Dai, H. Traumatic Brain Injury Imaging in the Second Near-Infrared Window with a Molecular Fluorophore *Adv. Mater.* **2016**, *28*, 6872.
- (36) Sun, Y.; Qu, C.; Chen, H.; He, M.; Tang, C.; Shou, K.; Hong, S.; Yang, M.; Jiang, Y.; Ding, B.; Xiao, Y.; Xing, L.; Hong, X.; Cheng, Z. Novel benzo-bis(1,2,5-thiadiazole) fluorophores for in vivo NIR-II imaging of cancer *Chem. Sci.* **2016**, *7*, 6203.
- (37) Antaris, A. L.; Chen, H.; Cheng, K.; Sun, Y.; Hong, G.; Qu, C.; Diao, S.; Deng, Z.; Hu, X.; Zhang, B.; Zhang, X.; Yaghi, O. K.; Alamparambil, Z. R.; Hong, X.; Cheng, Z.; Dai, H. A small-molecule dye for NIR-II imaging *Nat. Mater.* **2016**, *15*, 235.
- (38) Yang, Q.; Ma, Z.; Wang, H.; Zhou, B.; Zhu, S.; Zhong, Y.; Wang, J.; Wan, H.; Antaris, A.; Ma, R.; Zhang, X.; Yang, J.; Zhang, X.; Sun, H.; Liu, W.; Liang, Y.; Dai, H. Rational Design of Molecular Fluorophores for Biological Imaging in the NIR-II Window *Adv. Mater.* **2017**, *29*, 1.
- (39) Tao, Z.; Hong, G.; Shinji, C.; Chen, C.; Diao, S.; Antaris, A. L.; Zhang, B.; Zou, Y.; Dai, H. Biological Imaging Using Nanoparticles of Small Organic Molecules with Fluorescence Emission at Wavelengths Longer than 1000 nm *Angew. Chem.* **2013**, *125*, 13240.
- (40) Shao, A.; Xie, Y.; Zhu, S.; Guo, Z.; Zhu, S.; Guo, J.; Shi, P.; James, T. D.; Tian, H.; Zhu, W.-H. Far-Red and Near-IR AIE-Active Fluorescent Organic Nanoprobes with Enhanced Tumor-Targeting Efficacy: Shape-Specific Effects *Angew. Chem. Int. Ed.* **2015**, *54*, 7275.
- (41) Martinić, I.; Eliseeva, S. V.; Nguyen, T. N.; Pecoraro, V. L.; Petoud, S. Near-Infrared Optical Imaging of Necrotic Cells by Photostable Lanthanide-Based Metallacrowns *J. Am. Chem. Soc.* **2017**, *139*, 8388.
- (42) Starsich, F. H. L.; Gschwend, P.; Sergeyev, A.; Grange, R.; Pratsinis, S. E. Deep Tissue Imaging with Highly Fluorescent Near-Infrared Nanocrystals after Systematic Host Screening *Chem. Mater.* **2017**, *29*, 8158.

- (43) Accorsi, G.; Verri, G.; Bolognesi, M.; Armaroli, N.; Clementi, C.; Miliani, C.; Romani, A. The exceptional near-infrared luminescence properties of cuprorivaite (Egyptian blue) *Chem. Commun.* **2009**, 3392.
- (44) Johnson-McDaniel, D.; Barrett, C. A.; Sharafi, A.; Salguero, T. T. Nanoscience of an Ancient Pigment *J. Am. Chem. Soc.* **2013**, *135*, 1677.
- (45) Samanta, A.; Deng, Z.; Liu, Y. Infrared emitting quantum dots: DNA conjugation and DNA origami directed self-assembly *Nanoscale* **2014**, *6*, 4486.
- (46) Doffek, C.; Alzakhem, N.; Bischof, C.; Wahsner, J.; Güden-Silber, T.; Lügger, J.; Platas-Iglesias, C.; Seitz, M. Understanding the Quenching Effects of Aromatic C–H and C–D-Oscillators in Near-IR Lanthanoid Luminescence *J. Am. Chem. Soc.* **2012**, *134*, 16413.
- (47) Robinson, G. W.; Frosch, R. P. Theory of electronic energy relaxation in the solid phase *J. Chem. Phys.* **1962**, *37*, 1962.
- (48) Englman, R.; Jortner, J. The energy gap law for radiationless transitions in large molecules *Mol. Phys.* **1970**, *18*, 145.
- (49) Xiang, H.; Cheng, J.; Ma, X.; Zhou, X.; Chruma, J. J. Near-infrared phosphorescence: materials and applications *Chem. Soc. Rev.* **2013**, *42*, 6128.
- (50) Wang, P.; Wang, F.-F.; Chen, Y.; Niu, Q.; Lu, L.; Wang, H.-M.; Gao, X.-C.; Wei, B.; Wu, H.-W.; Cai, X.; Zou, D.-C. Synthesis of all-deuterated tris(2-phenylpyridine)iridium for highly stable electrophosphorescence: the "deuterium effect" *J. Mater. Chem. C* **2013**, *1*, 4821.
- (51) Martin-Ramos, P.; Ramos Silva, M.; Lahoz, F.; Martin, I. R.; Chamorro-Posada, P.; Eusebio, M. E. S.; Lavin, V.; Martin-Gil, J. Highly fluorinated erbium(III) complexes for emission in the C-band *J. Photochem. Photobiol., A* **2014**, *292*, 16.
- (52) Chi, Y.; Chou, P.-T. Transition-metal phosphors with cyclometalating ligands: fundamentals and applications *Chem. Soc. Rev.* **2010**, *39*, 638.
- (53) Valore, A.; Cariati, E.; Righetto, S.; Roberto, D.; Tessore, F.; Ugo, R.; Fragala, I. L.; Fragala, M. E.; Malandrino, G.; De Angelis, F.; Belpassi, L.; Ledoux-Rak, I.; Thi, K. H.; Zyss, J. Fluorinated β -Diketonate Diglyme Lanthanide Complexes as New Second-Order Nonlinear Optical Chromophores: The Role of f Electrons in the Dipolar and Octupolar Contribution to Quadratic Hyperpolarizability *J. Am. Chem. Soc.* **2010**, *132*, 4966.
- (54) Borisov, S. M.; Nuss, G.; Haas, W.; Saf, R.; Schmuck, M.; Klimant, I. New NIR-emitting complexes of platinum(II) and palladium(II) with fluorinated benzoporphyrins *J. Photochem. Photobiol., A* **2009**, *201*, 128.
- (55) Wang, J.; Wu, Q.; Wang, S.; Yu, C.; Li, J.; Hao, E.; Wei, Y.; Mu, X.; Jiao, L. Conformation-Restricted Partially and Fully Fused BODIPY Dimers as Highly Stable Near-Infrared Fluorescent Dyes *Org. Lett.* **2015**, *17*, 5360.
- (56) Wakamiya, A.; Murakami, T.; Yamaguchi, S. Benzene-fused BODIPY and fully-fused BODIPY dimer: impacts of the ring-fusing at the b bond in the BODIPY skeleton *Chem. Sci.* **2013**, *4*, 1002.
- (57) Cherumukkil, S.; Ghosh, S.; Praveen, V. K.; Ajayaghosh, A. An unprecedented amplification of near-infrared emission in a Bodipy derived [small pi]-system by stress or gelation *Chem. Sci.* **2017**, *8*, 5644.
- (58) Buenzli, J.-C. G.; Piguet, C. Taking advantage of luminescent lanthanide ions *Chem. Soc. Rev.* **2005**, *34*, 1048.
- (59) Hasegawa, Y.; Ohkubo, T.; Sogabe, K.; Kawamura, Y.; Wada, Y.; Nakashima, N.; Yanagida, S. Luminescence of Novel Neodymium Sulfonylamate Complexes in Organic Media *Angew. Chem., Int. Ed.* **2000**, *39*, 357.
- (60) Suffren, Y.; Zare, D.; Eliseeva, S. V.; Guénee, L.; Nozary, H.; Lathion, T.; Aboshyan-Sorgho, L.; Petoud, S.; Hauser, A.; Piguet, C. Near-Infrared to Visible Light-

- Upconversion in Molecules: From Dream to Reality *J. Phys. Chem. C* **2013**, *117*, 26957.
- (61) Gegiou, D.; Muszkat, K. A.; Fischer, E. Temperature dependence of photoisomerization. V. Effect of substituents on the photoisomerization of stilbenes and azobenzenes *J. Am. Chem. Soc.* **1968**, *90*, 3907.
- (62) Pschirer, N. G.; Kohl, C.; Nolde, F.; Qu, J.; Müllen, K. Pentarylene- and Hexarylenebis(dicarboximide)s: Near-Infrared-Absorbing Polyaromatic Dyes *Angew. Chem. Int. Ed.* **2006**, *45*, 1401.
- (63) Jiao, C.; Wu, J. Fused polycyclic aromatic compounds with near infrared absorption and emission *Synlett* **2012**, *23*, 171.
- (64) Nunzi, J.-M. Organic photovoltaic materials and devices *C. R. Phys.* **2002**, *3*, 523.
- (65) Charra, F.; Fichou, D.; Nunzi, J.-M.; Pfeffer, N. Picosecond photoinduced dichroism in solutions of thiophene oligomers *Chem. Phys. Lett.* **1992**, *192*, 566.
- (66) Lowry, M. S.; Bernhard, S. Synthetically Tailored Excited States: Phosphorescent, Cyclometalated Iridium(III) Complexes and Their Applications *Chem. - Eur. J.* **2006**, *12*, 7970.
- (67) Fayed, T. A. Extension of fluorescence response to the near-IR region *Rev. Fluoresc.* **2011**, *6*, 75.
- (68) Lu, W.; Mi, B.-X.; Chan, M. C. W.; Hui, Z.; Che, C.-M.; Zhu, N.; Lee, S.-T. Light-Emitting Tridentate Cyclometalated Platinum(II) Complexes Containing σ -Alkynyl Auxiliaries: Tuning of Photo- and Electrophosphorescence *J. Am. Chem. Soc.* **2004**, *126*, 4958.
- (69) Ajayaghosh, A. Donor-acceptor type low band gap polymers: polysquaraines and related systems *Chem. Soc. Rev.* **2003**, *32*, 181.
- (70) Kiyose, K.; Kojima, H.; Nagano, T. Functional Near-Infrared Fluorescent Probes *Chem. - Asian J.* **2008**, *3*, 506.
- (71) Qian, G.; Wang, Z. Y. Near-Infrared Organic Compounds and Emerging Applications *Chem. - Asian J.* **2010**, *5*, 1006.
- (72) Jiao, L.; Wu, Y.; Wang, S.; Hu, X.; Zhang, P.; Yu, C.; Cong, K.; Meng, Q.; Hao, E.; Vicente, M. G. H. Accessing Near-Infrared-Absorbing BF₂-Azadipyromethenes via a Push–Pull Effect *J. Org. Chem.* **2014**, *79*, 1830.
- (73) Runge, F. F. On some products of coal distillation *Ann. Phys. Chem.* **1834**, *65*.
- (74) Williamson, N. R.; Fineran, P. C.; Leeper, F. J.; Salmond, G. P. C. The biosynthesis and regulation of bacterial prodiginines *Nat. Rev. Microbiol.* **2006**, *4*, 887.
- (75) Fuerstner, A. Chemistry and biology of roseophilin and the prodigiosin alkaloids: a survey of the last 2500 years *Angew. Chem., Int. Ed.* **2003**, *42*, 3582.
- (76) Gulevich, A. V.; Dudnik, A. S.; Chernyak, N.; Gevorgyan, V. Transition Metal-Mediated Synthesis of Monocyclic Aromatic Heterocycles *Chem. Rev.* **2013**, *113*, 3084.
- (77) Ferreira, V. F.; de Souza, M. C. B. V.; Cunha, A. C.; Pereira, L. O. R.; Ferreira, M. L. G. Recent advances in the synthesis of pyrroles *Org. Prep. Proced. Int.* **2001**, *33*, 411.
- (78) Shrinivas, D. J.; Uttam, A. M.; Venkatrao, H. K.; Tejraj, M. A. Pyrrole: Chemical Synthesis, Microwave Assisted Synthesis, Reactions and Applications: A Review *Curr. Org. Chem.* **2013**, *17*, 2279.
- (79) Lubell, W. S.-C., D.; Dufour-Gallant, J.; Hopewell, R.; Boutard, N.; Kassem, T.; Dörr, A.; Zelli, R. 1-H Pyrroles (Update 2013) *Science of Synthesis* **2013**, *1*, 157.
- (80) Katrizky, A. R. in *Handbook of Heterocyclic Chemistry*; 1st ed.; Pergamon Press: New York, 1985
- (81) Danks, T. N. Microwave assisted synthesis of pyrroles *Tetrahedron Lett.* **1999**, *40*, 3957.
- (82) Baussanne, I.; Royer, J. Asymmetric routes towards polyfunctionalized pyrrolidines: synthesis and reactivity of a chiral silyloxyppyrrrole *Tetrahedron Lett.* **1996**, *37*, 1213.

- (83) Barton, D. H. R.; Kervagoret, J.; Zard, S. Z. A useful synthesis of pyrroles from nitroolefins *Tetrahedron* **1990**, *46*, 7587.
- (84) Gilchrist, T. L. in *Heterocyclic Chemistry*; 2nd ed.; John Wiley & Sons: New York, 1992
- (85) Fujii, H.; Yoshimura, T.; Kamada, H. Regioselective pyrrole synthesis from asymmetric β -diketone and conversion to sterically hindered porphyrin *Tetrahedron Lett.* **1997**, *38*, 1427.
- (86) Aoyagi, Y.; Mizusaki, T.; Ohta, A. Facile and efficient synthesis of pyrroles and indoles via palladium-catalyzed oxidation of hydroxy-enamines and -amines *Tetrahedron Lett.* **1996**, *37*, 9203.
- (87) Wang, B.; Gu, Y.; Luo, C.; Yang, T.; Yang, L.; Suo, J. Pyrrole synthesis in ionic liquids by Paal-Knorr condensation under mild conditions *Tetrahedron Lett.* **2004**, *45*, 3417.
- (88) Trautwein, A. W.; Sussmuth, R. D.; Jung, G. Hantzsch pyrrole synthesis on a solid support *Bioorg. Med. Chem. Lett.* **1998**, *8*, 2381.
- (89) Roomi, M. W.; MacDonald, S. F. Hantzsch pyrrole synthesis *Can. J. Chem.* **1970**, *48*, 1689.
- (90) Matiychuk, V. S.; Martyak, R. L.; Obushak, N. D.; Ostapiuk, Y. V.; Pidlypnyi, N. I. 3-aryl-2-chloropropanals in Hantzsch synthesis of pyrroles *Chem. Heterocycl. Compd. (N. Y., NY, U. S.)* **2004**, *40*, 1218.
- (91) Lei, T.; Liu, W.-Q.; Li, J.; Huang, M.-Y.; Yang, B.; Meng, Q.-Y.; Chen, B.; Tung, C.-H.; Wu, L.-Z. Visible Light Initiated Hantzsch Synthesis of 2,5-Diaryl-Substituted Pyrroles at Ambient Conditions *Org. Lett.* **2016**, *18*, 2479.
- (92) Barton, D. H. R.; Zard, S. Z. A new synthesis of pyrroles from nitro alkenes *J. Chem. Soc., Chem. Commun.* **1985**, 1098.
- (93) Burns, D. H.; Jabara, C. S.; Burden, M. W. A convenient preparation of benzyl 4-(R1)-3-(R2)pyrrole-2-carboxylates *Synth. Commun.* **1995**, *25*, 379.
- (94) Lash, T. D.; Wijesinghe, C.; Osuma, A. T.; Patel, J. R. Synthesis of novel porphyrin chromophores from nitroarenes: further applications of the Barton-Zard pyrrole condensation *Tetrahedron Lett.* **1997**, *38*, 2031.
- (95) Lash, T. D.; Thompson, M. L.; Werner, T. M.; Spence, J. D. Synthesis of novel pyrrolic compounds from nitroarenes and isocynoacetates using a phosphazene superbase *Synlett* **2000**, 213.
- (96) Lash, T. D.; Bellettini, J. R.; Bastian, J. A.; Couch, K. B. Synthesis of pyrroles from benzyl isocynoacetate *Synthesis* **1994**, 170.
- (97) Nakajima, S.; Osuka, A. Synthesis of a tetrakis(9-anthryl) substituted porphyrin and intramolecular charge-transfer emission in its dication *Tetrahedron Lett.* **1995**, *36*, 8457.
- (98) Dell'Erba, C.; Giglio, A.; Mugnoli, A.; Novi, M.; Petrillo, G.; Stagnaro, P. Synthetic exploitation of the ring-opening of 3,4-dinitrothiophene. 5. Base-induced cycloaddition of tosylmethyl or (tert-butoxycarbonyl)methyl isocyanide to 1,4-disubstituted 2,3-dinitro-1,3-butadienes. Access to 2,3-disubstituted 4-ethynylpyrroles *Tetrahedron* **1995**, *51*, 5181.
- (99) Abel, Y.; Haake, E.; Haake, G.; Schmidt, W.; Struve, D.; Walter, A.; Montforts, F.-P. A simple and flexible synthesis of pyrroles from α,β -unsaturated sulfones *Helv. Chim. Acta* **1998**, *81*, 1978.
- (100) Dijkstra, H. P.; ten Have, R.; van Leusen, A. M. A Direct Synthesis of 2-(Trimethylstannyl)pyrroles from Michael Acceptors and Stannylated Tosylmethyl Isocyanide *J. Org. Chem.* **1998**, *63*, 5332.

- (101) Chen, N.; Lu, Y.; Gadamasetti, K.; Hurt, C. R.; Norman, M. H.; Fotsch, C. A short, facile synthesis of 5-substituted 3-amino-1H-pyrrole-2-carboxylates *J. Org. Chem.* **2000**, *65*, 2603.
- (102) Toplak, R.; Svete, J.; Stanovnik, B.; Grdadolnik, S. G. The synthesis of methyl 2-(benzyloxycarbonyl)amino-3-dimethylaminopropenoate. The synthesis of trisubstituted pyrroles, 3-amino-2H-pyran-2-ones, fused 2H-pyran-2-ones and 4H-pyridin-4-ones *J. Heterocycl. Chem.* **1999**, *36*, 225.
- (103) Gupton, J. T.; Petrich, S. A.; Smith, L. L.; Bruce, M. A.; Vu, P.; Du, K. X.; Dueno, E. E.; Jones, C. R.; Sikorski, J. A. The application of vinylogous iminium salts and related synthons to the regiocontrolled preparation of 2,3- and 2,5-disubstituted pyrroles *Tetrahedron* **1996**, *52*, 6879.
- (104) Fuerstner, A.; Weintritt, H.; Hupperts, A. A New, Titanium-Mediated Approach to Pyrroles: First Synthesis of Lukianol A and Lamellarin O Dimethyl Ether *J. Org. Chem.* **1995**, *60*, 6637.
- (105) Braun, R. U.; Zeitler, K.; Mueller, T. J. J. A Novel One-Pot Pyrrole Synthesis via a Coupling-Isomerization-Stetter-Paal-Knorr Sequence *Org. Lett.* **2001**, *3*, 3297.
- (106) Bharadwaj, A. R.; Scheidt, K. A. Catalytic Multicomponent Synthesis of Highly Substituted Pyrroles Utilizing a One-Pot Sila-Stetter/Paal-Knorr Strategy *Org. Lett.* **2004**, *6*, 2465.
- (107) Banik, B. K.; Samajdar, S.; Banik, I. Simple Synthesis of Substituted Pyrroles *J. Org. Chem.* **2004**, *69*, 213.
- (108) Estevez, V.; Villacampa, M.; Menendez, J. C. Three-component access to pyrroles promoted by the CAN-silver nitrate system under high-speed vibration milling conditions: a generalization of the Hantzsch pyrrole synthesis *Chem. Commun.* **2013**, *49*, 591.
- (109) Balme, G.; Bouyssi, D.; Monteiro, N. Functionalized acetylenes as versatile building-blocks for the multicomponent assembling of polysubstituted furans and pyrroles *Heterocycles* **2007**, *73*, 87.
- (110) Agarwal, S.; Knoelker, H.-J. A novel pyrrole synthesis *Org. Biomol. Chem.* **2004**, *2*, 3060.
- (111) Estevez, V.; Villacampa, M.; Menendez, J. C. Recent advances in the synthesis of pyrroles by multicomponent reactions *Chem. Soc. Rev.* **2014**, *43*, 4633.
- (112) Portilla Zuniga, O. M.; Sathicq, A. G.; Martinez Zambrano, J. J.; Romanelli, G. P. Green Synthesis of Pyrrole Derivatives *Curr. Org. Synth.* **2017**, *14*, 865.
- (113) Michlik, S.; Kempe, R. A sustainable catalytic pyrrole synthesis *Nat. Chem.* **2013**, *5*, 140.
- (114) Baltazzi, E.; Krimen, L. I. Recent Advances in the Chemistry of Pyrrole *Chem. Rev.* **1963**, *63*, 511.
- (115) Bean, R. A. J. G. P. in *The Chemistry of Pyrroles* Academic Press 1977
- (116) Cordell, G. A. 2-Halopyrroles. Synthesis and chemistry *J. Org. Chem.* **1975**, *40*, 3161.
- (117) Sundberg, R. J.; Elsevier: 1996; Vol. 2, p 119.
- (118) Bouit, P.-A.; Kamada, K.; Feneyrou, P.; Berginc, G.; Toupet, L.; Maury, O.; Andraud, C. Two-photon absorption-related properties of functionalized BODIPY dyes in the infrared range up to telecommunication wavelengths *Adv. Mater.* **2009**, *21*, 1151.
- (119) Bessette, A.; Hanan, G. S. Design, synthesis and photophysical studies of dipyrromethene-based materials: insights into their applications in organic photovoltaic devices *Chem. Soc. Rev.* **2014**, *43*, 3342.
- (120) Boens, N.; Leen, V.; Dehaen, W. Fluorescent indicators based on BODIPY *Chem. Soc. Rev.* **2012**, *41*, 1130.

- (121) Singh, S. P.; Gayathri, T. Evolution of BODIPY Dyes as Potential Sensitizers for Dye-Sensitized Solar Cells *Eur. J. Org. Chem.* **2014**, *2014*, 4689.
- (122) Yuan, L.; Lin, W.; Zheng, K.; He, L.; Huang, W. Far-red to near infrared analyte-responsive fluorescent probes based on organic fluorophore platforms for fluorescence imaging *Chem. Soc. Rev.* **2013**, *42*, 622.
- (123) Kamkaew, A.; Lim, S. H.; Lee, H. B.; Kiew, L. V.; Chung, L. Y.; Burgess, K. BODIPY dyes in photodynamic therapy *Chem. Soc. Rev.* **2013**, *42*, 77.
- (124) Awuah, S. G.; You, Y. Boron dipyrromethene (BODIPY)-based photosensitizers for photodynamic therapy *RSC Adv.* **2012**, *2*, 11169.
- (125) Treibs, A.; Kreuzer, F.-H. Difluorboryl-Komplexe von Di- und Tripyrrylmethenen *Liebigs Ann. Chem.* **1968**, *718*, 208.
- (126) Loudet, A.; Burgess, K. BODIPY dyes and their derivatives: Syntheses and spectroscopic properties *Chem. Rev.* **2007**, *107*, 4891.
- (127) Ulrich, G.; Ziesel, R.; Harriman, A. The chemistry of fluorescent Bodipy dyes: versatility unsurpassed *Angew. Chem., Int. Ed.* **2008**, *47*, 1184.
- (128) Xiao, S.; Cao, Q.; Dan, F. Solid-emissive BODIPY derivatives: design, synthesis and applications *Curr. Org. Chem.* **2012**, *16*, 2970.
- (129) Lu, H.; Mack, J.; Yang, Y.; Shen, Z. Structural modification strategies for the rational design of red/NIR region BODIPYs *Chem. Soc. Rev.* **2014**, *43*, 4778.
- (130) Ntziachristos, V.; Ripoll, J.; Wang, L. V.; Weissleder, R. Looking and listening to light: the evolution of whole-body photonic imaging *Nat. Biotechnol.* **2005**, *23*, 313.
- (131) Li, X.; Huang, S.; Hu, Y. Diversity-oriented derivatization of BODIPY based on regioselective bromination *Org. Biomol. Chem.* **2012**, *10*, 2369.
- (132) Lakshmi, V.; Rajeswara Rao, M.; Ravikanth, M. Halogenated boron-dipyrromethenes: synthesis, properties and applications *Org. Biomol. Chem.* **2015**, *13*, 2501.
- (133) Rohand, T.; Baruah, M.; Qin, W.; Boens, N.; Dehaen, W. Functionalisation of fluorescent BODIPY dyes by nucleophilic substitution *Chem. Commun.* **2006**, 266.
- (134) Boens, N.; Verbelen, B.; Dehaen, W. Postfunctionalization of the BODIPY Core: Synthesis and Spectroscopy *Eur. J. Org. Chem.* **2015**, *2015*, 6577.
- (135) Fischer, H.; Orth, H. *Die Chemie des Pyrrols* **1937**, *II*.
- (136) Rothmund, P. Porphyrin studies. III. The structure of the porphine ring system *J. Am. Chem. Soc.* **1939**, *61*, 2912.
- (137) Adler, A. D.; Longo, F. R.; Finarelli, J. D.; Goldmacher, J.; Assour, J.; Korsakoff, L. A simplified synthesis for meso-tetraphenylporphine *J. Org. Chem.* **1967**, *32*, 476.
- (138) Lindsey, J. S.; Schreiman, I. C.; Hsu, H. C.; Kearney, P. C.; Marguerettaz, A. M. Rothmund and Adler-Longo reactions revisited: synthesis of tetraphenylporphyrins under equilibrium conditions *J. Org. Chem.* **1987**, *52*, 827.
- (139) Lindsey, J. S.; Wagner, R. W. Investigation of the synthesis of ortho-substituted tetraphenylporphyrins *J. Org. Chem.* **1989**, *54*, 828.
- (140) Arsenault, G. P.; Bullock, E.; MacDonald, S. F. Pyrromethanes and porphyrins therefrom *J. Am. Chem. Soc.* **1960**, *82*, 4384.
- (141) Hiroto, S.; Miyake, Y.; Shinokubo, H. Synthesis and Functionalization of Porphyrins through Organometallic Methodologies *Chem. Rev.* **2017**, *117*, 2910.
- (142) Kadish, K. M.; Smith, K. M.; Guillard, R.; Editors in *The Porphyrin Handbook; Volume 6, Applications: Past, Present and Future*; Academic Press, 2000
- (143) Perry, J. W.; Mansour, K.; Lee, I. Y. S.; Wu, X. L.; Bedworth, P. V.; Chen, C. T.; Ng, D.; Marder, S. R.; Miles, P.; Wada, T.; Tian, M.; Sasabe, H. Organic optical limiter with a strong nonlinear absorptive response *Science* **1996**, *273*, 1533.
- (144) Calvete, M.; Yang, G. Y.; Hanack, M. Porphyrins and phthalocyanines as materials for optical limiting *Synth. Met.* **2004**, *141*, 231.

- (145) Senge, M. O.; Fazekas, M.; Notaras, E. G. A.; Blau, W. J.; Zawadzka, M.; Locos, O. B.; Mhuircheartaigh, E. M. N. Nonlinear optical properties of porphyrins *Adv. Mater.* **2007**, *19*, 2737.
- (146) Yella, A.; Lee, H.-W.; Tsao, H. N.; Yi, C.; Chandiran, A. K.; Nazeeruddin, M. K.; Diao, E. W.-G.; Yeh, C.-Y.; Zakeeruddin, S. M.; Gratzel, M. Porphyrin-sensitized solar cells with cobalt (II/III)-based redox electrolyte exceed 12 percent efficiency *Science* **2011**, *334*, 629.
- (147) Imahori, H.; Umeyama, T.; Ito, S. Large π -Aromatic Molecules as Potential Sensitizers for Highly Efficient Dye-Sensitized Solar Cells *Acc. Chem. Res.* **2009**, *42*, 1809.
- (148) Zhao, Q.; Huang, C.; Li, F. Phosphorescent heavy-metal complexes for bioimaging *Chem. Soc. Rev.* **2011**, *40*, 2508.
- (149) Escobedo, J. O.; Rusin, O.; Lim, S.; Strongin, R. M. NIR dyes for bioimaging applications *Curr. Opin. Chem. Biol.* **2010**, *14*, 64.
- (150) Ethirajan, M.; Chen, Y.; Joshi, P.; Pandey, R. K. The role of porphyrin chemistry in tumor imaging and photodynamic therapy *Chem. Soc. Rev.* **2011**, *40*, 340.
- (151) Deng, F.; Sommer, J. R.; Myahkostupov, M.; Schanze, K. S.; Castellano, F. N. Near-IR phosphorescent metalloporphyrin as a photochemical upconversion sensitizer *Chem. Commun.* **2013**, *49*, 7406.
- (152) Esipova, T. V.; Vinogradov, S. A. Synthesis of Phosphorescent Asymmetrically π -Extended Porphyrins for Two-Photon Applications *J. Org. Chem.* **2014**, *79*, 8812.
- (153) Suijkerbuijk, B. M. J. M.; Klein, G. R. J. M. Merging porphyrins with organometallics: synthesis and applications *Angew. Chem., Int. Ed.* **2008**, *47*, 7396.
- (154) Papkovsky, D. B.; O'Riordan, T. C. Emerging applications of phosphorescent metalloporphyrins *J. Fluoresc.* **2005**, *15*, 569.
- (155) Baldo, M. A.; O'Brien, D. F.; You, Y.; Shoustikov, A.; Sibley, S.; Thompson, M. E.; Forrest, S. R. Highly efficient phosphorescent emission from organic electroluminescent devices *Nature* **1998**, *395*, 151.
- (156) Perepichka, D. F.; Meng, H.; Ling, M.-M. In *Organic Light Emitting Materials and Devices*; Li, Z., Meng, H., Eds.; CRC: **2006**.

Chapter 2

Tuning Photophysics via Modular Aryl Moiety in a Family of Novel PtAr₄TBIP Dyes

This chapter delves into the synthesis and electronic/photophysical properties for peripherally functionalized alkylimide Pt (II) complexes of Ar₄TBP. Convenience in their preparation at scale and improved solubility/stability over prototypical PtPh₄TBP directed efforts towards enhancement of photoluminescence as the overarching goal of the project. PtPh₄TBIP along with its deuterated (PtPh₄TBIP-*d*₂₀) counterpart were prepared characterized spectroscopically. Structure-property relationships were extracted to glean insight into photophysics of a prominent, yet not fully explored class of dyes. Part of this work has been published.¹

2.1 Introduction to π -Extended Porphyrins

Symmetrically tetraannulated tetrabenzoporphyrins **1** (TBPs), tetranaphtho[2,3]porphyrins **2** (TNPs) and tetraanthra[2,3]porphyrins **3** (TAPs) are part of the class of π -extended porphyrins, depicted in Figure 2.1 with IUPAC-recommended numbering.² Modification of optical properties by aromatic ring annulation to the porphyrin macrocycle to obtain materials like these is a growing field in modern synthetic and theoretical

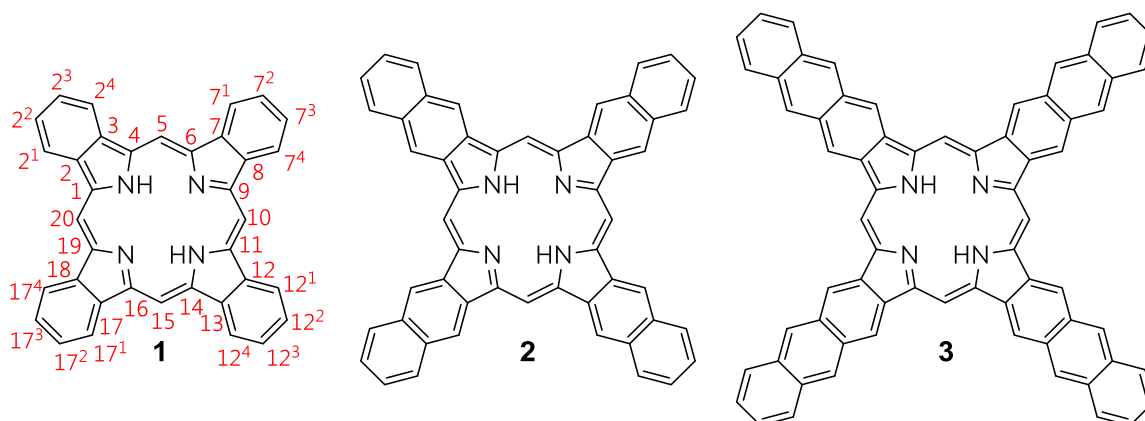


Figure 2.1 Core structures of π -extended porphyrins TBP **1**, TNP **2** and TAP **3**.

porphyrin chemistry. A condensed summary of Cheprakov's insightful theoretical analysis³ of π -extended porphyrins is presented in this section. The quantity and variety of π -extended porphyrins has exploded in the last 30 years, efforts which were in large part galvanized by the need to develop novel NIR chromophores. Yet, the bathochromic shifts observed in the myriad of novel benzo-annulated porphyrins prepared fell short of expectations; it seemed that the fused moieties were unable to effectively disrupt the basic porphyrin π -electron system. Under the formal rules of aromatic fusion (summation of π -electrons within the system), TBP would be considered a 34-electron aromatic system, which does not fall in line with experimentally-determined optoelectronic properties.⁵ Gouterman's four orbital model^{6,7} describing main porphyrin transitions is simulated from a fully symmetrical [18]-annulene. Indeed, the aromatic porphyrin system can be understood as a set of [18]-

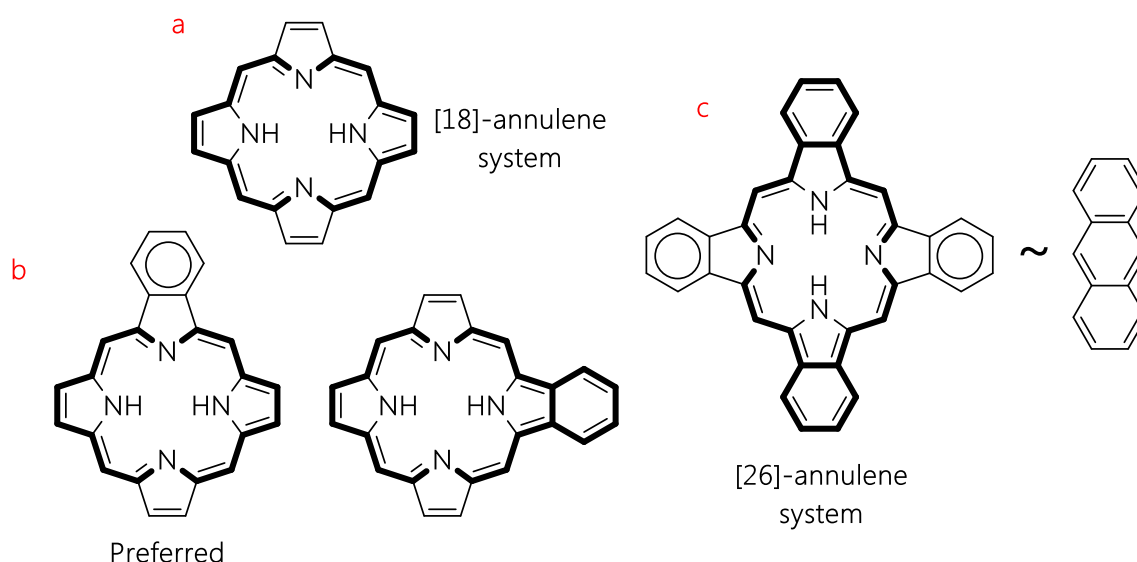


Figure 2.2 a) Representation of the [18]-annulene system permeating the porphyrin ring. b) Localization of aromaticity in monoannulated porphyrin according to Clar's theory. c) [26]-annulene TBP system and analogy to linear acene.

annulenes traversing a robust framework of aromatic five-membered rings (Figure 2.2a). Clar's theory of localized sextets⁸ states that polycyclic systems tend to localize aromaticity in smaller subsystems. Monoannulation (Figure 2.2b) will likely make monobenzoporphyrin (MBP) behave as a true benzene sextet isolated from [18]-annulene. Extending this idea to four annealed benzo rings (divided into the two inequivalent sets), [26]-annulene TBP could be viewed as a simple linear acene⁹ (Figure 2.2c). Indeed, "dilution of aromaticity"¹⁰ encountered within linear acenes manifests also itself within TBP. The porphyrinic character

of the system maintained in part by the peripheral sextets by helping shift electron density onto benzene rings which act as weak π -electron withdrawing substituents. This would decrease basicity of nitrogen atoms and concomitantly increase π -acidity of the TBP ligand.¹² An interesting corollary to the progressively weakening aromaticity in porphyrins (upon successive linear annulation) is to the extent to which TNP and TAP are prone to degradation via endoperoxide formation. Interestingly, the same mechanism of endoperoxide formation is currently being exploited to develop very sensitive O₂ molecular probes.¹⁵⁻¹⁷ Q-band enhancement epitomized in metalloporphyrins is one of the most meaningful and unique consequences of linear annelation. This effect is particularly prominent in the PhMe spectrum of PtPh₄TBP (Figure 2.3). In some cases, Q-bands surpass Soret bands in intensity and reach well into the NIR region.¹⁵ It should be noted however, that Soret bands experience a far weaker disturbance with progressive annelation increasing the Soret/Q-band gap. Macrocycle distortion (*i.e.* ruffling, saddling) in non-extended porphyrins hinders photophysical properties, namely inducing a large reduction in PLQY.^{18,19} This distortion of the core is a result of two competing¹¹ forces: (a) the drive to planarize the macrocycle to regain aromatic stability and (b) relief of steric congestion between *meso*-rings and β,β' -substituents on the pyrrole. The annulated benzo rings do indeed contribute to steric congestion in TBP, yet it is generally found that distortion does

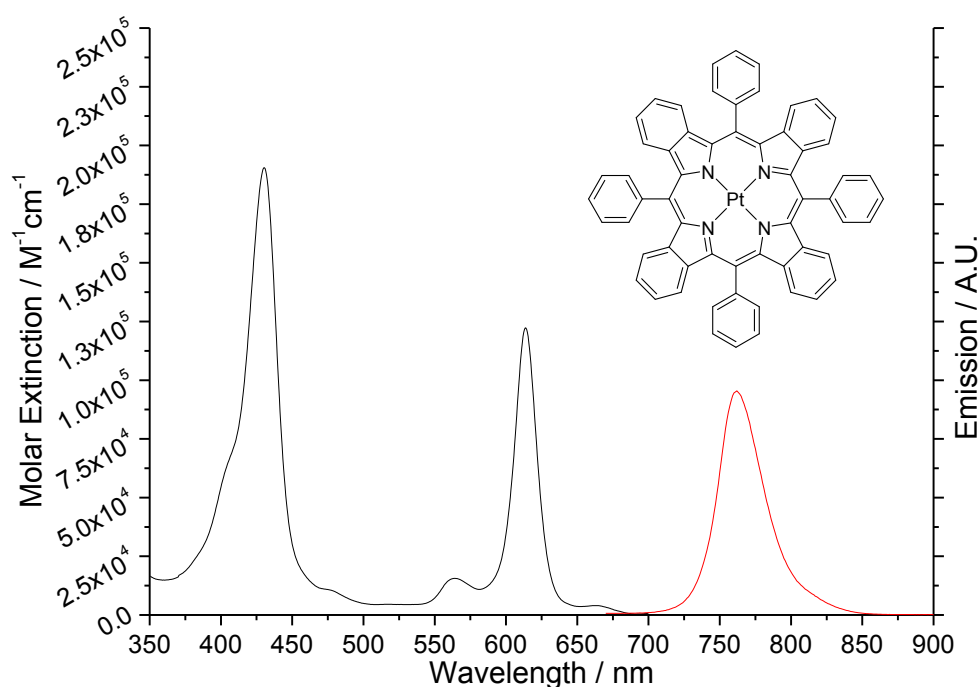


Figure 2.3 Absorption (black line)/emission (red line) spectra of PtPh₄TBP in PhMe.

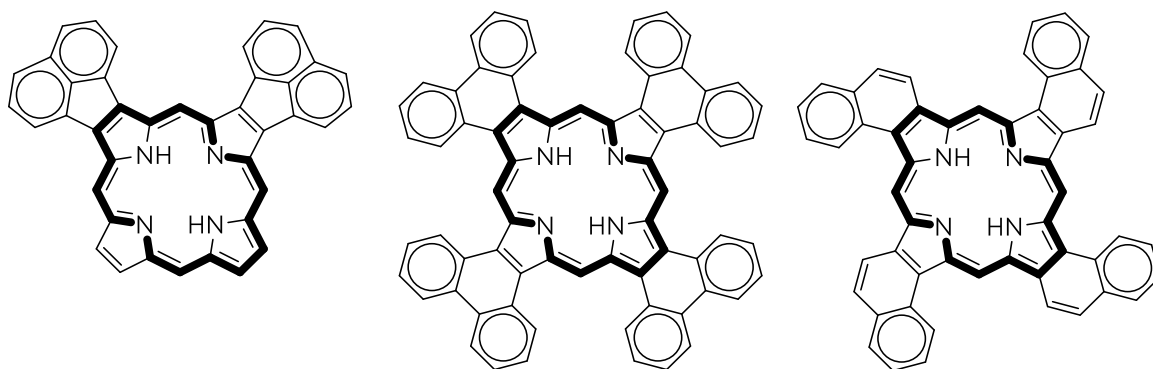


Figure 2.4 Examples of angularly annulated systems. Left to right: acenaphthoporphyrin, tetraphenanthro[9,10]porphyrin and tetranaphtho[1,2]-porphyrin.

not significantly ruin emissivity. In fact, as the number of annulated rings increases (i.e. TNPs, TAPs) the detrimental effect that distortion exerts loses severity.²⁰ In the context of π -extended porphyrins (as is the case for regular porphyrins), macrocycles bearing substituents at the 5,10,15,20-positions are more synthetically accessible due to improved solubility and ease of handle. Indeed, owing to relatively easier access,²¹ TBPs and their spectroscopic properties have been studied substantially more than any other extended porphyrin. While the linear system TBP is the sole focus of this chapter, angularly-annulated systems (Figure 2.4) deserve short mention. Since the synthesis of these systems does not involve unstable isoindoles, most materials had been explored long before the increasing interest in linear systems. Sub-localization of aromaticity in such systems (Clar's localized sextets) is always expected and they are therefore considered to be more aromatic and more stable than their linearly annulated counterparts. Unlike TBPs however, they do not form an extended π -electron system despite bearing highly conjugated subsystems, which largely restricts their optical properties to the visible region like regular porphyrins.²³⁻²⁵

2.1.1 Applications

Applications for porphyrins are as numerous and diverse as their published structures. In that sense, TBPs readily lend themselves to any application for which regular porphyrins are suitable for. For a detailed survey, the reader is referred back to subsection 1.6.3. However, their unique optoelectronic properties allow them to bridge the gap in areas where regular porphyrins would otherwise prove inadequate. For example, efficient NIR emission with extremely low self-absorption demonstrated by PtPh₄TBP was the key enabling a breakthrough in performance for luminescent light concentrators. Pt(II) and Pd(II)

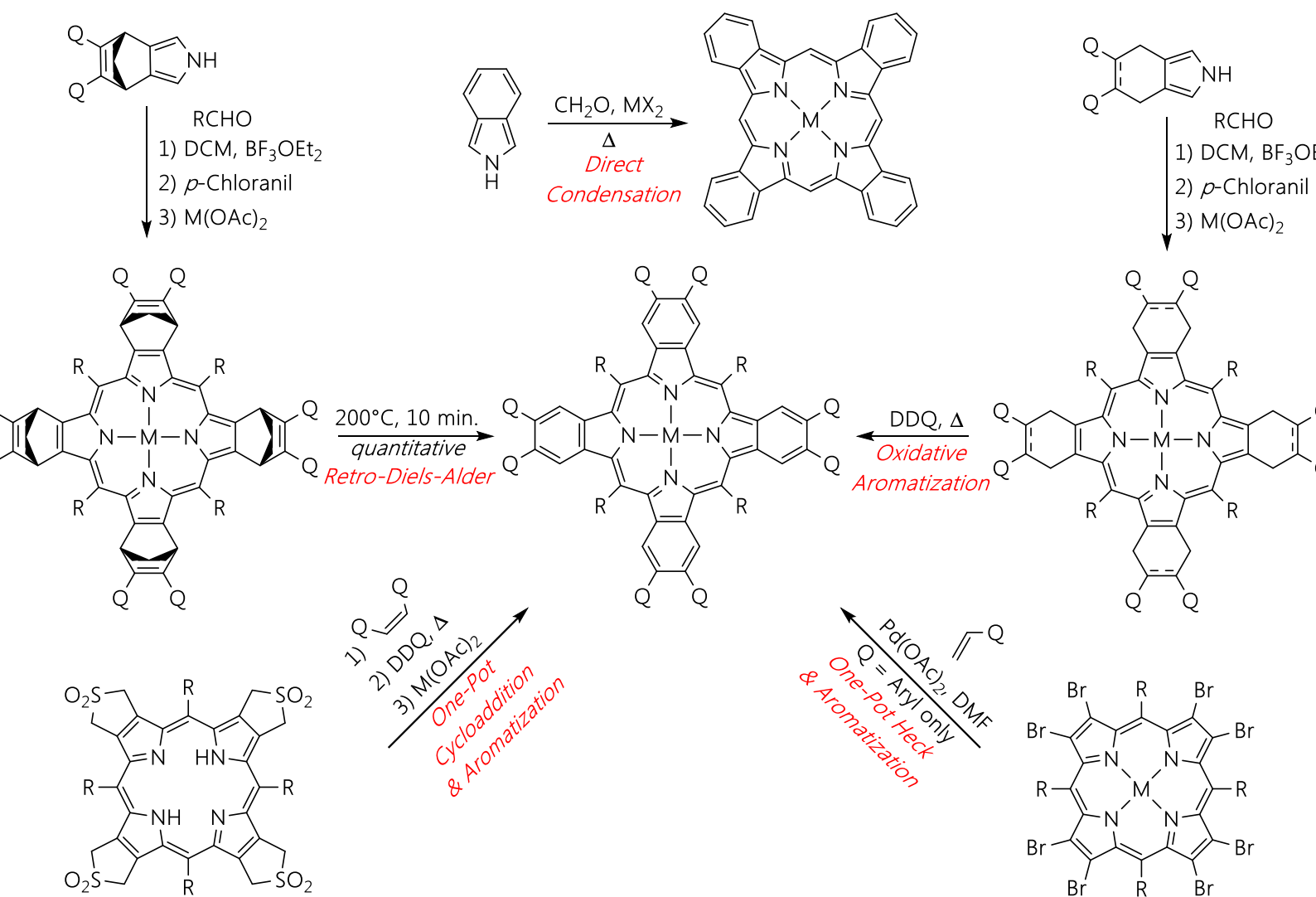
complexes of TBP are widely considered to be the most useful NIR phosphors as they find application in light harvesting/emitting arrays, biometrics and have come into their own as quintessential photosensitizers in TTA photon-upconversion.

2.1.2 Synthetic Methodology

Since their earliest synthesis in 1938 by direct condensation of isoindoles, newer higher-yielding and cleaner synthetic approaches have been developed: retro-Diels-Alder, one-pot Heck/aromatization, one-pot cycloaddition/aromatization and oxidative aromatization. Of particular importance are the last two methods, variations of which are still currently being used in TBP synthesis. Each of these methods as outlined (Scheme 2.1) and discussed below, with a focus on Ar₄TBPs.

A brute force direct-condensation approach yielded trace amounts of TBP, complex and nearly inseparable side-products obscured the intended product. Additionally, low functional group tolerance and vanishingly small solubility of the resulting macrocycles made purification tedious. Ono and co-workers introduced the concept of using a “masked” isoindole synthon^{41,42,41,42,41,42} during assembly of the porphyrin macrocycle. This allowed them to overcome the inherent instability of the unsubstituted isoindole heterocycle. The resulting porphyrin and its metal complexes could be easily handled and dissolved in common organic solvents, overcoming previous challenges related to solubility. Heating the porphyrin at 200 °C extrudes ethylene gas in a Retro-Diels-Alder type reaction resulting in quantitative conversion to tetrabenzoporphyrin. While an elegant improvement over the direct condensation of isoindole, availability of starting materials, reliance on hazardous compounds for synthesis of the pyrrole precursor and limited opportunity for functionalization left room for improvement.

The oxidative aromatization pathway, primarily carved out by Vinogradov and co-workers^{21,43,44} introduced a greater degree of freedom in terms of compatible substituents while starting from inexpensive, readily available materials. This method, much like Ono's, relies on an isoindole precursor, namely 4,5,6,7-tetrahydroisoindole which is ultimately aromatized by prolonged heating with DDQ. While this was once again an improvement over the previous method, yields of the final porphyrins suffered from harsh aromatization conditions. Synthesis from partially aromatized 4,7-dihydroisoindole was proposed by Cheprakov as a workaround for low yields, since aromatization could now be driven to



2.1 Summary of most commonly used synthetic methodologies in TBP synthesis.

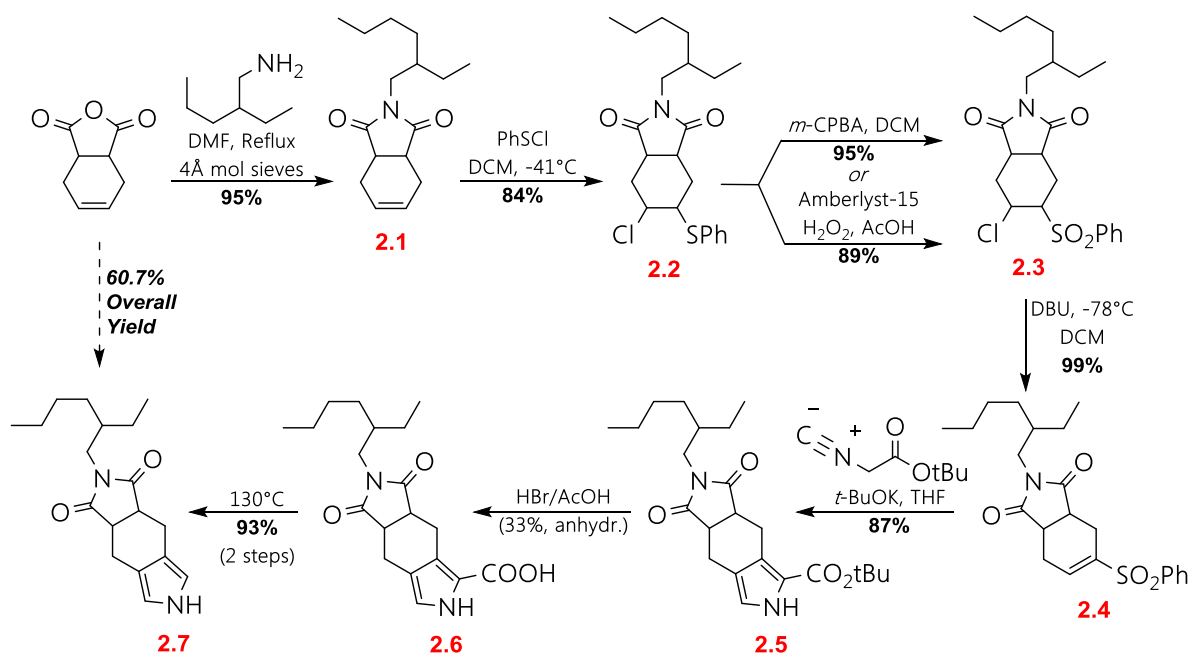
completion at much lower temperatures. The oxidative aromatization method is still used to this day and accounts for a significant majority of all TBP, TNP and TAP complexes synthesized. Dienophiles react readily with sulfolenopyrrole once the latter undergoes thermal extrusion of SO₂.⁴⁶ A convenient way to access sulfolenopyrroles is via Barton-Zard chemistry,^{47,48} alternatively via classical pyrrole synthesis starting from 3,4-dimethylsulfolene.⁴⁹ This method represents an attractive way to generate multiple derivatives using the same precursor, if low solubility of the tetra-sulfolene porphyrin derivatives can be overcome. In a recent development, β-octabromoporphyrin was reacted with 4-vinylpyridine in a concerted Heck reaction to generate Ar₄TBP in one-step. Although not as widely applied as the Retro-Diels-Alder or the oxidative aromatization method, it is growing in popularity despite limitation in substituent choice. This section outlined the most relevant synthetic pathways to TBPs, it is by no means exhaustive. Literature TBP syntheses use methods presented here (or iterations thereof). It should be noted that all chemistry presented in section 1.6 is equally applicable to π-extended porphyrins discussed in this chapter. If required, the reader is referred to more comprehensive reviews^{3,52,53} dealing with the topic.

2.2 Synthesis of *meso*-Aryl Tetrabenzoporphyrins

2.2.1 Synthesis of 4,5,6,7-Tetrahydroisoindole Precursor

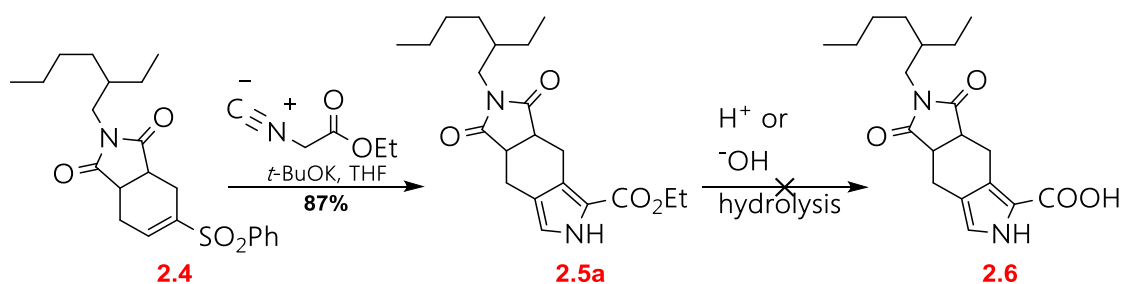
Assembly of the pyrrole ring in the 4,5,6,7-tetrahydroisoindole precursor was achieved through a modified Barton-Zard condensation reaction.¹ Subsequent de-esterification/decarboxylation of the pyrrole afforded the unsubstituted 4,5,6,7-tetrahydroisoindole precursor (Scheme 2.2).

Condensation of two inexpensive and widely available compounds *cis*-1,2,3,6-tetrahydrophthalic anhydride and 2-ethylhexylamine in dimethylformamide resulted in nearly quantitative conversion into imide **2.1** on a 300 g scale. PhSH was treated with NCS to generate phenylsulfinyl chloride *in-situ* for the chlorosulfanylation of **2.1** to yield phenylsulfane **2.2**. Expedient oxidation of sulfanes to sulfones is typically accomplished with *m*-CPBA. However, this material is a health/safety hazard and the desire for a cost-effective oxidation of **2.2** led to H₂O₂/AcOH as an alternate peroxycarboxylic acid source. When catalysed with Amberlyst-15, it provides a high yielding and greener alternative to halogenated solvents and expensive halogenated peroxycarboxylic acids (i.e. *m*-CPBA). Both

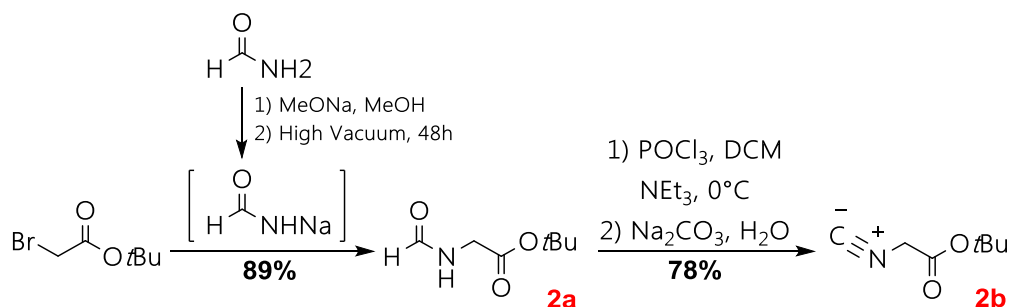


Scheme 2.2 Large scale synthesis of 4,5,6,7-tetrahydroisindole precursor **2.7**.

methods were tested and $\text{H}_2\text{O}_2/\text{AcOH}$ proved to be an acceptable substitute to generate sulfone **2.3**; while oxidation with *m*-CPBA provides a marginally greater yield and faster workup on a smaller scale, *m*-CPBA precipitate was found to hinder stirring at lower temperatures and complicate workups. Peroxyacetic acid/Amberlyst-15 was found to be more appropriate for such preparative work. Rapid DBU-promoted dehydrochlorination at -78°C afforded sulfonylcyclohexene **2.4** in quantitative yield. It should be noted that treatment of **2.3** with DBU at room temperature or even -40°C results in a complex mixture of several closely-eluting products. Similar results are obtained if DBU is added in a slow, dropwise fashion at -78°C . It is possible that competitive proton abstraction reactions are occurring when DBU is added above cryogenic temperatures. It was found that rapid addition (within fifteen seconds) was key in obtaining sufficiently pure quantities of **2.4**. Initial synthetic efforts to assemble the pyrrole ring were focused on Barton-Zard condensation of **2.4** (Scheme 2.3) with the commercially available ethyl isocyanoacetate. However, it was unexpectedly found that ethyl 4,5,6,7-tetrahydroisindole-2-carboxylate **2.5a** did not undergo clean de-esterification without concomitant hydrolysis of the imide moiety. *tert*-Butyl pyrrole 2-carboxylates have long been known to undergo facile decarboxylation in neat TFA. Unlike its ethyl counterpart, *tert*-butyl isocyanoacetate **2b** is not readily commercially available. It was reproducibly synthesized⁵⁴ (Scheme 2.4) on a 250 g scale starting from *tert*-butyl bromoacetate and formamide. Barton-Zard



Scheme 2.3 Barton-Zard condensation of **2.4** with ethyl isocyanoacetate.

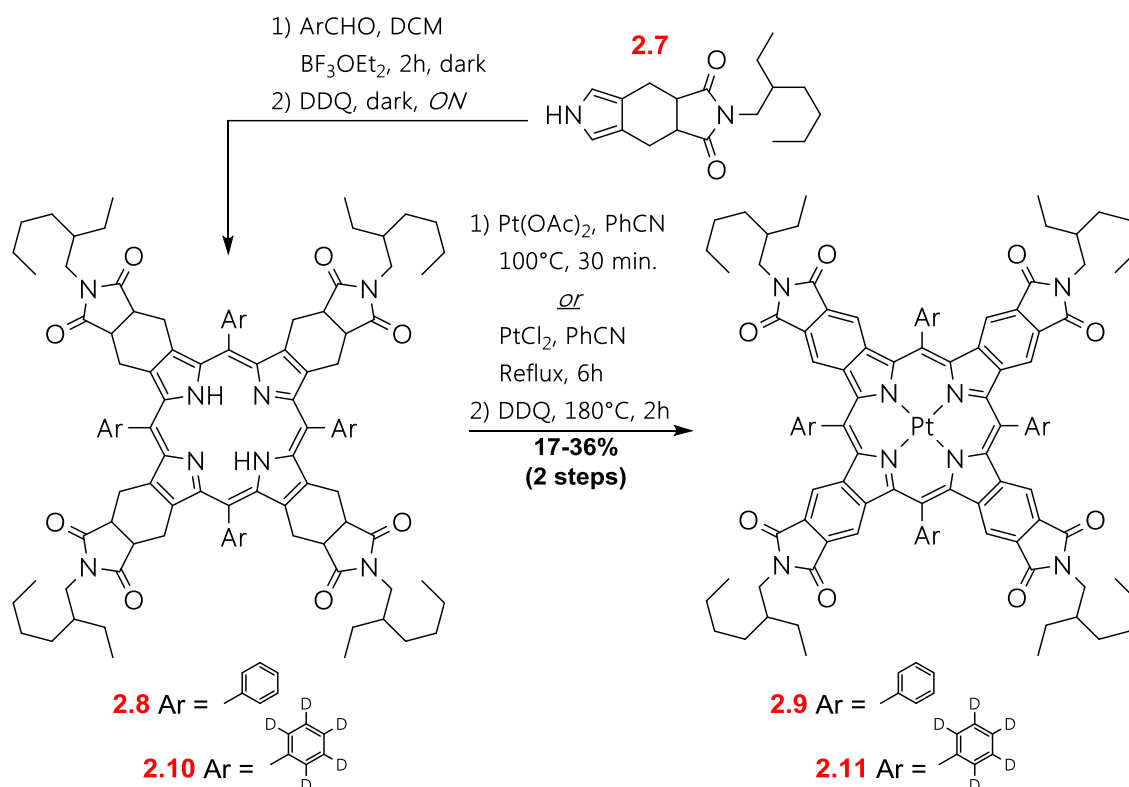


Scheme 2.4 Synthesis of tert-butyl isocyanoacetate **2b**.

condensation of **2.4** with *tert*-butyl isocyanoacetate afforded the *tert*-butyl 4,5,6,7-tetrahydroisoindole-2-carboxylate **2.5** in high yields (86%) as an amorphous solid. **2.5** can be prepared in >100 g batches in 65% overall yield from *cis*-1,2,3,6-tetrahydrophthalic anhydride and is a convenient stable intermediate in the synthesis. Treatment of **2.5** with 33% HBr in AcOH resulted in de-esterification and partial decarboxylation; ^1H NMR of the crude mixture revealed a 9:1 of **2.6** and **2.7**, respectively. Heating this mixture between 130-150 °C for 1h completed the decarboxylation and afforded 4,5,6,7-tetrahydroisoindole **2.7** in good yield (93%). It should be noted that decarboxylation was also attempted with TFA, but failed to yield **2.7** in significant yield. It was found that the white, fluffy crystalline form of **2.7** (obtained by recrystallization from Et₂O/pentane) displays benchtop stability for over days in contact with air/light and may be stored for months under N₂ at -20 °C. This is in contrast to significant instability encountered with unsubstituted 4,5,6,7-tetrahydroisoindole, which begins to darken upon exposure to light and air.

2.2.2 Synthesis of Pt(II)Ar₄TBIPs

Oxidative condensation of 4,5,6,7-tetrahydroisoindole **2.7** with the appropriate aromatic aldehyde (PhCHO, C₆D₅CDO and C₆F₅CHO) under modified Lindsey conditions⁵⁵ afforded their respective hexadecahydro- precursors H₂Ar₄TCIP **2.8**, **2.10** (Scheme 2.5).



Scheme 2.5 Synthesis of Pt(II)Ar₄TBIP derivatives via oxidative aromatization method under Lindsey conditions.

Due to overly complicated NMR spectra caused by stereogenic centers, non-planarity of the macrocycle and the diastereomeric nature of the 4,5,6,7-tetrahydroisoindole precursor, H₂Ar₄TCIPs were partially purified without extensive characterization (only UV-Vis and HRMS). Typically, this is accomplished by either short-path column chromatography with NEt₃ as a co-eluent and/or slow crystallization of the bis(hydrochloride)/bis(trifluoroacetate) porphyrinium salts. Depending on the basicity of the H₂TCIP ligand, Pt insertion was accomplished with PtCl₂ in refluxing PhCN and Pt(OAc)₂ in warm PhCN was used for difficult cases or where scarcity of the starting material made yield a top priority. Aromatization with excess DDQ in boiling 1,2,4-TCB afforded the intended Pt(II)Ar₄TBIP (Ar = Ph and Ph-d₅) dyes. In certain cases, metalation of the macrocycle and aromatization was achieved as a one-pot reaction. For example, PtPh₄TBIP **2.9** was prepared on a multigram scale one-pot reaction in 36% yield (22% overall yield from inexpensive *cis*-1,2,3,6-tetrahydrophthalic anhydride starting material). It should be noted that due to excellent solubility of the pyrrole building block, laborious chromatographic purification of otherwise insoluble π -extended porphyrins is simplified. Often, exploitation of crystallization differences between porphyrins and oligomeric side-products removes the

need for chromatographic separation. However, crude purification and isolation of PtAr₄TBIPs **2.9** and **2.11** via crystallization is no longer viable when both product and impurities are functionalized extensively with aliphatic side-chains. As a result, PtAr₄TBIPs will crystallize out of fractions more effectively if first purified with column chromatography.

2.3 Solubility and Stability Studies

There is a discernible lack of solubility values for TBP dyes in the literature, either due to insufficient quantities of material prepared or excessive insolubility/aggregation of the dyes which prevents accurate determination of extinction coefficients and solution saturation points. The large scale synthesis of PtPh₄TBIP provided an opportunity to probe spectroscopic and solubility parameters in multiple solvents, shown in Table 2.1. A key focus in the design of the PtPh₄TBIP molecule was improving its solubility over the parent PtPh₄TBP, which was thought could to be accomplished with peripheral aliphatic moieties. Indeed, a polarizable aromatic core and aliphatic chains make PtPh₄TBIP most soluble in medium polarity solvents. The achieved exceptionally high solubility, up to 600 g/L in PhMe, can be attributed to the four branched 2-EH chains with stereogenic centers and reduced macrocyclic planarity via *meso*-Ph substituents. It is interesting that although dichloromethane is generally considered to be a better solvent for porphyrin dyes, PhMe is more effective in preventing PtPh₄TBIP from forming aggregates. Photodegradation⁵⁶ of organic/organometallic dyes is the major drawback to their application, particularly in harvesting solar energy. We hypothesized that the fused electron-withdrawing imide

Table 2.1 Solution Saturation Points of PtPh₄TBIP In Organic Solvents at Room Temperature with Corresponding Absorption Maxima

Solvent	$E_T(30)$	Solubility		λ_{max}/nm ($\log(\epsilon)$)	
		g/L	mol/L	Soret	Q-band
methanol	55.4	0.12	7.0×10^{-5}	462 (5.11)	633 (4.89)
CH ₃ CN	45.6	0.65	3.8×10^{-4}	461 (5.26)	631 (5.02)
dichloromethane	40.7	400	0.23	464 (5.39)	634 (5.20)
tetrahydrofuran	37.4	510	0.30	461 (5.35)	631 (5.14)
PhMe	33.9	600	0.35	463 (5.37)	633 (5.19)
Hexanes	31	2.2	1.3×10^3	457 (5.36)	628 (5.23)

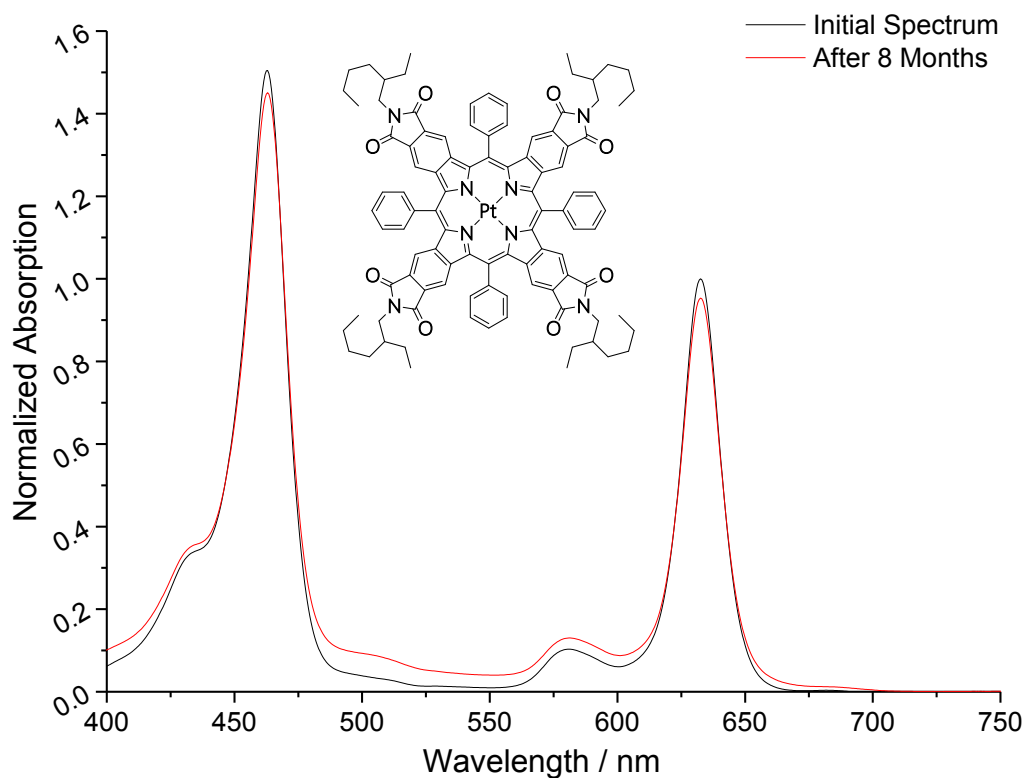


Figure 2.5 Long-term stability study of PtPh₄TBIP (spectrum in dichloromethane).

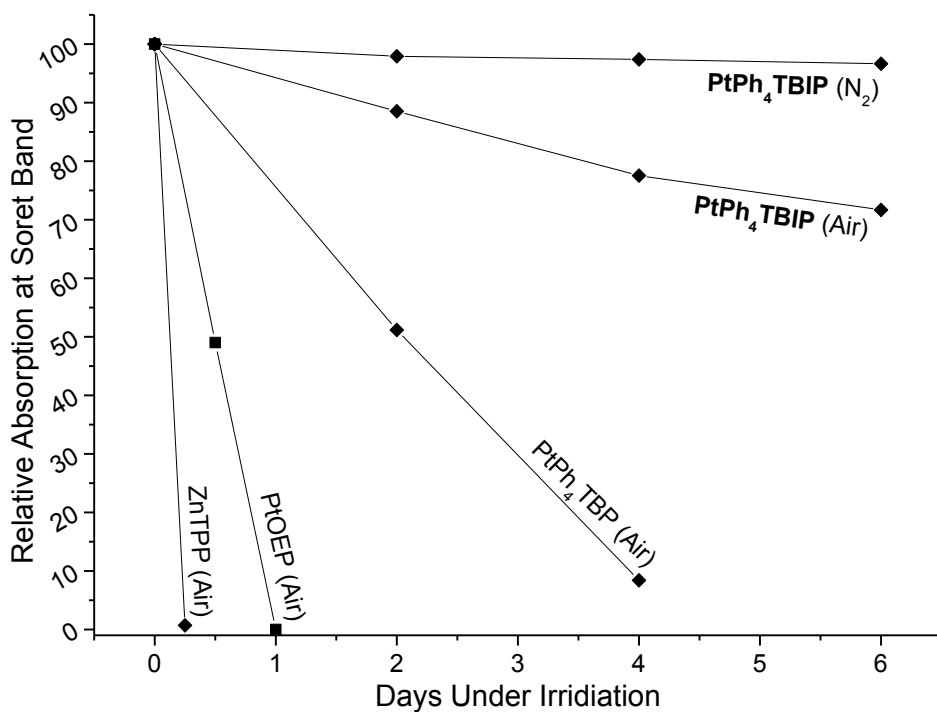


Figure 2.6 Accelerated photodegradation of representative porphyrins followed through decrease of Soret band intensity (500 W halogen lamp, 90 °C, PhMe, 10⁻⁵ M).

substituents at the periphery of the Ph₄TBP macrocycle would suppress the photo-oxidation by lowering the HOMO level of the molecule. Indeed, virtually no degradation was observed under ambient light for over 8 months, and either the solid-state or in PhMe solution (Figure 2.4). To assess the limits of photostability for PtPh₄TBIP, an accelerated photodegradation study (Figure 2.5) was carried out by illuminating its PhMe with a 500 W halogen/tungsten lamp at ~90 °C (radiative heating). Almost⁵⁷ no degradation was observed when PtPh₄TBIP was subjected to these conditions under a N₂ atmosphere. Even in an air-saturated solution <30% degradation was observed after 6 days of continuous irradiation. The parent PtPh₄TBP showed a ~5 times faster degradation profile under identical conditions, while other common porphyrin dyes, PtOEP and ZnPh₄P, showed ~20 and ~80 times faster degradation, respectively. The mechanism of the observed photooxidation is based on sensitized generation of singlet oxygen, and the observed stability of PtPh₄TBIP under these conditions is remarkable. In fact, the above photodegradation experiment with PtPh₄TBIP generates > 200 times as much solvent decomposition products compared to the loading of the dye (benzylic alcohol, benzaldehyde, benzoic acid, and uncharacterized oligomers).

2.4 Crystal Structures

Remarkably, although PtPh₄TBIP should exist as a statistical mixture of six stereoisomers, slow evaporation of its solution in a PhH/methanol/CHCl₃ mixture produced

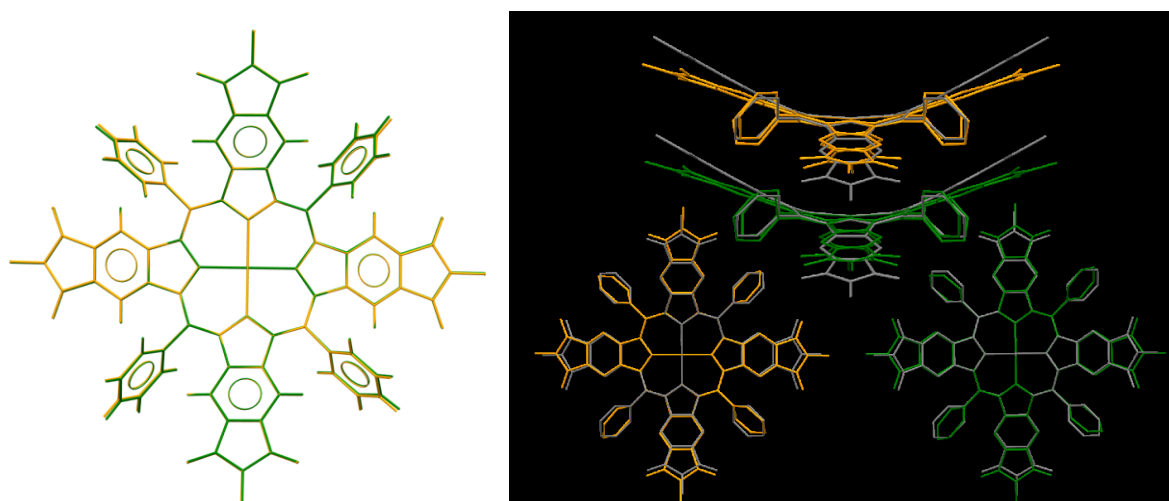


Figure 2.7 (Left) Skeletal overlay of X-ray structures for PtPh₄TBIP (orange) and its deuterated analogue **2.11** (green), 2-EH aliphatic chains committed for clarity. (Right) X-ray skeletal structures overlaid with their respective predicted geometries (B3LYP/6-31G*) in grey.

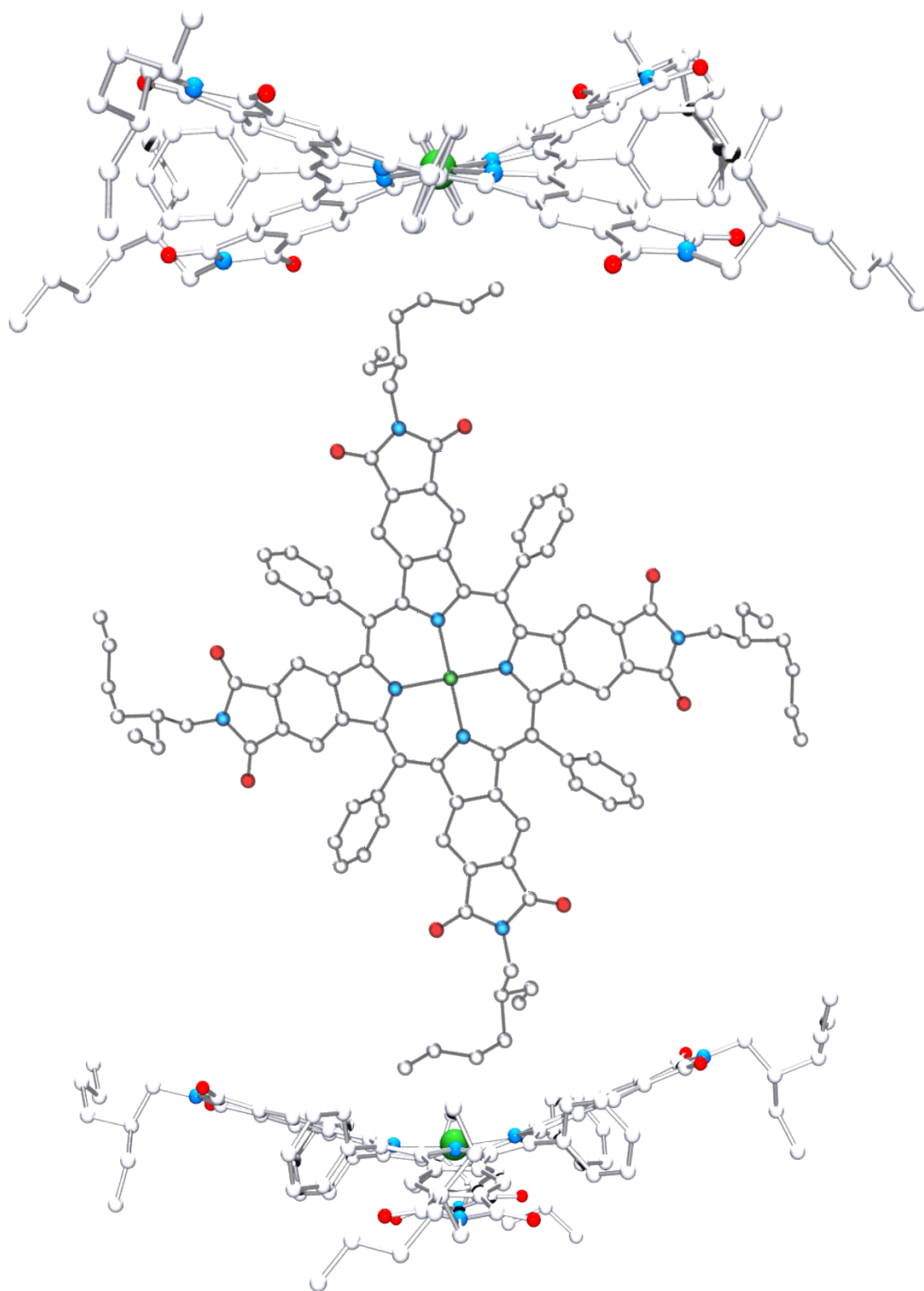


Figure 2.6 (Top) Axial view through C_m -Pt- C_m (C_m = meso-carbon) (Middle) X-ray structure of (*R,S,R,S*)- PtPh₄TBIP. (Bottom) Axial view through N-Pt-N, displaying the prominent saddle shape of the macrocycle.

on a single crystal (Figure 2.6) of the pure (*R,S,R,S*)-**2.9**. Its X-ray analysis revealed a saddle-shape conformation, typical⁵⁸ for related TPTBPs. Normal-coordinate structural decomposition (NSD) analysis⁵⁹ revealed PtPh₄TBIP to have a relatively low out-of-plane distortion ($D_{oop} = 2.27 \text{ \AA}$ compared to 2.83 \AA for PtPh₄TBP)²⁸ almost completely described by the B_{2u} mode (2.24 \AA) associated with saddling. This could be a result of the depleted electron density on CH bonds of the isoindole moiety reducing repulsion with *meso*-Ph rings. Despite being grown under identical conditions, PtPh₄TBIP-*d*₂₀ **2.11** (D_{2d} point group), X-ray analysis failed to show any significant differences in macrocyclic distortion or orientation of Ph rings. Aside from slight orthogonal bending of the Ph rings (Figure 2.7, left), the crystal structures are essentially superimposable.

NSD analysis of X-ray structures revealed a significantly smaller mean displacement D_{oop} for **2.9/2.11** (2.27 \AA) compared to PtPh₄TBP (2.83 \AA). Since *oop* distortion stems from the Ph ring/sp² CH interaction, this difference can be explained by the depleted electron density of benzo CH bonds alleviating steric clashing. It is noteworthy that D_{oop} is completely insensitive to isotopic substitution of Ph rings⁶⁰ in **2.9/2.11**, disproving the presence or involvement of peri-type interactions in the observed RTP-QY enhancement. Hypsochromic spectral shifting and increased PLQY from PtPh₄TBP (773 nm , $\Phi_P = 0.35$) to PtPh₄TBIP **2.9** (755 nm , $\Phi_P = 0.45$) can be rationalized in terms of reduced D_{oop} . Lessened HOMO destabilization in **2.9** brings the geometry closer to the planar TBP configuration characterized by higher PLQY, longer T₁ lifetimes and blue-shifted spectra.^{58,61}

2.5 Electronic and Photophysical Properties

As is the case for other π -extended porphyrin derivatives, PtPh₄TBIP **2.9** is an exceptionally strong absorber in the blue ($\lambda_{max} = 465 \text{ nm}$, $\log(\epsilon) = 5.39$, Soret band) and red ($\lambda_{max} = 633 \text{ nm}$, $\log(\epsilon) = 5.20$, Q-band) regions of the spectrum (Table 2.2). Compared to PtPh₄TBP, the Soret and Q-band are bathochromically shifted by 35 nm and 21 nm , respectively. However, emission is hypsochromically shifted by 25 nm , indicative a lowered HOMO level. Exciting at either Soret or Q-band leads to NIR phosphorescence ($\lambda_{max} = 755 \text{ nm}$). A PLQY of 0.45 was obtained for PtPh₄TBIP **2.9** using PtPh₄TBP as a reference standard ($\Phi_P = 0.35$) measured at room temperature in argon-degassed PhMe (Figure 2.8). Interestingly, ${}^3\tau_{em}$ for **2.9** ($14 \mu\text{s}$) in argon-saturated PhMe is considerably shorter, to our knowledge, than any known Pt porphyrin including the parent PtPh₄TBP ($29.9 \mu\text{s}$). This corresponds to a ~ 3 times faster radiative transition in the former ($k_r = 3.2 \times 10^4 \text{ s}^{-1}$ and

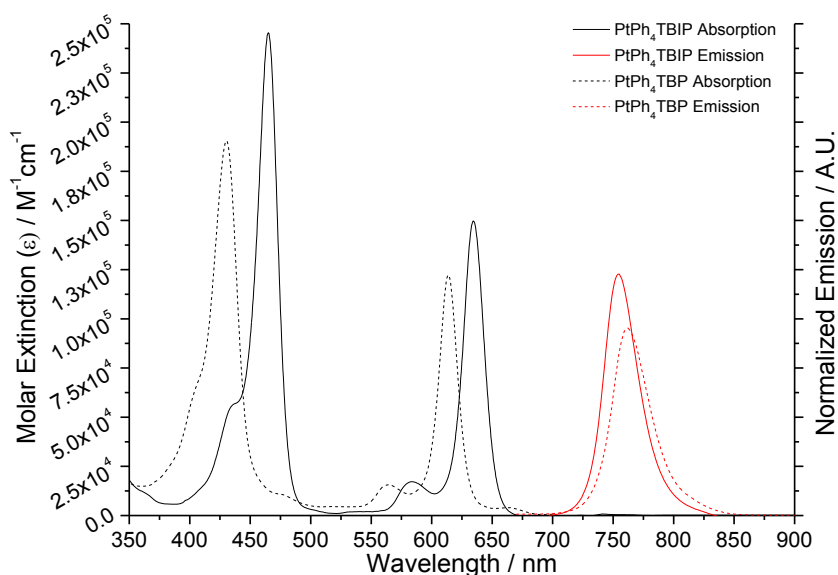
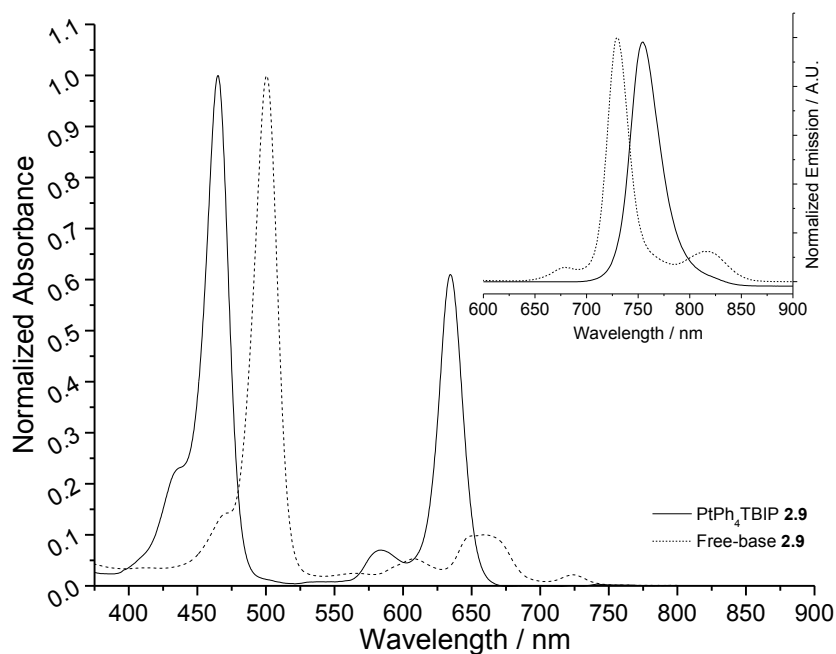


Figure 2.8 (Top) Overlay of normalized absorption spectra of **2.9** in dichloromethane and its free-base form $\text{H}_2\text{Ph}_4\text{TBIP}$. The inset shows the overlay of normalized emission spectra for both compounds. (Bottom) Overlay of absorption and emission spectra for PtPh_4TBP and **2.9** in de-gassed PhMe at 298K.

$1.2 \times 10^4 \text{ s}^{-1}$ for **2.9** and PtPh_4TBP , respectively), which minimizes quenching and photodegradation processes. The freebase form of **2.9** ($\text{H}_2\text{Ph}_4\text{TBIP}$), which was chromatographically recovered as a side-product in the synthesis of **2.9**, displays an intense Soret band but opposing transition dipoles of the contributing transitions result in weak and

fragmented Q-bands, which coalesce upon Pt insertion (Figure 2.8). Although the freebase shows fluorescence beyond 700 nm, it is quite weak ($\Phi_F < 3\%$).

2.5.1 Effect of Deuteration

Initial photophysical studies (Table 2.2) have revealed the deuterated isotopomer PtPh₄TBIP-*d*₂₀ **2.11** to have a slightly longer-lived triplet state lifetime ($\tau_{em} \sim 16 \mu s$) and an unusually high PLQY (an up to $\sim 50\%$ increase over **2.9**) which prompted further investigation. Particularly, there was an interest in ascertaining reproducibility of this effect in the well-studied isoskeletal PtPh₄TBP⁵. Given that this apparent effect was seldom seen in organic dyes and not well understood at the time, scientific literature was scoured for published examples of similar effects in an effort to explain why such an increase in PLQY was observed. It should be noted that photophysical properties (PLQY, τ_{em}) for these phosphorescent dyes are highly sensitive to residual oxygen, which affects reproducibility of measurements. In fact, this property is what makes these dyes such good O₂ probes.

2.5.1.1 Literature precedents

The fundamental hurdle in uncovering the full potential of any NIR-emissive material lies in suppression of non-radiative decay (k_{nr}) rates. By virtue of their narrow HOMO-LUMO gap, NIR dyes prove to be consistently weaker emitters compared to their UV-Vis counterparts. This relationship is expressed by a basic statement⁶³⁻⁶⁵ of the Energy Gap law (eq. 5, Chapter 1). Theoretical and spectroscopic study of these underlying photophysical processes helped established general strategies to be applied towards preserving and improving PLQY in NIR materials. These include increasing chromophore rigidity and planarity, reducing self-aggregation via steric substitution as well as removing intrinsic contributors⁶⁷ to k_{nr} through isotopic substitution and fluorination.^{68,69} The latter has proven itself a powerful tool for PLQY enhancement, a result particularly well documented⁷⁰ for Ln complexes. However, fluorine's electronegative nature effects significant change in dipole/ k_r , often leading to unexpected photophysical modification. Notably, *p*-fluorination of *meso*-Ph rings in PtPh₄TBP resulted in $\sim 20\%$ relative PLQY enhancement while further fluorination drastically reduces PLQY and lifetime.⁷¹ Conversely, isotopic substitution (*i.e.* deuteration) does not modulate electronic properties and remains the sole viable option for tuning photophysics while preserving molecular geometry and spectral characteristics.

Table 2.2 Initial Photophysical Data with Calculated Rate Constants for Pt(II)Ph₄TBPs and their Deuterated Analogues in PhMe at 298K

Compound	λ_{\max} / nm (log ϵ_{\max} / E ⁻¹ cm ⁻¹) ^a	λ_{em} nm ^b	$\Phi_{\text{p}}^{b, c}$ (τ_{em} / μs^b)	Rel. Enh.	$k_{\text{r}} / 10^4 \text{ s}^{-1}$ ^d	$k_{\text{nr}} / 10^4 \text{ s}^{-1}$ ^e
PtPh ₄ TBP	430 (5.28), 612 (5.13)	770	0.35 ± 0.05 (29.5)	1.00	1.2 ± 0.17	2.2 ± 0.17
PtPh ₄ TBP- <i>d</i> ₂₀ (2.14)	430 (5.29), 612 (5.14)	770	0.35 ± 0.05 (29.6)	1.00 ± 0.03	1.2 ± 0.17	2.2 ± 0.17
PtPh ₄ TBIP (2.9)	465 (5.39), 633 (5.20)	755	0.45 ± 0.07 (14.0)	1.00	3.2 ± 0.50	3.9 ± 0.50
PtPh ₄ TBIP- <i>d</i> ₂₀ (2.11)	465 (5.39), 633 (5.20)	755	0.65 ± 0.09 (16.3)	1.44 ± 0.01	4.0 ± 0.55	2.1 ± 0.55

^a Absorbance data in PhMe solution for Soret/Q-band, respectively. ^b Measured in deoxygenated spectroscopy-grade PhMe. ^c PtPh₄TBIP measured against PtPh₄TBP ($\Phi_{\text{p}} = 0.35 \pm 0.05$ in PhMe). ^d Calculated as $k_{\text{r}} = \Phi_{\text{p}}k$. ^e Calculated as $k_{\text{nr}} = k - k_{\text{r}}$.

A longstanding strategy in systems prone to excited state deactivation⁷² through vibronic coupling to X-H oscillators (i.e. lanthanides) is to minimize k_{nr} by perdeuteration/fluorination⁷³ of ligands. “Promoter” modes induce significant nuclear displacement to access geometries facilitating conical intersections for non-radiative T₁/S₁ → S₀ surface crossings.⁷⁴ Low-energy (< 800 cm⁻¹) aromatic C=C and C-H distortion modes (i.e. C=C twisting, C-H out-of-plane bending) have been identified as some of the most efficient promoters of non-radiative decay.⁷⁵ Comparable low-energy modes were shown to account for the majority (>50%) of reorganizational energy in model aromatic systems. Non-radiative decay is commonly ascribed to high-frequency vibrations (i.e. C-H stretching); however, these “acceptor” modes show minimal nuclear displacement and serve almost exclusively as inert energy sinks for vibronic quanta. Non-radiative decay of triplet states in Pt(II) monomers and polymers has been shown⁷⁶ to quantitatively follow the energy gap law. Nevertheless, deuteration of a Pt(II) phenylene ethynylene derivative failed⁷⁷ to improve lifetime ($\tau_{\text{em}} = 140 \mu\text{s}$) or emission efficiencies. An enhancement⁷⁸ ($\Phi_{\text{p}} = 6.2 \pm 0.5\%$ from $3.0 \pm 0.3\%$) was reported for blue RTP in a purely aromatic molecule upon deuteration. This

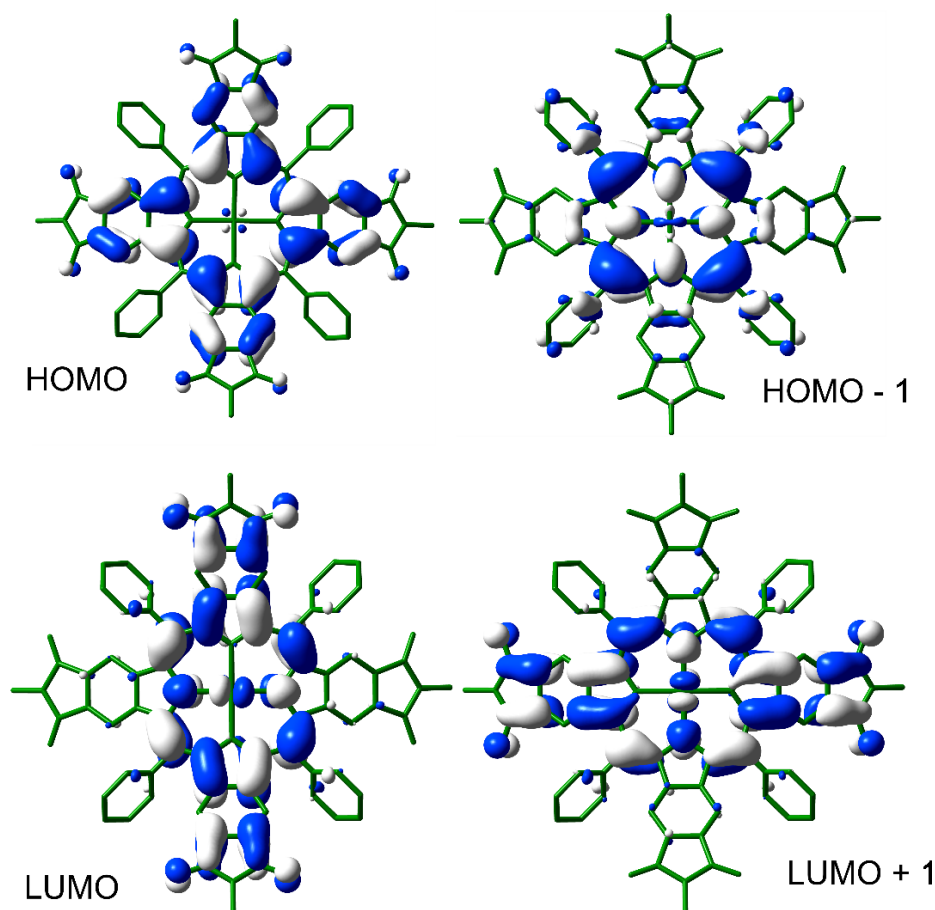


Figure 2.9 Calculated orbital coefficients for **2.9** at the B3LYP/Def2SVPP level.

was attributed to an increase in $k_{\text{ISC}}(S_1 \rightarrow T_1)$ rather than reduced k_{nr} . Fluorescence yields or lifetimes of the ^2H isotopomer were left unchanged ($\Phi_{\text{F}} = 47 \pm 4\%$, $\tau_{\text{em}} = 1.7 \pm 0.1$ ns). Similarly, perylene- d_{12} displayed a 45% increase in relative triplet-triplet annihilation upconversion efficiency (PtPh₄TBP acting as triplet sensitizer) compared to its ^4H isotopomer. Efficient and persistent red-green-blue RTP ($\Phi_{\text{P}} > 0.10$, $\tau_{\text{em}} > 1\text{s}$) in a purely organic host/guest amorphous material⁷⁹ was observed upon deuteration of the guest, attenuating k_{nr} while the rigid β -estradiol host minimized quenching of long-lived triplet excitons. Despite these examples, there has not yet been a reported instance of PLQY enhancement upon deuteration of NIR-emissive organic dyes.

2.5.1.2 Photophysical Effects of Deuteration

In contrast to PtPh₄TBIP- d_{20} **2.11**, presence of Ph- d_5 moieties in PtPh₄TBP- d_{20} **2.14** effected no change in Φ_{P} or τ_{em} (Table 2.2). This might be due to low-frequency skeletal modes of benzo moieties (*i.e.* C=C twisting/bending, C-H bending) enabling efficient non-

radiative decay. Potential photophysical enhancements upon deuteration are therefore likely to be depreciated by these rate-dominating distortion modes. Contrastingly, the latent effects of isotopic substitution on k_{nr} are revealed when these same modes are attenuated in **2.9/2.11** by fused imide moieties. Partial deuteration experiments^{80,81} performed on acenes have shown the non-radiative decay to be influenced by C-H modes only when the π, π^* excited state is at least partially localized on them. Intuitively, *meso*-Ph moieties and their isotopomers are expected to have a negligible influence on photophysical properties given their near-orthogonal orientation to the macrocycle. The minimal FMO density of *meso*-Ph moieties is confirmed by quantum mechanical calculations at the B3LYP/Def2SVPP level and their minimal involvement in excited-states (Figure 2.9). Nevertheless, their presence imparts a prominent saddle-shaped distortion onto most metalloporphyrins, an effect which stems from a balance of conjugation between Ph/porphyrin core and steric effects. The identity of the *meso*-substituents (Ph/Ph- d_5) obviously has negligible influence on sterics of **2.9/2.11** yet could serve a small but impactful role in the porphyrin's vibronic scaffold as evidenced by the apparent increase in

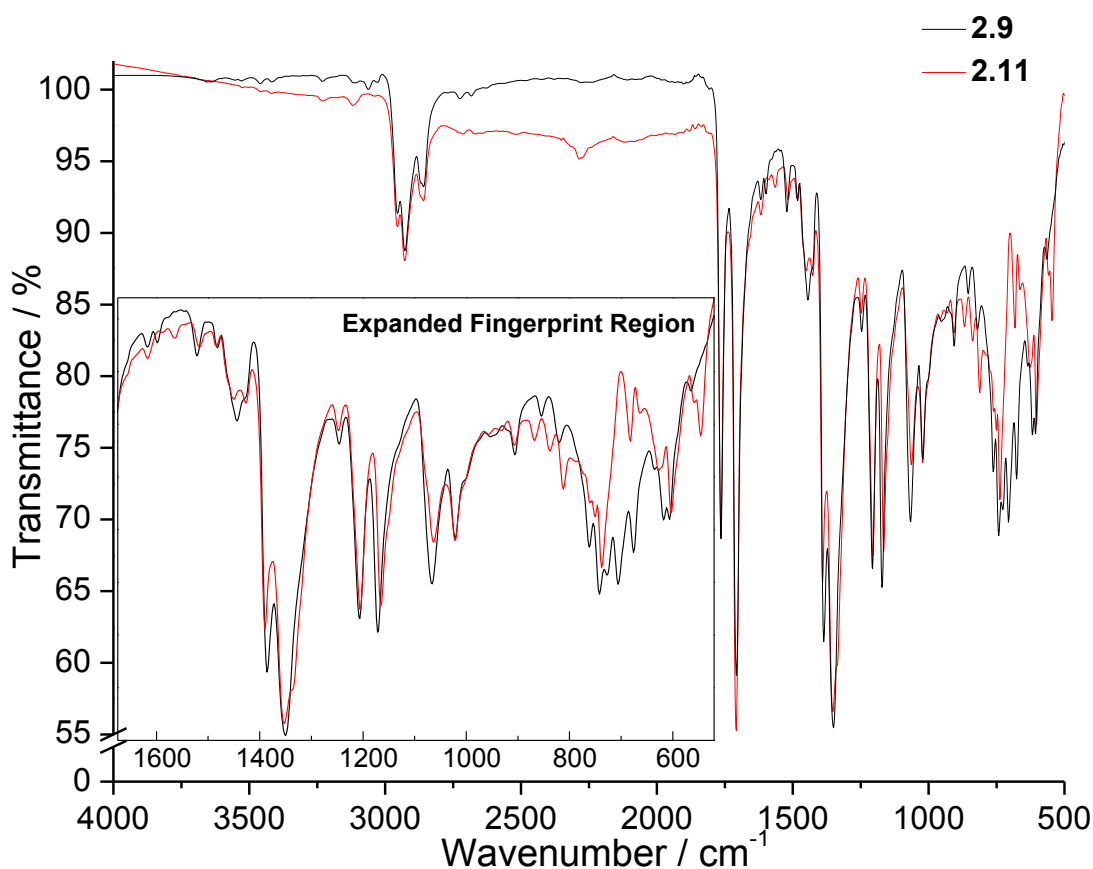


Figure 2.10 Overlap of **2.9/2.11** FTIR spectra.

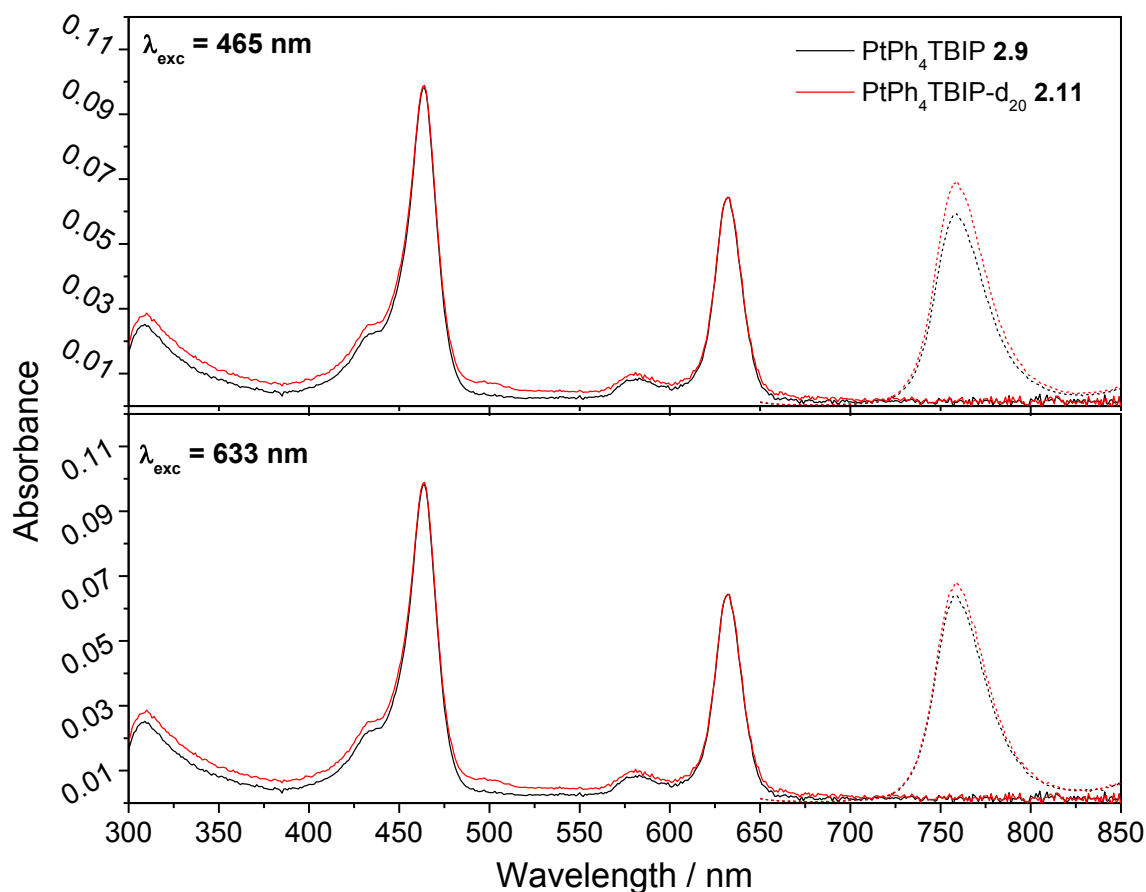


Figure 2.11 Overlap of absorption and emission spectra for PtPh₄TBIP **2.9** (black) and PtPh₄TBIP-*d*₂₀ **2.11** excited at the Soret band (top graph) and the Q-band (bottom graph) in degassed PhMe. Spectrum obtained from Meyer group at UNC Chapel Hill.

Φ_P . Liquid benzene was shown to undergo significant rearrangement of its vibrational tiers and relaxation dynamics upon deuteration.⁸³ A change in the intramolecular vibrational redistribution (IVR) rate of the triplet excited state onto the *meso*-Ph acceptor modes is likely impeded in isotopomers PtPh₄TBP-*d*₂₀/PtPh₄TBP, thereby removing a possible contributor to k_{nr} . Funnels along excited-state PES have been proposed as refinements of the energy gap law in non-planar porphyrins;^{61,86} distortion of the latter in the excited state may help access funnel geometries with greater Frank-Condon vibrational overlap integrals leading to increased k_{nr} . Efficiently restricting access to these geometries relies on a number of factors of which decreased effective molecular motion towards funnel points is key. This is accomplished by modulating vibrational frequencies on Ph moieties, altering excited-state conformational dynamics⁸⁷. Thus, a plausible explanation for the Φ_P enhancement could reside in the altered excited-state dynamics of **2.11** via low-energy distortion modes; *i.e.* deuteration of PtPh₄TBIP **2.9** reduces amplitude for out-of-plane Ph C-H bending (similarly

to α -deuterated stilbene⁷⁵) and by extension, rates of non-emissive surface crossings by restricting access to pivotal geometries. This view is supported by the juxtaposition of 2.9/2.11 FTIR spectra (Figure 2.10) which reveals some attenuation of $\sim 700\text{ cm}^{-1}$ vibration in 2.11, typically ascribed to out-of-plane aromatic C-H(D) bending.

2.5.2 Excitation Wavelength Dependence of Φ_P

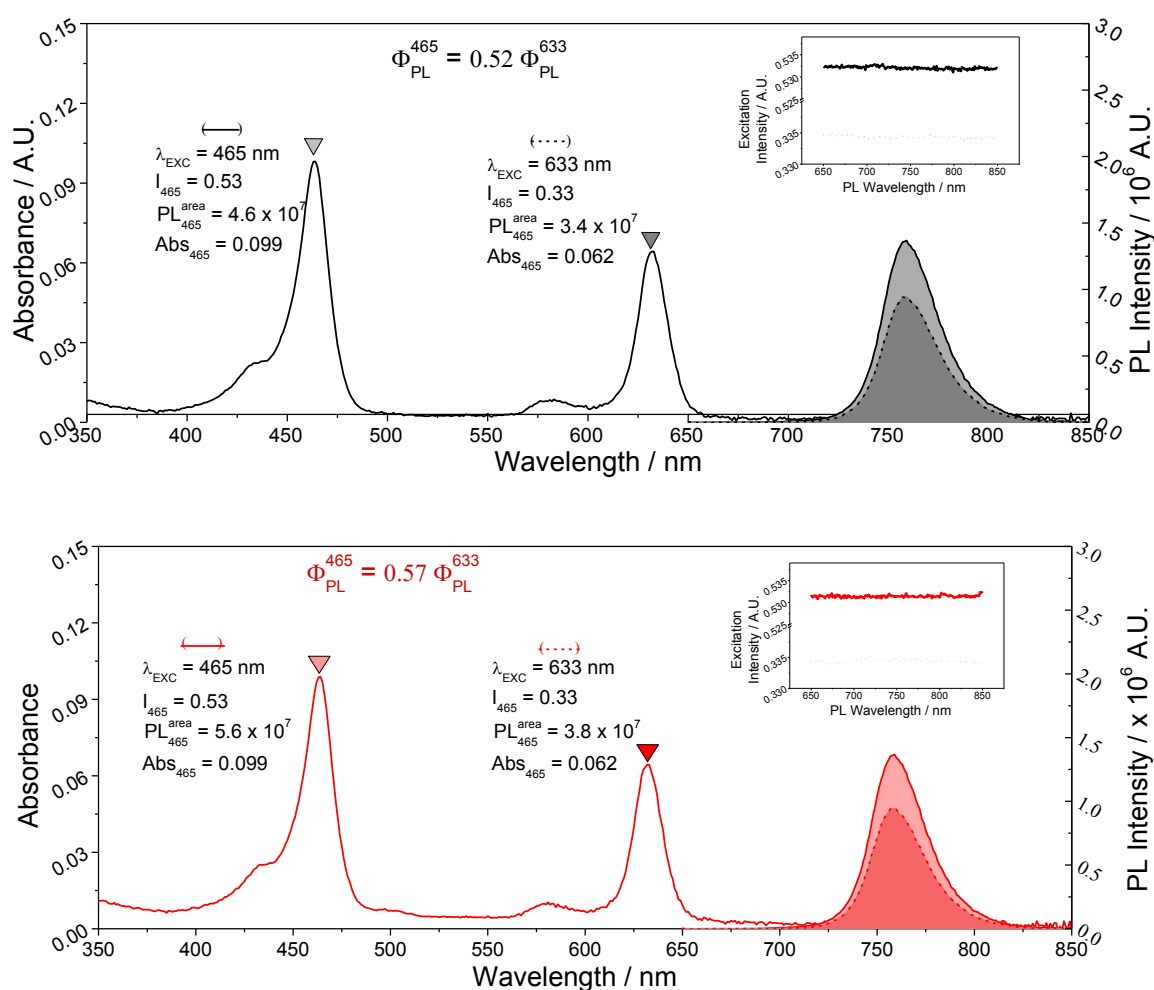


Figure 2.12 Steady-state UV-Vis absorption and emission spectra for PtPh₄TBIP 2.9 (top) and PtPh₄TBIP-d₂₀ 2.11 (bottom). PL spectra were measured with 465 nm (solid lines) and 633 nm (dashed lines) excitation. The inset shows the monitored intensity of the indicated excitation wavelengths. Internal calibration of the data provided the relative Φ_P . *Note:* Internal calibration of the PL data was performed by normalizing the integrated PL by both the absorption at λ_{ex} and the intensity of the light excitation. Spectrum obtained from Meyer group at UNC Chapel Hill.

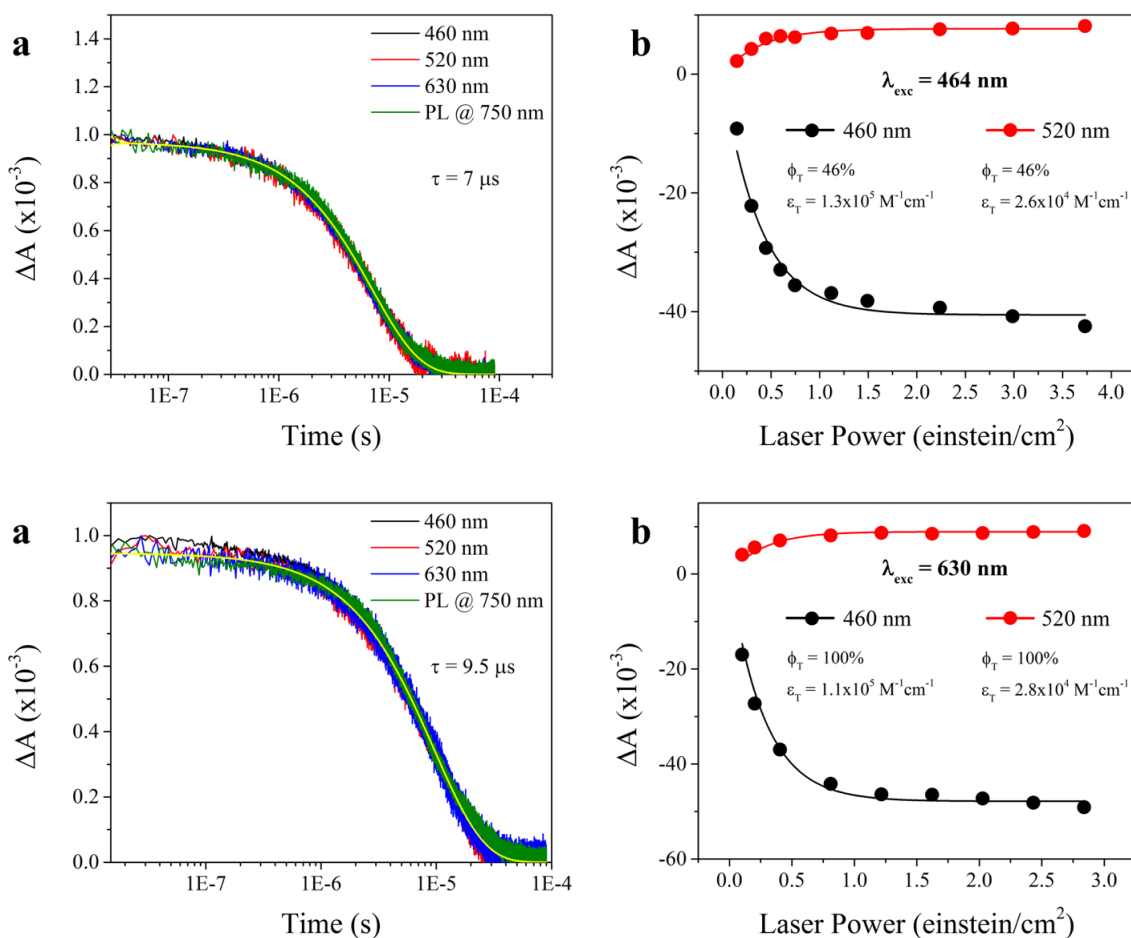
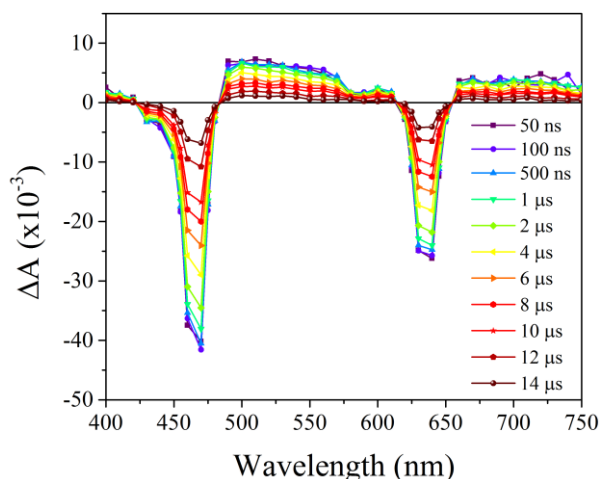


Figure 2.13 (a) Single wavelength transient-absorption spectroscopy (TAS) kinetics and photoluminescence of PtPh₄TBIP-*d*₂₀ **2.11** in argon-purged PhMe. A global analysis to the kinetic data resulted in monoexponential decays with ${}^3\tau_{em} = 7 \mu\text{s}$ (top, $\lambda_{ex} = 464 \text{ nm}$) and ${}^3\tau_{em} = 9.5 \mu\text{s}$ (bottom, $\lambda_{ex} = 630 \text{ nm}$). B) Power dependency of TAS kinetics measured at 460 nm and 520 nm enabled calculation of ISC QY and extinction coefficients through the partial saturation method. Spectra for Figures 2.13 and 2.14 obtained from Meyer group at UNC Chapel Hill.

Figure 2.14 Transient absorption spectrum of PtPh₄TBIP **2.9** in Ar-purged PhMe after 464 nm-pulsed light excitation at the indicated time delays.



Initially, conditions for PLQY measurements of these dyes were modelled after literature procedures for similar compounds. Virtually all metalloporphyrins and π -extended metalloporphyrins were excited exclusively at the Q-band. This preference is understandable because persistent impurities in porphyrin samples tend to manifest optically in the blue/green region (i.e. chlorins) whereas porphyrin Q-bands tended to reside unaccompanied in the red region (excitation in the red region avoids these problems). Ordinarily, PLQY is assumed to be independent of excitation wavelength (Vavilov's rule); higher excited states undergo non-radiative decay to the lowest excited state before any radiative processes may occur. However, lack of a red laser in the midst of photophysical characterization restricted excitation to the Soret band. PLQY and τ_{em} values obtained were inconsistent with those derived from Q-band excitation. Further investigation revealed that choice of excitation wavelength (Figure 2.11) produces a noticeable effect on Φ_P . **2.11** shows a ~17% increase in measured PLQY over its non-deuterated counterpart **2.9** when excited at the Soret band (465 nm). This perceived increase in drops down to ~6% when comparing both dyes excited at the Q-band (633 nm).

Interestingly, lifetimes determined through single-wavelength transient absorption spectroscopy (Figure 2.13) show **2.9** has no dependence on excitation wavelength (${}^3\tau_{em,460} = {}^3\tau_{em,620} = 11 \mu s$) whereas deuterated isotopomer **2.11** revealed (Figure 2.13) a marked dependence (${}^3\tau_{em,460} = 7 \mu s$, ${}^3\tau_{em,630} = 9.5 \mu s$). This suggests an increase in k_r is required in order to account for the observed changes in photophysical properties. Theoretical models of so-called "dark states"⁸⁸ which can influence photophysical processes in porphyrins have been proposed by spectroscopists working within the field. These dark states would potentially compete with the expected non-radiative decay to S_1 of coupled S_2 and S_3 states. Perdeuteration of the *meso*-Ph moieties might alter the extent of coupling to dark states, which would manifest itself through QY differences of Soret-generated triplets. Further studies are required to elucidate the mechanism through which conflicting photophysical properties are observed within the same dye.

2.6 Conclusions

A couple of highly phosphorescent PtAr₄TBIP dyes with varying aryl groups (Ph, C₆D₅) at the *meso*-positions were synthesized and characterized. Deuteration at the *meso*-positions resulted in unusual photophysical properties: PLQY measurements for **2.11**

revealed a ~17% increase over its non-deuterated counterpart **2.9** when excited at the Soret band. Transient absorption spectroscopy studies revealed that while excitation at the Q-band leads to quantitative triplet formation, Soret band excitation results in a ~50% loss in triplet yield, presumably via coupling to “dark states” accessible from S₂. Further studies are required to gain an understanding of the effects deuteration may have on the photophysical properties of these dyes.

2.7 Experimental

All reaction solvents were purified prior to use by passing them through a solvent column of activated A-1 alumina on the MBraun MB-SPS solvent purification system. Unless specified, all chemicals were used as purchased without further purification. All glassware was flame-dried under vacuum prior to use. NMR spectra were acquired in CDCl₃ with a Bruker 300 MHz spectrometer for ¹³C NMR and with a Bruker 400 MHz spectrometer for ¹H NMR. Column chromatography was performed using 60-200µm irregular silica as stationary phase unless otherwise noted. Mass spectra were recorded on the Bruker Maxis UHR-TOF instrument. PtPh₄TBP was purchased from Frontier Scientific and used as received.

Single dark purple block-shaped crystals of (PtPh₄TBIP-*d*₂₀) were grown from a mixture of methanol and benzene by slow evaporation. A suitable crystal (0.53×0.29×0.23 mm) was selected and mounted on a MITIGEN holder in Paratone oil on a Rigaku Oxford Diffraction SuperNova diffractometer. The crystal was kept at *T* = 120 K during data collection. Using Olex2 (Dolomanov et al., 2009), the structure was solved with the PLATON structure solution program, using the SQUEEZE methods solution method. The model was refined with version of ShelXL (Sheldrick, 2008) using Least Squares minimisation.

N-Formyl-*tert*-butyl glycinate (2a) NaOMe (150 g, 2.78 mol) was added in portions to a 4500 mL boiling flask equipped with a magnetic stir bar and methanol (800 mL) was added under N₂ atmosphere. The flask was immersed into an ice bath, allowed to cool to 0 °C before adding quickly adding formamide (400 mL, xs). After stirring at room temperature for 30 min, methanol was distilled away under reduced pressure and the contents of the flask were subjected to high vacuum for 48h. If the contents of the flask solidify, heat gently on a steam bath until the solids melt (around 70 °C). *tert*-Butyl bromoacetate (500 g, 2.56

mol) was added dropwise over vigorous stirring at such a rate to keep the internal temperature of the flask around 60 °C. After completing addition, the flask was kept at 60 °C for another 6 hours. The resulting clear, light-yellow solution was stirred with saturated Na₂CO₃ solution (4L) overnight. The biphasic mixture was passed through a short pad of Celite and the aqueous phase was extracted with dichloromethane (5 x 500 mL). The combined organic fractions were washed with brine (2 x 500 mL) and dried over Na₂SO₄ before removing the solvent under reduced pressure to leave behind a light-yellow oil which was fractionally distilled to afford the title compound as a clear colourless oil (362.8, 89%). Spectral data matches published values. ¹H NMR (300 MHz, CDCl₃) δ 8.21 (s, 1H), 6.37 (br s, 1H), 3.95 (d, J = 4 Hz, 2H), 1.45 (s, 9H); ¹³C NMR (75 MHz, CDCl₃) δ 168.58, 161.02, 82.58, 40.56, 27.94.

tert-Butyl Isocynoacetate⁸⁹⁸⁹⁸⁹ (**2b**) N-formyl-tert-butyl glycinate (360 g, 2.26 mol) and trimethylamine (945 mL, 6.78 mol) were added to dichloromethane (3000 mL) in a 10 L boiling flask equipped with a magnetic stir bar. The flask was immersed into an ice bath and the contents were allowed to cool to 0 °C before adding POCl₃/phosphorus oxychloride (210g, 2.26 mol) dropwise such that the internal temperature of the flask did not exceed 4 °C. After complete addition, the contents of the flask were stirred for another 6h at 0 °C before quenching with saturated Na₂CO₃ solution (5L). The organic fraction was isolated and the aqueous fractions were extracted with dichloromethane (3×1000 mL). The combined organic fractions were concentrated *in vacuo* down to ca. 2000 mL, washed with brine (1000 mL) and dried over Na₂SO₄. After removing the solvent under reduced pressure, the resulting orange oil was distilled under vacuum to afford **2b** as a colorless, foul-smelling liquid (249 g, 78%). The compound was stored under N₂ atmosphere at -20 °C, where it crystallizes into a white solid. Spectral data matches published values. ¹H NMR (300 MHz, CDCl₃) δ 4.11 (s, 2H), 1.48 (s, 9H).

2-(2-Ethylhexyl)-3a,4,7,7a-tetrahydro-1H-isoindole-1,3(2H)-dione (**2.1**) *cis*-1,2,3,6-tetrahydrophthalic anhydride (140.0g, 0.92 mol) and 4A molecular sieves (200 g) were stirred in dimethylformamide (400 mL) until the anhydride is dissolved followed by addition of 2-ethylhexylamine (130.8g, 1.012 mol). The contents were refluxed for 24h under N₂ before acquiring a yellow color. dimethylformamide was removed under reduced pressure and the resulting yellow oil was distilled under reduced pressure (0.5 mmHg, 180 °C) to afford 2-(2-ethylhexyl)-3a,4,7,7a-tetrahydro-1H-isoindole-1,3(2H)-dione **2.1** (242 g, 94.9%)

as a yellow oil with a carotenoid odor. ^1H NMR (300 MHz, CDCl_3) δ 5.89 (t, $J = 3.2$ Hz, 2H), 3.35 (d, $J = 7.4$ Hz, 2H), 3.06 (t, $J = 2.6$ Hz, 2H), 2.61 (m, 2H), 2.19 (m, 2H), 1.67 (m, 1H), 1.22 (m, 8H), [0.87 (t, $J = 6.8$ Hz), 0.85 (t, $J = 7.2$ Hz)] (6H); ^{13}C NMR (75 MHz, CDCl_3) δ 180.5, 127.8, 42.8, 39.0, 37.3, 30.2, 28.4, 23.65, 23.62, 23.0, 14.0, 10.3; HRMS ESI, m/z for $\text{C}_{16}\text{H}_{25}\text{NO}_2+\text{H}$ calcd 264.1958, found 264.1961.

5-Chloro-2-(2-ethylhexyl)-6-(phenylthio)hexahydro-1H-isoindole-1,3(2H)-dione (2.2) NCS (123 g, 0.904 mol) was completely dissolved in dichloromethane (400 mL) in a 2 L round-bottom flask. The flask was immersed in an ice/water bath (0°C) and stirred under N_2 atmosphere for 30 min. PhSH/thiophenol (95.8 mL, 0.904 mol) was added dropwise (3 mL/min, exothermic reaction) giving rise to an intense orange solution. The content was stirred for 10 min. at room temperature. The flask was immersed into a $\text{CH}_3\text{CN}/\text{CO}_2$ bath (-41°C) followed by slow addition (20 mL/min) of imide **2.1** (224 g, 0.853 mol) as a solution in dichloromethane (500 mL). The mixture was brought to room temperature, stirred for 1h and subsequently filtered to remove succinimide by-product. The solvent was removed under reduced pressure and the resulting orange oil was purified on a column of silica (hexane/EtOAc, 6' ID, 2' length). **2.2** was isolated as a yellow oil (292 g, 83.9%). ^1H NMR (300 MHz, CDCl_3) δ 7.45-7.41 (m, 2H), 7.37-7.30 (m, 3H), 4.25-4.17 (m, 1H), 3.57 (q, $J = 4.2$ Hz, 1H), 3.40-3.38 (m, 2H), 3.19-3.05 (m, 1H), 2.90 (td, $J = 4.0$ Hz, 8.0 Hz, 1H), 2.66-2.36 (m, 2H), 2.33-2.28 (dd, $J = 3.7$ Hz, 9 Hz, 1H), 2.22-2.09 (m, 1H), 1.83-1.71 (m, 1H), 1.29-1.21 (br m, 8H), 0.92-0.84 (m, 6H); ^{13}C NMR (75 MHz, CDCl_3) δ 179.24, 179.22, 178.4, 178.1, 132.8, 132.7, 132.4, 132.3, 129.4, 129.3, 128.1, 57.5, 57.1, 48.4, 42.3, 37.4, 36.7, 36.2, 35.7, 30.3, 28.3, 26.7, 26.6, 25.4, 23.6, 22.9, 14.0, 10.3, 10.2; HRMS ESI, m/z for $\text{C}_{22}\text{H}_{30}\text{ClNO}_2\text{S}+\text{Na}$ calcd 430.1578, found 430.1585.

5-Chloro-2-(2-ethylhexyl)-6-(phenylsulfonyl)hexahydro-1H-isoindole-1,3(2H)-dione (2.3)

Note: *m*-CPBA was received as a 77% mixture with H_2O and *m*-CBA. It was purified before use by dissolving in dichloromethane (5 mL/g of mixture) and washing (3 x 600 mL) with pH 7.5 buffer (820 mL 0.1M NaOH, 500 mL 0.2M KH_2PO_4 , diluted up to 2L). The organic layer was dried over Na_2SO_4 and evaporated at room temperature under reduced pressure to give pure *m*-CPBA/*meta*-chloroperoxybenzoic acid. Caution: as all peroxides, dry *m*-CPBA has a potential for spontaneous decomposition; this manipulation should be carried out behind explosion protection shield; contamination with heavy metals should be avoided (eg, no metallic spatulas). A solution of sulfide **2.2** (280 g, 0.686 mol) in 2000 mL of

dichloromethane was prepared in a 3 L round-bottom flask. The flask was immersed into an ice/water bath (0°C) and the contents were stirred for 30 min. *m*-CPBA (310 g, 1.79 mol) was added in portions (~10 g per 10s, exothermic reaction), resulting in a milky white opaque solution towards the end of the addition. The flask was brought to room temperature, stirred for 1h and subsequently filtered to remove *m*-CBA. The filtrate was washed with dichloromethane (200 mL x 3) and the combined organic solutions were concentrated under reduced pressure to ca. 1 L volume. The organic phase was washed with Na₂CO₃ solution (10%, 200 mL x 3), dried over Na₂SO₄ and the solvent was removed under reduced pressure to afford **2.3** as a yellow oil (286 g, 94.8%) used directly in the next reaction. ¹H NMR (300 MHz, CDCl₃) δ 7.87 (dd, 2H, *J* = 1.5 Hz, 7.2Hz), 7.70-7.65 (tt, *J* = 1.2 Hz, 7.4 Hz, 1H), 7.60-7.54 (m, 2H), 4.63-4.57 (m, 1H), 3.48-3.42 (m, 1H), 3.34-3.27 (m, 3H), 3.04-2.96 (m, 1H), 2.58-2.50 (m, 1H), 2.38-2.14 (m, 2H), 2.19-2.01 (m, 1H), 1.72-1.58 (br m, 1H), 1.26-1.12 (br m, 8H), 0.83-0.78 (m, 6H); ¹³C NMR (75 MHz, CDCl₃) δ 178.4, 177.9, 136.8, 134.4, 129.5, 128.5, 64.64, 64.61, 50.6, 42.5, 37.2, 36.2, 35.1, 30.27, 30.22, 29.30, 29.26, 28.18, 28.15, 22.79, 22.77, 19.7, 19.6, 13.9, 10.2; HRMS ESI, *m/z* for C₂₂H₃₀ClNO₄S+Na calcd 462.1476, found 462.1484.

2-(2-Ethylhexyl)-5-(phenylsulfonyl)-3a,4,7,7a-tetrahydro-1H-isoindole-1,3(2H)-dione (2.4)

Chlorosulfone **2.3** (68.5 g, 0.156 mol) was dissolved in dichloromethane (600 mL) in a 3 L round-bottom flask, immersed in a isopropyl alcohol/CO₂ bath (-78°C) and stirred for 30 min under N₂ atmosphere. 1,8-Diazabicycloundec-7-ene (30.0 g, 0.192 mol) was then added rapidly, producing a dark green colored solution which progressed to a dark brown color by the end of the addition. The flask was immersed into an ice/water bath (0°C) and was allowed to stir for 10 min. The mixture was washed with HCl (5%, 300 mL), dried over Na₂SO₄ and the solvent was subsequently removed under reduced pressure to afford **2.4** as a yellow oil (62 g, >99%). ¹H NMR (300 MHz, CDCl₃) δ 7.82 (d, *J* = 8 Hz, 2H), 7.64 (t, *J* = 7.6 Hz, 1H), 7.54 (t, *J* = 7.5 Hz, 2H), 7.16 (br t, *J* = 2.8 Hz, 1H), 3.22-3.02 (m, 4H), 2.91-2.79 (m, 2H), 2.52-2.43 (m, 2H), 1.60-1.49 (m, 1H), 1.24-1.15 (br m, 8H), 0.89-0.79 (m, 6H); ¹³C NMR (75 MHz, CDCl₃) δ 178.6, 177.6, 141.2, 138.37, 138.36, 137.0, 133.6, 129.2, 128.2, 42.80, 42.76, 38.5, 37.73, 37.71, 37.2, 37.1, 30.3, 30.2, 28.4, 28.1, 24.5, 23.7, 23.5, 23.0, 22.87, 22.85, 14.0, 10.3, 10.0; HRMS ESI, *m/z* for C₂₂H₂₉NO₄S+Na calcd 426.1710, found 426.1724.

tert-Butyl 6-(2-ethylhexyl)5,7-dioxo-2,4,4a,5,6,7,7a,8-octahydropyrrolo[3,4-f]isoindole-1-carboxylate (2.5) KOtBu (33.5 g, 0.289 mol) was dissolved in dry tetrahydrofuran (3000 mL) in a 10 L round-bottom flask through vigorous magnetic stirring, producing a bright yellow solution. The flask was thoroughly flushed with N₂ gas and subsequently immersed in an ice/water bath for 30 min. *t*-Butyl 2-isocynoacetate **2b** (43.0 g, 0.306 mol) was added rapidly to the stirred solution, yielding a progressively darker orange transparent solution. The reaction mixture was stirred for an additional 45 min while immersed in the ice bath. Dipolarophile **2.4** (62.0 g, 0.154 mol) was added dropwise into the flask as a tetrahydrofuran solution (200 mL) with the aid of an addition funnel. The flask was brought to room temperature and was allowed to stir for 1h; the reaction was monitored by TLC (hexanes/EtOAc). The solvent was removed under reduced pressure, re-dissolved in dichloromethane (500 mL) and subsequently washed with brine (3 x 200 mL). The combined organic fractions were dried over Na₂SO₄ and dichloromethane was removed under reduced pressure to afford orange oil. The crude product was purified using flash chromatography (hexanes/EtOAc, 3'' ID, 2' length) to afford **2.5** as a yellow powder (54 g, 87%). ¹H NMR (300 MHz, CDCl₃) δ 9.97 (br s, 1H), 6.60 (d, *J* = 2.6 Hz, 1H), 3.74 (dd, *J* = 3.0 Hz, 15.5 Hz, 1H), 3.16-3.06 (m, 5H), 2.68-2.54 (m, 2H), 1.50 (s, 9H), 1.40-1.28 (br m, 1H), 1.12-0.98 (m, 4H), 0.90-0.50 (m, 10H); ¹³C NMR (75 MHz, CDCl₃) δ 180.1, 179.8, 161.2, 123.6, 123.5, 119.21, 119.16, 118.94, 118.93, 117.89, 117.87, 80.7, 42.3, 42.2, 40.14, 40.07, 39.8, 39.7, 36.9, 36.7, 29.61, 29.60, 28.4, 28.2, 28.1, 27.9, 22.8, 22.7, 22.64, 22.57, 22.4, 22.3, 22.2, 21.7, 13.8, 10.2, 9.8; HRMS ESI, *m/z* for C₂₃H₃₄N₂O₄+Na calcd 425.2424, found 425.2411.

6-(2-Ethylhexyl)5,7-dioxo-2,4,4a,5,6,7,7a,8-octahydropyrrolo[3,4-f]isoindole-1-carboxylic acid (2.6) To a 250 mL round-bottom flask was added *t*-butyl ester **2.6** (45.1 g, 0.112 mol) and thoroughly purged with N₂ gas and covered with aluminium foil. 33% HBr in AcOH (100 mL, excess) was added to the flask over vigorous stirring, dissolving **2.5** and turning the solution bright orange. The content was stirred for 30 min and subsequently poured onto a cold (0°C) KH₂PO₄ solution (10%, 500 mL). The aqueous phase was extracted with EtOAc (3 x 200 mL) and the combined organic fractions were dried over Na₂SO₄. The solvent was removed under reduced pressure to afford brown semi-crystalline product (39 g, >99%) in a 100 mL round-bottom flask equipped with a magnetic stir bar. The product (carboxylic acid/pyrrole in a 4:1 ratio) is used in the next step without purification. A sample of the carboxylic acid **2.6** was isolated (liquid chromatography, silica, hexanes/EtOAc) and

characterized: ^1H NMR (300 MHz, CDCl_3) δ 9.32 (br s, 1H), 6.80 (br s, 1H), 3.82 (d, $J = 15.4$ Hz, 1H), 3.34-3.18 (m, 5H), 2.81 (dd, $J = 6.7$ Hz, 15.4 Hz, 1H), 2.70 (dd, $J = 6.2$ Hz, 14.6 Hz, 1H), 1.55-1.42 (br s, 1H), 1.22-1.10 (m, 4H), 1.02-0.74 (m, 7H), 0.74-0.65 (m, 3H); ^{13}C NMR (75 MHz, CDCl_3) δ 180.3, 180.1, 165.64, 165.61, 126.8, 120.0, 119.70, 119.65, 117.35, 117.32, 42.7, 40.2, 40.1, 39.8, 39.7, 37.0, 30.0, 29.9, 28.3, 28.0, 23.1, 23.0, 22.9, 22.20, 22.17, 21.78, 21.76, 14.0, 10.4, 10.2; HRMS ESI, m/z for $\text{C}_{19}\text{H}_{26}\text{N}_2\text{O}_4 + \text{Na}$ calcd 369.1789, found 369.1785.

2-(2-Ethylhexyl)3a,4,8,8a-tetrahydropyrrolo[3,4-f]isoindole-1,3(2H,6H)-dione (2.7) The 100 mL round-bottom flask containing **2.6** (39 g) from the previous step was placed in a preheated oil bath 130°C and subjected to vacuum for 30 seconds in order to remove trace amounts of solvent. The flask was refilled with N_2 gas, covered with aluminium foil and was allowed to stir for 45 mins. The brown crystalline oil melted and eventually started to bubble (release of CO_2 gas). The flask was cooled to room temperature and the contents were dissolved in eluent (2 parts hexanes/1 part EtOAc) and subsequently passed through a short pad of silica gel. All fractions were collected and the solvent was removed under reduced pressure yielding yellow flakes (31.5 g, 93%). The solid was dried in a 250 mL round-bottom flask under vacuum at room temperature, covered with aluminium foil (light-sensitive). ^1H NMR (300 MHz, CDCl_3) δ 8.00 (br s, 1H), 6.50 (d, $J = 2.4$ Hz, 2H), 3.23-3.15 (m, 6H), 2.76-2.70 (m, 2H), 1.50-1.41 (m, 1H), 1.25-1.09 (m, 5H), 0.86-0.82 (m, 6H), 0.71-0.66 (m, 3H); ^{13}C NMR (75 MHz, CDCl_3) δ 180.68, 180.66, 116.9, 113.40, 113.31, 113.27, 42.5, 40.7, 40.6, 37.0, 29.8, 28.2, 22.89, 22.86, 22.14, 22.11, 14.1, 10.3; HRMS ESI, m/z for $\text{C}_{22}\text{H}_{26}\text{N}_2\text{O}_2 + \text{H}$ calcd 303.2067, found 303.2070.

Platinum (II) 5,10,15,20-tetraphenyl-tetrabenzoimido[*b, g, l, q*]porphyrin (2.9) *Note:* dichloromethane used in this reaction was dried over 4A molecular sieves for 3 weeks prior to use. To a 2 L round-bottom flask was added freshly distilled PhCHO (1.60 g, 16.1 mmol) as a dichloromethane solution (100 mL). dichloromethane (1300 mL) and 4A molecular sieves (100 g) were added to the flask and argon gas was passed through the solution for 1h while stirring. Pyrrole **2.7** (4.43 g, 14.9 mmol) was added to the flask as a solution in previously de-oxygenated dichloromethane (100 mL). The flask was shielded from light and the mixture was stirred under argon for 20 min. BF_3OEt_2 (0.49g, 3.50 mmol) was added to the flask dropwise, immediately producing a dark green color. The reaction is monitored through UV-Vis spectroscopy by the growth of a sharp Soret band at approximately 460 nm

(see Figure S1). Volumetric aliquots were withdrawn every 20 min; once the Soret band no longer showed a marked increase in intensity, the reaction was quenched. The contents were stirred for 60 min after which DDQ (4.00 g, 17.6 mmol) was added rapidly to the stirring mixture. The solution was allowed to stir at room temperature for an additional 3h. The solvent was removed under reduced pressure and the dark blue oil was dissolved in tetrahydrofuran (200 mL) and the sieves were filtered off. The sieves were extracted with tetrahydrofuran (3 x 200 mL). The fractions were combined, tetrahydrofuran removed in vacuo and the bluish solids re-dissolved in CHCl₃ (50 mL). The solution was passed through a short pad of silica and eluted with CHCl₃/tetrahydrofuran. The organic phase was washed with Na₂CO₃ (200mL, 10%), brine and was dried over Na₂SO₄. The solvent was removed under reduced pressure and the crude mixture was used in the next step without further purification. Purification and characterization by NMR of the complex porphyrin mixture is hampered by a large number of diastereomers. The identity of **2.8** is established through HRMS and UV-Vis spectroscopy. HRMS ESI, *m/z* for C₁₀₀H₁₁₅N₈O₈ [M+H]⁺ calcd 1555.8832, found 1555.8815.

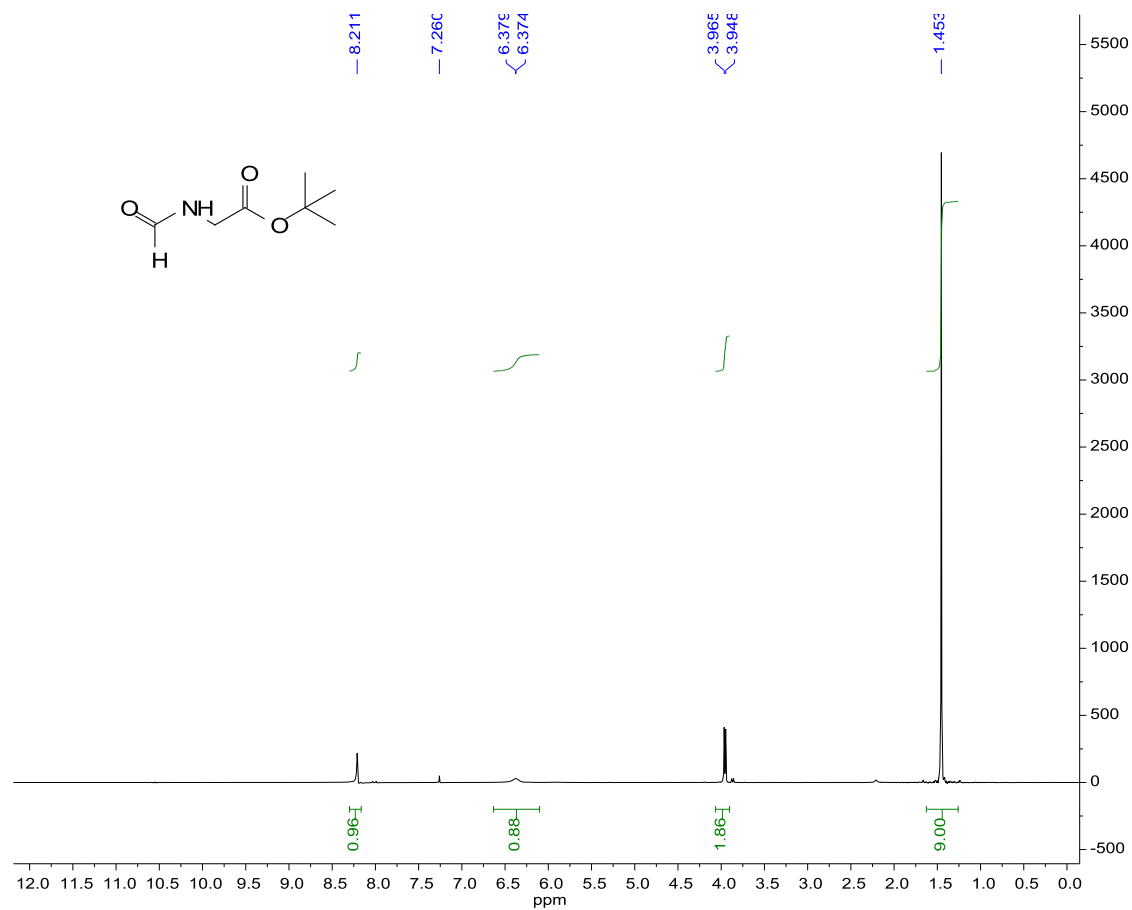
The crude mixture from the previous step containing **2.8** is dissolved in PhCN (150 mL) and added to a 500 mL round-bottom flask. PtCl₂ (0.400g, 1.47 mmol) is added to the flask over vigorous stirring under argon atmosphere. The reaction was monitored by UV-Vis spectroscopy; the appearance of a Soret band at approximately 418 nm indicated insertion of Pt into the porphyrin ring. The rise in the 418 nm band is accompanied by a concurrent decrease in the intensity of the free-base porphyrin Q-band at around 680 nm. The contents of the flask were refluxed for 4h at which point DBU (0.50 g, 3.3 mmol) was added in one portion and the mixture was refluxed for an additional hour. DDQ (4.00 g, 17.6 mmol) was added in small portions and the mixture was allowed to reflux for 5-10 min until no increase in Q-band at 633 nm was noticed. PhCN was distilled off under reduced pressure and the crude mixture was purified by column chromatography (silica, 43-60 μm) using hexane as eluent to wash away fast-moving colored impurities and residual PhCN, followed by a CHCl₃/*i*Pr₂O gradient (0 to 2.5% *i*Pr₂O) to obtain **2.9** as a dark green fraction (2.35 g, 36.4%). ¹H NMR (300 MHz, CDCl₃) δ 8.26 (d, *J* = 7.0 Hz, 8H), 8.19 (t, *J* = 7.6 Hz, 4H), 8.04 (t, *J* = 7.7 Hz, 8H), 7.47 (s, 8H), 3.56-3.54 (d, *J* = 7.2 Hz, 8H), 1.85-1.75 (m, 4H), 1.62 (s, H₂O) 1.37-1.20 (m, 37H), 0.91-0.86 (27H); ¹³C NMR (75 MHz, CDCl₃) 168.2, 140.7, 139.4, 137.0, 133.2, 131.1, 130.3, 128.9, 121.0, 119.7, 42.2, 38.4, 30.6, 28.6, 23.9, 23.0, 14.1, 10.4; HRMS ESI, *m/z* for C₁₀₀H₉₆N₈O₈Pt calcd 1731.6993, found 1731.7004. Comb. Analysis Calc.: C 69.31%, H 5.58%, N 6.47%; found C 69.01%, H 5.59%, N 6.39%.

Platinum (II) 5,10,15,20-tetrakis(perdeuterophenyl)-tetrabenzoimido[*b, g, l, q*]porphyrin (2.11) To a 3L round-bottom flask equipped with a magnetic stir bar (elliptical, 70 mm length) was added dichloromethane (2500 mL, previously dried over 4A molecular sieves at 10% v/v). Pyrrole **2.7** (540 mg, 1.78 mmol) was added to the flask and dry N₂ gas was bubbled (18G needle) through the solution for 1h with stirring. The flask was shielded from light with aluminium foil and *d*₆-benzaldehyde (200 mg, 1.78 mmol) was added in one portion. After an additional 15 min of bubbling N₂ gas, the needle was retracted and BF₃OEt₂ (0.28 mL, 2 mmol) was added to the flask in one portion, quickly darkening the solution. The contents were stirred for 2h at which point DDQ (0.568 g, 2.5 mmol) was added in one portion to the stirring mixture. The solution was allowed to stir at room temperature overnight and was subsequently concentrated under reduced pressure to ~500 mL and was washed with 10% Na₂SO₃ (500 mL), H₂O (500 mL), 5% HCl (500 mL) and brine (500 mL). The organic phase was dried over Na₂SO₄ (25 g) and the solvent was removed under reduced pressure to a metallic green paste which was dissolved in Et₂O (15 mL), carefully layered with hexanes (60 mL) and left to slowly crystallize over the weekend. The black supernatant was filtered off to leave behind bright green metallic crystals (170 mg) which were rinsed with copious amounts of cold (-41 °C) Et₂O. The mother liquor was concentrated and left to crystallize overnight to yield a second crop of black/green crystals with a metallic lustre (35 mg). An overall yield of 205 mg of porphyrin *bis*(hydrochloride) salt was obtained and used without further purification.

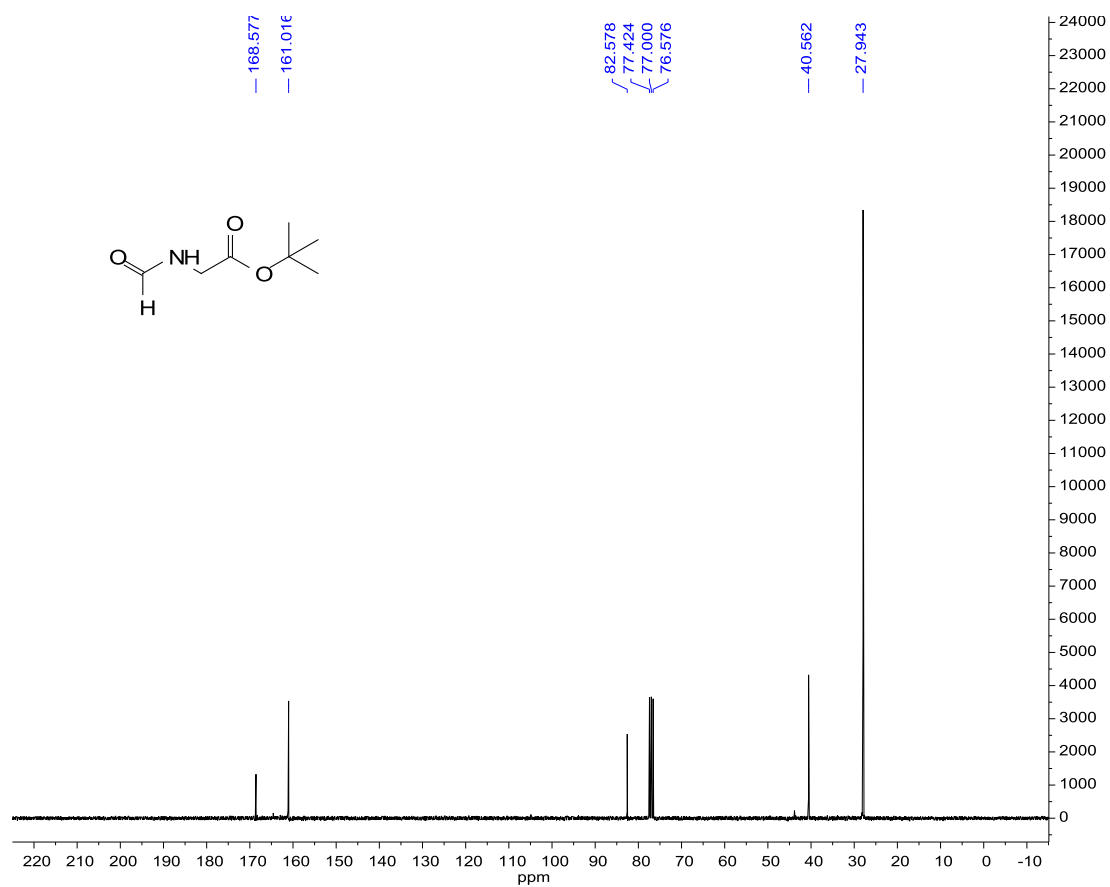
PtCl₂ (30 mg, 113 μmol) was added to a flame-dried 50 mL round-bottom flask equipped with a magnetic stir bar. Dry PhCN (25 mL) was added before bringing the flask to 120 °C and stirring overnight. The *bis*(hydrochloride) salt of the porphyrin (20 mg) was added to a 100 mL round-bottom flask equipped with a magnetic stir bar and was dissolved in Ph₂O (30 mL). N₂ gas was bubbled through the solution (18G syringe) for 30 min before transferring the dissolved Pt/PhCN solution through a cannula. The temperature of the porphyrin solution was maintained at 100 °C during the transfer. After complete addition of the platinum reagent, DBU (20 mg, 131 μmol) was added, the solution was brought to 180 °C and was stirred for an additional 2h. DDQ (200 mg, 881 μmol) was added in one portion and the solution was kept for 180 °C for an additional hour (until no further change in the Q-band at 633 nm is detected). The solvent was distilled away under reduced pressure and crude mixture was purified by column chromatography using hexanes/dichloromethane to wash away fast-moving colored impurities and residual

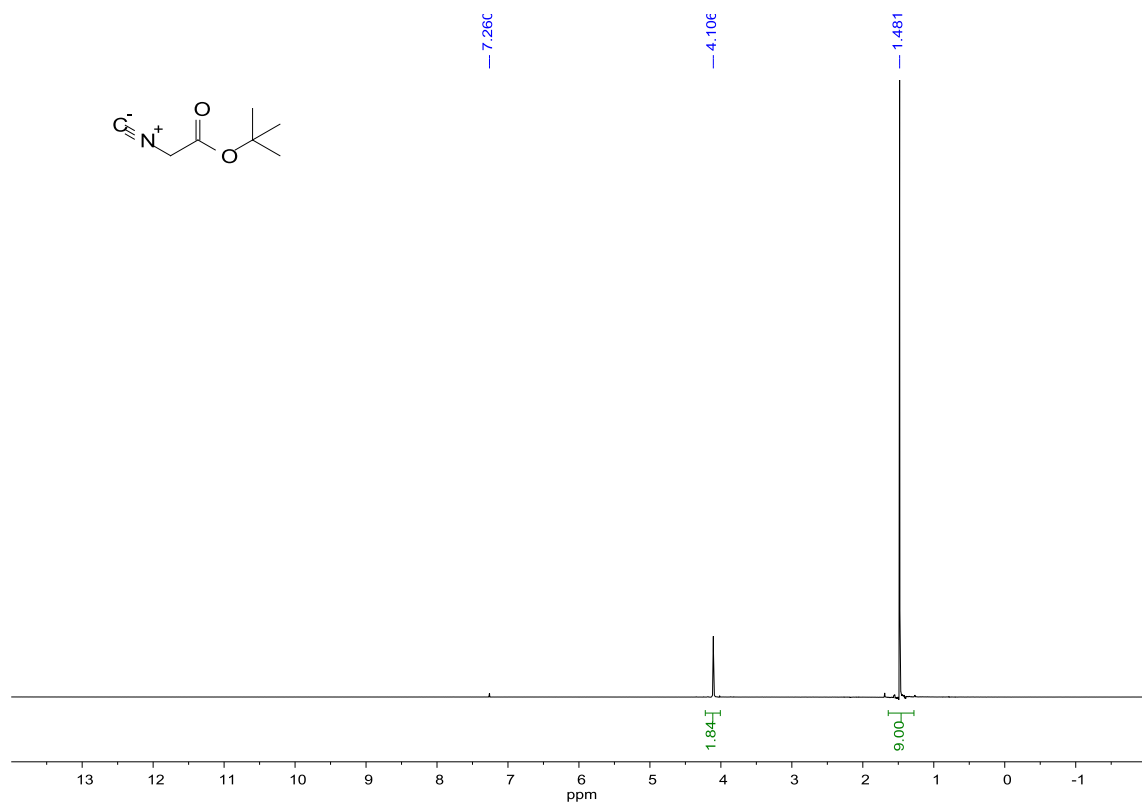
PhCN/Ph₂O, followed by elution with CHCl₃/(iPr)₂O, collecting the bright green fraction. The solvent was evaporated and the solids were crystallized by layering a concentrated solution of porphyrin in dichloromethane with a 10 fold excess of methanol to afford the title compound as bright green crystals with a metallic lustre (21 mg, 98%). ¹H NMR (500 MHz, CDCl₃) δ 7.46 (s, 8H), 3.55 (d, 7.2 Hz, 8H), 1.81 (m, 4H), 1.29 (m, 32 H), 0.89 (m, 24H); ¹³C NMR (125 MHz, CDCl₃) δ 168.30, 140.91, 139.42, 137.14, 132.91, 130.73, 121.17, 119.83, 42.33, 38.52, 30.75, 28.76, 27.44, 24.05, 23.12, 14.21, 10.57; HRMS ESI, *m/z* for C₁₀₀H₇₆D₂₀N₈O₈ calcd 1751.8249, found 1751.8243.

Solubility Measurements – The solubility of PtPh₄TBIP **2.9** was determined spectroscopically from saturated solutions. 50 mg samples of the porphyrin were added to a 25 mL vial along with 2-3 mL of the appropriate solvent. If complete dissolution occurred at room temperature (298K), more porphyrin was added until a saturation point was reached (precipitate observable on the bottom and sides of the vials). The contents of the vial were subsequently refluxed for 10 min and cooled to room temperature. If no precipitate was observed, more porphyrin was added and the vial's contents were once again brought to and kept at reflux for 10 min. If precipitate was visible after heating, solvent was incrementally added and heated to reach a point of minimal precipitate at room temperature. This was taken to be the saturation point of a given solvent at room temperature. The solution was filtered through a 0.45 μ PTFE syringe filter and an aliquot (~50 μL) was withdrawn with the aid of an analytical glass syringe and dispensed into a 100 mL or 250 mL “Class A” volumetric flask. The volumetric solution was made up with the appropriate solvent and further diluted using “Class A” volumetric glassware until a satisfactory optical density was achieved to record the absorbance spectrum. To accurately calculate the saturation concentration, the extinction coefficients at the Soret band and the Q-band were determined for each solvent. The absorption at the Soret band was related to *c*_{sat} (saturation concentration) by using the Beer's law ($A = \epsilon cl$) and the appropriate dilution factor.

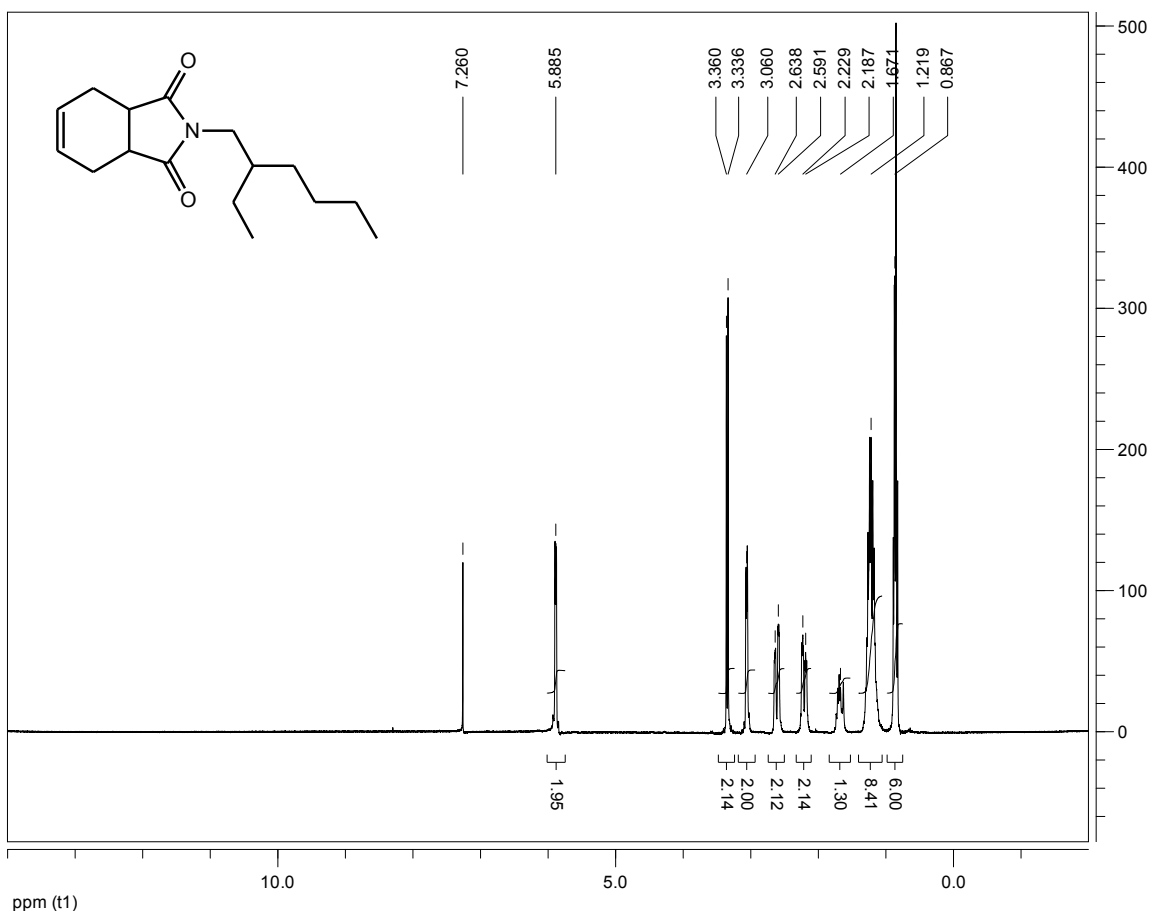


^1H NMR (top) and ^{13}C NMR (bottom) spectra for **2a** in CDCl_3 .

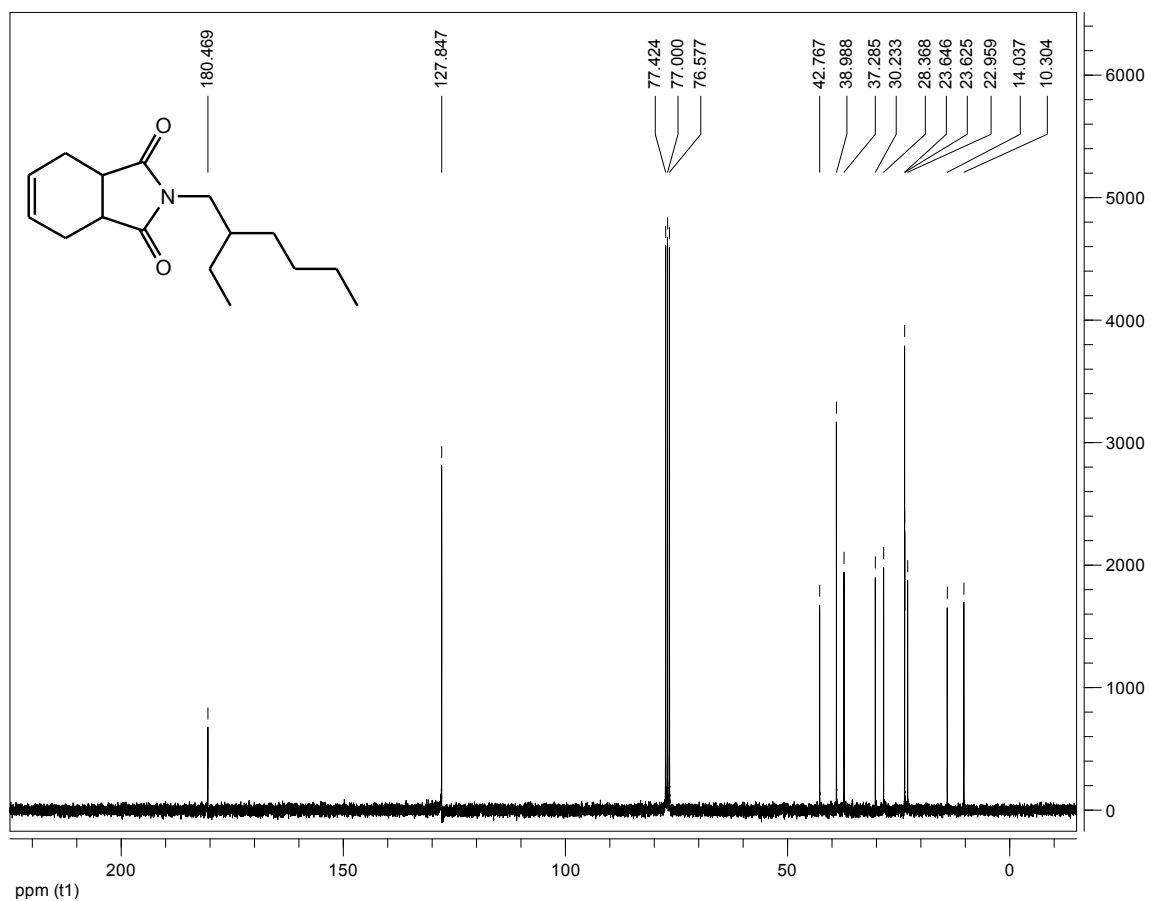


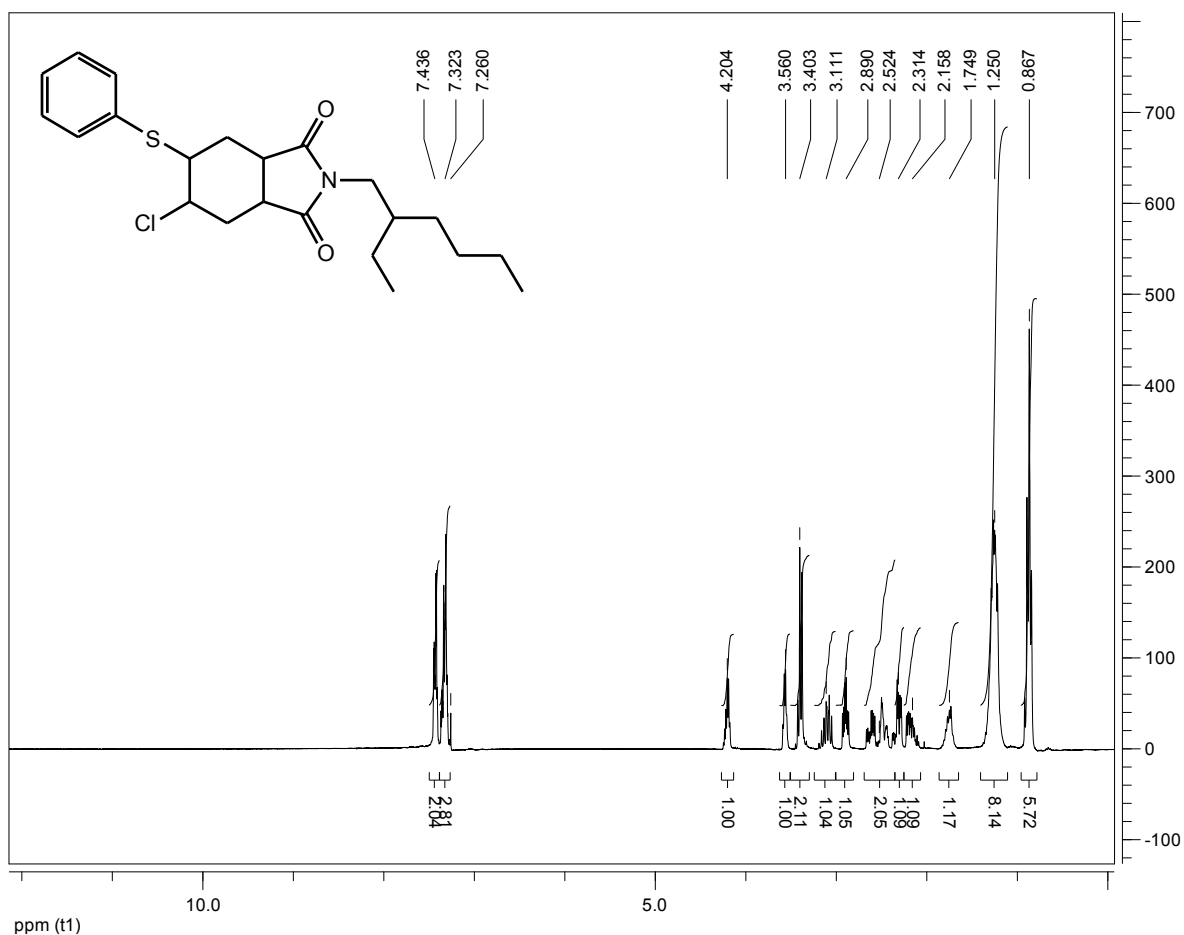


^1H NMR spectrum for **2b** in CDCl_3 .

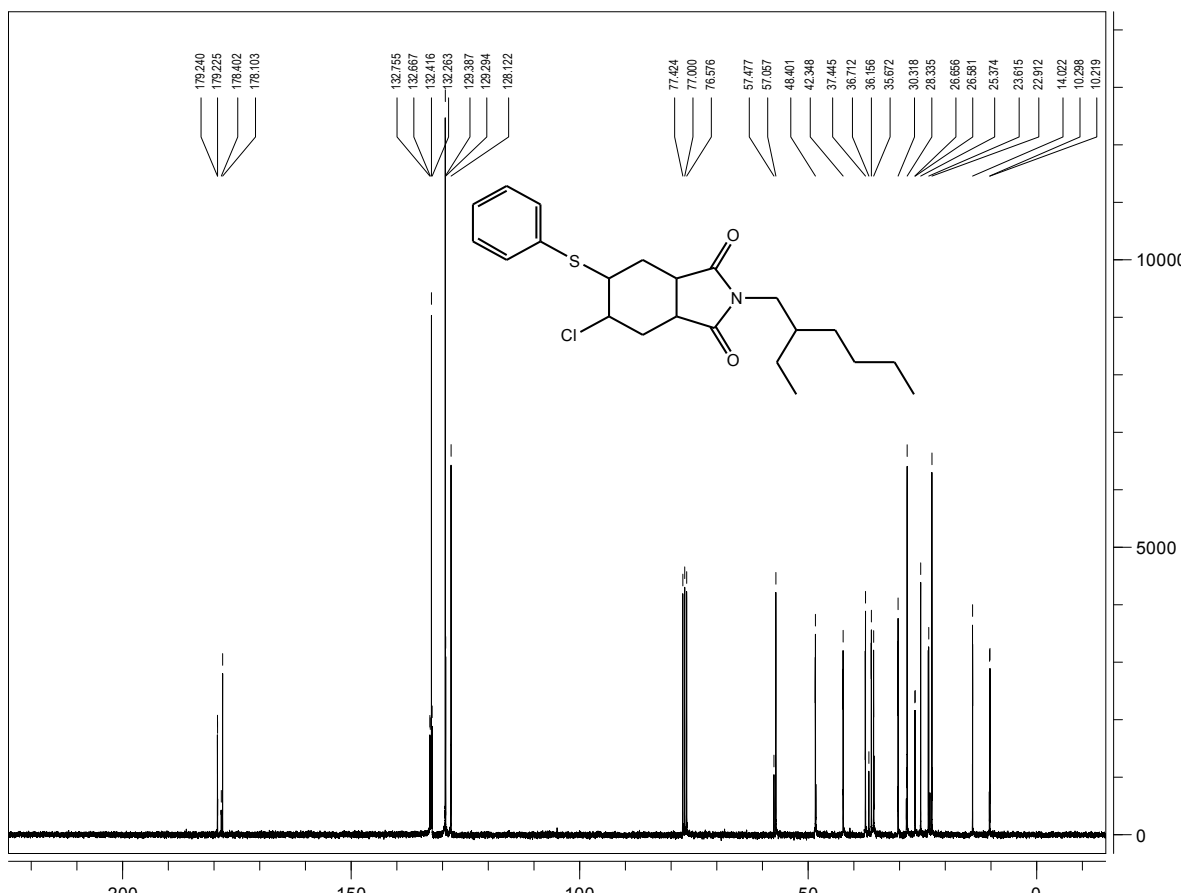


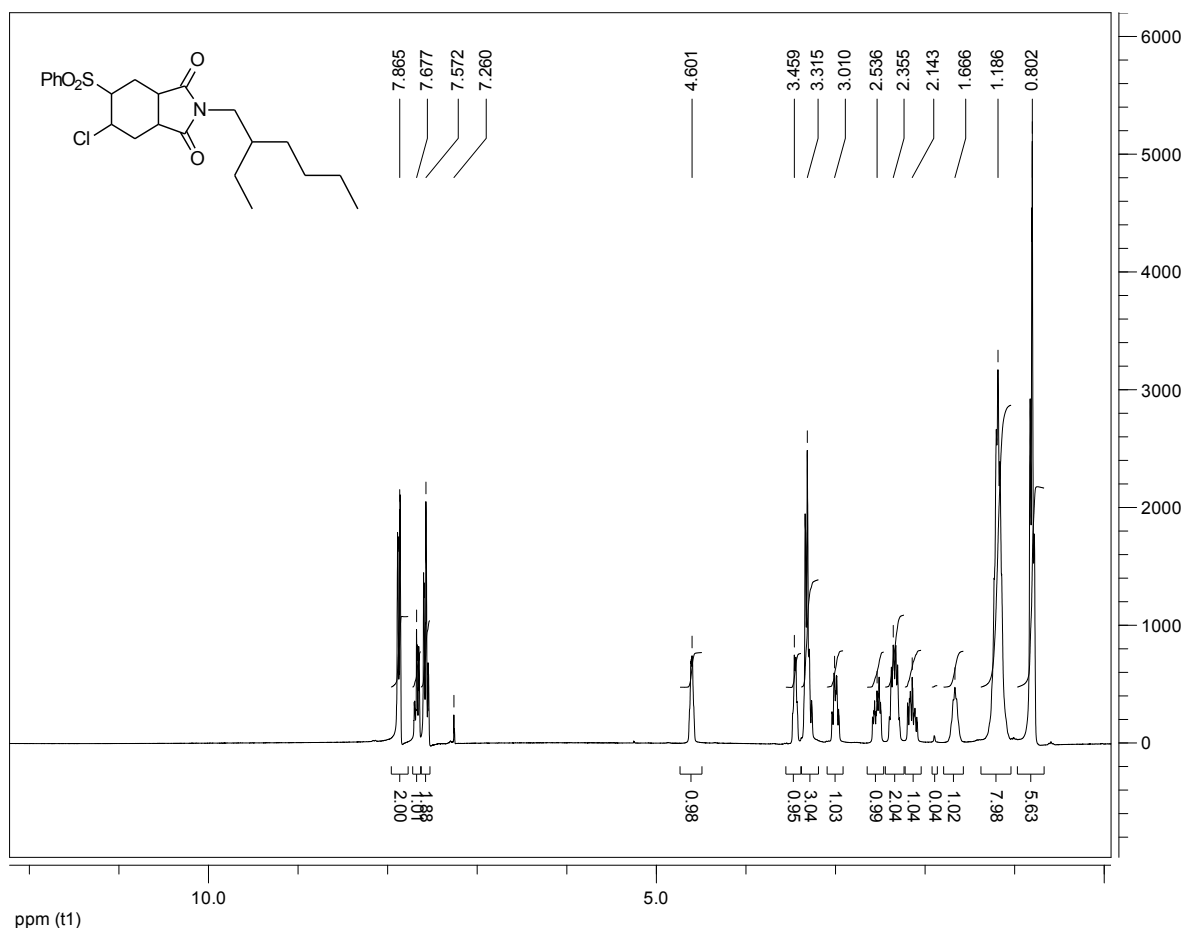
^1H NMR (top) and ^{13}C NMR (bottom) spectra for **2.1** in CDCl_3 .



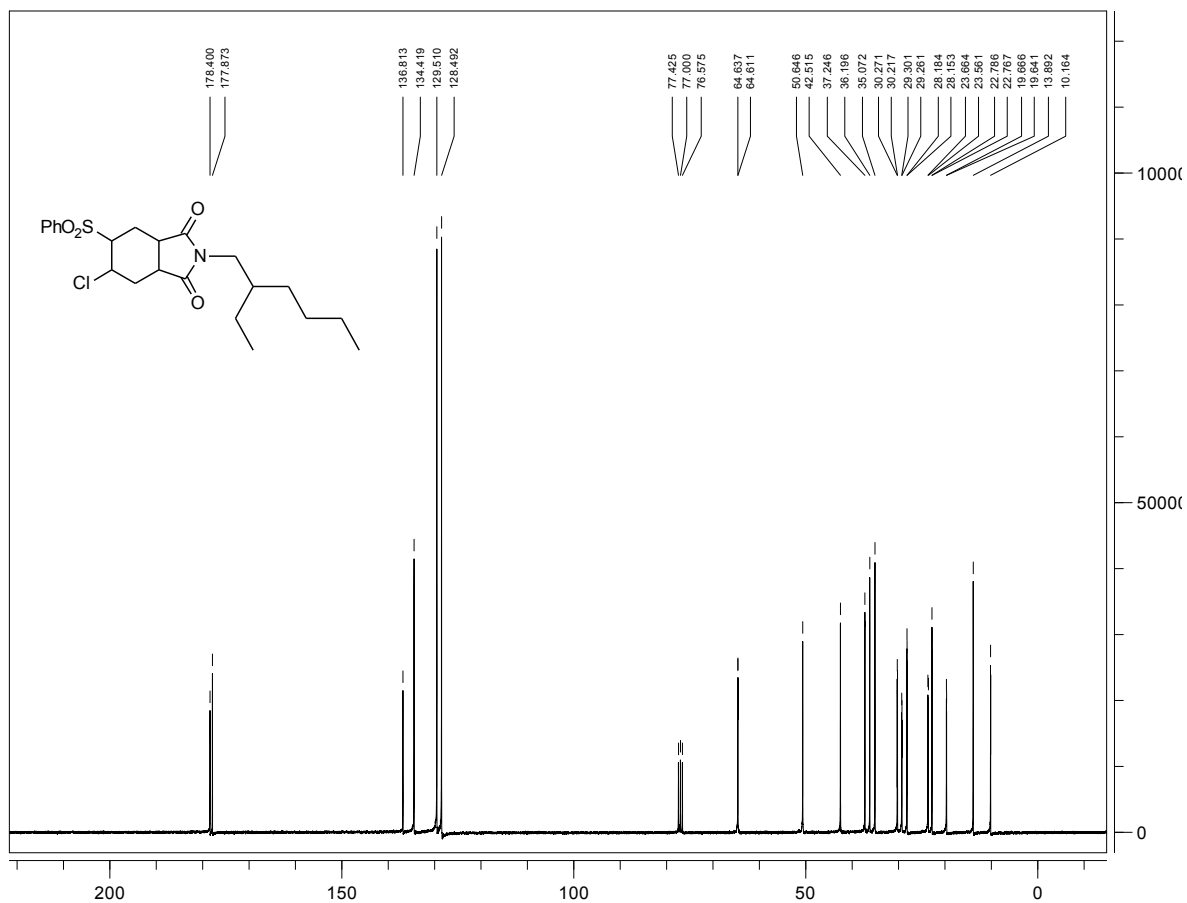


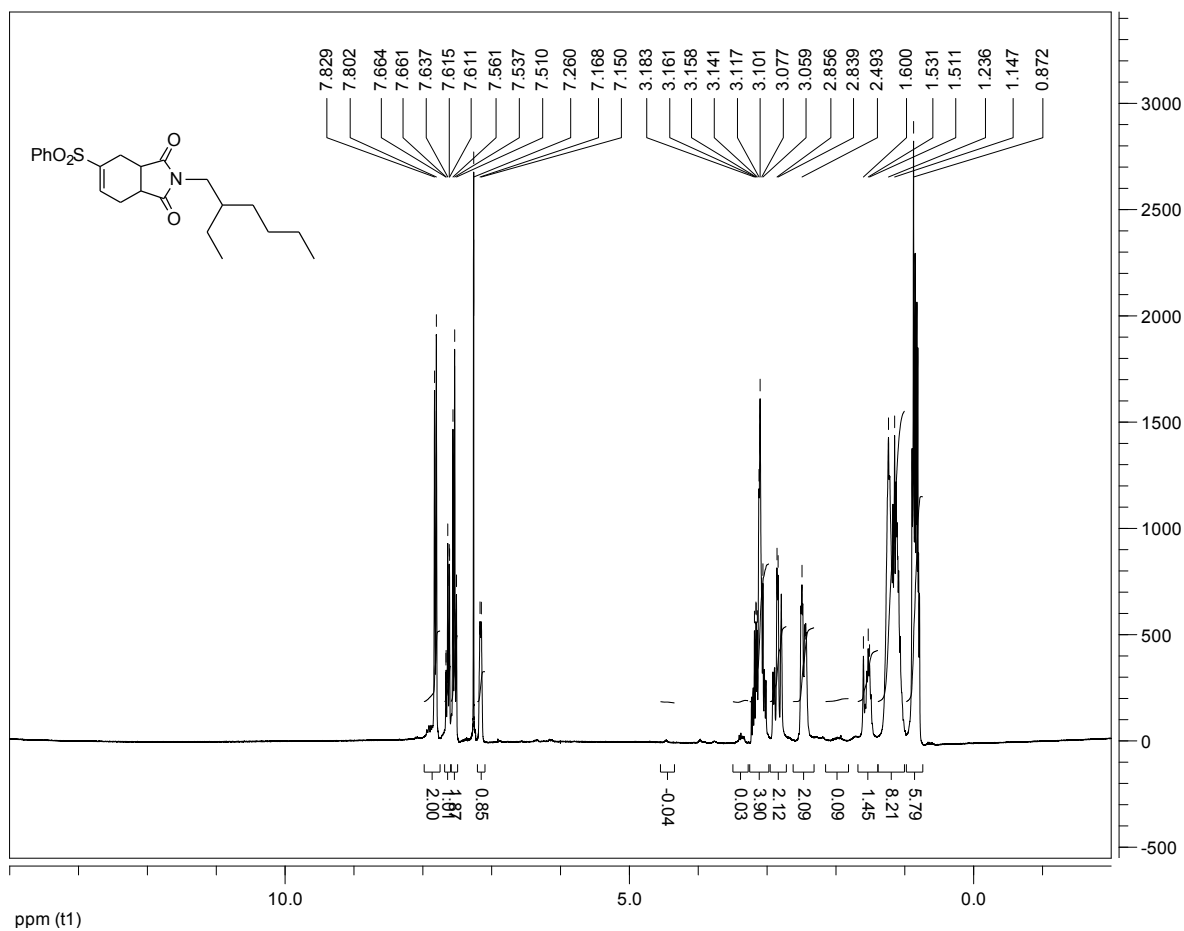
¹H NMR (top) and ¹³C NMR (bottom) spectra for 2.2 in CDCl₃.



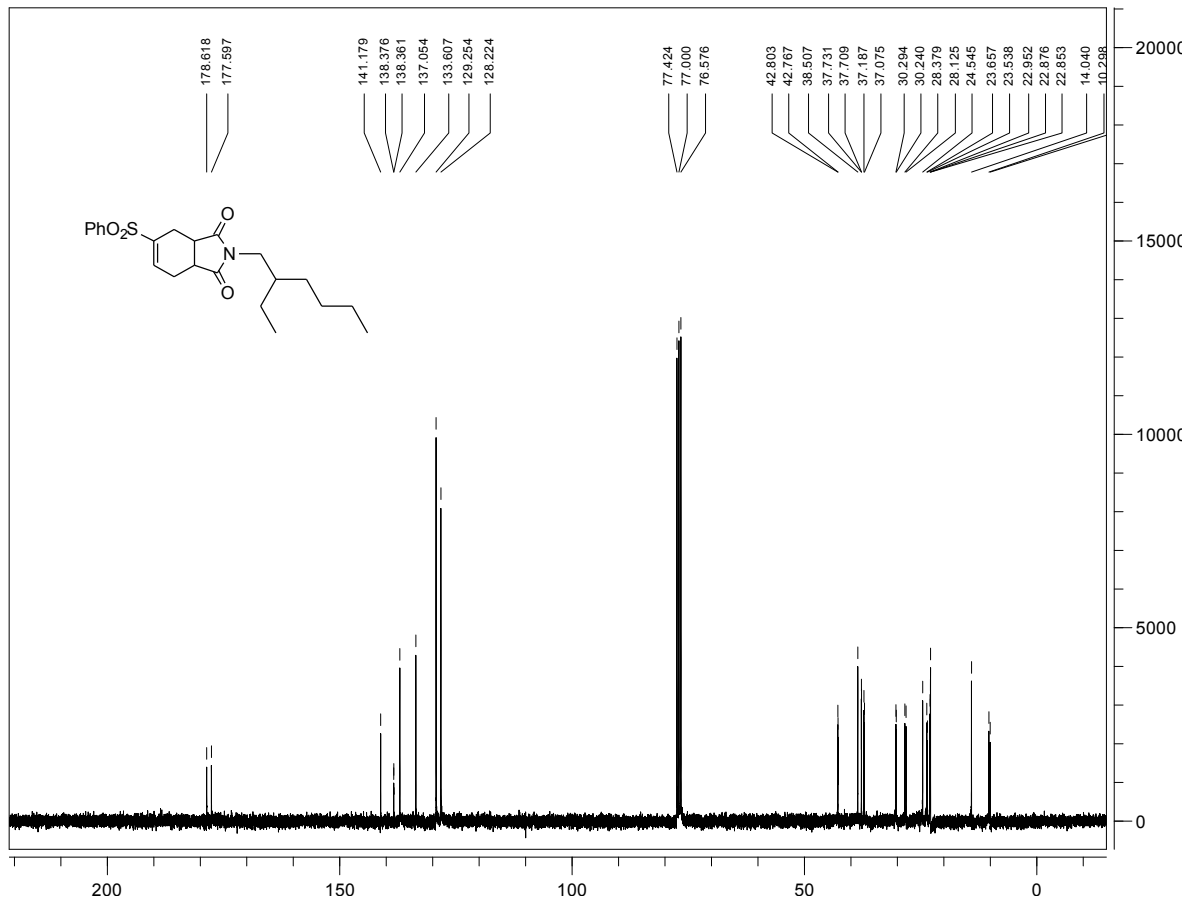


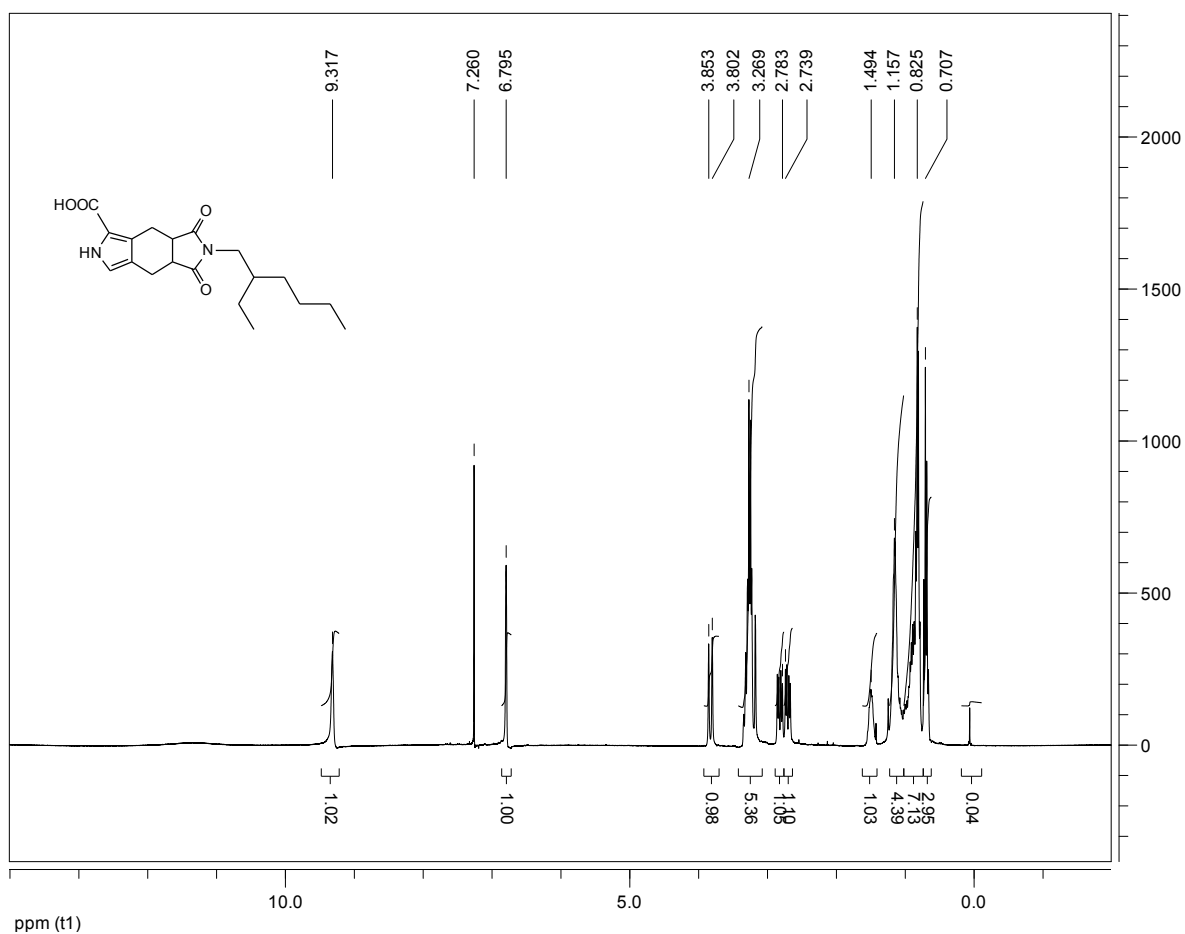
^1H NMR (top) and ^{13}C NMR (bottom) spectra for **2.3** in CDCl_3 .



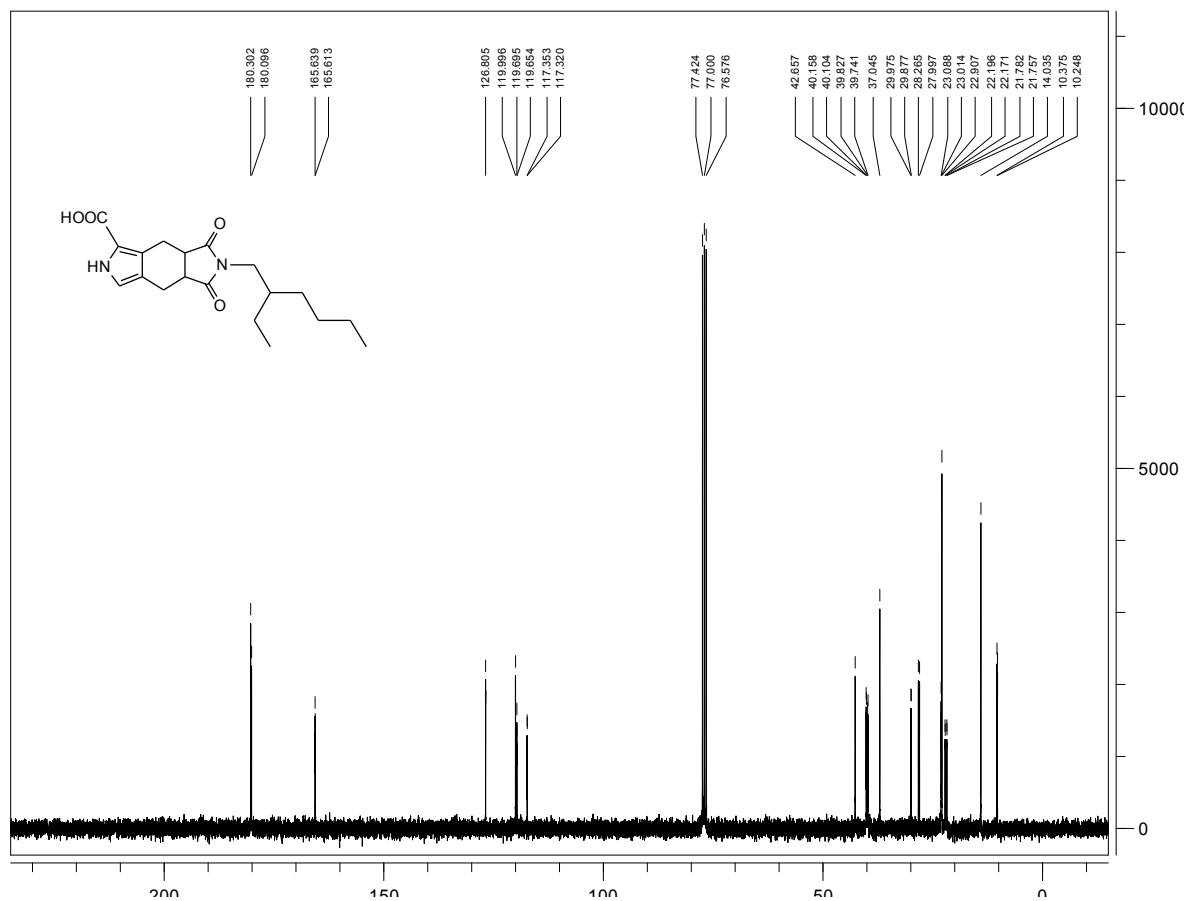


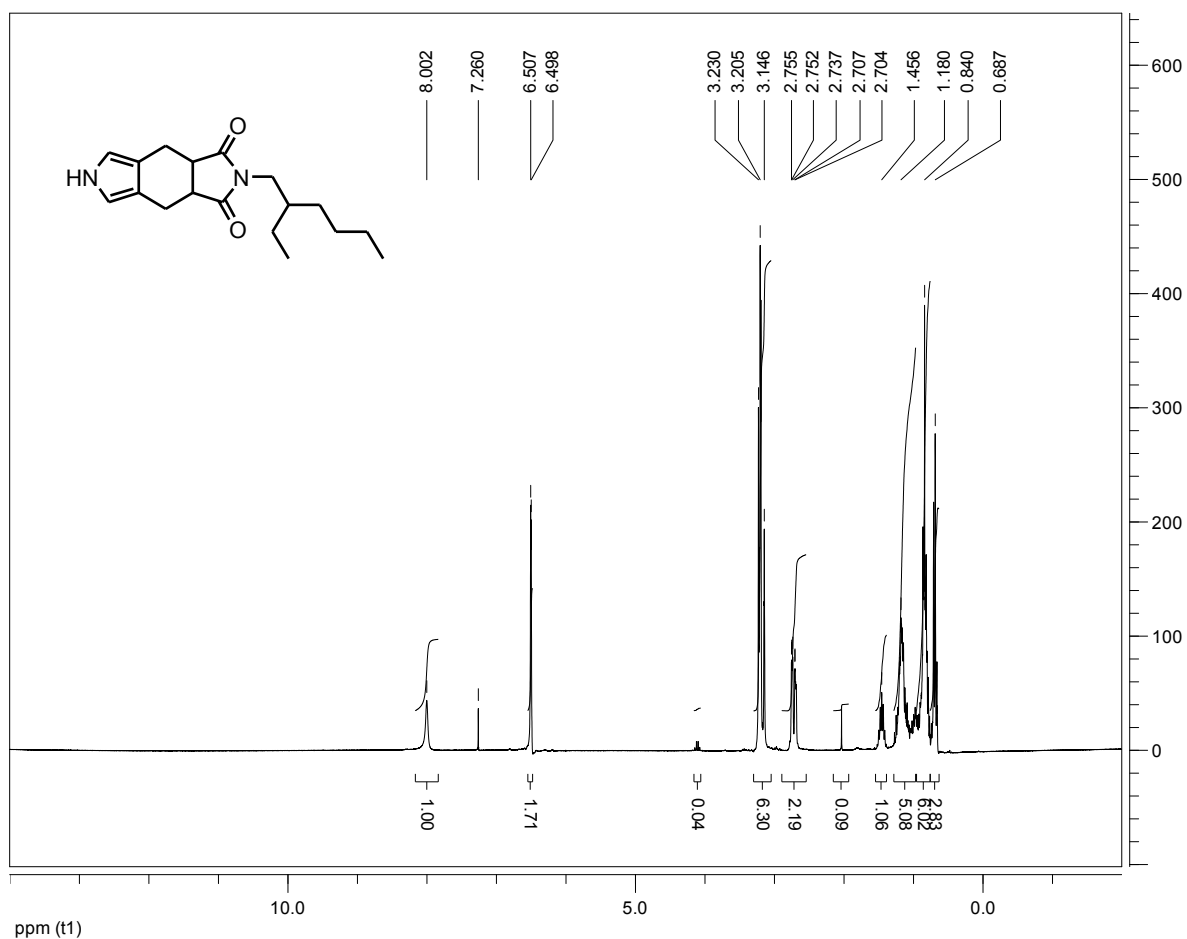
^1H NMR (top) and ^{13}C NMR (bottom) spectra for **2.4** in CDCl_3 .



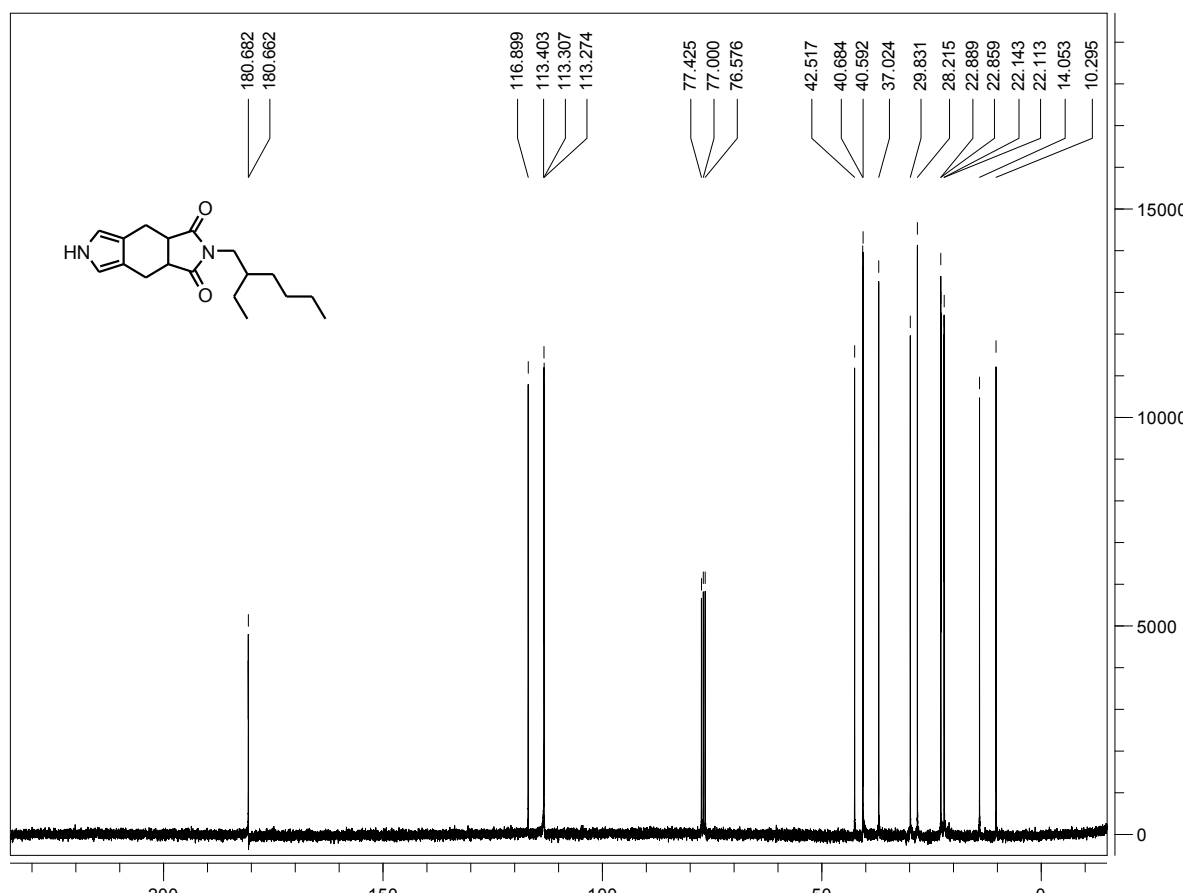


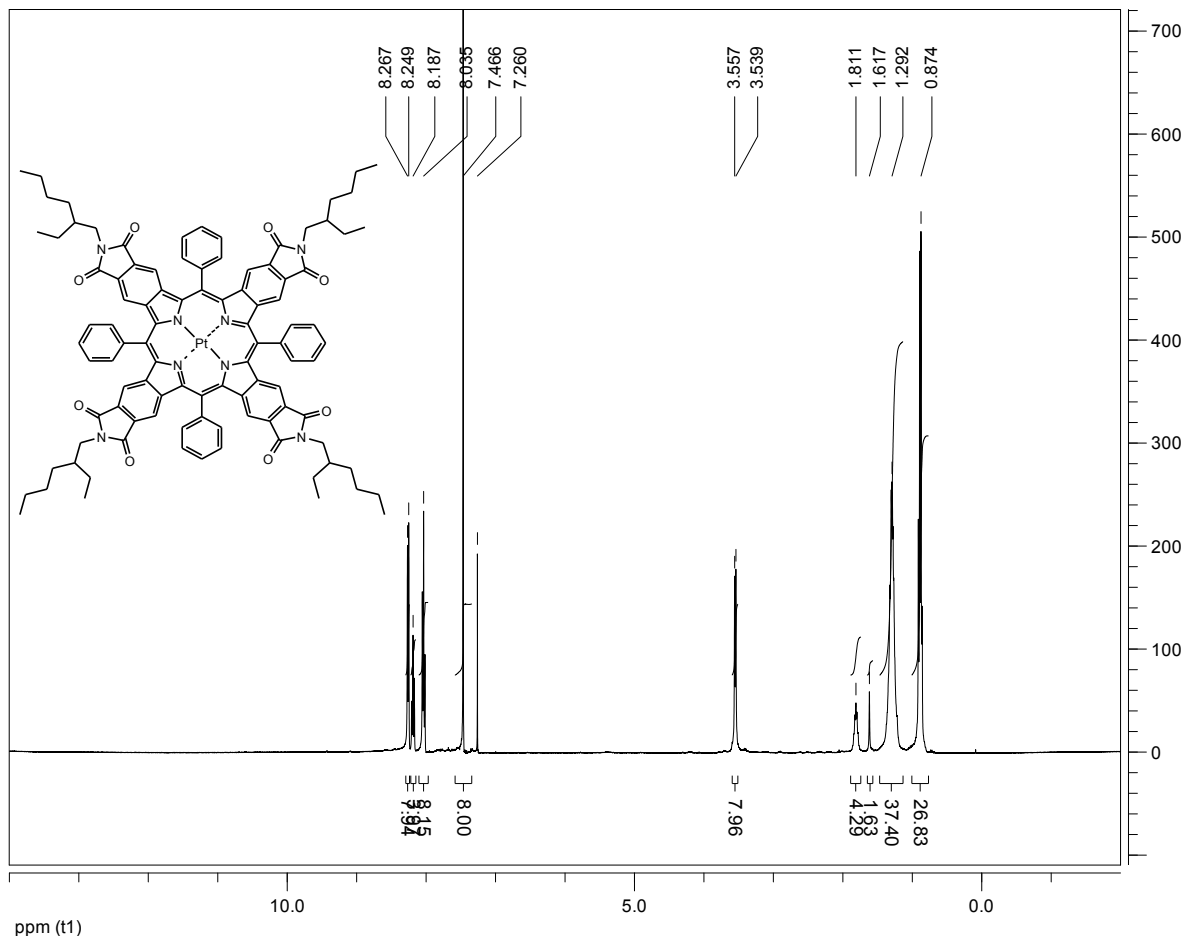
^1H NMR (top) and ^{13}C NMR (bottom) spectra for **2.6** in CDCl_3 .



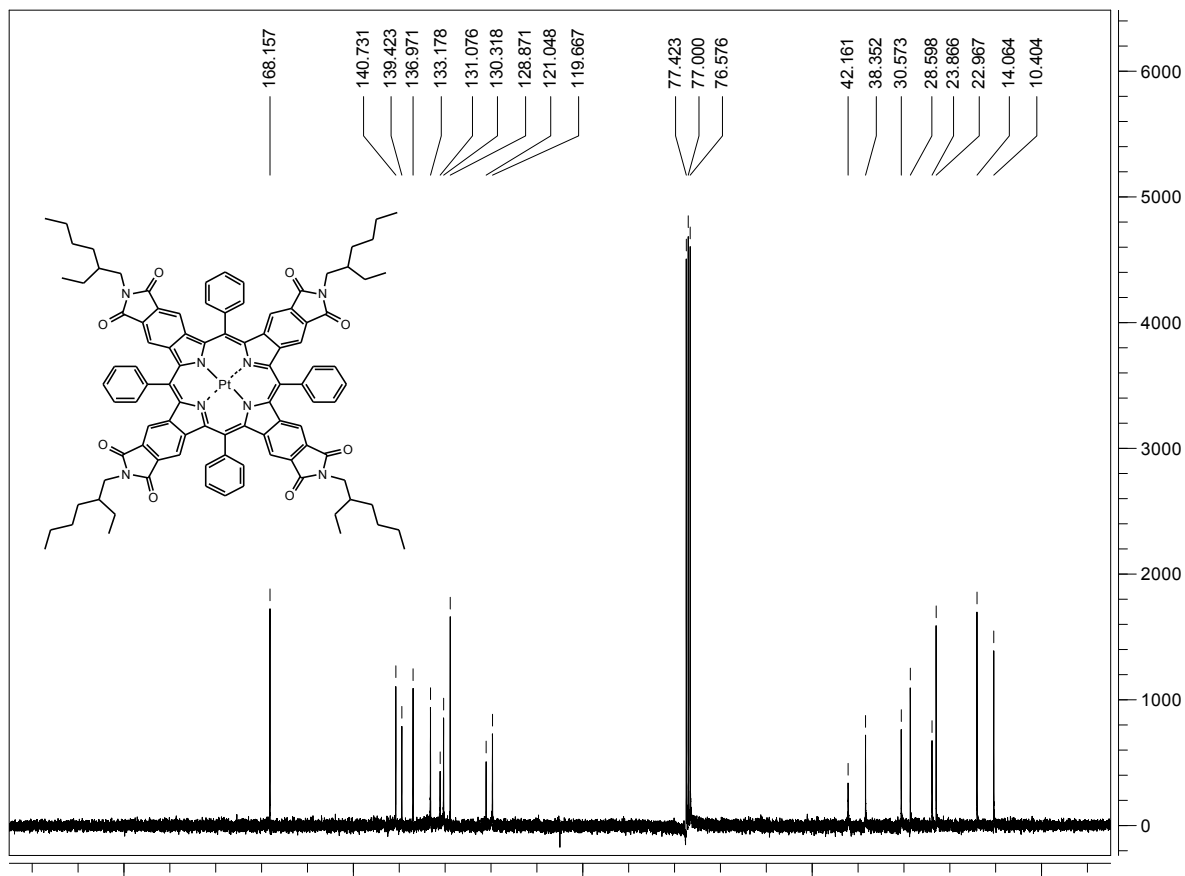


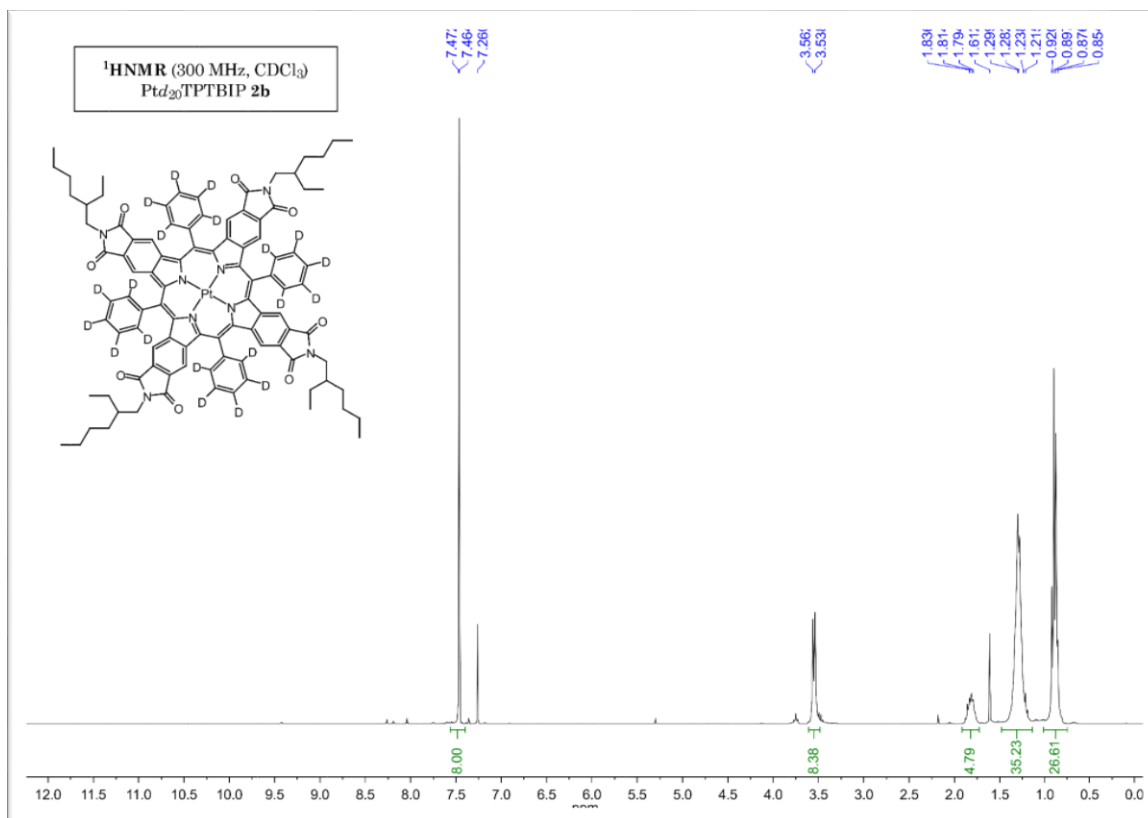
^1H NMR (top) and ^{13}C NMR (bottom) spectra for **2.7** in CDCl_3 .



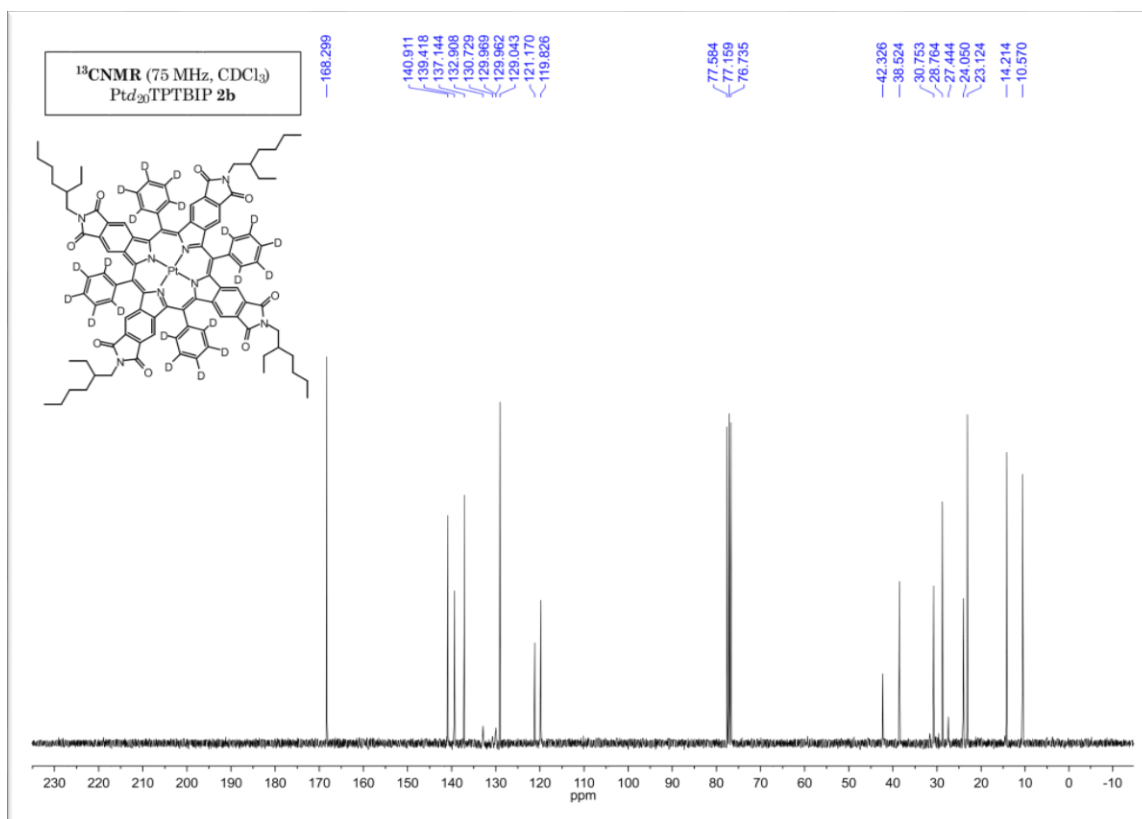


^1H NMR (top) and ^{13}C NMR (bottom) spectra for **2.9** in CDCl_3 .





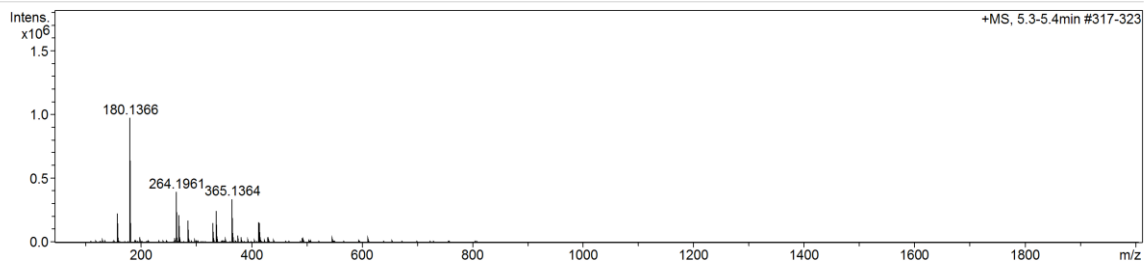
¹H NMR spectrum of **2.11** in CDCl₃.



¹³C NMR spectrum of **2.11** in CDCl₃.

Acquisition Parameter

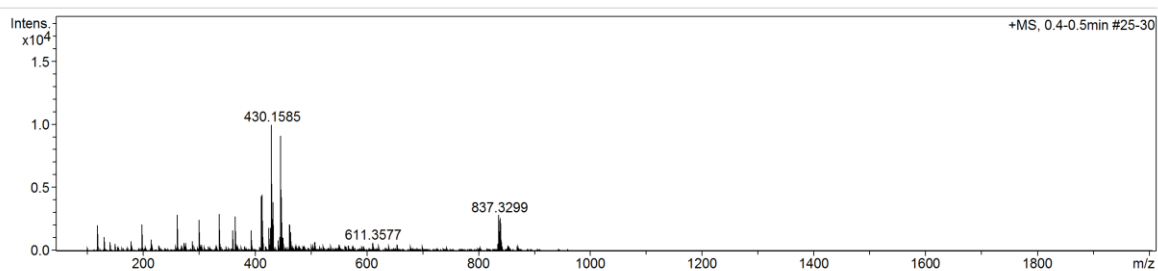
Source Type	ESI	Ion Polarity	Positive	Set Nebulizer	1.0 Bar
Focus	Active	Set Capillary	3000 V	Set Dry Heater	200 °C
Scan Begin	50 m/z	Set End Plate Offset	-500 V	Set Dry Gas	4.0 l/min
Scan End	2000 m/z	Set Collision Cell RF	600.0 Vpp	Set Divert Valve	Source



Meas. m/z	#	Ion Formula	m/z	err [ppm]	mSigma	Score	rdb	e ⁻ Conf	N-Rule
264.1961	1	C ₁₆ H ₂₆ NO ₂	264.1958	-1.2	3.1	100.00	4.5	even	ok
286.1782	1	C ₁₄ H ₂₀ N ₇	286.1775	-2.6	4.9	100.00	8.5	even	ok
	1	C ₁₆ H ₂₅ NNaO ₂	286.1777	-1.6	3.1	100.00	4.5	even	ok

HRMS spectrum of **2.1**.**Acquisition Parameter**

Source Type	ESI	Ion Polarity	Positive	Set Nebulizer	1.0 Bar
Focus	Active	Set Capillary	3000 V	Set Dry Heater	200 °C
Scan Begin	50 m/z	Set End Plate Offset	-500 V	Set Dry Gas	4.0 l/min
Scan End	2000 m/z	Set Collision Cell RF	600.0 Vpp	Set Divert Valve	Source

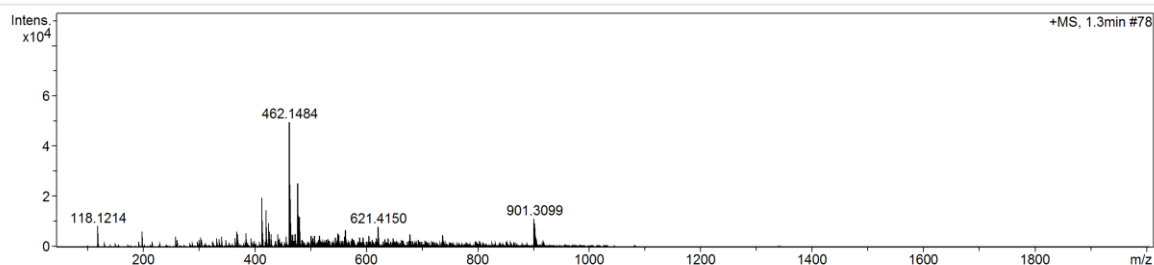


Meas. m/z	#	Ion Formula	m/z	err [ppm]	mSigma	Score	rdb	e ⁻ Conf	N-Rule
430.1585	1	C ₂₂ H ₃₀ CINNaO ₂ S	430.1578	-1.7	3.8	100.00	7.5	even	ok

HRMS spectrum of **2.2**.

Acquisition Parameter

Source Type	ESI	Ion Polarity	Positive	Set Nebulizer	1.0 Bar
Focus	Active	Set Capillary	3000 V	Set Dry Heater	200 °C
Scan Begin	50 m/z	Set End Plate Offset	-500 V	Set Dry Gas	4.0 l/min
Scan End	2000 m/z	Set Collision Cell RF	600.0 Vpp	Set Divert Valve	Source

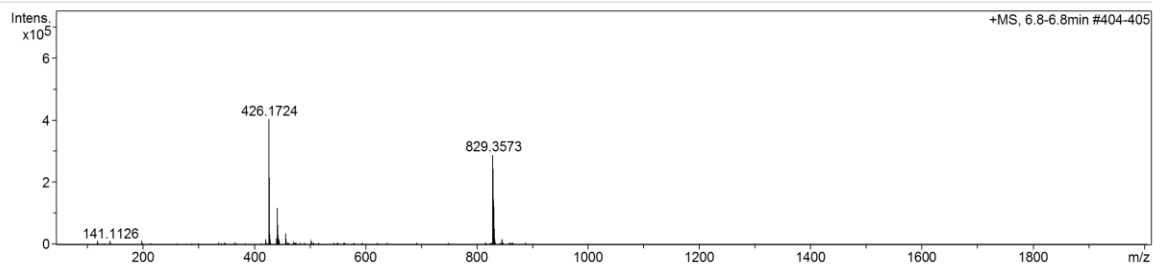


Meas. m/z	#	Ion Formula	m/z	err [ppm]	mSigma	Score	rdb	e ⁻ Conf	N-Rule
462.1484	1	C22H30ClNNaO4S	462.1476	-1.6	9.7	100.00	7.5	even	ok
	2	C17H31Cl2N5NaO2S	462.1468	-3.5	134.4	0.51	3.5	even	ok
478.1219	1	C22H30ClKNO4S	478.1216	-0.8	3.0	100.00	7.5	even	ok

HRMS spectrum of **2.3**.

Acquisition Parameter

Source Type	ESI	Ion Polarity	Positive	Set Nebulizer	1.0 Bar
Focus	Active	Set Capillary	3000 V	Set Dry Heater	200 °C
Scan Begin	50 m/z	Set End Plate Offset	-500 V	Set Dry Gas	4.0 l/min
Scan End	2000 m/z	Set Collision Cell RF	600.0 Vpp	Set Divert Valve	Source

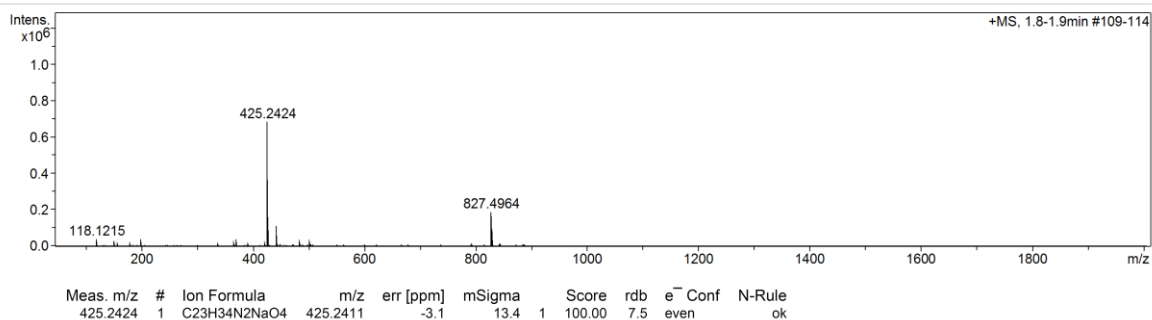


Meas. m/z	#	Ion Formula	m/z	err [ppm]	mSigma	Score	rdb	e ⁻ Conf	N-Rule
426.1724	1	C22H29NNaO4S	426.1710	-3.3	4.5	100.00	8.5	even	ok
442.1462	1	C22H29KNO4S	442.1449	-2.9	4.3	100.00	8.5	even	ok
	2	C19H33KNO4S2	442.1483	4.7	24.4	39.17	3.5	even	ok

¹H NMR spectrum of **2.4**.

Acquisition Parameter

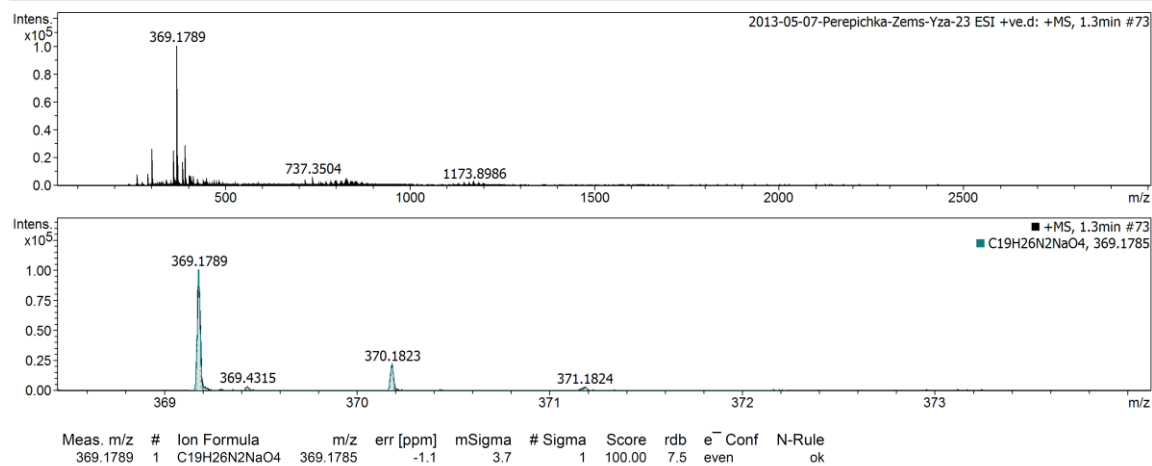
Source Type	ESI	Ion Polarity	Positive	Set Nebulizer	1.0 Bar
Focus	Active	Set Capillary	3000 V	Set Dry Heater	200 °C
Scan Begin	50 m/z	Set End Plate Offset	-500 V	Set Dry Gas	4.0 l/min
Scan End	2000 m/z	Set Collision Cell RF	600.0 Vpp	Set Divert Valve	Source



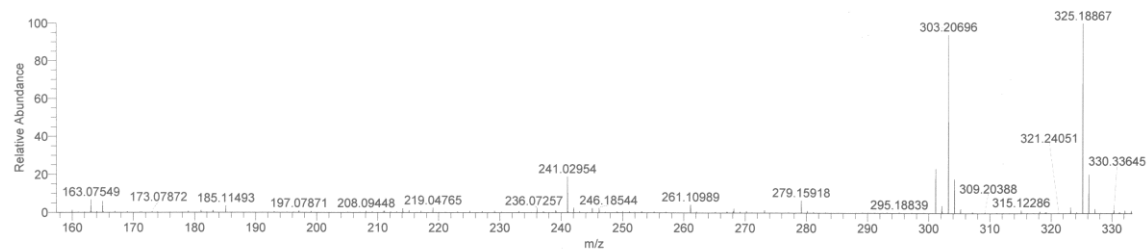
HRMS spectrum of 2.5.

Acquisition Parameter

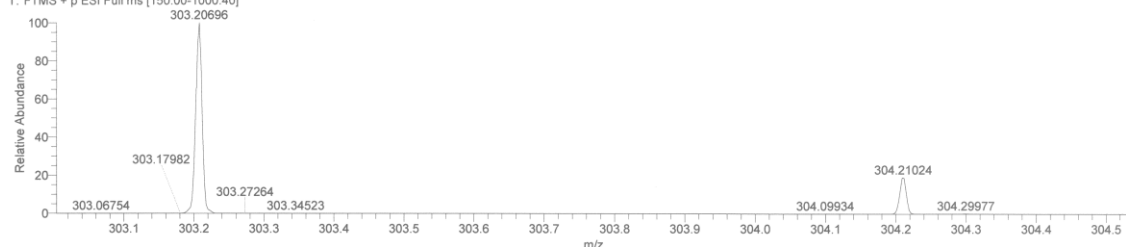
Source Type	ESI	Ion Polarity	Positive	Set Nebulizer	0.6 Bar
Focus	Active	Set Capillary	4500 V	Set Dry Heater	180 °C
Scan Begin	50 m/z	Set End Plate Offset	-500 V	Set Dry Gas	4.0 l/min
Scan End	3000 m/z	Set Collision Cell RF	1500.0 Vpp	Set Divert Valve	Source



HRMS spectrum of 2.6.



130503-HRESI02-Perepichka-yaroslav-YZa-24#238-245 RT: 0.56-0.58 AV: 8 NL: 8.55E7
T: FTMS + p ESI Full ms [150.00-1000.40]



130503-HRESI02-Perepichka-yaroslav-YZa-24#238-245 RT: 0.56-0.58 AV: 8

T: FTMS + p ESI Full ms [150.00-1000.40]

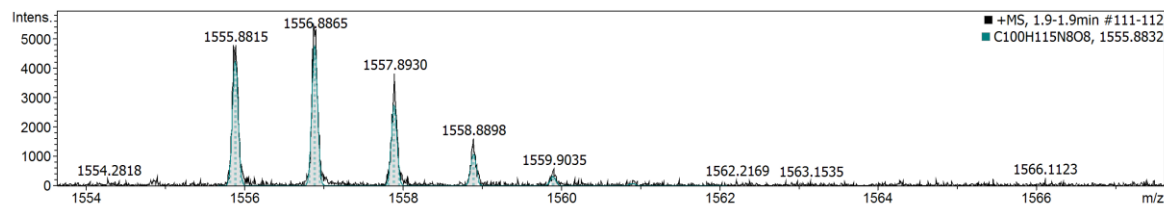
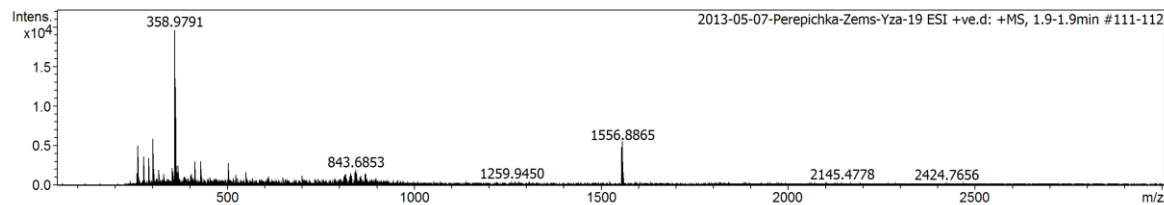
m/z = 303.18873-303.21720

m/z	Intensity	Relative	Resolution	Charge	Theo. Mass	Delta (ppm)	RDB equiv.	Composition
303.20696	85895848.0	100.00	30959.10	1.00	303.20670	0.86	6.5	C ₁₈ H ₂₇ O ₂ N ₂

HRMS spectrum of 2.7.

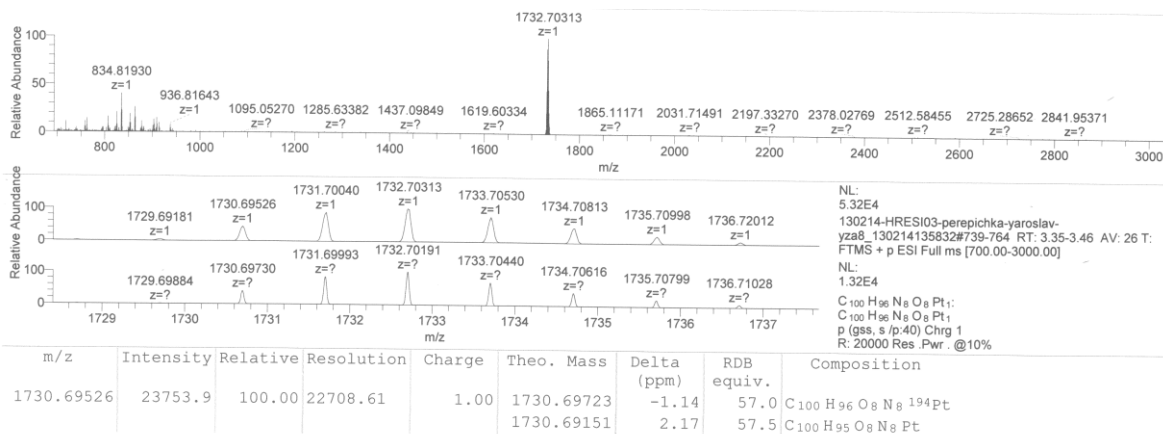
Acquisition Parameter

Source Type	ESI	Ion Polarity	Positive	Set Nebulizer	0.6 Bar
Focus	Active	Set Capillary	4500 V	Set Dry Heater	180 °C
Scan Begin	50 m/z	Set End Plate Offset	-500 V	Set Dry Gas	4.0 l/min
Scan End	3000 m/z	Set Collision Cell RF	1500.0 Vpp	Set Divert Valve	Source



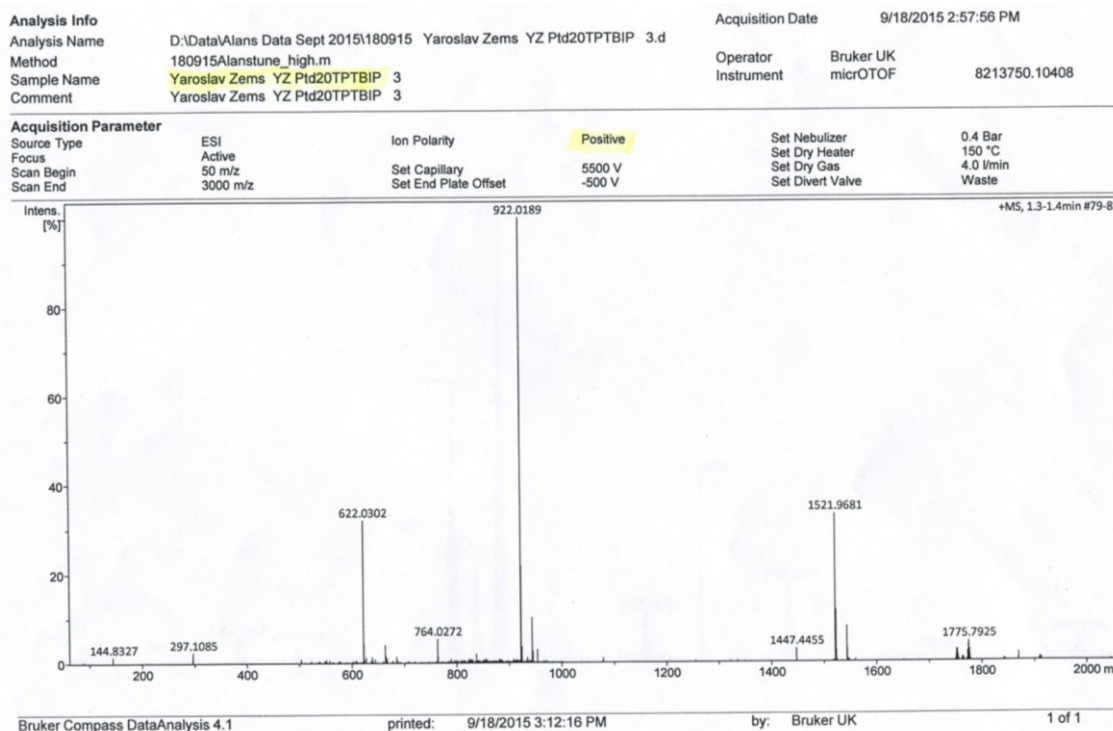
Meas. m/z	#	Ion Formula	m/z	err [ppm]	mSigma	# Sigma	Score	rdb	e ⁻ Conf	N-Rule
1555.8815	1	C100H115N8O8	1555.8832	-1.1	76.2	1	100.00	47.5	even	ok
1555.8832	1	C100H115N8O8	1555.8832	-1.1	76.2	1	100.00	47.5	even	ok

HRMS spectrum of 2.8.



m/z	Intensity	Relative	Resolution	Charge	Theo. Mass	Delta (ppm)	RDB equiv.	Composition
1731.70040	47646.5	100.00	22516.65	1.00	1731.69934	0.62	57.0	C ₁₀₀ H ₉₆ O ₈ N ₈ Pt

HRMS spectrum of 2.9.



HRMS of 2.11.

2.8 References

- (1) Zems, Y.; Moiseev, A. G.; Perepichka, D. F. Convenient Synthesis of a Highly Soluble and Stable Phosphorescent Platinum Porphyrin Dye *Org. Lett.* **2013**, *15*, 5330.
- (2) Moss, G. P. Nomenclature of tetrapyrroles. Recommendations 1986 *Eur. J. Biochem.* **1988**, *178*, 277.
- (3) Cheprakov, A. V. In *58 The Synthesis of π -Extended Porphyrins*; World Scientific Publishing Company: **2012**, p 1.
- (4) Lash, T. D. Modification of the porphyrin chromophore by ring fusion: identifying trends due to annelation of the porphyrin nucleus *J. Porphyr. Phthalocya.* **2001**, *5*, 267.
- (5) Sommer, J. R.; Shelton, A. H.; Parthasarathy, A.; Ghiviriga, I.; Reynolds, J. R.; Schanze, K. S. Photophysical Properties of Near-Infrared Phosphorescent π -Extended Platinum Porphyrins *Chem. Mater.* **2011**, *23*, 5296.
- (6) Gouterman, M. Spectra of porphyrins *J. Mol. Spectrosc.* **1961**, *6*, 138.
- (7) Gouterman, M.; Wagniere, G.; Snyder, L. C. Spectra of porphyrins. II. Four-orbital model *J. Mol. Spectrosc.* **1963**, *11*, 108.
- (8) Clar, E. in *The Aromatic Sextet*; Wiley, 1972
- (9) Qu, Z.; Zhang, D.; Liu, C.; Jiang, Y. Open-Shell Ground State of Polyacenes: A Valence Bond Study *J. Phys. Chem. A* **2009**, *113*, 7909.
- (10) Suresh, C. H.; Gadre, S. R. Clar's Aromatic Sextet Theory Revisited via Molecular Electrostatic Potential Topography *J. Org. Chem.* **1999**, *64*, 2505.
- (11) Finikova, O. S.; Cheprakov, A. V.; Carroll, P. J.; Dalosto, S.; Vinogradov, S. A. Influence of Nonplanarity and Extended Conjugation on Porphyrin Basicity *Inorg. Chem.* **2002**, *41*, 6944.
- (12) Cheng, R.-J.; Lin, S.-H.; Mo, H.-M. Spectroscopic and Oxidation Studies of meso-Tetraphenyltetrabenzoporphyrin Carbonyl Complexes of Ruthenium(II): CO as the Probe to Elucidate the Bonding Characteristics of Porphyrins *Organometallics* **1997**, *16*, 2121.
- (13) Filatov, M. A.; Senge, M. O. Molecular devices based on reversible singlet oxygen binding in optical and photomedical applications *Molecular Systems Design & Engineering* **2016**, *1*, 258.
- (14) Kobayashi, N.; Nevin, W. A.; Mizunuma, S.; Awaji, H.; Yamaguchi, M. Ring-expanded porphyrins as an approach towards highly conductive molecular semiconductors *Chem. Phys. Lett.* **1993**, *205*, 51.
- (15) Filatov, M. A.; Balushev, S.; Ilieva, I. Z.; Enkelmann, V.; Miteva, T.; Landfester, K.; Aleshchenkov, S. E.; Cheprakov, A. V. Tetraaryltetraanthra[2,3]porphyrins: synthesis, structure, and optical properties *J. Org. Chem.* **2012**, *77*, 11119.
- (16) Filatov, M. A.; Heinrich, E.; Busko, D.; Ilieva, I. Z.; Landfester, K.; Balushev, S. Reversible oxygen addition on a triplet sensitizer molecule: protection from excited state depopulation *Phys. Chem. Chem. Phys.* **2015**, *17*, 6501.
- (17) Filatov, M. A.; Balushev, S.; Landfester, K. Protection of densely populated excited triplet state ensembles against deactivation by molecular oxygen *Chem. Soc. Rev.* **2016**, *45*, 4668.
- (18) Gentemann, S.; Medforth, C. J.; Forsyth, T. P.; Nurco, D. J.; Smith, K. M.; Fajer, J.; Holten, D. Photophysical Properties of Conformationally Distorted Metal-Free Porphyrins. Investigation into the Deactivation Mechanisms of the Lowest Excited Singlet State *J. Am. Chem. Soc.* **1994**, *116*, 7363.

- (19) Senge, M. O.; Kalisch, W. W. Synthesis and Structural Characterization of Nonplanar Tetraphenylporphyrins and Their Metal Complexes with Graded Degrees of β -Ethyl Substitution *Inorg. Chem.* **1997**, *36*, 6103.
- (20) Finikova, O. S.; Cheprakov, A. V.; Vinogradov, S. A. Synthesis and luminescence of soluble meso-unsubstituted tetrabenz- and tetranaphtho[2,3]porphyrins *J. Org. Chem.* **2005**, *70*, 9562.
- (21) Finikova, O. S.; Cheprakov, A. V.; Beletskaya, I. P.; Carroll, P. J.; Vinogradov, S. A. Novel Versatile Synthesis of Substituted Tetrabenzoporphyrins *J. Org. Chem.* **2004**, *69*, 522.
- (22) Sundberg, R. J.; Elsevier: 1996; Vol. 2, p 119.
- (23) Novak, B. H.; Lash, T. D. Porphyrins with Exocyclic Rings. 11. Synthesis and Characterization of Phenanthroporphyrins, a New Class of Modified Porphyrin Chromophores *J. Org. Chem.* **1998**, *63*, 3998.
- (24) Lash, T. D.; Novak, B. H. Porphyrins with exocyclic rings. Part 6. Tetraphenanthro[9,10-b:9,10-g:9,10-l:9,10-q]porphyrin, a new highly conjugated porphyrin system *Angew. Chem., Int. Ed. Engl.* **1995**, *34*, 683.
- (25) Lash, T. D.; Lin, Y.; Novak, B. H.; Parikh, M. D. Porphyrins with exocyclic rings. Part 19: Efficient syntheses of phenanthrolineporphyrins *Tetrahedron* **2005**, *61*, 11601.
- (26) Currie, M. J.; Mapel, J. K.; Heidel, T. D.; Goffri, S.; Baldo, M. A. High-Efficiency Organic Solar Concentrators for Photovoltaics *Science* **2008**, *321*, 226.
- (27) Sun, Y.; Borek, C.; Hanson, K.; Djurovich, P. I.; Thompson, M. E.; Brooks, J.; Brown, J. J.; Forrest, S. R. Photophysics of Pt-porphyrin electrophosphorescent devices emitting in the near infrared *Appl. Phys. Lett.* **2007**, *90*, 213503/1.
- (28) Borek, C.; Hanson, K.; Djurovich, P. I.; Thompson, M. E.; Aznavour, K.; Bau, R.; Sun, Y.; Forrest, S. R.; Brooks, J.; Michalski, L.; Brown, J. Highly efficient, near-infrared electrophosphorescence from a Pt-metalloporphyrin complex *Angew. Chem., Int. Ed.* **2007**, *46*, 1109.
- (29) Borisov, S. M.; Nuss, G.; Haas, W.; Saf, R.; Schmuck, M.; Klimant, I. New NIR-emitting complexes of platinum(II) and palladium(II) with fluorinated benzoporphyrins *J. Photochem. Photobiol., A* **2009**, *201*, 128.
- (30) Sommer, J. R.; Farley, R. T.; Graham, K. R.; Yang, Y.; Reynolds, J. R.; Xue, J.; Schanze, K. S. Efficient Near-Infrared Polymer and Organic Light-Emitting Diodes Based on Electrophosphorescence from (Tetraphenyltetranaphtho[2,3]porphyrin)platinum(II) *ACS Appl. Mater. Interfaces* **2009**, *1*, 274.
- (31) Yamada, H.; Kuzuhara, D.; Takahashi, T.; Shimizu, Y.; Uota, K.; Okujima, T.; Uno, H.; Ono, N. Synthesis and Characterization of Tetraanthroporphyrins *Org. Lett.* **2008**, *10*, 2947.
- (32) Miteva, T.; Yakutkin, V.; Nelles, G.; Balushev, S. Annihilation assisted upconversion: all-organic, flexible and transparent multicolour display *New J. Phys.* **2008**, *10*, No pp. given.
- (33) Rietveld, I. B.; Kim, E.; Vinogradov, S. A. Dendrimers with tetrabenzoporphyrin cores: near infrared phosphors for in vivo oxygen imaging *Tetrahedron* **2003**, *59*, 3821.
- (34) Esipova, T. V.; Karagodov, A.; Miller, J.; Wilson, D. F.; Busch, T. M.; Vinogradov, S. A. Two New "Protected" Oxyphors for Biological Oximetry: Properties and Application in Tumor Imaging *Anal. Chem.* **2011**, *83*, 8756.
- (35) Yakutkin, V.; Filatov, M. A.; Ilieva, I. Z.; Landfester, K.; Miteva, T.; Balushev, S. Upconverting the IR-A Range of the Sun Spectrum using Palladium Tetraaryl tetraanthra[2,3]porphyrins *Photochem. Photobiol. Sci.* **2015**, Ahead of Print.
- (36) Wohnhaas, C.; Mailaender, V.; Droege, M.; Filatov, M. A.; Busko, D.; Avlasevich, Y.; Balushev, S.; Miteva, T.; Landfester, K.; Turshatov, A. Triplet-Triplet Annihilation

- Upconversion Based Nanocapsules for Bioimaging Under Excitation by Red and Deep-Red Light *Macromol. Biosci.* **2013**, *13*, 1422.
- (37) Deng, F.; Sommer, J. R.; Myahkostupov, M.; Schanze, K. S.; Castellano, F. N. Near-IR phosphorescent metalloporphyrin as a photochemical upconversion sensitizer *Chem. Commun.* **2013**, *49*, 7406.
- (38) Cui, X.; Zhao, J.; Yang, P.; Sun, J. Zinc(II) tetraphenyltetrabenzoporphyrin complex as triplet photosensitizer for triplet-triplet annihilation upconversion *Chem. Commun.* **2013**, *49*, 10221.
- (39) Danos, A.; MacQueen, R. W.; Cheng, Y. Y.; Dvořák, M.; Darwish, T. A.; McCamey, D. R.; Schmidt, T. W. Deuteration of Perylene Enhances Photochemical Upconversion Efficiency *J. Phys. Chem. Lett.* **2015**, *6*, 3061.
- (40) Zhao, J.; Ji, S.; Guo, H. Triplet-triplet annihilation based upconversion: from triplet sensitizers and triplet acceptors to upconversion quantum yields *RSC Adv.* **2011**, *1*, 937.
- (41) Ito, S.; Murashima, T.; Ono, N.; Uno, H. A new synthesis of benzoporphyrins using 4,7-dihydro-4,7-ethano-2H-isoindole as a synthon of isoindole *Chem. Commun.* **1998**, 1661.
- (42) Ito, S.; Murashima, T.; Ono, N. A new synthesis of pyrroles fused with polycyclic skeletons *J. Chem. Soc., Perkin Trans. 1* **1997**, 3161.
- (43) Finikova, O.; Cheprakov, A.; Beletskaya, I.; Vinogradov, S. An expedient synthesis of substituted tetraaryltetrabenzoporphyrins *Chem. Commun.* **2001**, 261.
- (44) Finikova, O. S.; Cheprakov, A. V.; Vinogradov, S. A. Synthesis and Luminescence of Soluble meso-Unsubstituted Tetrabenzo- and Tetranaphtho[2,3]porphyrins *J. Org. Chem.* **2005**, *70*, 9562.
- (45) Filatov, M. A.; Cheprakov, A. V.; Beletskaya, I. P. A Facile and Reliable Method for the Synthesis of Tetrabenzoporphyrin from 4,7-Dihydroisoindole *Eur. J. Org. Chem.* **2007**, *2007*, 3468.
- (46) Segura, J. L.; Martin, N. o-Quinodimethanes: Efficient Intermediates in Organic Synthesis *Chem. Rev.* **1999**, *99*, 3199.
- (47) Vicente, M. G. H.; Tome, A. C.; Walter, A.; Cavaleiro, J. A. S. Synthesis and cycloaddition reactions of pyrrole-fused 3-sulfolenes: a new versatile route to tetrabenzoporphyrins *Tetrahedron Lett.* **1997**, *38*, 3639.
- (48) Johnstone, K. D.; Pearce, W. A.; Pyke, S. M. Porphyrin building blocks: Using a modified Barton-Zard approach to construct annulated pyrroles *J. Porphyr. Phthalocya.* **2002**, *6*, 661.
- (49) Ando, K.; Kankake, M.; Suzuki, T.; Takayama, H. New building blocks, 3,5-dihydro-1H-thieno-3,4-c]pyrrole 2,2-dioxides; preparation and their Diels-Alder reaction with dimethyl acetylenedicarboxylate *Tetrahedron* **1995**, *51*, 129.
- (50) Rieder, A.; Kraeutler, B. Loading a Porphyrin with Fullerene Units *J. Am. Chem. Soc.* **2000**, *122*, 9050.
- (51) Jiang, L.; Zaenglein, R. A.; Engle, J. T.; Mittal, C.; Hartley, C. S.; Ziegler, C. J.; Wang, H. Water-soluble ionic benzoporphyrins *Chem. Commun.* **2012**, *48*, 6927.
- (52) Carvalho, C. M. B.; Brocksom, T. J.; Thiago, d. O. K. Tetrabenzoporphyrins: synthetic developments and applications *Chem. Soc. Rev.* **2013**, *42*, 3302.
- (53) Ono, N.; Yamada, H.; Okujima, T. In *7 Synthesis of Porphyrins Fused with Aromatic Rings*; World Scientific Publishing Company: **2012**, p 1.
- (54) Meduna, V.; Sawlewicz, P.; Vogt, R. N-Formylglycine tert-butyl ester *Synth. Commun.* **1989**, *19*, 1487.
- (55) Lindsey, J. S.; Schreiman, I. C.; Hsu, H. C.; Kearney, P. C.; Marguerettaz, A. M. Rothmund and Adler-Longo reactions revisited: synthesis of tetraphenylporphyrins under equilibrium conditions *J. Org. Chem.* **1987**, *52*, 827.

- (56) Schmidbauer, S.; Hohenleutner, A.; Koenig, B. Chemical Degradation in Organic Light-Emitting Devices: Mechanisms and Implications for the Design of New Materials *Adv. Mater.* **2013**, *25*, 2114.
- (57) Residual degradation (3%) is likely due to slow penetration of oxygen into the flask over 6 days.
- (58) Lebedev, A. Y.; Filatov, M. A.; Cheprakov, A. V.; Vinogradov, S. A. Effects of Structural Deformations on Optical Properties of Tetrabenzoporphyrins: Free-Bases and Pd Complexes *J. Phys. Chem. A* **2008**, *112*, 7723.
- (59) Jentzen, W.; Ma, J.-G.; Shelnut, J. A. Conservation of the conformation of the porphyrin macrocycle in hemoproteins *Biophys. J.* **1998**, *74*, 753.
- (60) Sazanovich, I. V.; Galievsky, V. A.; van Hoek, A.; Schaafsma, T. J.; Malinovskii, V. L.; Holten, D.; Chirvony, V. S. Photophysical and Structural Properties of Saddle-Shaped Free Base Porphyrins: Evidence for an "Orthogonal" Dipole Moment *J. Phys. Chem. B* **2001**, *105*, 7818.
- (61) Gentemann, S.; Medforth, C. J.; Forsyth, T. P.; Nurco, D. J.; Smith, K. M.; Fajer, J.; Holten, D. Photophysical Properties of Conformationally Distorted Metal-Free Porphyrins. Investigation into the Deactivation Mechanisms of the Lowest Excited Singlet State *J. Am. Chem. Soc.* **1994**, *116*, 7363.
- (62) Graham, K. R.; Yang, Y.; Sommer, J. R.; Shelton, A. H.; Schanze, K. S.; Xue, J.; Reynolds, J. R. Extended Conjugation Platinum(II) Porphyrins for use in Near-Infrared Emitting Organic Light Emitting Diodes *Chem. Mater.* **2011**, *23*, 5305.
- (63) Doffek, C.; Alzakhem, N.; Bischof, C.; Wahsner, J.; Güden-Silber, T.; Lügger, J.; Platas-Iglesias, C.; Seitz, M. Understanding the Quenching Effects of Aromatic C–H- and C–D-Oscillators in Near-IR Lanthanoid Luminescence *J. Am. Chem. Soc.* **2012**, *134*, 16413.
- (64) Robinson, G. W.; Frosch, R. P. Theory of electronic energy relaxation in the solid phase *J. Chem. Phys.* **1962**, *37*, 1962.
- (65) Englman, R.; Jortner, J. The energy gap law for radiationless transitions in large molecules *Mol. Phys.* **1970**, *18*, 145.
- (66) Xiang, H.; Cheng, J.; Ma, X.; Zhou, X.; Chruma, J. J. Near-infrared phosphorescence: materials and applications *Chem. Soc. Rev.* **2013**, *42*, 6128.
- (67) Wang, P.; Wang, F.-F.; Chen, Y.; Niu, Q.; Lu, L.; Wang, H.-M.; Gao, X.-C.; Wei, B.; Wu, H.-W.; Cai, X.; Zou, D.-C. Synthesis of all-deuterated tris(2-phenylpyridine)iridium for highly stable electrophosphorescence: the "deuterium effect" *J. Mater. Chem. C* **2013**, *1*, 4821.
- (68) Martin-Ramos, P.; Ramos Silva, M.; Lahoz, F.; Martin, I. R.; Chamorro-Posada, P.; Eusebio, M. E. S.; Lavin, V.; Martin-Gil, J. Highly fluorinated erbium(III) complexes for emission in the C-band *J. Photochem. Photobiol., A* **2014**, *292*, 16.
- (69) Chi, Y.; Chou, P.-T. Transition-metal phosphors with cyclometalating ligands: fundamentals and applications *Chem. Soc. Rev.* **2010**, *39*, 638.
- (70) Valore, A.; Cariati, E.; Righetto, S.; Roberto, D.; Tessore, F.; Ugo, R.; Fragala, I. L.; Fragala, M. E.; Malandrino, G.; De Angelis, F.; Belpassi, L.; Ledoux-Rak, I.; Thi, K. H.; Zyss, J. Fluorinated β -Diketonate Diglyme Lanthanide Complexes as New Second-Order Nonlinear Optical Chromophores: The Role of f Electrons in the Dipolar and Octupolar Contribution to Quadratic Hyperpolarizability *J. Am. Chem. Soc.* **2010**, *132*, 4966.
- (71) Borisov, S. M.; Nuss, G.; Haas, W.; Saf, R.; Schmuck, M.; Klimant, I. New NIR-emitting complexes of platinum(II) and palladium(II) with fluorinated benzoporphyrins *J. Photochem. Photobiol., A* **2009**, *201*, 128.
- (72) Buenzli, J.-C. G.; Piguet, C. Taking advantage of luminescent lanthanide ions *Chem. Soc. Rev.* **2005**, *34*, 1048.

- (73) Hasegawa, Y.; Ohkubo, T.; Sogabe, K.; Kawamura, Y.; Wada, Y.; Nakashima, N.; Yanagida, S. Luminescence of Novel Neodymium Sulfonylamine Complexes in Organic Media *Angew. Chem., Int. Ed.* **2000**, *39*, 357.
- (74) Gegiou, D.; Muszkat, K. A.; Fischer, E. Temperature dependence of photoisomerization. V. Effect of substituents on the photoisomerization of stilbenes and azobenzenes *J. Am. Chem. Soc.* **1968**, *90*, 3907.
- (75) Sharafy, S.; Muszkat, K. A. Viscosity dependence of fluorescence quantum yields *J. Am. Chem. Soc.* **1971**, *93*, 4119.
- (76) Wilson, J. S.; Chawdhury, N.; Al-Mandhary, M. R. A.; Younus, M.; Khan, M. S.; Raithby, P. R.; Köhler, A.; Friend, R. H. The Energy Gap Law for Triplet States in Pt-Containing Conjugated Polymers and Monomers *J. Am. Chem. Soc.* **2001**, *123*, 9412.
- (77) Koehler, A.; Khan, A. L. T.; Wilson, J. S.; Dosche, C.; Al-Suti, M. K.; Shah, H. H.; Khan, M. S. The role of C-H and C-C stretching modes in the intrinsic non-radiative decay of triplet states in a Pt-containing conjugated phenylene ethynylene *J. Chem. Phys.* **2012**, *136*, 094905/1.
- (78) Hirata, S.; Totani, K.; Watanabe, T.; Kaji, H.; Vacha, M. Relationship between room temperature phosphorescence and deuteration position in a purely aromatic compound *Chem. Phys. Lett.* **2014**, *591*, 119.
- (79) Hirata, S.; Totani, K.; Zhang, J.; Yamashita, T.; Kaji, H.; Marder, S. R.; Watanabe, T.; Adachi, C. Efficient Persistent Room Temperature Phosphorescence in Organic Amorphous Materials under Ambient Conditions *Adv. Funct. Mater.* **2013**, *23*, 3386.
- (80) McClanahan, S. F.; Kincaid, J. R. 3MLCT lifetimes of tris(2,2'-bipyridine)ruthenium(II). Position-dependent deuterium effects *J. Am. Chem. Soc.* **1986**, *108*, 3840.
- (81) Henry, B. R.; Charlton, J. L. Position-dependent deuterium effects on radiationless transitions in anthracene *J. Am. Chem. Soc.* **1973**, *95*, 2782.
- (82) Parusel, A. B. J.; Wondimagegn, T.; Ghosh, A. Do Nonplanar Porphyrins Have Red-Shifted Electronic Spectra? A DFT/SCI Study and Reinvestigation of a Recent Proposal *J. Am. Chem. Soc.* **2000**, *122*, 6371.
- (83) Seong, N.-H.; Fang, Y.; Dlott, D. D. Vibrational Energy Dynamics of Normal and Deuterated Liquid Benzene *J. Phys. Chem. A* **2009**, *113*, 1445.
- (84) Moss, D. B.; Parmenter, C. S. Acceleration of intramolecular vibrational redistribution by methyl internal rotation. A chemical timing study of p-fluorotoluene and p-fluorotoluene-d₃ *J. Chem. Phys.* **1993**, *98*, 6897.
- (85) Nesbitt, D. J.; Field, R. W. Vibrational Energy Flow in Highly Excited Molecules: Role of Intramolecular Vibrational Redistribution *J. Phys. Chem.* **1996**, *100*, 12735.
- (86) Chirvony, V. S.; van Hoek, A.; Galievsky, V. A.; Sazanovich, I. V.; Schaafsma, T. J.; Holten, D. Comparative Study of the Photophysical Properties of Nonplanar Tetraphenylporphyrin and Octaethylporphyrin Diacids *J. Phys. Chem. B* **2000**, *104*, 9909.
- (87) Gentemann, S.; Nelson, N. Y.; Jaquinod, L.; Nurco, D. J.; Leung, S. H.; Medforth, C. J.; Smith, K. M.; Fajer, J.; Holten, D. Variations and Temperature Dependence of the Excited State Properties of Conformationally and Electronically Perturbed Zinc and Free Base Porphyrins *J. Phys. Chem. B* **1997**, *101*, 1247.
- (88) Liang, Y.; Bradler, M.; Klinger, M.; Schalk, O.; Balaban, M. C.; Balaban, T. S.; Riedle, E.; Unterreiner, A.-N. Ultrafast Dynamics of meso-Tetraphenylmetalporphyrins: The Role of Dark States *ChemPlusChem* **2013**, *78*, 1244.
- (89) Franchino, A.; Jakubec, P.; Dixon, D. J. Enantioselective synthesis of (-)-chloramphenicol via silver-catalysed asymmetric isocynoacetate aldol reaction *Org. Biomol. Chem.* **2016**, *14*, 93.

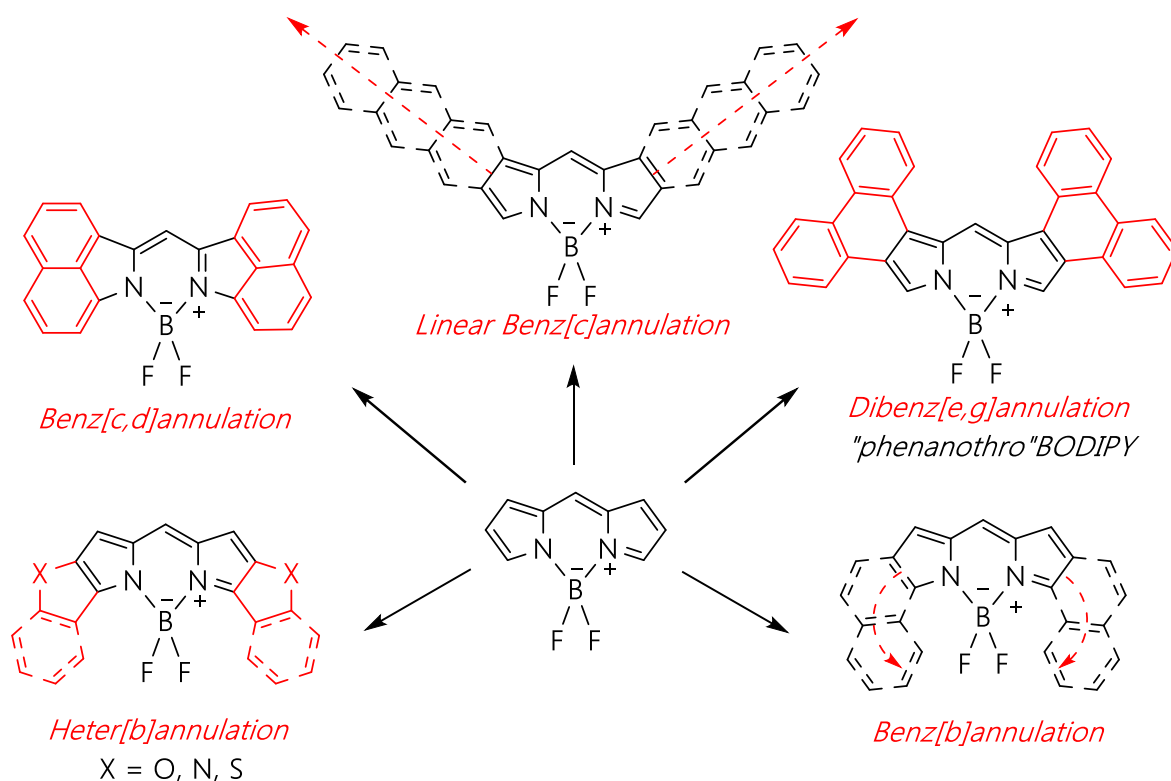
Chapter 3

Remarkably Bright NIR Emission in Novel π -extended BODIPYs

This chapter describes the synthesis of highly soluble and stable red/NIR-luminescent BODIPY dyes exhibiting Φ_F up to unity in select cases. As is the case for materials described in Chapter 2, these BODIPY dyes are functionalized peripherally with 2-EH imide moieties. Often called “porphyrin’s little sister”, exploration of BODIPYs evolved organically from work done with the π -extended porphyrins. The goal of this project was to see how far optical properties could be shifted into the NIR without sacrificing PLQY. To that end, a series of 3,5-halogenated benzo-annulated BODIPY dyes 3,5- X_2 Bz₂[c]BODIPY (X = Cl, Br) were prepared, characterized and used for Pd-catalyzed post-synthetic/nucleophilic modification of the BODIPY core. Influence of molecular structure on photophysical properties of these π -extended dyes are discussed within the context of bright NIR chromophore design.

3.1 Introduction to π -Extended BODIPYs

Much like the π -extended porphyrins described in Chapter 2, research into BODIPYs with red-shifted optical properties has flourished in recent years, due to increased demand for bright NIR chromophores for numerous applications. Drawing on the generalized methods discussed in Chapter 1, BODIPY-specific red-shifting strategies¹⁷ can be divided into 5 different categories: (i) extending π -conjugation through unsaturated and aromatic moieties (ii) incorporation of heteroatoms¹⁸, (iii) fusion of aromatic rings to the BODIPY framework, (iv) incorporation of nitrogen at the meso-position¹⁹ (aza-BODIPY) (v) modification at/of the boron core. It should be noted however, that aryl/alkyne substitution of fluorine at the boron center exerts limited effect on optical properties, as they are not brought into conjugation with the BODIPY core. Alternative methods include promoting phosphorescence²¹ via heavy atom effect and multi-chromophore systems. The work in



Scheme 3.1 Most commonly encountered ring-fusion modes in BODIPY systems.

this chapter explores the effect of linear benz[c]annulation with halogen/ene/yne substitution at the 3,5-positions. Scheme 3.1 depicts the most widely employed fusion patterns to generate π -extended BODIPY's.

Structural rigidity plays a large role in determining how emissive a given BODIPY structure could be. Functionalization of BODIPYs with freely-rotating substituents (especially at the *meso*- and 3,5-positions) tends to increase k_{nr} , thereby reducing PLQY. For example, while 3,5-arylated BODIPYs display red-shifting of optical properties compared with their 3,5-alkylated counterparts, introduction of freely-rotating Ar rings drastically quenches emission.^{24,25} Fusion of aromatic moieties to the BODIPY core represents a sensible approach to red-shift spectral properties without compromising molecular rigidity and PLQY. Figure 3.1 shows representative examples of this class of compound.²⁶ The most optimal properties were observed with [c]annulated BODIPY: Bz₂[c]BODIPY ($\Phi_f = 0.87$, $\lambda_{em} = 606$ nm) and phenanthro[c]BODIPY (not shown, $\Phi_f = 0.94$, $\lambda_{em} = 647$ nm). Empirically, [b]annulation results in lower quantum yields and loss of characteristic spectral BODIPY features (sharp and narrow peaks). The strategies discussed above (alkylation, styrylation and [c]annulation) have been applied systematically to BODIPY systems, albeit in a separate fashion, in order to extract clear structure-property relationships in this important class of dye. However, a combination of these approaches which pushes spectral features to the

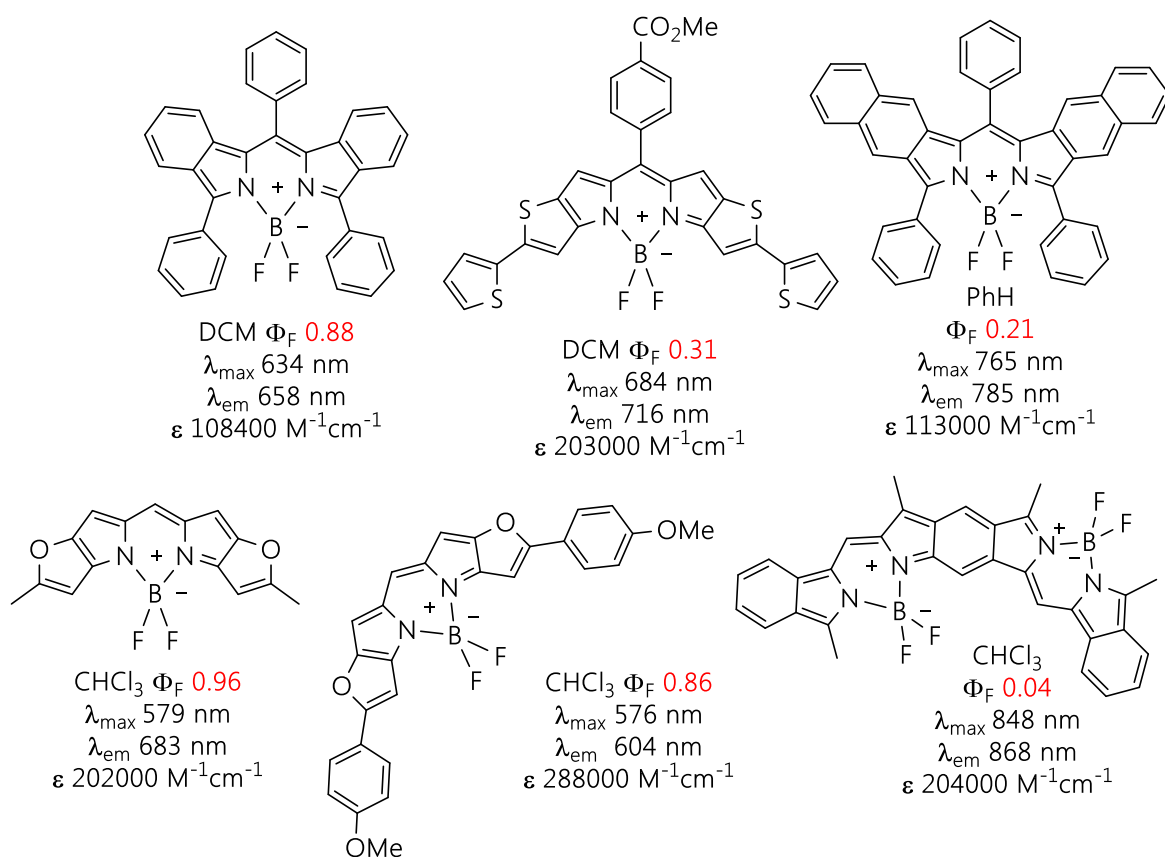


Figure 3.1 Representative examples of published BODIPY structures bearing fused aromatic moieties taken from (10).

NIR while retaining high PLQY ($\Phi > 0.75$) has not yet been achieved. The few promising published examples describe asymmetrically substituted BODIPY dyes such as 3-styryl-Bz[c]BODIPY ($\Phi_F = 0.24$, $\lambda_{em} = 741$ nm) and 3-pyrrolo-5-styryl Bz[c]BODIPY ($\Phi_F = 0.75$, $\lambda_{em} = 705$ nm). The more successful attempts at red-shifting spectral properties involved bis-alkylation and bis-styrylation at the 3,5-positions (Figure 3.2). BODIPY B bearing phenylethynyl moieties at 3,5-positions is an excellent red-emitter²⁷ ($\Phi_F = 1.0$, $\lambda_{em} = 628$ nm), representing a bathochromic shift of 107 nm compared to the 3,5-unsubstituted BODIPY A while 2,6-substitution leads to a weaker-emitting and less red-shifted species C ($\Phi_F = 0.60$, $\lambda_{em} = 594$ nm). Styryl substituents have proven to be even more potent red-shifters within the BODIPY framework. Mono-styrylated BODIPY D at the 3-position ($\Phi_F = 0.70$, $\lambda_{em} = 569$ nm) exhibits a 60 nm bathochromic shift compared to the parent BODIPY while 3,5-distyryl BODIPY E⁴ ($\Phi_F = 0.59$, $\lambda_{em} = 641$ nm) boasts an impressive 129 nm shift. Once again, only a modest shift is observed in the nearly non-emissive ($\Phi_F = 0.01$, $\lambda_{em} = 633$ nm) 2,6-distyryl F²⁸ analogue.

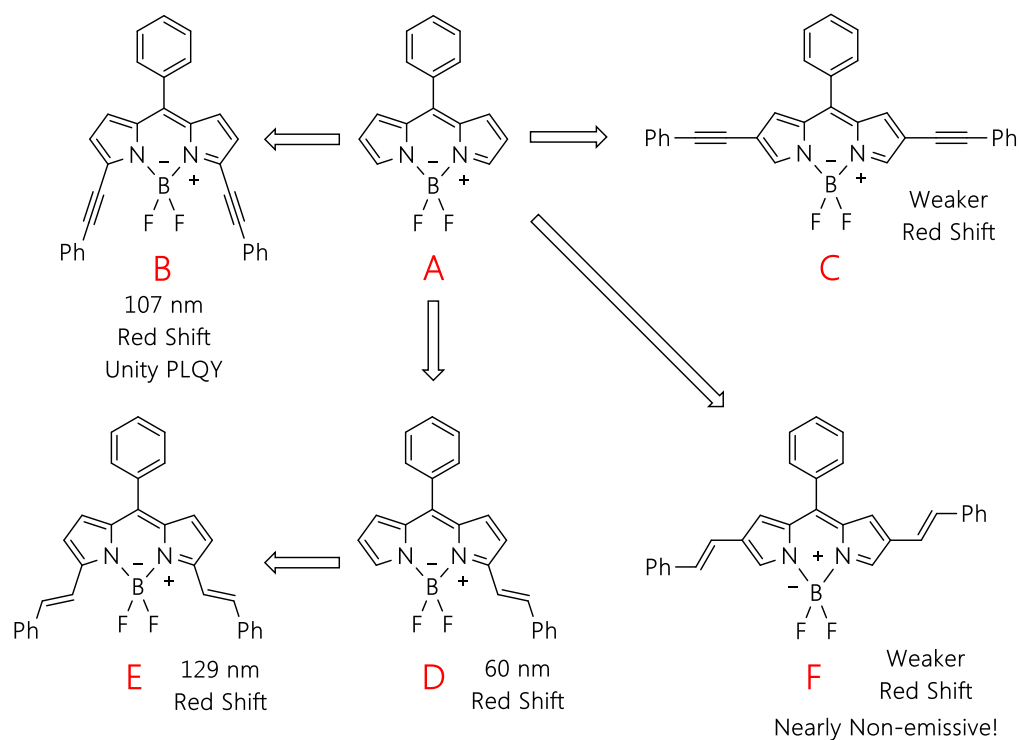
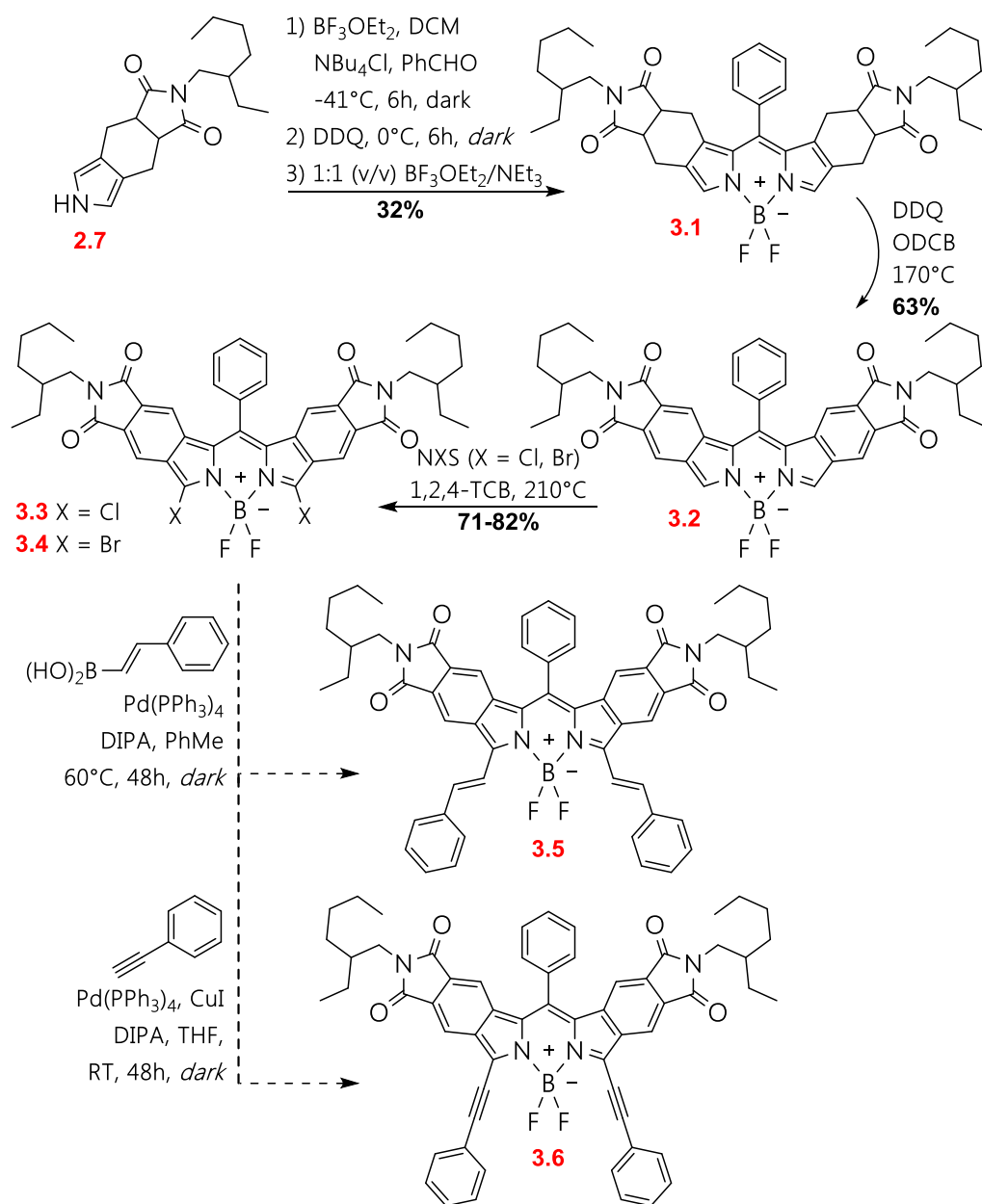


Figure 3.2 Representation of photophysical properties after 3,5- and 2,6-substitution with phenylethynyl and styryl moieties.

3.2 Synthesis of Bz₂-Annulated BODIPYs

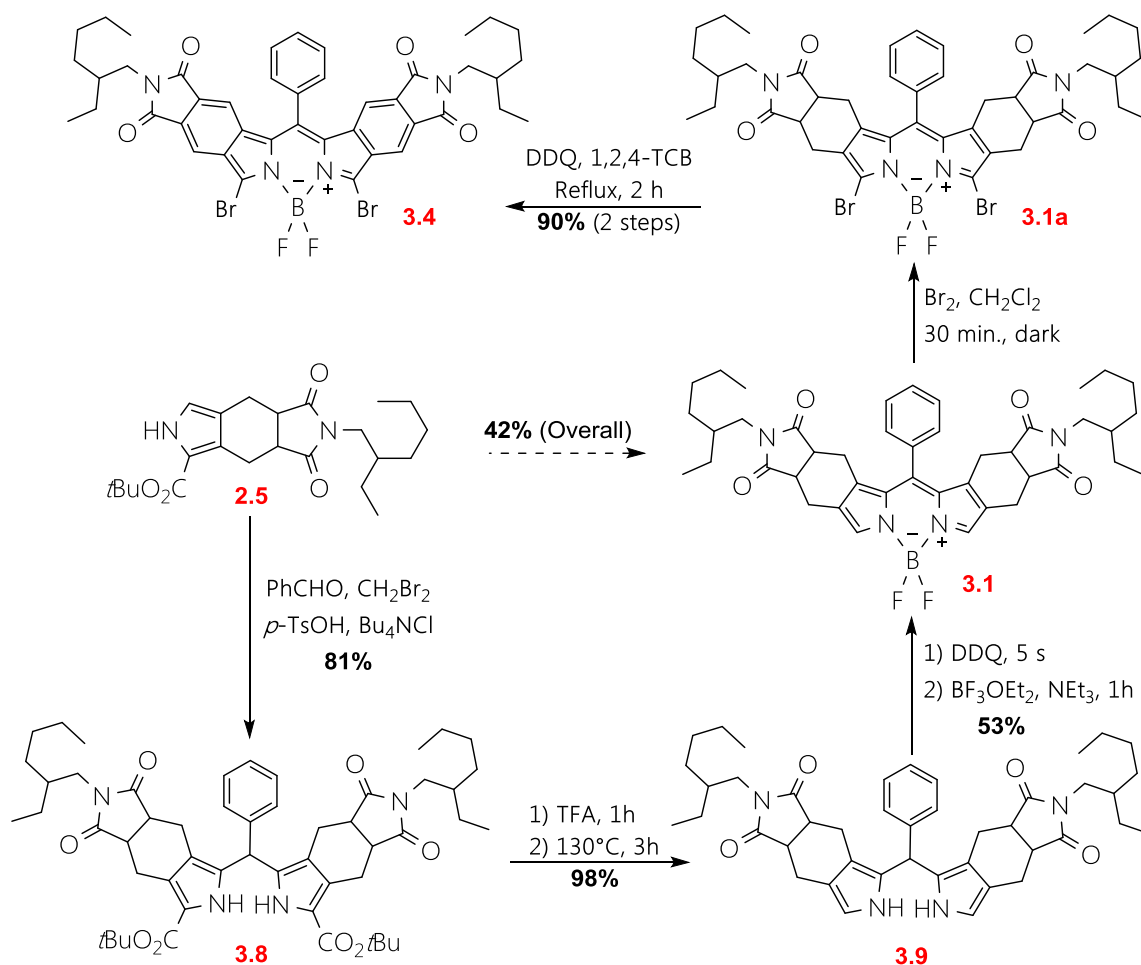
Investigation into π -extended BODIPYs was aimed at obtaining symmetrical 3,5-(CCPh)₂Bz₂[c]BODIPY **3.5** and 3,5-(CCHPh)₂Bz₂[c]BODIPY **3.6** (Scheme 3.1). Four equivalents of **2.7** were titrated with one equivalent of PhCHO/benzaldehyde at -41°C to form BODIPY **3.1** after successive treatment with DDQ and BF₃OEt₂/NEt₃. It was found that stoichiometric condensation (4:1 pyrrole/aldehyde) at reduced temperature in the presence of Bu₄NCl was effective in achieving controlled condensation. Reaction yield also proved contingent upon oxidation with DDQ at the correct time determined by monitoring reaction progress (dipyrrmethane formation) by UV-Vis spectroscopy.

A higher yielding and reproducible route to **3.1** (Scheme 3.2) was developed beginning with *tert*-butyl 3,3'-dipyrrmethane carboxylate **3.8**, obtained from acid-catalyzed condensation of **2.5** with PhCHO/benzaldehyde in CH₂Br₂. This synthesis offers simplified purification by avoiding closely-eluting condensation products (tripyrane and prodigiosin-type dyes), along with greater economy of exotic starting material **2.7**. Additive Bu₄NCl increased yield of **3.8** driving the equilibrium forward.²⁰ It is noteworthy that use of typical



Scheme 3.1 Synthesis of π -extended 3,5- $\text{X}_2\text{Bz}_2[\text{c}]\text{BODIPY}$ (X = Cl, Br) and their Pd-catalyzed functionalization leading to 3,5-(styryl) $_2\text{Bz}_2[\text{c}]\text{BODIPY}$ **3.5** and 3,5-(CCPh) $_2\text{Bz}_2[\text{c}]\text{BODIPY}$ **3.6** and via Suzuki/Sonogashira coupling, respectively.

halomethane solvents (*i.e.* dichloromethane, CHCl_3) resulted in incomplete condensation; neat CH_2Br_2 was required for the reaction to proceed to completion. The presence of stereomeric 2-EH aliphatic chains and stereogenic annulated cyclohexano- moieties produces mesomeric compounds which exhibit different retention times on silica (verified by HRMS of each fraction). De-esterification of **3.8** was accomplished with neat TFA, followed by decarboxylation of the neat material at 130°C for 3 hours. The decarboxylated product **3.9** was obtained as a dense, light purple oil which is used immediately without



Scheme 3.2 Synthesis of starting BODIPY **3.1** via controlled condensation of pyrrole 2-carboxylate **2.5** and milder two-step synthesis of useful precursor **3.4**.

further purification or characterization. Subsequent oxidation with DDQ for 5 seconds followed by treatment with BF₃OEt₂/NEt₃ results in **3.1** in 42% overall yield starting from **2.5**. It is imperative that that oxidation with DDQ be allowed to proceed only for 5 seconds (using vigorous stirring); extending oxidation with DDQ to only 60 seconds reduces the yield of BODIPY from 53% to 12% (half of which is an unwanted, closely-eluting BODIPY dye).

Subsequent aromatization with DDQ in refluxing *o*-DCB yielded 3,5-H₂Bz₂[c]BODIPY **3.2** which was treated with NXS (X= Cl, Br) in refluxing 1,2,4-TCB to generate highly fluorescent halogenated derivatives 3,5-Cl₂Bz₂[c]BODIPY **3.3** and 3,5-Br₂Bz₂[c]BODIPY **3.4**. It should be noted that a one-pot aromatization/halogenation from **3.1** is possible if 1,2,4-TCB is chosen as the aromatization solvent. **3.4** can also readily be prepared by room temperature treatment of **3.2** with Br₂ in dry tetrahydrofuran. Selective halogenation of a BODIPY dye bearing fused aromatic moieties has not been reported. Of noteworthy significance is the inert nature of the benzo moieties in **3.2** towards electrophilic reagents

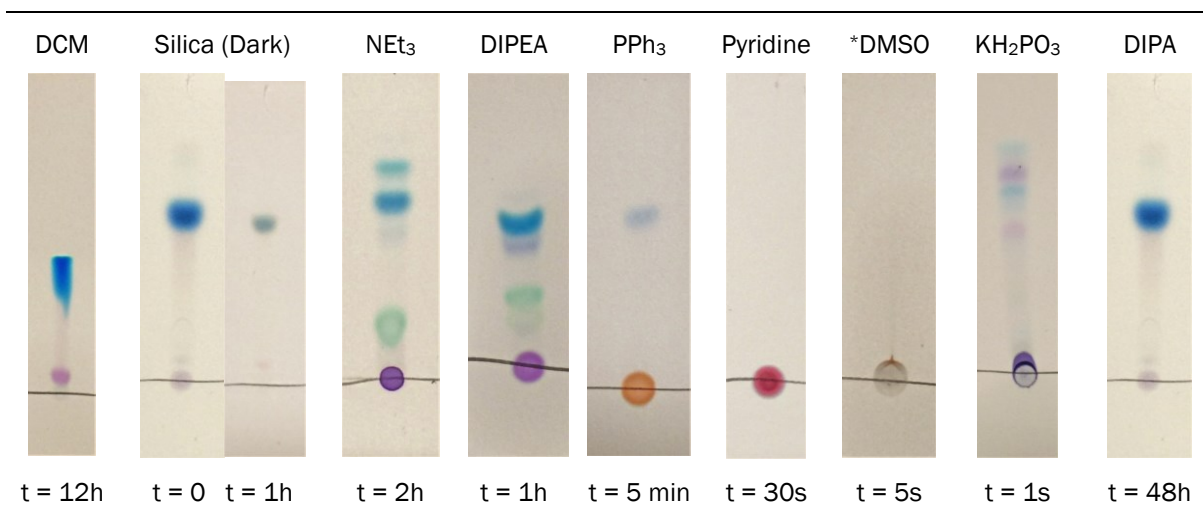
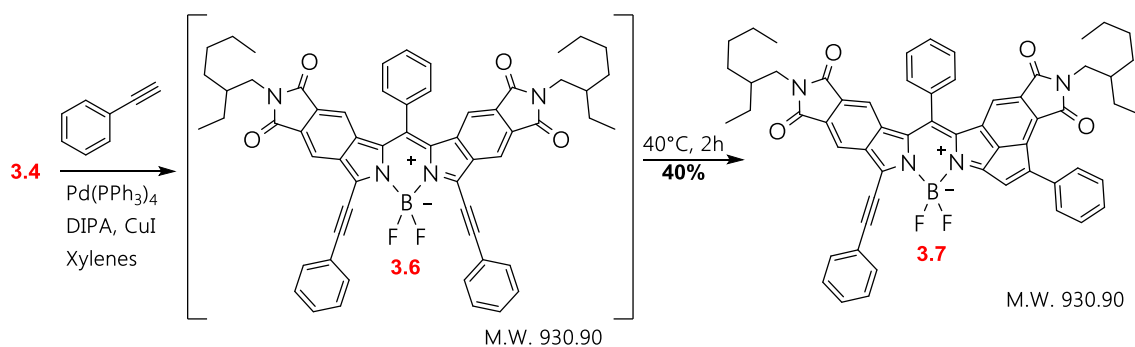


Figure 3.3 Reactivity of the blue BODIPY **3.4** with various solvents and reagents at room temperature visually demonstrated by TLC after indicated time. *At 60 °C.

(e.g. NCS, NBS, Br₂). Indeed, the dye emerged unscathed from all but the most draconian conditions, requiring 2 hours in 1,2,4-TCB/NCS at 210 °C for complete chlorination at the 3,5-positions. In contrast, NCS perchlorinates the BODIPY skeleton at room temperature.¹⁸ Such behavior can be rationalized by the benzo moieties delocalizing an already electron-deficient BODIPY core and by effective HOMO stabilization through the in-plane imide moieties. A superior route to **3.4** was developed (Scheme 3.2), generating a cleaner material through a two-step synthesis: room temperature bromination to afford **3.1a** (no purification or characterization) followed by immediate aromatization generating **3.4** in 90% overall yield from **3.1**. Numerous attempts at Pd-catalyzed functionalization of BODIPYs **3.3** and **3.4** resulted in complex mixtures of dyes with no observable formation of intended products **3.5** and **3.6**. The problem was traced back to the choice of base, which seemed to have a profound effect on the 3,5-halogenated starting materials. Despite exhibiting remarkable stability towards electrophiles, BODIPYs **3.3** and **3.4** seem to react easily with a variety of nucleophiles. Figure 3.3 shows quick, irreversible reaction of the blue starting material with many reagents and solvents, many of which are traditionally considered non-nucleophilic nor problematic (i.e. dichloromethane, water & triethylamine). However, diisopropylamine did not react or cause decomposition even after prolonged (48 h) contact with the starting material. After these findings, diisopropylamine was the base of choice for all Pd-catalyzed reactions which were performed with **3.4** under modified²⁹ Sonogashira and Suzuki conditions in attempts to produce 3,5-(CCHPh)₂Bz₂[c]BODIPY **3.5** and 3,5-(CCPh)₂Bz₂[c]BODIPY **3.6**. The former was never isolated nor was its formation confirmed (i.e. by HRMS) in the crude product; the Suzuki couplings resulted in bright green solids



Scheme 3.3 Unexpected formation of cyclized side product in the Sonogashira coupling.

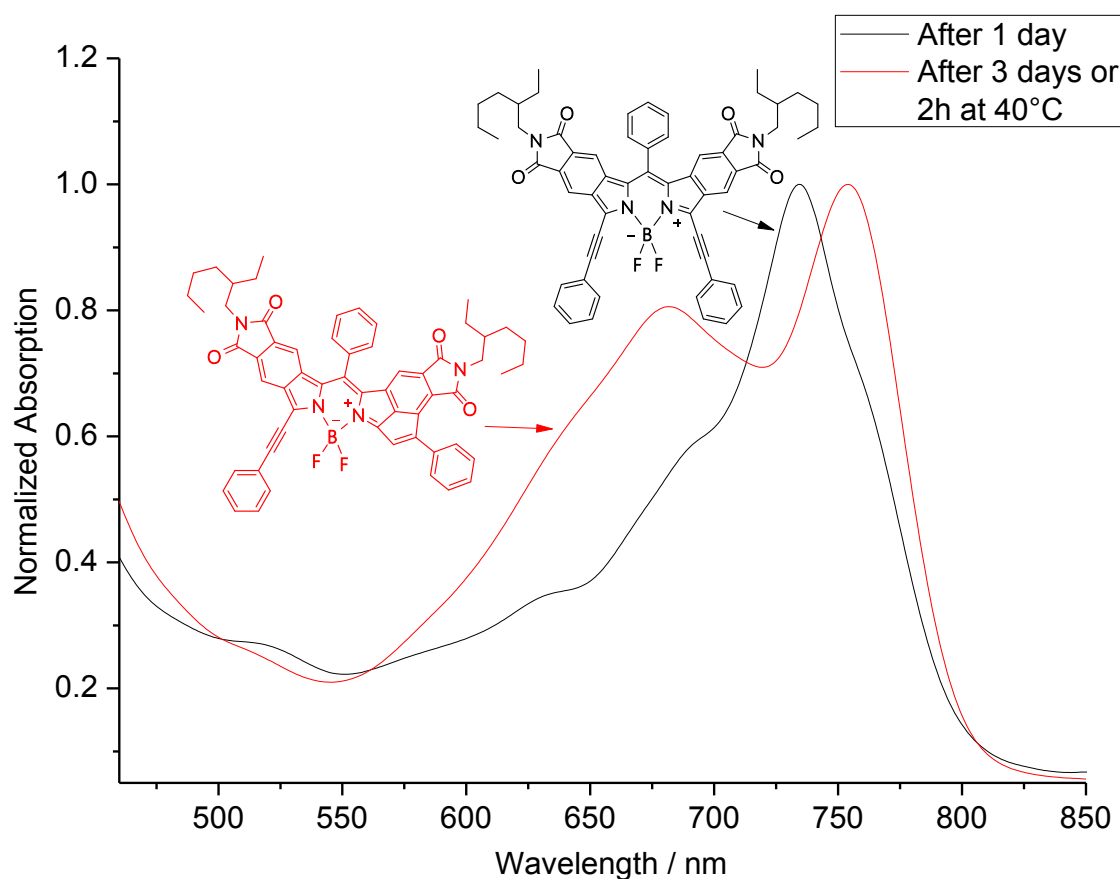
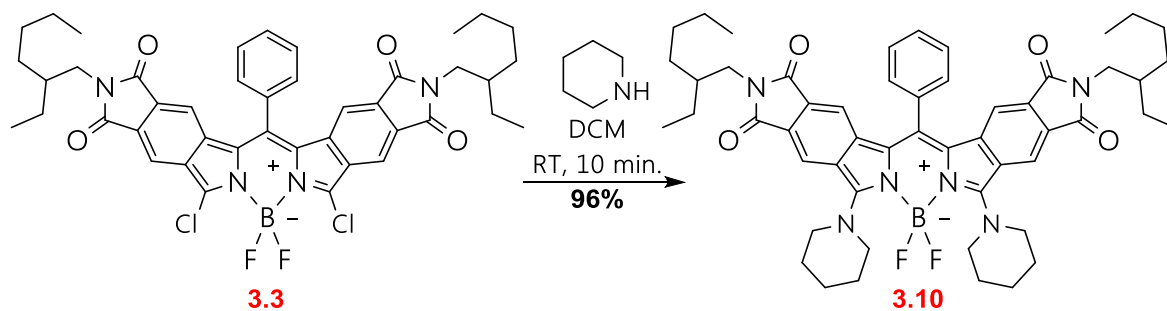


Figure 3.4 Observation of hypothesized *in-situ* intermediate **3.6** before temperature-mediated cyclization to **3.7**.

which displayed red-shifted spectra yet were composed of complex mixtures of dyes. However, Sonogashira coupling appeared to be more successful: a major product was recovered which exhibited red-shifted spectral properties characteristic of a BODIPY dye corresponding to **3.6** on the basis of HRMS data. However, ^1H NMR and ^{13}C NMR data suggest the formation of an asymmetric structure to which we propose the cyclized side product shown in Scheme 3.3. Formation of such a structure would most likely proceeded



Scheme 3.4 Piperidine-mediated aminolysis of **3.3** with piperidine to produce **3.10**.

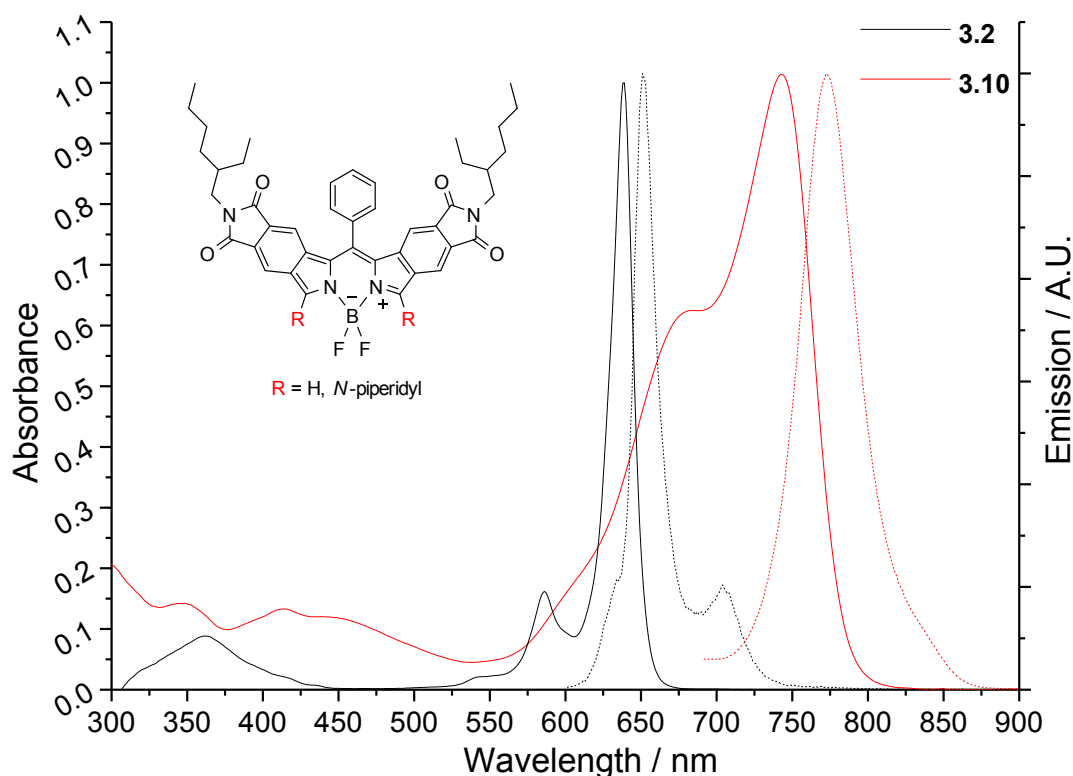


Figure 3.5 Overlap of normalized absorption (solid) and emission (dotted) spectra for **3.2** (black) and 3,5-(pip)₂Bz₂[c]BODIPY **3.11** in PhMe.

through the symmetrically substituted intermediate **3.6**. This view is supported by UV-Vis and TLC data collected during the Sonogashira coupling reaction, showing formation of an intermediate BODIPY band followed by its red-shift associated with a prolonged reaction time and/or heat (Figure 3.4).

The reactive nature of the halogenated BODIPYs towards nucleophiles was exploited for aminolysis of 3,5-Cl₂Bz₂[c]BODIPY **3.3** by piperidine; reaction with the base occurs instantly upon at room temperature to generate dark green 3,5-(pip)₂Bz₂[c]BODIPY **3.10** (Scheme 3.4). Its optical characterization revealed a >100 nm red-shift of the absorption

band in PhMe compared to **3.2** (Figure 3.5). While nucleophilic attack at halogenated 3,5-positions by primary and secondary amines is known,³⁰ **3.3** has also demonstrated unusual reactivity with alcohols at room temperature. Attempted recrystallization from dichloromethane/methanol by slow evaporation at room temperature resulted in a dramatic colour change (blue to green) and noted spectral broadening. Although this green product was never isolated, its optical properties fall in line with other 3,5-alkoxide BODIPY derivatives.³¹

3.3 Physical Properties

These compounds are exceptionally soluble in all organic solvents (**3.3** and **3.4** react with alcohols) and exhibit remarkable bench-top stability in solid-state (no change detected by TLC). Given that 3,5-unsubstituted π -extended BODIPYs have been demonstrated to be more prone to oxidation than their substituted counterparts, it is surprising that **3.2** shows only minimal degradation if left exposed to air and ambient light for several days. Additionally, it should be noted that **3.3**, **3.4**, **3.7** and **3.10** are not indefinitely photostable when adsorbed onto silica and should be eluted off the stationary phase promptly or better yet purified in a dark environment.

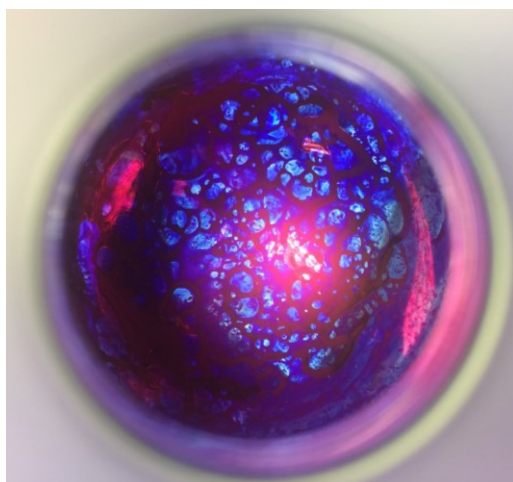


Figure 3.7 Red-blue optical dualism in **3.3** observed in solid-state (round-bottom flask).

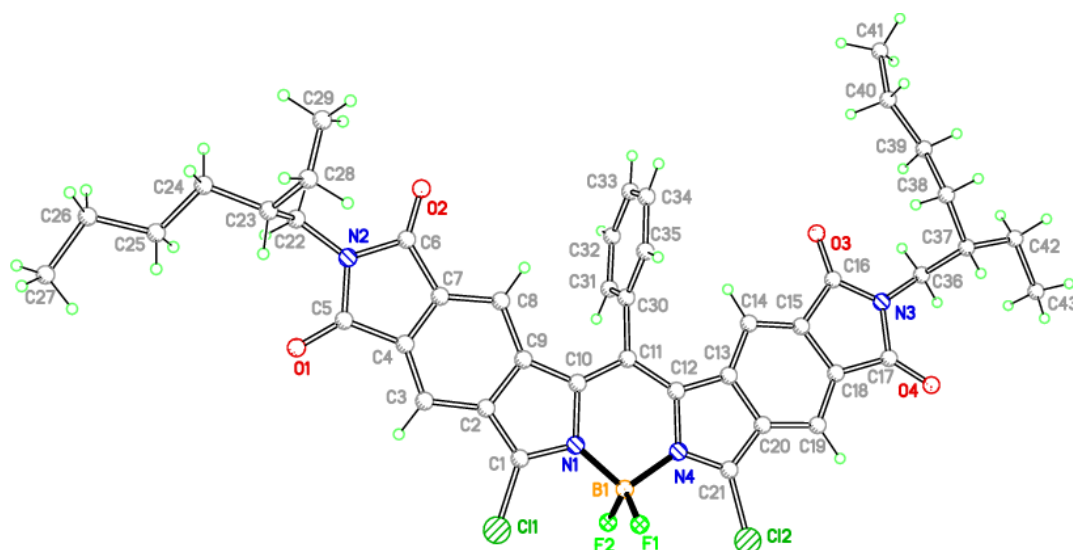
3.3.1 Crystal Structure

BODIPY compounds are known to crystallize easily into single-crystals routinely without any special precautions. While these materials are functionalized with 2-EH

Table 3.1 Photophysical Data for various Bz₂[c]BODIPYs in Aerated Solution at 298K.

BODIPY	Solvent	$\lambda_{\text{max}} / \text{nm}$ ($\epsilon_{\text{max}} / \text{E}^{-1}\text{cm}^{-1}$) ^a	$\lambda_{\text{em}} / \text{nm}$ ^b	Φ_{F}
3.2	PhMe	619 (140000)	623	1.00 ± 0.04 ^a
3.3	PhMe	640 (118000)	670	1.00 ± 0.03 ^b
3.4	PhMe	647 (109000)	672	0.43 ± 0.06 ^b
3.7	PhMe	767 (148000)	776	0.11 ± 0.04 ^c
3.10	PhMe	742 (133000)	773	0.12 ± 0.06 ^d

^a Measured against cresyl violet ($\Phi_{\text{F}} = 0.53 \pm$ in methanol) ^b Measured against Rhodamine-101 ($\Phi_{\text{F}} = 0.913 \pm 0.046$ in EtOH) ^c Measured against indocyanine green ($\Phi_{\text{F}} = 0.106 \pm 0.005$ in DMF). ^d Measured against 1,1',3,3,3',3'-hexamethylindotricarbocyanine iodide (HITCI) ($\Phi_{\text{F}} = 0.283 \pm 0.017$ in EtOH).

**Figure 3.6** X-ray crystal structure for **3.3**.

aliphatic chains, a crystal structure was nevertheless obtained for **3.3** (Figure 3.6) and is in excellent agreement with published 3,5-haloBODIPY crystal structures. Minimal root-mean-squared (RMS) deviation of the Bz₂[c]BODIPY core reveals a high degree of planarity. The *meso*-Ph ring is essentially orthogonal to the core, which is consistent with similar aromatic benz[c]annulated BODIPYs where bulky β, β' substituents on the pyrrole subunit restrict free rotation of the aryl ring.²⁶

3.3.2 Photophysical Properties

Unmistakable during their synthesis, the Bz₂[c]BODIPY compounds are deep blue in solution but fluoresce brightly with a vivid red color even under ambient light (Figure 3.7). Not surprisingly, both **3.2** and **3.3** showed unity quantum yield ($\Phi_F = 1.00 \pm 0.04$ and $\Phi_F = 1.00 \pm 0.03$, respectively) for red emission in PhMe solution. Interestingly, although **3.4** bears two heavy atoms affixed directly to the core (heavy-atom effect increasing k_{ISC}), it remains modestly fluorescent ($\Phi_F = 0.43 \pm 0.06$). Halogenation at the 3,5-positions seems to have a small impact (21 nm) on absorption maxima when comparing **3.2** and **3.3** but a much more pronounced effect on fluorescence wavelength (47 nm). The red-shift observed for absorption bands is in line with similar published examples of 3,5-haloBODIPYs. Both **3.7** and **3.10** are good absorbers ($\epsilon > 130000 \text{ M}^{-1}\text{cm}^{-1}$) and exhibit sizable red-shifts of their optical properties compared to **3.2**. The biggest red-shifting of spectral properties is observed in **3.7** with the absorption at 767 nm and emission at 776 nm. However, due to the asymmetrical nature of the molecule and the likely bent conformation of the BODIPY core due to [b]-fusion, the PLQY is significantly lower (0.11 ± 0.04) compared to the starting material **3.4**. Upon aromatization of **3.1** to **3.2**, a marked sharpening of spectral features is

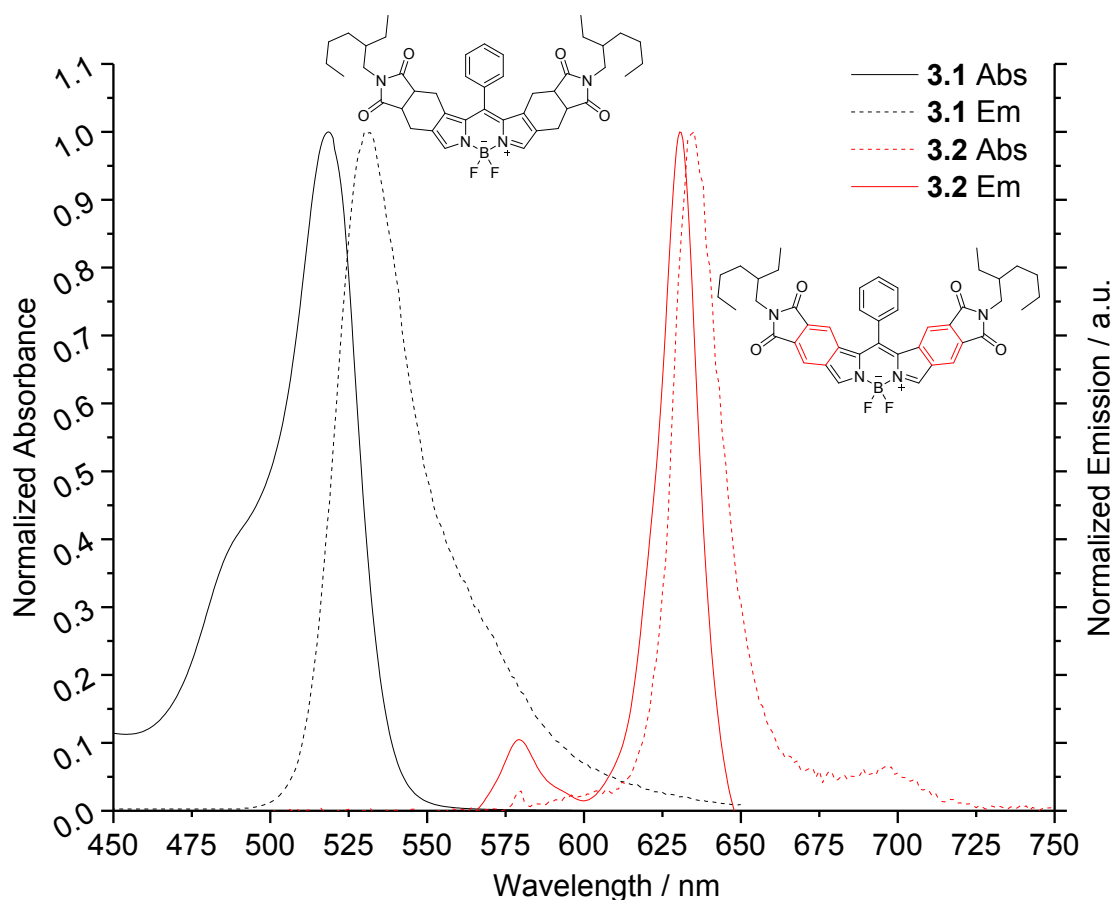


Figure 3.7 Overlap of absorption/emission spectra for **3.1** and **3.2** in dichloromethane.

observed (Figure 3.7) along with a reduction in the Stokes shift, indicative of enhanced molecular rigidity and lower reorganizational energy in the excited state. With the myriad of π -extended BODIPYs and libraries of 3,5-functionalized BODIPYs published and studied,^{12,17,33} it is puzzling to find a lack of examples where both ring-annulation and *ene/yne* substitution at the 3,5-positions is integrated into a single BODIPY material. This is perhaps indicative of the significant synthetic challenges involved in creating materials such as **3.5** and **3.6**. Nevertheless, as is shown in Figure 3.4, there is a chance of isolating a yet unidentified species (likely **3.6**) by adjusting the reaction conditions or terminating the reaction earlier.

3.4 Conclusions

To summarize, a high-yielding approach to 3,5-halogenated dibenz[*c*]annulated BODIPYs **3.3** and **3.4** was developed which were then used as starting materials for Pd-catalyzed and nucleophilic functionalization of the BODIPY core. Sonogashira coupling produced an unexpected [*b*]-cyclized BODIPY is the major product, possibly being formed through **3.6** as an intermediate. BODIPYs **3.2-3.3** were shown to have unity quantum yield in the red/far-red region. These spectral properties along, with excellent photostability make these π -extended BODIPYs an appealing choice for a myriad of practical applications, particularly bio-medical imaging.³⁴

3.5 Experimental

Unless specified, all chemicals were used as purchased without further purification. All glassware was flame-dried under vacuum prior to use. NMR spectra were acquired in CDCl₃ or CD₂Cl₂ (Cambridge Isotope Laboratories) with a Bruker Avance 500 MHz spectrometer equipped with a DCH cryoprobe. High resolution mass spectra were collected on a Bruker micrOTOF mass spectrometer. Thin-layer chromatography was performed using Millipore-Merck EMD silica gel TLC plates with F254 indicator. Column chromatography purification was performed on Geduran Si60 silica gel (40-63 μ m).

3,5-H₂BODIPY (3.1) A 500 mL round-bottom flask was equipped with a stir bar and thoroughly flushed with argon gas. Pyrrole **2.7** (1.0g, 3.3 mmol) and PhCHO (0.175g, 0.168 mL, 1.65 mmol) were added to the flask and dissolved in dichloromethane (400 mL). The solution was stirred and vigorously degassed with Ar gas for 30 min at room temperature.

The flask was immersed in a dry ice/isopropyl alcohol bath (-77 °C) and degassed further for 30 additional min. The flask was covered with aluminum foil and BF₃OEt₂ (0.115g, 0.10 mL, 0.8 mmol) was added to the flask, producing a yellowish solution. After degassing for an additional 30 min, the solution was allowed to slowly warm up in an CH₃CN/CO₂ bath (-41 °C). The reaction is monitored by TLC (hexanes/EtOAc) and is quenched with the addition of DDQ (0.400g, 1.75 mmol) when most of the aldehyde was consumed. The flask is brought to room temperature before subsequent addition of NEt₃ (5 mL) and BF₃OEt₂ (5 mL). The contents were stirred in the dark overnight before removing the solvent under reduced pressure to yield a dark brown residue which was purified using column chromatography (silica, hexanes/EtOAc). The title compound **3.1** was obtained as a copper-red solid (0.412 g, 32%). ¹H NMR (CD₂Cl₂) δ 7.63-7.52 (m, 5H), 7.20 (d, *J*=7.5 Hz, 2H), 3.13-3.00 (m, 8H), 2.85 (t, *J*=7.5 Hz, 2H), 2.50 (dd, *J*=7.5 Hz, *J*=15.3 Hz, 2H), 2.12-1.88 (m, 4H), 1.48-1.36 (m, 2H), 1.18-0.57 (m, 25H); ¹³C NMR (CD₂Cl₂) δ 178.56, 178.51, 177.89, 144.59, 140.36, 139.70, 131.58, 130.59, 129.04, 128.04, 127.72, 127.69, 127.49, 38.65, 36.23, 29.38, 27.58, 22.23, 22.19, 22.12, 13.03, 9.13, 9.04; ¹⁹F NMR (CD₂Cl₂) δ -145.62 (m); HRMS ESI, *m/z* for C₄₃H₅₃BF₂N₄O₄ + Na calcd 761.4028 found 761.4054.

3,5-H₂Bz₂[c]BODIPY (3.2) A 50 mL round-bottom flask was equipped with a stir bar and flushed with nitrogen gas. BODIPY **3.1** (40 mg, 54.0 μmol) was dissolved in *o*-DCB (25 mL) and added to the flask. DDQ (57 mg, 250 μmol) was added to flask and the stirring solution was thoroughly degassed by bubbling argon gas through the solvent for 30 min. The flask was sealed with a Teflon-lined glass stopper, covered with aluminum foil and immersed in an oil bath preheated to 170 °C. The solution was stirred for 1 hour at 170 °C and brought back to room temperature. The solution was poured onto a short pad of silica and washed thoroughly with hexanes to elute *o*-DCB. The product was eluted with EtOAc and the solvent was removed under reduced pressure. The crude residue was purified using column chromatography (silica, hexanes/EtOAc) and recrystallized from pentane/ether to yield **3.2** as greenish-blue flakes (25.5 mg, 63%). ¹H NMR (300 MHz, CDCl₃) δ 8.66 (s, 2H), 8.24 (s, 2H), 7.88 (t, *J* = 7.8 Hz, 1H), 7.80 (t, *J* = 7.8 Hz, 2H), 7.58 (d, *J* = 7.6 Hz, 2H), 6.72 (s, 2H), 3.54 (d, *J* = 3.6 Hz), 1.79 (m, 2H), 1.26 (m, 18 H), 0.88 (m, 12 H); ¹³C NMR (75 MHz, CDCl₃) δ 167.68, 141.69, 141.43, 137.48, 132.94, 132.13, 131.72, 131.50, 130.51, 128.74, 128.25, 128.01, 120.19, 117.86, 42.38, 38.40, 30.70, 28.69, 24.01, 23.09, 14.19, 10.54; HRMS APCI, *m/z* for C₄₃H₄₆BF₂N₄O₄ + H calcd 731.35747 found 731.35903.

3,5-Cl₂Bz[c]BODIPY (3.3) A 200 mL round-bottom flask was equipped with a stir bar and flushed with N₂ gas. BODIPY **3.2** (120 mg, 165 μmol) was dissolved in 1,2,4-TCB (80 mL) and added to the flask. DDQ (230 mg, 1.00 mmol) was added to flask and the stirring solution was thoroughly degassed by bubbling N₂ gas through the solvent for 1h. A reflux condenser was fitted to the top of the flask (covered with aluminum foil) and the mixture was slowly brought to reflux (~210°C) by immersion into an oil bath. There was a progressive colour change from dark orange to deep blue as the temperature rose. The solution was stirred at reflux until only one visible sharp absorption band ($\lambda_{\text{max}} = 620$ nm in dichloromethane) was visible. The flask was cooled down to ~120°C before adding NCS (400 mg, 3 mmol) in one portion. The flask was re-immersed into the oil bath and slowly heated up to reflux once more. After 2 hours, λ_{max} moves to 640 nm and the flask was cooled. The solvent was removed via distillation under vacuum at low temperature (<40°C) and the blue residue was re-dissolved in dichloromethane (500 mL) followed by washing with Na₂SO₃ (10%, 500 mL), HCl (5%, 500 mL), brine (500 mL) and dried over Na₂SO₄. The crude residue was purified using column chromatography (silica, dichloromethane/(iPr)₂O) and recrystallized from pentane/Et₂O to yield **3.3** as crimson/blue flakes (89 mg, 71%). ¹H NMR (300 MHz, CD₂Cl₂) δ 8.23 (s, 2H), 7.96 (t, *J* = 8 Hz, 1H), 7.84 (t, *J* = 8 Hz, 2H), 7.61 (d, *J* = 7.61 Hz, 2H), 6.56 (s, 2H), 3.52 (d, *J* = 3.5 Hz, 4H), 1.76 (m, 2H), 1.28 (m, 17H), 0.88 (m, 12H); ¹³C NMR (75 MHz, CD₂Cl₂) δ 167.63, 167.59, 142.66, 138.72, 137.06, 133.03, 132.52, 131.72, 131.47, 130.95, 129.20, 128.87, 127.86, 118.70, 117.99, 42.69, 38.89, 31.09, 29.11, 24.39, 23.52, 14.37, 10.72.

3,5-Br₂Bz[c]BODIPY (3.4) BODIPY **3.1** (770 mg, 1042 μmol) was transferred to a 100 mL round bottom flask equipped with a magnetic stir bar and dissolved in dichloromethane (40 mL). The vial was covered with aluminium foil and Br₂/dichloromethane solution (12.8 mL of a 0.488M solution) was quickly added. The vial was capped and the reaction was monitored by UV-Vis spectroscopy every 15 minutes. After 30 minutes, the reaction was diluted with dichloromethane (100 mL) and washed with sodium thiosulfate (2 x 100 mL), followed by water (2 x 100 mL). The combined organic fractions were dried over magnesium sulfate and the solvent was removed under reduced pressure to leave behind bright pink/green solids. The solids were re-dissolved in dichloromethane (100 mL) and passed through a short pad of silica (very important step!). After removing the solvent, the pink solids were dissolved in 1,2,4-trichlorobenzene (15 mL) and transferred to a dry 125 mL round-bottom flask equipped with a magnetic stir bar and 2,3-dichloro-5,6-dicyano-1,4-

benzoquinone (928 mg, 4088 μmol). The solvent was sparged with Ar for 10 minutes with stirring (18G needle) before fitting a reflux condenser to the flask. The flask was immersed into an oil bath and the temperature was slowly increased (50 °C/20 minutes) until a temperature of 170 °C was achieved. At 170 °C, the see-through pink solution started darkening, taking on a dark pink/red colour. At 180 °C (5 minutes later), the solution took on a deep purple colour. At 195-200 °C (10 minutes later), the solution took on a characteristic deep blue colour associated with Bz₂BODIPYs. An additional 10 minutes of stirring at 200 °C no longer results in a red-shift of λ_{max} . The reaction was brought back to room temperature when two consecutive aliquots revealed no discernable change by UV-Vis spectroscopy. The reaction mixture was diluted with dichloromethane (50 mL) and hexanes (200 mL) before loading it on a short pad of silica. A 1:1 mixture of hexanes and dichloromethane was used to elute the trichlorobenzene and neat dichloromethane was used to elute and collect the first blue band. The solvent was removed under reduced pressure to leave behind blue/red flakes which were recrystallized from boiling acetonitrile, affording **3.4** as thin green needles with a metallic lustre (830 mg, 90%). ¹H NMR (500 MHz, CD₂Cl₂) δ 8.20 (s, 2H), 7.96 (t, *J* = 8 Hz, 1H), 7.85 (t, *J* = 7.9 Hz, 2H), 7.62 (d, *J* = 7.6 Hz, 2H), 6.55 (s, 2H), 3.52 (d, *J* = 3.5 Hz, 4H), 1.76 (m, 2H), 1.28 (m, 18 H), 0.88 (m, 13 H); ¹³C NMR (125 MHz, CD₂Cl₂) δ 167.08, 136.60, 133.82, 132.38, 131.94, 131.68, 131.12, 130.37, 129.29, 128.58, 128.54, 119.15, 118.16, 117.36, 42.12, 38.32, 30.53, 20.54, 23.82, 22.94, 13.79, 10.15.

Asymmetrically fused Bz[c]BODIPY (3.7)

- Diisopropylamine **4** was distilled from sodium hydroxide under Ar atmosphere and atmospheric pressure, collecting the middle fraction only. The colorless distillate was thoroughly sparged with Ar (18 G needle, 1h) before storage in a screw-cap (PTFE) glass test tube (oven dried).
- Xylenes were dried over 4A molecular sieves.
- Immediately before use, phenylacetylene was passed through basic alumina repeatedly (Brockmann 1) until it eluted as a colorless liquid.

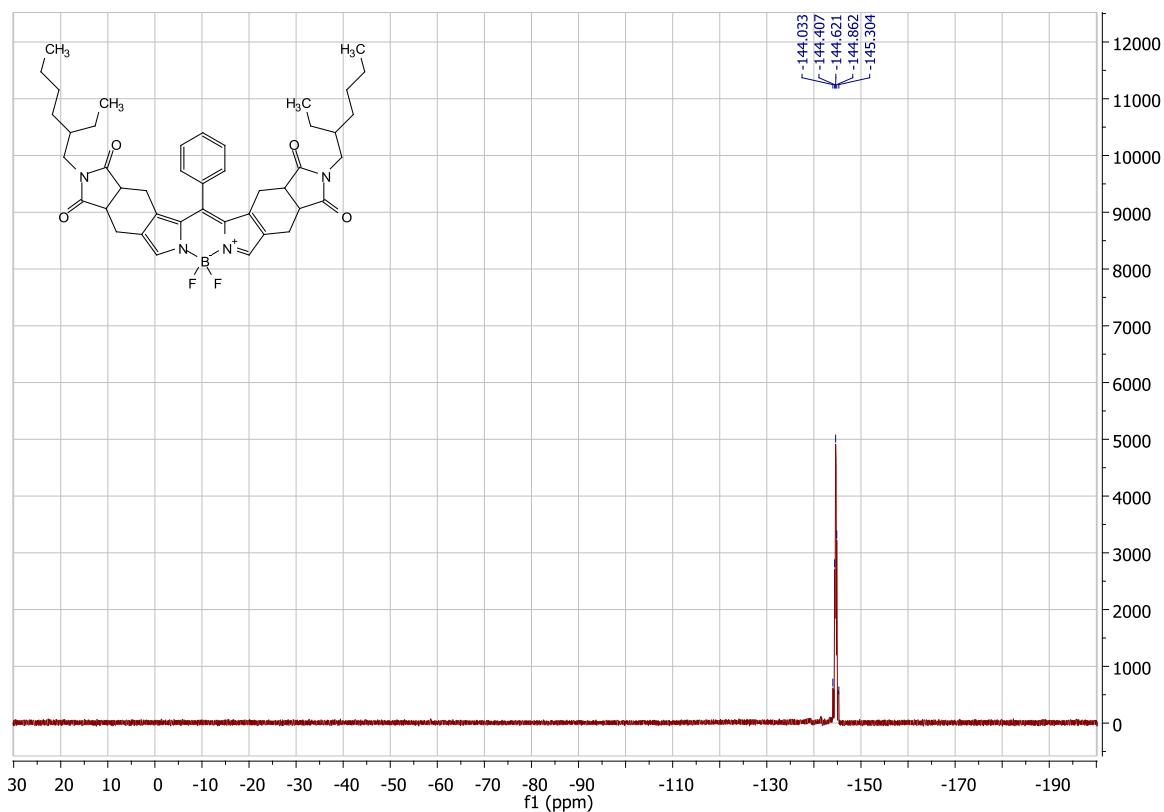
BODIPY **3.4** (100 mg, 112 μmol) was added to a 48 mL Schlenk tube equipped with a magnetic stir bar. Xylenes (2.0 mL) and diisopropylamine (200 μL , 1428 μmol) were added to the flask. The blue solution was sparged with Ar (18G needle) for 30 minutes before adding tetrakis(triphenylphosphine)palladium(0) (40 mg, 35 μmol) and copper (I) iodide (0.4 mg, 2.1 μmol) as quickly as possible. Sparging continued for an additional 15 minutes

before replacing the septum with the screw-thread cap over positive Ar pressure. The reaction started turning progressively greener over the next few hours and was left to stir at room temperature in the dark for 14 hours. The reaction was slowly heated (~10°C/30 min.) to 40°C and stirred at that temperature for 2 hours before diluting with hexanes (100 mL) and passing them through a short pad of silica with 95:5 dichloromethane/ethyl acetate, collecting the green fraction. The solvent was removed under reduced pressure and the resulting green solids were purified with column chromatography (hexanes/ethyl acetate), affording **3.7** as dark green solids (42 mg, 40%). ¹H NMR (500 MHz, CD₂Cl₂) δ 8.30 (s, 1H), 7.86 (t, *J* = 7.8 Hz, 1H), 7.76 (t, *J* = 7.8 Hz, 2H), 7.70 (d, *J* = 7.8 Hz, 2H), 7.59 (m, 4H), 7.44 (m, 3H), 7.36 (m, 3H), 7.24 (s, 1H), 6.82 (s, 1H), 6.53 (s, 1H), 6.42 (s, 1H), 3.50 (d, *J* = 3.5 Hz, 2H), 3.40 (d, *J* = 3.5 Hz, 2H), 1.78 (m, 2H), 1.28 (m, 22H), 0.87 (m, 14H); ¹³C NMR (125 MHz, CD₂Cl₂) δ 168.82, 168.64, 167.95, 167.78, 163.07, 159.74, 140.28, 137.26, 135.26, 134.82, 134.02, 132.81, 132.44, 132.09, 131.94, 131.82, 131.45, 130.54, 130.39, 129.88, 129.35, 129.09, 128.49, 127.75, 126.51, 126.19, 123.53, 121.93, 121.43, 118.71, 118.51, 117.67, 102.21, 98.64, 82.37, 42.35, 38.93, 38.86, 31.16, 31.08, 29.19, 29.08, 24.43, 23.56, 23.53, 21.54, 14.40, 14.37 10.79; HRMS APCI, *m/z* for C₅₉H₅₃BF₂N₄O₄ + C₆H₁₅N calcd 1032.54052 found 1032.53978.

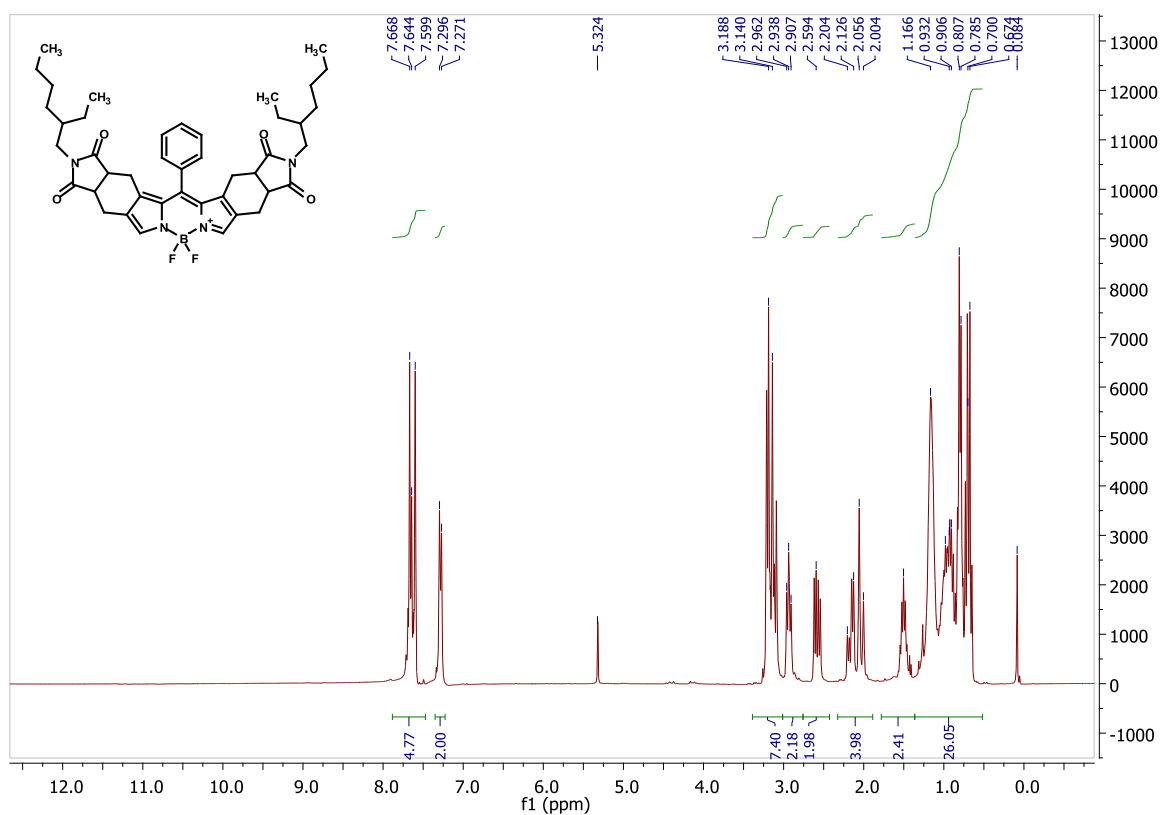
di-tert-Butyl 3,3'-(phenylmethylene)bis(6-(2-ethylhexyl)-5,7-dioxo-2,4,4a,5,6,7,7a,8-octahydropyrrolo[3,4-*f*]isoindole-1-carboxylate) (3.8) Pyrrole **2.5** (10.0 g, 24.8 mmol), benzaldehyde (1.27 g, 12.4 mmol), *para*-toluenesulfonic acid (213 mg, 1.24 mmol) and tetrabutylammonium chloride (693 mg, 2.50 mmol) were added to a flame-dried 250 mL round-bottom flask equipped with a magnetic stir bar and dissolved in dibromomethane (80 mL). The round-bottom flask was purged with nitrogen gas and sealed. After 24h stirring at room temperature, the solution took on a dark orange/burgundy color. The burgundy color disappears immediately upon spotting on TLC, leaving a light yellow spot. Heat gun treatment of the TLC plate (5-10 seconds, max heat) confirms the presence of dipyrromethane entities due to progressive darkening of the yellow spot into an orange one. Additionally, a previously invisible spot appears around R_f = 0.3 and quickly turns orange. The solution was poured into sat. NaHCO₃ (300 mL), immediately turning light yellow. Washing with NaHCO₃, brine, drying over Na₂SO₄ (10g) and removing the solvent under reduced pressure afforded an oily orange solid which was purified with column chromatography (hexanes/EtOAc) and dried under vacuum to give the title compound (8.98 g, 81.0 %). Crunchy, light yellow solids. TLC: R_f = 0.45 (hexanes/EtOAc 3:1). ¹H NMR (500 MHz, CD₂Cl₂) δ 8.61 (t, 1H), 8.47 (d, *J* = 18.3 Hz, 1H), 7.38 – 7.22 (m, 3H), 7.16 – 7.06 (m,

2H), 5.51 (d, $J = 11.5$ Hz, 1H), 3.73 – 3.65 (m, 2H), 3.38 – 3.09 (m, 8H), 2.95 – 2.62 (m, 4H), 2.39 – 2.21 (m, 2H), 1.53 (s, 9H), 1.51 (s, 9H), 1.48 – 0.17 (m, 32H). ^{13}C NMR (125 MHz, CD_2Cl_2) δ 180.52, 180.36, 180.31, 180.29, 180.24, 179.88, 179.86, 179.83, 160.48, 160.44, 160.37, 160.34, 139.62, 139.54, 139.52, 139.43, 130.12, 130.04, 130.02, 129.98, 129.88, 128.90, 128.84, 128.15, 128.12, 128.09, 127.33, 127.32, 127.27, 127.26, 124.50, 124.46, 124.44, 124.42, 124.33, 119.10, 119.03, 118.99, 118.97, 118.94, 118.88, 117.60, 117.58, 117.54, 117.51, 117.46, 117.42, 117.39, 117.35, 80.65, 80.63, 80.61, 80.59, 80.57, 53.84, 53.62, 53.41, 53.19, 52.98, 42.80, 42.68, 42.66, 42.48, 42.45, 42.43, 40.70, 40.41, 40.39, 40.27, 40.08, 40.04, 39.97, 39.95, 39.91, 39.87, 39.79, 39.74, 37.16, 37.11, 37.09, 37.07, 36.96, 36.88, 36.86, 36.83, 30.28, 30.18, 30.01, 29.99, 28.55, 28.52, 28.16, 28.13, 28.12, 28.10, 28.08, 23.27, 23.24, 23.22, 23.19, 22.96, 22.93, 22.91, 22.88, 22.87, 22.82, 22.75, 22.69, 22.63, 22.59, 22.56, 22.51, 20.55, 20.52, 20.50, 20.47, 20.45, 20.41, 13.84, 13.82, 13.78, 10.19, 10.14, 10.09, 9.51, 9.48, 9.42, 9.36; HRMS (EI) for $\text{C}_{53}\text{H}_{72}\text{N}_4\text{O}_8\text{Na}$ ($\text{M}+\text{Na}$) $^+$: m/z calcd 915.5242 found 915.5230.

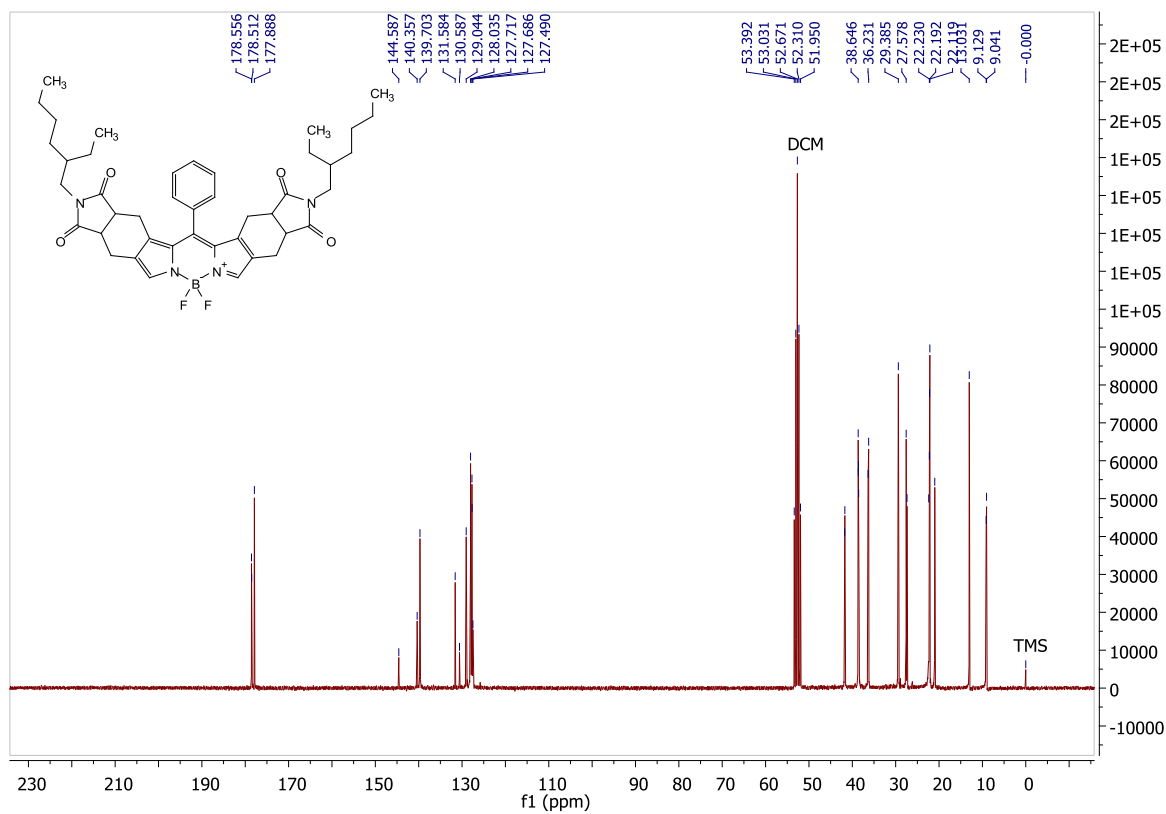
3,5-(pip)₂Bz[c]BODIPY (3.10) BODIPY **3.3** (30 mg, 37 μmol) was added to a flame-dried 50 mL round-bottom flask. A magnetic stir bar and piperidine (10 mL) was added. The color changed immediately from blue to dark green. The solution was stirred for an additional 10 min at room temperature. The reaction was quenched with 2% HCl (300 mL), and extracted with dichloromethane (2 x 100 mL). The combined organic fractions were washed with H_2O (200 mL) and dried over sodium sulfate (25 g). The solvent was removed under reduced pressure and the crude solids were purified by column chromatography (hexanes/EtOAc, covered in aluminium foil) to afford green solids after recrystallization of its bis(hydrobromide) salt and conversion to freebase (23.6 mg, 71%). ^1H NMR (500 MHz, CDCl_3) δ 8.22 (s, 1H), 8.17 (s, 1H), 7.78 (t, $J = 7.8$ Hz, 1H), 7.69 (t, $J = 7.8$ Hz, 2H), 7.45 (d, $J = 7.5$ Hz, 2H), 6.73 (m, 1H), 6.53 (s, 1H), 6.41 (s, 1H), 3.87 (m, 2H), 3.71 (m, 4H), 3.50 (t, $J = 3.5$ Hz, 4H), 1.89 (m, 6H), 1.77 (m, 4H), 1.25 (m, 28H), 0.87 (m, 14H); ^{13}C NMR (125 MHz, CD_2Cl_2) δ 168.56, 168.22, 168.06, 167.64, 154.06, 153.50, 138.46, 134.22, 133.77, 131.50, 130.46, 130.37, 129.59, 128.66, 128.47, 125.79, 124.85, 123.92, 123.76, 123.60, 123.15, 120.69, 119.98, 118.29, 118.18, 114.21, 53.68, 45.44, 42.29, 42.16, 38.42, 38.38, 32.08, 30.75, 29.88, 29.85, 29.82, 29.51, 28.91, 28.77, 28.73, 26.65, 24.43, 24.04, 23.12, 23.11, 22.85, 22.43, 14.27, 14.20, 14.08, 10.59; HRMS APCI, m/z for $\text{C}_{53}\text{H}_{63}\text{BF}_2\text{N}_6\text{O}_4$ calcd 866.94675 found 866.94912.



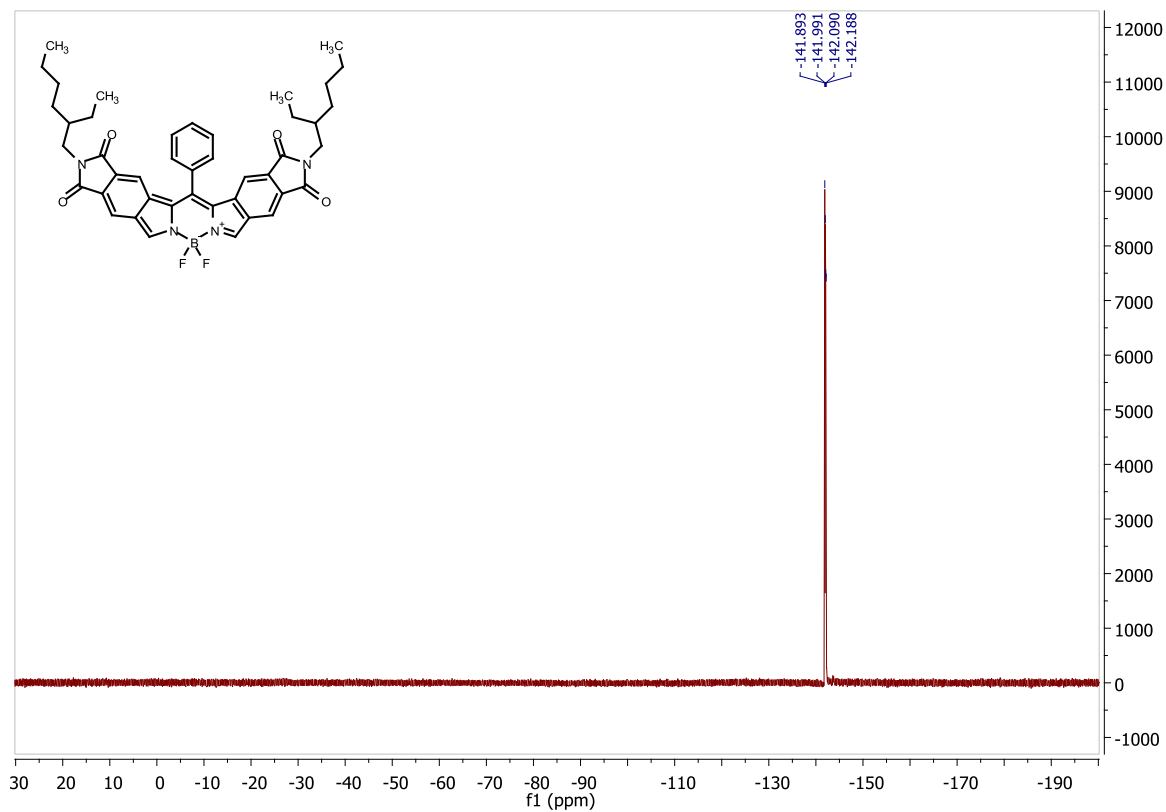
¹⁹F NMR spectrum of **3.1** in CDCl₃.



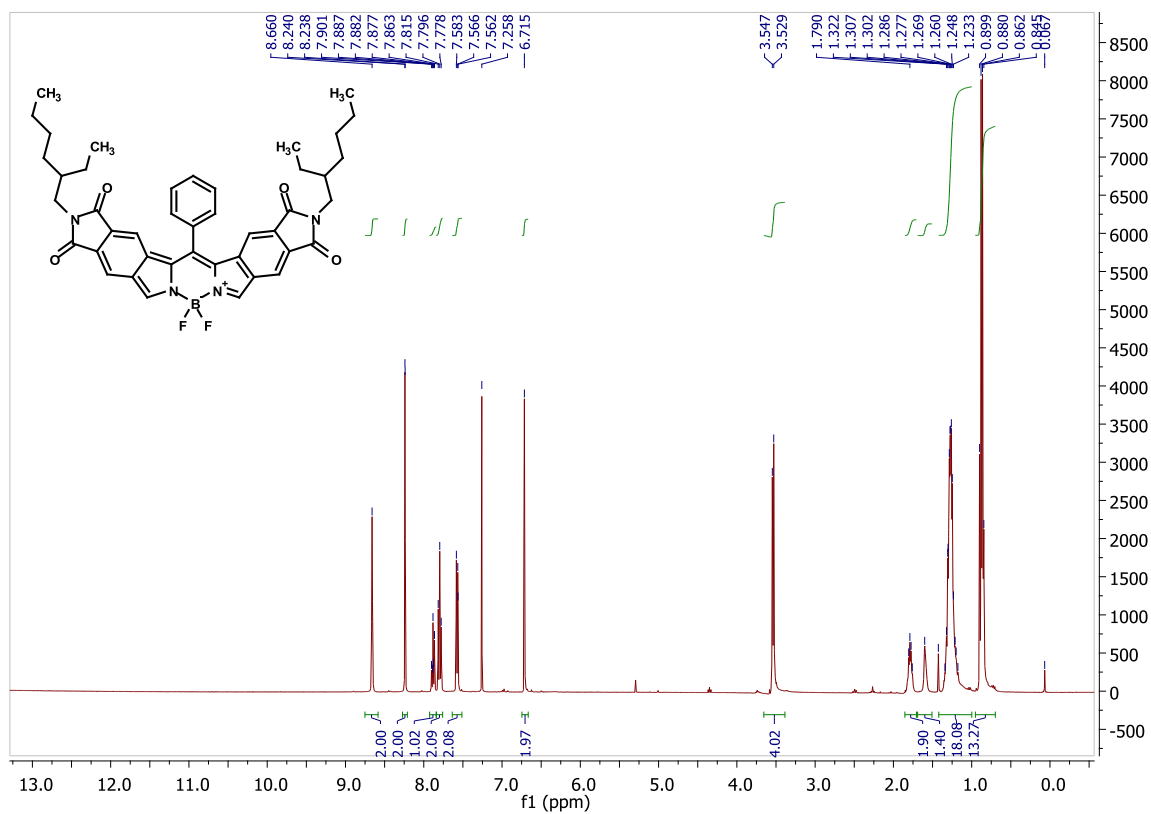
¹H NMR spectrum of **3.1** in CDCl₃.



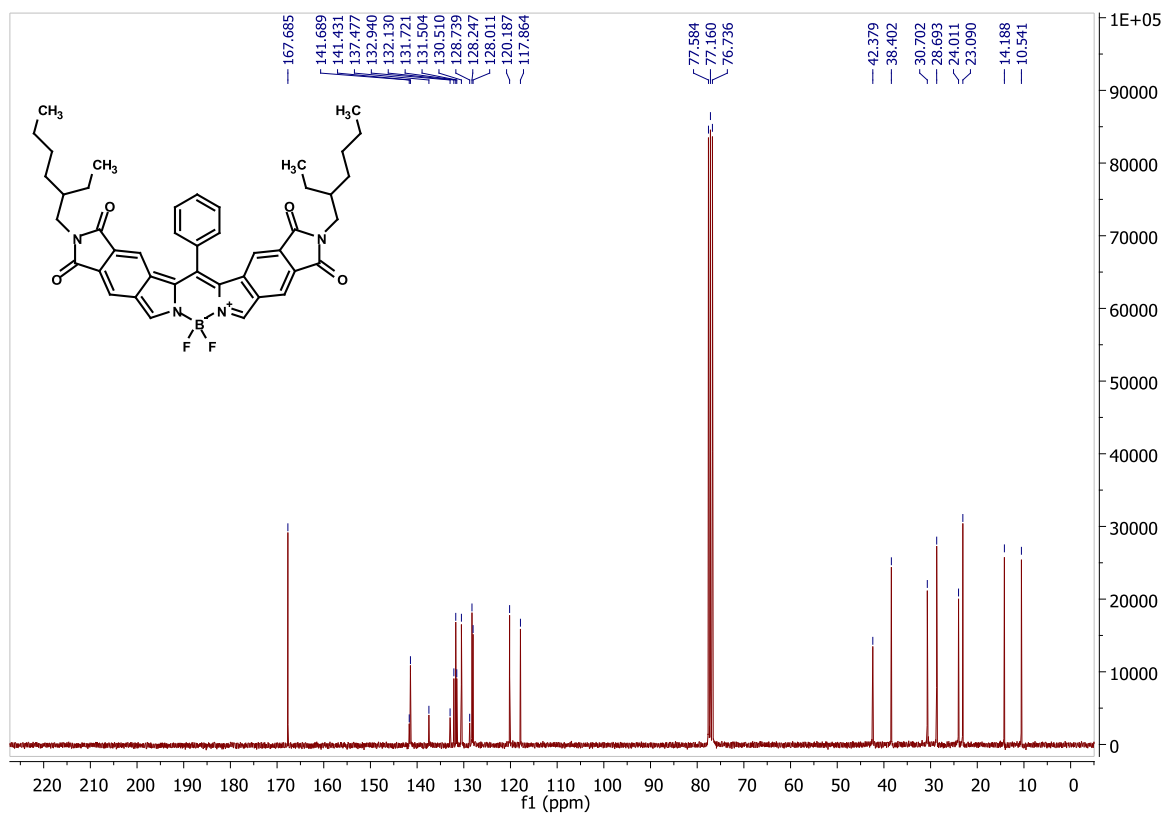
¹³C NMR spectrum of **3.1** in CDCl₃.



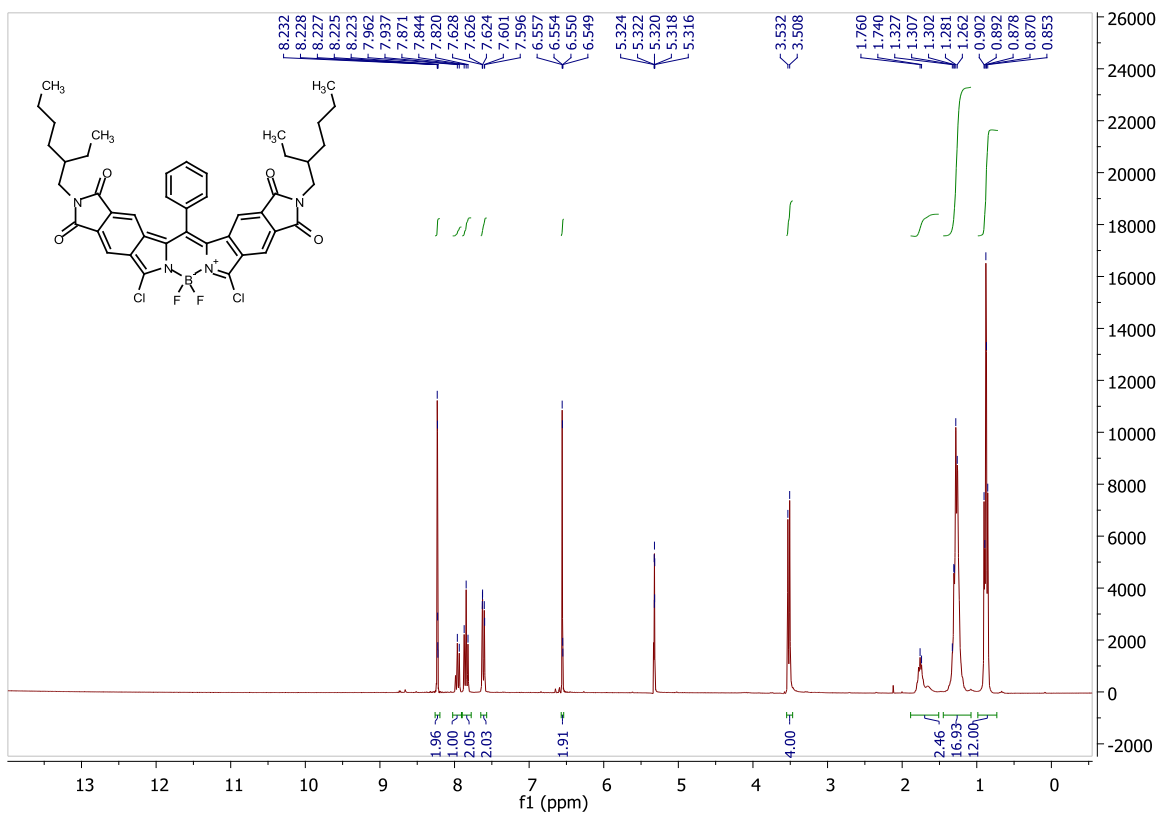
¹⁹F NMR spectrum of **3.2** in CDCl₃.



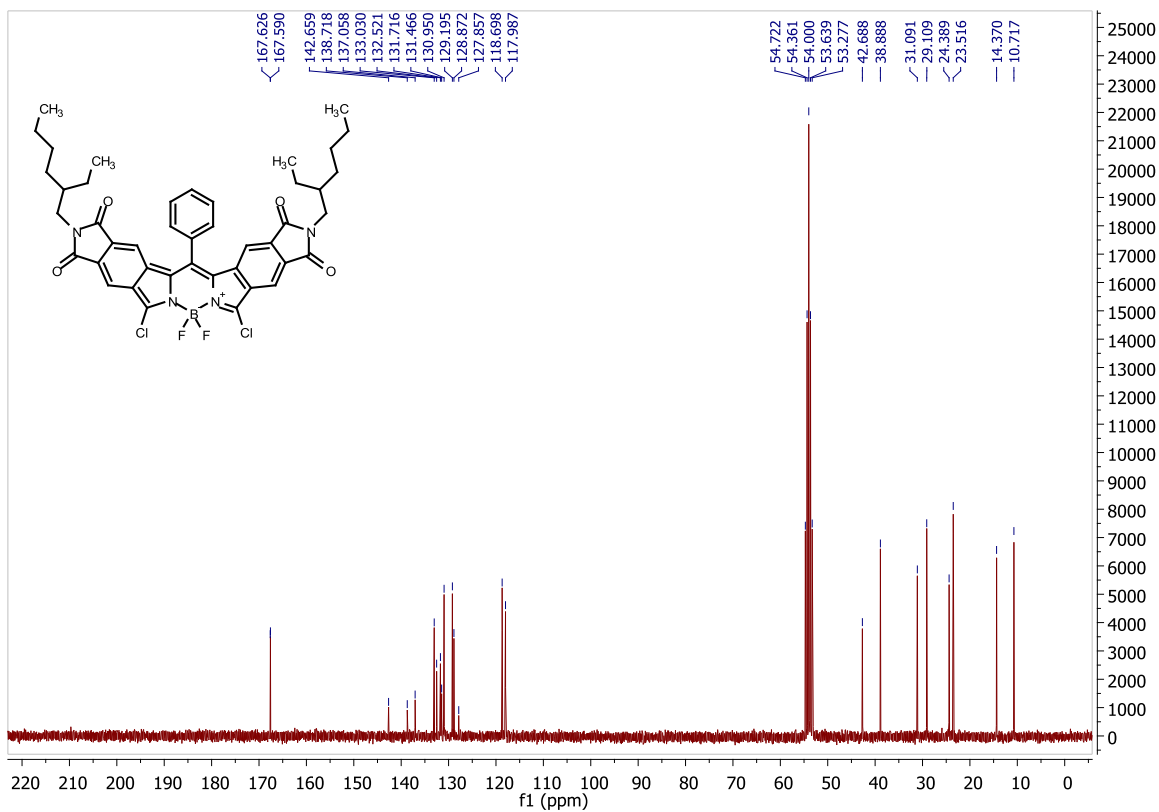
¹H NMR spectrum of **3.2** in CDCl₃.



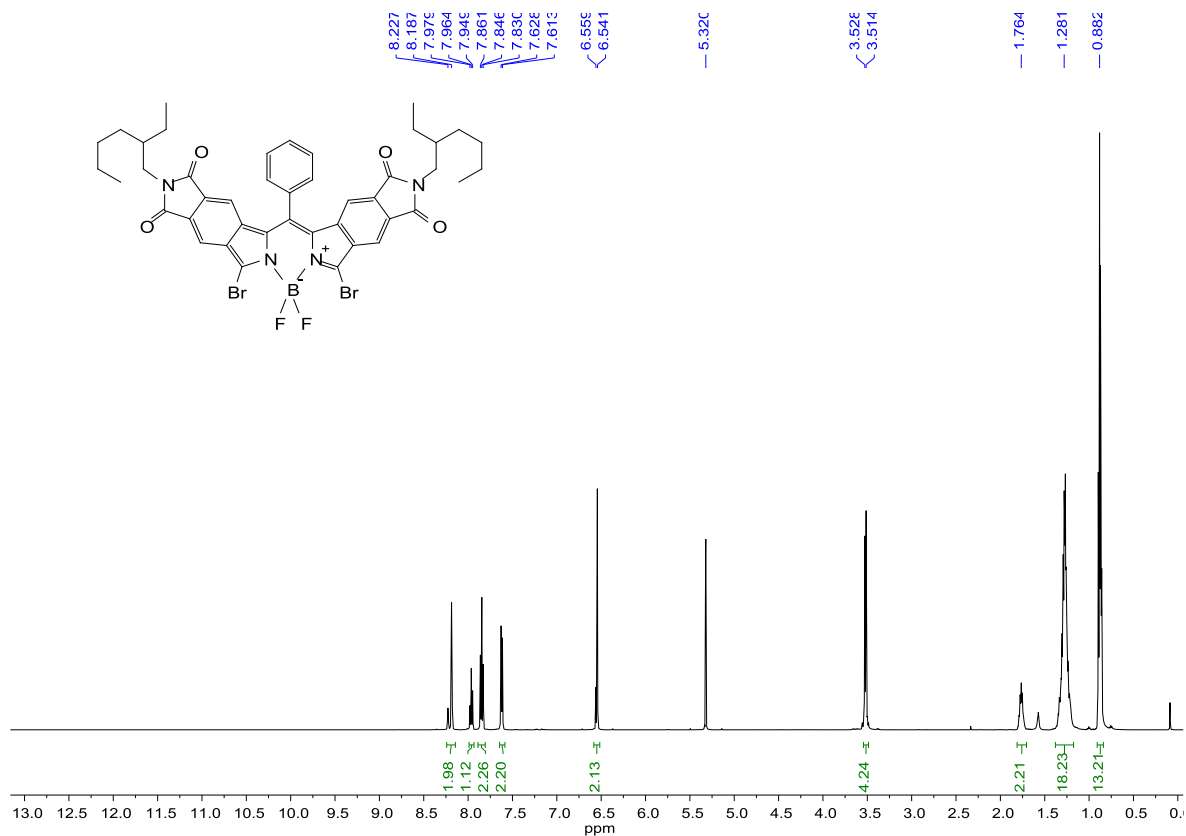
¹³C NMR spectrum of **3.2** in CDCl₃.



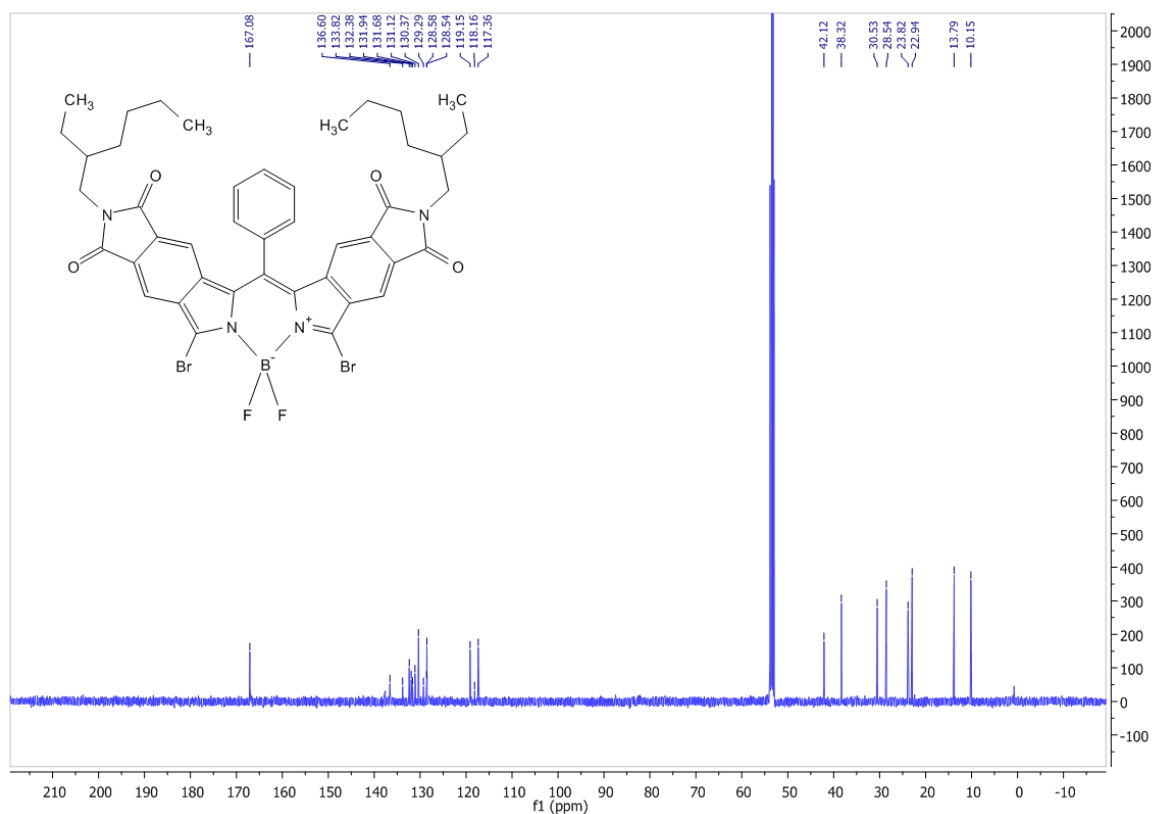
¹H NMR spectrum of **3.3** in CD₂Cl₂.



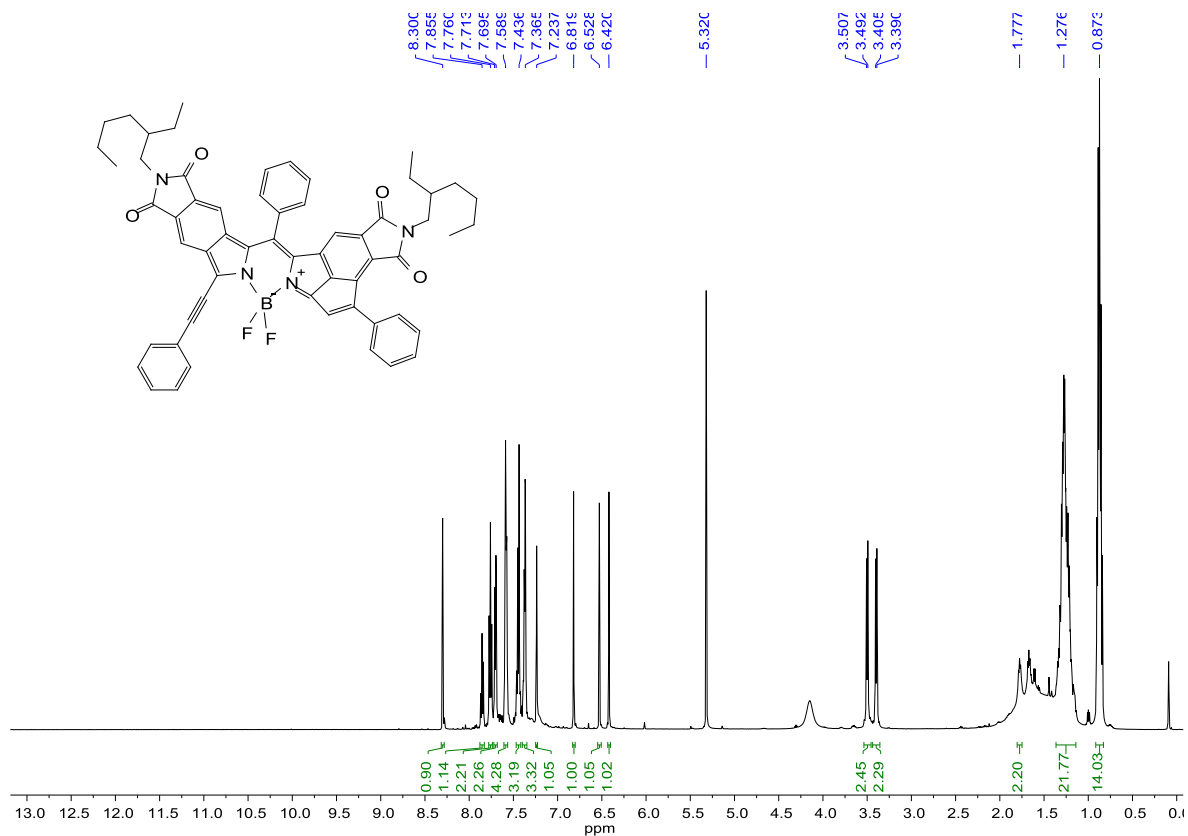
¹³C NMR spectrum of **3.3** in CD₂Cl₃.



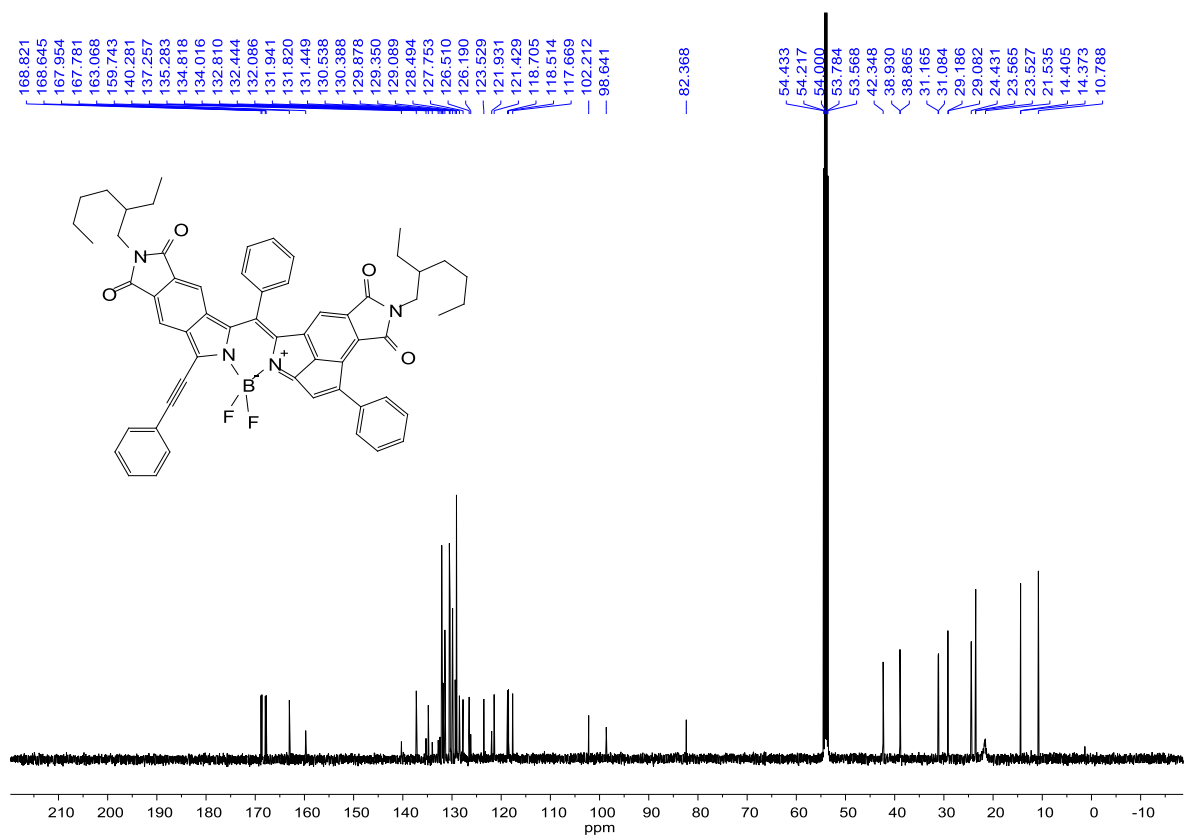
¹H NMR spectrum of **3.4** in CD₂Cl₂.



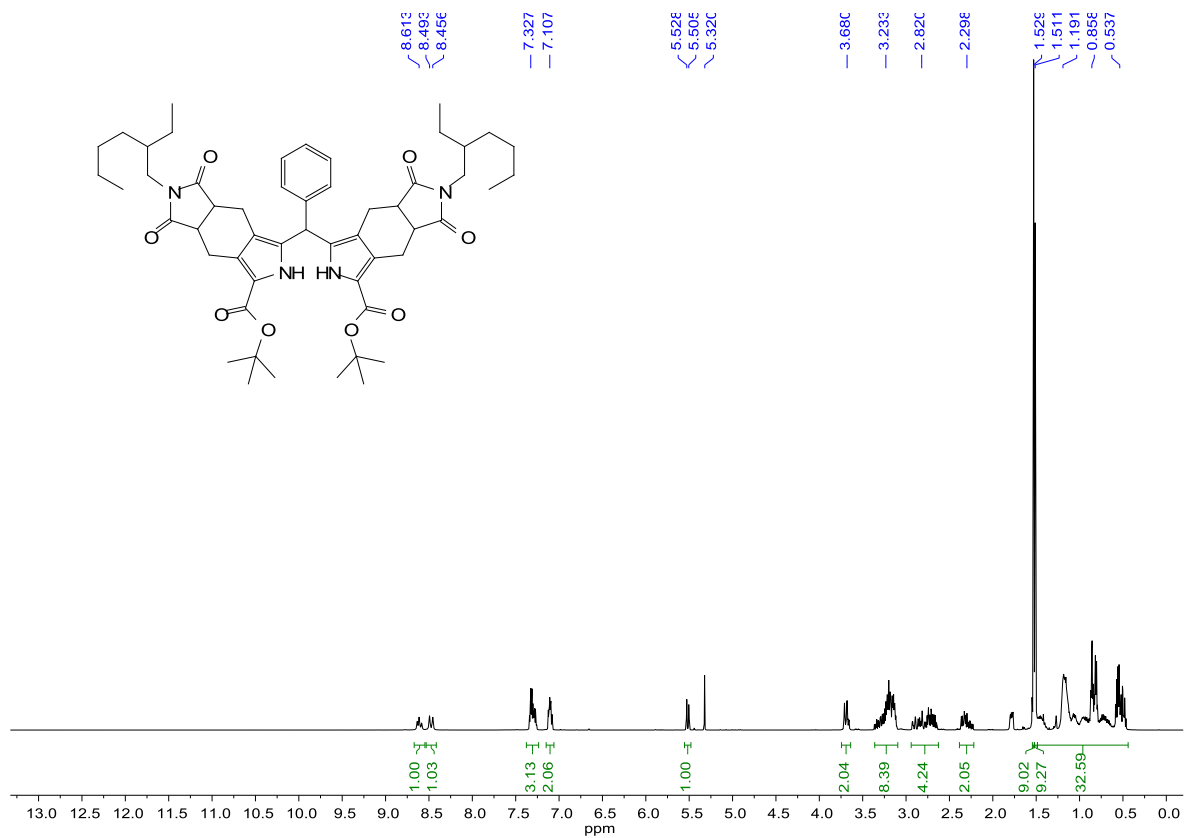
¹³C NMR spectrum of **3.4** in CD₂Cl₂.



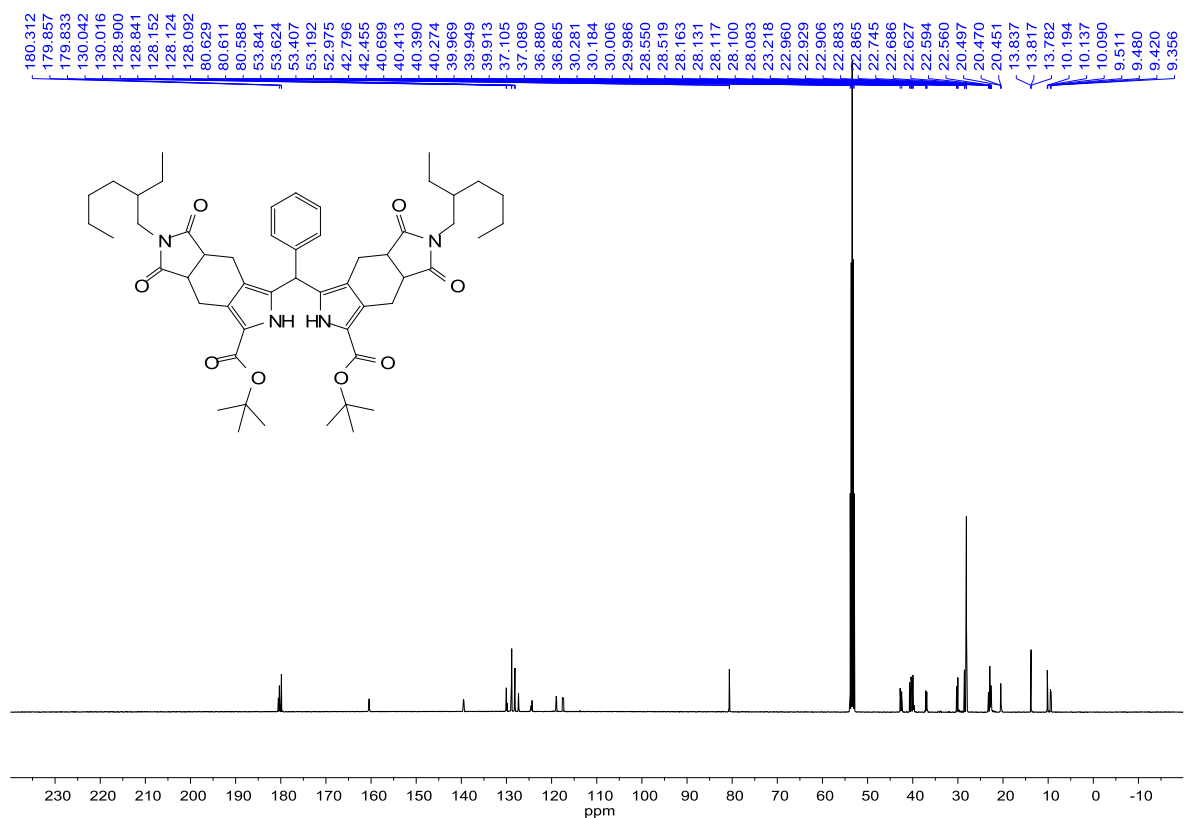
¹H NMR spectrum of 3.7 in CD₂Cl₂.



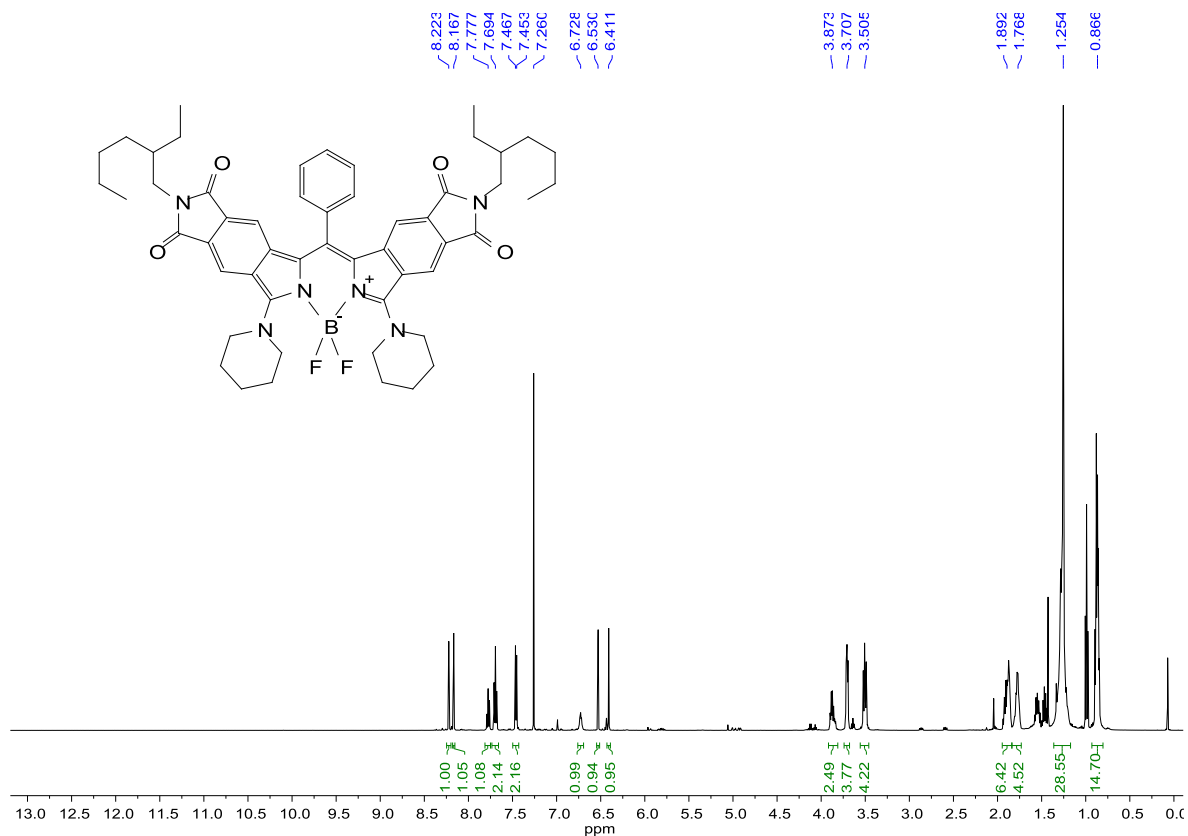
¹³C NMR spectrum of 3.7 in CD₂Cl₂.



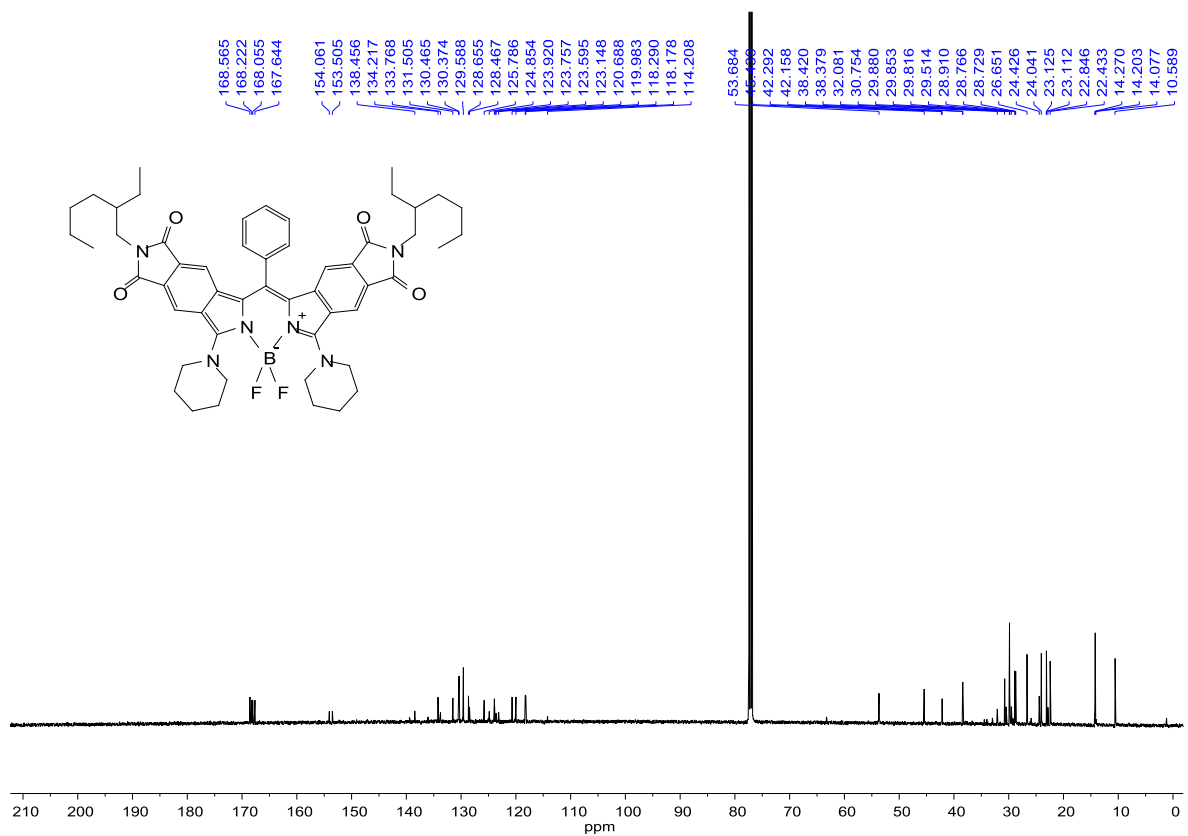
¹H NMR spectrum of **3.8** in CD₂Cl₂.



¹³C NMR spectrum of **3.8** in CD₂Cl₂.



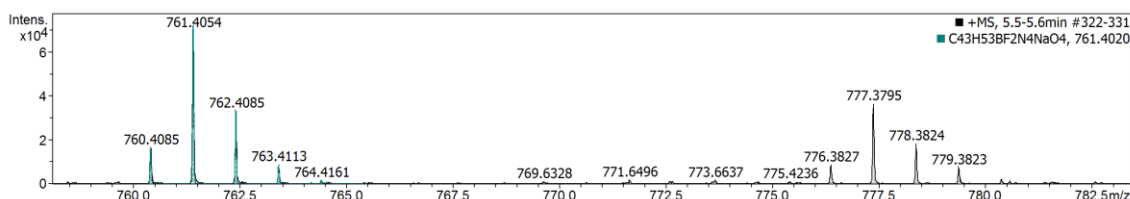
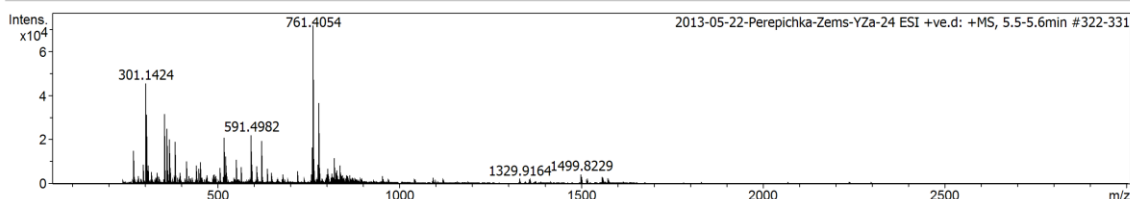
¹H NMR spectrum of 3.10 in CDCl₃.



¹³C NMR spectrum of 3.10 in CDCl₃.

Acquisition Parameter

Source Type	ESI	Ion Polarity	Positive	Set Nebulizer	0.6 Bar
Focus	Active	Set Capillary	4500 V	Set Dry Heater	180 °C
Scan Begin	50 m/z	Set End Plate Offset	-500 V	Set Dry Gas	4.0 l/min
Scan End	3000 m/z	Set Collision Cell RF	1500.0 Vpp	Set Divert Valve	Source



Meas. m/z	#	Ion Formula	m/z	err [ppm]	mSigma	# Sigma	Score	rdb	e ⁻ Conf	N-Rule
761.4054	1	C43H53BF2N4NaO4	761.4028	3.5	3.6	1	40.00	18.5	even	ok
	2	C44H49BF2N8Na	761.4041	-1.7	9.7	2	100.00	23.5	even	ok
	3	C36H57BF2N4NaO9	761.4085	-4.1	30.3	3	14.84	9.5	even	ok
777.3795	1	C44H49BF2KN8	777.3780	1.8	5.7	1	100.00	23.5	even	ok
	2	C43H53BF2KN4O4	777.3767	-3.6	8.5	2	33.05	18.5	even	ok

Bruker Compass DataAnalysis 4.1

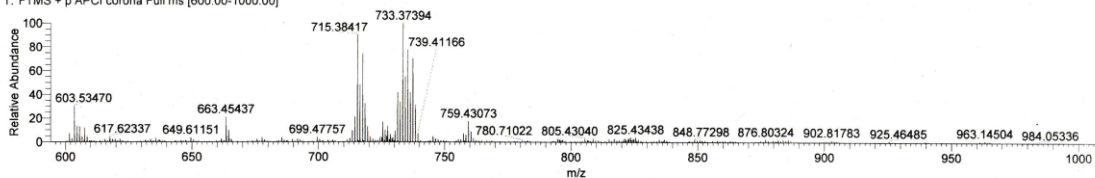
printed: 5/22/2013 12:19:04 PM

by: ADM

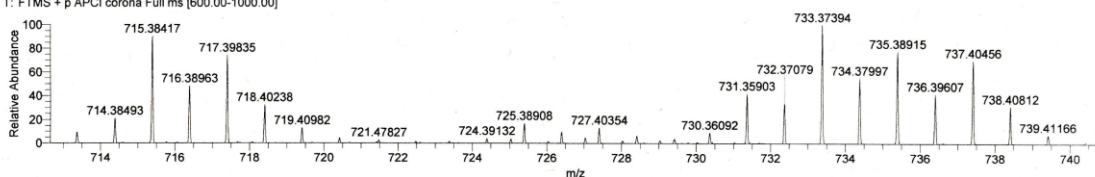
Page 1 of 1

HRMS spectrum of 3.1.

130523-03HRESI-Perepichka-Yaroslav-YZA24 #318-328 RT: 26.59-26.62 AV: 11 NL: 3.91E6
T: FTMS + p APCI corona Full ms [600.00-1000.00]

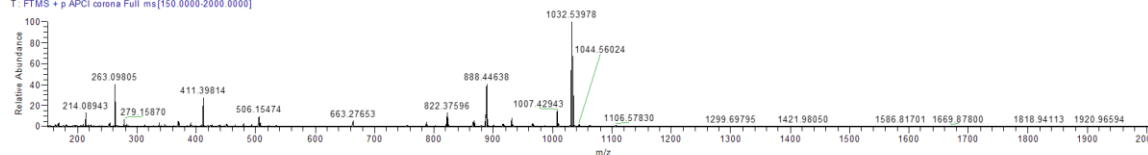


130523-03HRESI-Perepichka-Yaroslav-YZA24 #318-328 RT: 26.59-26.62 AV: 11 NL: 3.91E6
T: FTMS + p APCI corona Full ms [600.00-1000.00]

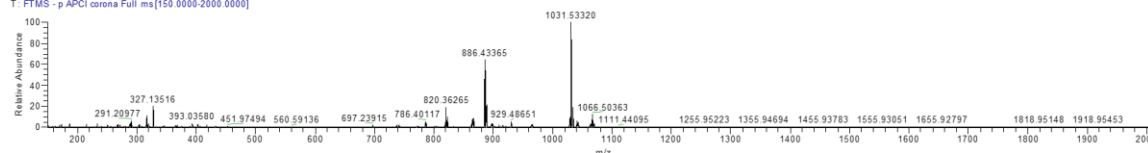


m/z	Intensity	Relative	Resolution	Charge	Theo. Mass	Delta (ppm)	RDB equiv.	Composition
731.35903	1647368.4	100.00	20419.09	1.00	731.35881	0.30	22.0	C ₄₅ H ₄₈ O ₅ N ₄ BF ₂
					731.36033	-1.77	22.5	C ₄₄ H ₄₈ O ₅ N ₄ F
					731.35747	2.14	22.5	C ₄₃ H ₄₆ O ₄ N ₄ BF ₂

HRMS spectrum of 3.2.

180827-05APCHR-Perepichka-ZemsYZ-M49 #669-702 RT: 3.06-3.14 AV: 34 NL: 8.46E7
T: FTMS + p APCI corona Full ms(150.0000-2000.0000)

m/z	Intensity	Relative	Resolution	Charge	Theo. Mass	Delta (ppm)	RDB equiv.	Composition
1032.53978	85067664.0	100.00	17081.93	1.00	1032.54052	-0.71	33.5	C ₆₅ H ₆₉ O ₄ N ₅ B F ₂
					1032.53670	2.99	33.0	C ₆₅ H ₇₀ O ₆ N ₄ B F

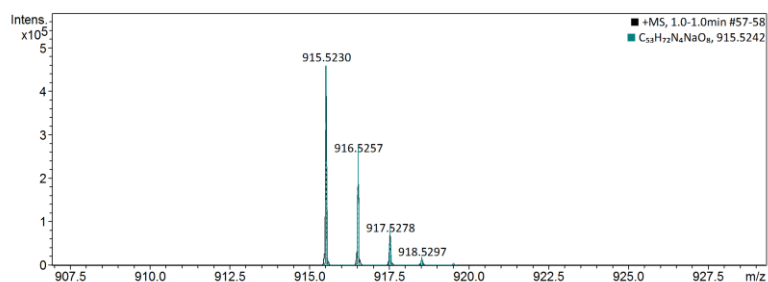
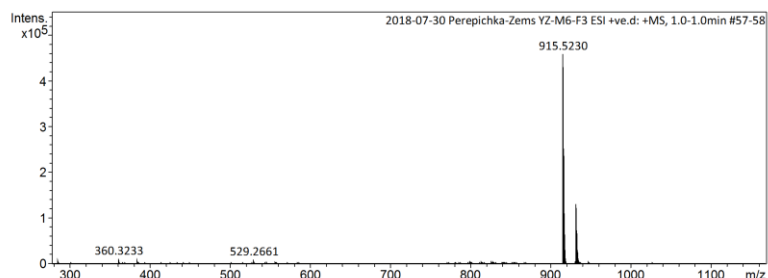
180827-05APCHR-Perepichka-ZemsYZ-M49 #709-738 RT: 3.16-3.23 AV: 30 NL: 4.43E6
T: FTMS - p APCI corona Full ms(150.0000-2000.0000)

m/z	Intensity	Relative	Resolution	Charge	Theo. Mass	Delta (ppm)	RDB equiv.	Composition
1031.53320	4443617.5	100.00	16774.57	1.00	1031.53379	-0.57	34.0	C ₆₅ H ₆₈ O ₄ N ₅ B F ₂
					1031.52997	3.14	33.5	C ₆₅ H ₆₉ O ₆ N ₄ B F

HRMS spectrum of 3.7.

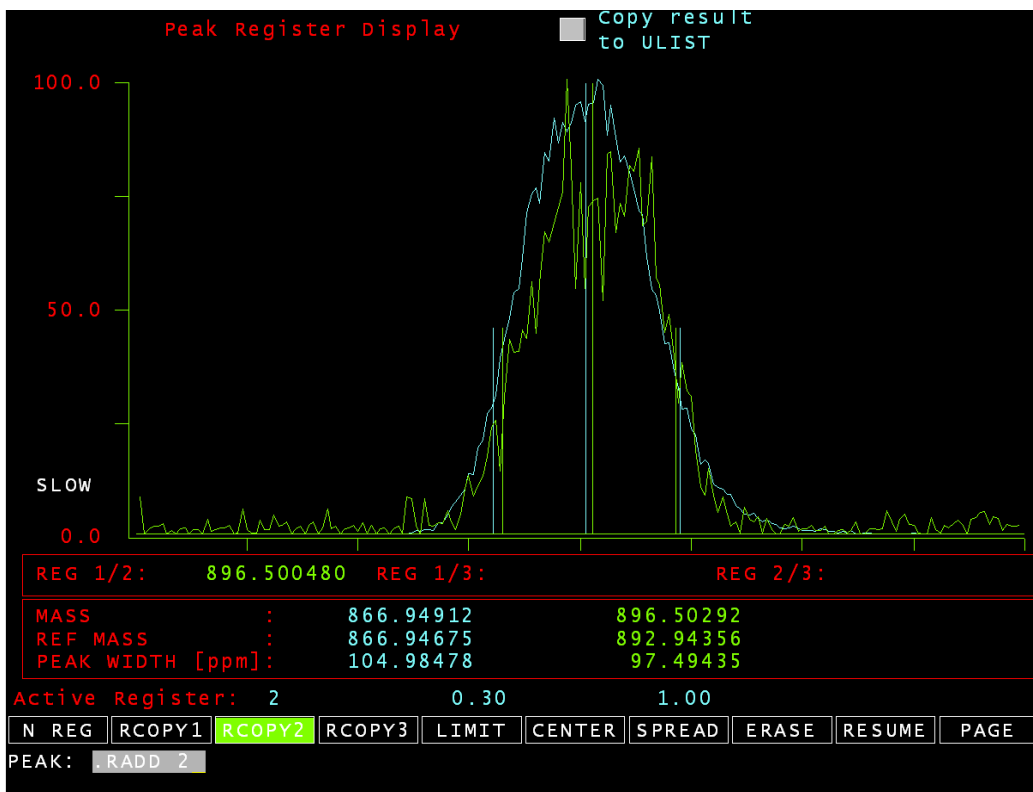
Acquisition Parameter

Source Type	ESI	Ion Polarity	Positive	Set Nebulizer	0.6 Bar
Focus	Not active	Set Capillary	4500 V	Set Dry Heater	180 °C
Scan Begin	90 m/z	Set End Plate Offset	-500 V	Set Dry Gas	4.0 l/min
Scan End	1200 m/z	Set Charging Voltage	2000 V	Set Divert Valve	Source
		Set Corona	0 nA	Set APCI Heater	0 °C



Meas. m/z	#	Ion Formula	m/z	err [ppm]	mSigma	# mSigma	Score	rdb	e ⁻ Conf	N-Rule
915.5230	1	C ₄₉ H ₆₈ N ₁₀ NaO ₆	915.5216	-1.6	21.4	1	41.34	20.5	even	ok
	2	C ₅₂ H ₇₆ NaO ₁₂	915.5229	-0.1	23.7	2	100.00	14.5	even	ok
	3	C ₅₀ H ₆₄ N ₁₄ NaO ₂	915.5229	-0.1	32.0	3	65.30	25.5	even	ok
	4	C ₅₃ H ₇₂ N ₄ NaO ₈	915.5242	1.4	35.9	4	32.38	19.5	even	ok
	5	C ₆₅ H ₆₈ N ₂ NaO	915.5224	-0.6	92.4	5	8.06	32.5	even	ok

HRMS spectrum of 3.8.



Elemental composition search on mass 896.50

m/z= 891.50-901.50

m/z	Theo. Mass	Delta (ppm)	RDB equiv.	Composition
896.50048	896.50023	0.25	23.5	C ₅₂ H ₆₅ O ₇ N ₆ ¹¹ B ₁
	896.49950	0.98	25.0	C ₅₄ H ₆₅ O ₅ N ₆ F ₁
	896.50157	-1.09	23.0	C ₅₄ H ₆₇ O ₈ N ₃ ¹¹ B ₁
	896.50198	-1.50	26.0	C ₅₂ H ₆₂ O ₂ N ₁₀ F ₂
	896.50199	-1.51	20.5	C ₅₃ H ₆₈ O ₇ N ₃ F ₂
	896.49816	2.32	25.5	C ₅₂ H ₆₃ O ₄ N ₉ F ₁
	896.50332	-2.84	25.5	C ₅₄ H ₆₄ O ₃ N ₇ F ₂
	896.50405	-3.57	24.0	C ₅₂ H ₆₄ O ₅ N ₇ ¹¹ B ₁ F ₁
	896.49664	3.84	24.5	C ₅₃ H ₆₃ O ₄ N ₆ ¹¹ B ₁ F ₂
	896.49568	4.80	24.5	C ₅₄ H ₆₆ O ₇ N ₅
	896.50540	-4.92	23.5	C ₅₄ H ₆₆ O ₆ N ₄ ¹¹ B ₁ F ₁

HRMS spectrum of **3.10**.

3.7 References

- (1) Bouit, P.-A.; Kamada, K.; Feneyrou, P.; Berginc, G.; Toupet, L.; Maury, O.; Andraud, C. Two-photon absorption-related properties of functionalized BODIPY dyes in the infrared range up to telecommunication wavelengths *Adv. Mater.* **2009**, *21*, 1151.
- (2) Lakhe, D.; Jairaj, K. K.; Pradhan, M.; Ladiwala, U.; Agarwal, N. Synthesis and photophysical studies of heteroaryl substituted-BODIPY derivatives for biological applications *Tetrahedron Lett.* **2014**, *55*, 7124.
- (3) Ortiz, M. J.; Agarrabeitia, A. R.; Duran-Sampedro, G.; Banuelos Prieto, J.; Lopez, T. A.; Massad, W. A.; Montejano, H. A.; Garcia, N. A.; Lopez Arbeloa, I. Synthesis and functionalization of new polyhalogenated BODIPY dyes. Study of their photophysical properties and singlet oxygen generation *Tetrahedron* **2012**, *68*, 1153.
- (4) Huang, L.; Yu, X.; Wu, W.; Zhao, J. Styryl Bodipy-C60 Dyads as Efficient Heavy-Atom-Free Organic Triplet Photosensitizers *Org. Lett.* **2012**, *14*, 2594.
- (5) Xiao, S.; Cao, Q.; Dan, F. Solid-emissive BODIPY derivatives: design, synthesis and applications *Curr. Org. Chem.* **2012**, *16*, 2970.
- (6) Umezawa, K.; Citterio, D.; Suzuki, K. New trends in near-infrared fluorophores for bioimaging *Anal. Sci.* **2014**, *30*, 327.
- (7) Benniston, A. C.; Copley, G. Lighting the way ahead with boron dipyrromethene (Bodipy) dyes *Phys. Chem. Chem. Phys.* **2009**, *11*, 4124.
- (8) Yogo, T.; Urano, Y.; Ishitsuka, Y.; Maniwa, F.; Nagano, T. Highly Efficient and Photostable Photosensitizer Based on BODIPY Chromophore *J. Am. Chem. Soc.* **2005**, *127*, 12162.
- (9) Boens, N.; Leen, V.; Dehaen, W. Fluorescent indicators based on BODIPY *Chem. Soc. Rev.* **2012**, *41*, 1130.
- (10) Singh, S. P.; Gayathri, T. Evolution of BODIPY Dyes as Potential Sensitizers for Dye-Sensitized Solar Cells *Eur. J. Org. Chem.* **2014**, *2014*, 4689.
- (11) Bessette, A.; Hanan, G. S. Design, synthesis and photophysical studies of dipyrromethene-based materials: insights into their applications in organic photovoltaic devices *Chem. Soc. Rev.* **2014**, *43*, 3342.
- (12) Ulrich, G.; Ziessel, R.; Harriman, A. The chemistry of fluorescent Bodipy dyes: versatility unsurpassed *Angew. Chem., Int. Ed.* **2008**, *47*, 1184.
- (13) Ziessel, R.; Ulrich, G.; Harriman, A. The chemistry of Bodipy: A new El Dorado for fluorescence tools *New J. Chem.* **2007**, *31*, 496.
- (14) Rao, M. R.; Mobin, S. M.; Ravikanth, M. Boron-dipyrromethene based specific chemodosimeter for fluoride ion *Tetrahedron* **2010**, *66*, 1728.
- (15) Kamkaew, A.; Lim, S. H.; Lee, H. B.; Kiew, L. V.; Chung, L. Y.; Burgess, K. BODIPY dyes in photodynamic therapy *Chem. Soc. Rev.* **2013**, *42*, 77.
- (16) Yamazawa, S.; Nakashima, M.; Suda, Y.; Nishiyabu, R.; Kubo, Y. 2,3-Naphtho-Fused BODIPYs as Near-Infrared Absorbing Dyes *J. Org. Chem.* **2016**, *81*, 1310.
- (17) Lu, H.; Mack, J.; Yang, Y.; Shen, Z. Structural modification strategies for the rational design of red/NIR region BODIPYs *Chem. Soc. Rev.* **2014**, *43*, 4778.
- (18) Lakshmi, V.; Rajeswara Rao, M.; Ravikanth, M. Halogenated boron-dipyrromethenes: synthesis, properties and applications *Org. Biomol. Chem.* **2015**, *13*, 2501.
- (19) Zhao, W.; Carreira, E. M. Conformationally restricted aza-bodipy: A highly fluorescent, stable, near-infrared-absorbing dye *Angew. Chem., Int. Ed.* **2005**, *44*, 1677.
- (20) Filatov, M. A.; Lebedev, A. Y.; Mukhin, S. N.; Vinogradov, S. A.; Cheprakov, A. V. π -Extended Dipyrins Capable of Highly Fluorogenic Complexation with Metal Ions *J. Am. Chem. Soc.* **2010**, *132*, 9552.

- (21) Zhao, J.; Xu, K.; Yang, W.; Wang, Z.; Zhong, F. The triplet excited state of Bodipy: formation, modulation and application *Chem. Soc. Rev.* **2015**, *44*, 8904.
- (22) Diring, S.; Puntoriero, F.; Nastasi, F.; Campagna, S.; Ziesel, R. Star-shaped multichromophoric arrays from bodipy dyes grafted on truxene core *J. Am. Chem. Soc.* **2009**, *131*, 6108.
- (23) Whited, M. T.; Djurovich, P. I.; Roberts, S. T.; Durrell, A. C.; Schlenker, C. W.; Bradforth, S. E.; Thompson, M. E. Singlet and triplet excitation management in a bichromophoric near-infrared-phosphorescent BODIPY-benzoporphyrin platinum complex *J. Am. Chem. Soc.* **2011**, *133*, 88.
- (24) Thoresen, L. H.; Kim, H.; Welch, M. B.; Burghart, A.; Burgess, K. Synthesis of 3,5-diaryl-4,4-difluoro-4-bora-3a,4a-diaza-s-indacene (BODIPY) dyes *Synlett* **1998**, 1276.
- (25) Burghart, A.; Kim, H.; Welch, M. B.; Thoresen, L. H.; Reibenspies, J.; Burgess, K.; Bergstroem, F.; Johansson, L. B. A. 3,5-Diaryl-4,4-difluoro-4-bora-3a,4a-diaza-s-indacene (BODIPY) dyes: synthesis, spectroscopic, electrochemical, and structural properties *J. Org. Chem.* **1999**, *64*, 7813.
- (26) Lu, H.; Mack, J.; Yang, Y.; Shen, Z. Structural modification strategies for the rational design of red/NIR region BODIPYs *Chem. Soc. Rev.* **2014**, *43*, 4778.
- (27) Qin, W.; Rohand, T.; Dehaen, W.; Clifford, J. N.; Driesen, K.; Beljonne, D.; Van Averbek, B.; Van der Auweraer, M.; Boens, N. Boron Dipyrromethene Analogs with Phenyl, Styryl, and Ethynylphenyl Substituents: Synthesis, Photophysics, Electrochemistry, and Quantum-Chemical Calculations *J. Phys. Chem. A* **2007**, *111*, 8588.
- (28) Gai, L.; Mack, J.; Lu, H.; Yamada, H.; Kuzuhara, D.; Lai, G.; Li, Z.; Shen, Z. New 2,6-Distyryl-Substituted BODIPY Isomers: Synthesis, Photophysical Properties, and Theoretical Calculations *Chem. - Eur. J.* **2014**, *20*, 1091.
- (29) Rohand, T.; Qin, W.; Boens, N.; Dehaen, W. Palladium-Catalyzed Coupling Reactions for the Functionalization of BODIPY Dyes with Fluorescence Spanning the Visible Spectrum *Eur. J. Org. Chem.* **2006**, *2006*, 4658.
- (30) Rohand, T.; Baruah, M.; Qin, W.; Boens, N.; Dehaen, W. Functionalisation of fluorescent BODIPY dyes by nucleophilic substitution *Chem. Commun.* **2006**, 266.
- (31) Boens, N.; Verbelen, B.; Dehaen, W. Postfunctionalization of the BODIPY Core: Synthesis and Spectroscopy *Eur. J. Org. Chem.* **2015**, *2015*, 6577.
- (32) Jiao, L.; Pang, W.; Zhou, J.; Wei, Y.; Mu, X.; Bai, G.; Hao, E. Regioselective Stepwise Bromination of Boron Dipyrromethene (BODIPY) Dyes *J. Org. Chem.* **2011**, *76*, 9988.
- (33) Loudet, A.; Burgess, K. BODIPY dyes and their derivatives: Syntheses and spectroscopic properties *Chem. Rev.* **2007**, *107*, 4891.
- (34) Ni, Y.; Wu, J. Far-red and near infrared BODIPY dyes: synthesis and applications for fluorescent pH probes and bio-imaging *Org. Biomol. Chem.* **2014**, *12*, 3774.

Chapter 4

Concluding Remarks

A new useful building block (**2.7**) was developed¹ from very inexpensive materials for pyrrole-based dyes with unique properties. Compared to similar 2,5-unsubstituted pyrroles, it exhibits remarkable stability at room temperature as a white crystalline solid. In addition to improving stability, the alkylimide moiety greatly enhances solubility of the building block which improved synthetic yield of target dyes (avoiding the “crashing-out” of in-situ polypyrromethane intermediates) and subsequent ease of chromatographic purification. Based on this new building block, a novel series of π -extended luminescent dyes were prepared for two popular and well-studied classes of dye: porphyrins in Chapter 2 and BODIPYs in Chapter 3.

Compared to parent dye PtTPTBP, PtPh₄TBIP **2.9** was shown to be more stable, soluble as well as an exceptional absorber ($\epsilon \sim 250000 \text{ M}^{-1}\text{cm}^{-1}$) and phosphorescent emitter. Similar properties were observed in deuterated analogue **2.11**, along with some unusual photophysical properties such as increased PLQY.¹ Compared to other porphyrins, **2.9** showed a significantly reduced rate of the photodegradation in stability experiments (up to 80 times slower compared to popular ZnTPP). This is an important property for materials science applications, where prolonged interaction with photons would lead to premature degradation of photoactive dyes. In addition, exceptionally high solubilities are achieved (up to 600 g/L) which are attributed to the four branched 2-ethylhexyl chains with stereogenic centers and saddle-shaped porphyrin core preventing π -stacking. Such a strong solubility would be considered an asset for incorporation into polymers (i.e. PMMA) for application in materials research. The preparation of this material was achieved on a multi-gram scale, which facilitates access to sufficient quantities of this type of material for practical applications. Efficient luminescence at 755 nm ($\Phi = 0.45$) and negligible self-absorption make PtTPTBIP **2.9** a highly desirable material for further photophysical study and practical applications. Seeking improvement of the photophysical properties seen in **2.9**, deuteration of the *meso*-Ph moieties in the PtAr₄TBIP family of dyes led to a modest ($\sim 17\%$) increase in PLQY when excited at the Soret band but a much smaller increase ($\sim 6\%$) when excited at

the Q-band. Such wavelength-dependant behaviour in Φ_P is not consistent with Kasha/Vavilov's rule and is thought to occur due to ultrafast funneling of the S_2 state to dark states with high k_{ISC} , potentially avoiding non-radiative relaxation in S_1 . Although further photophysical studies are required to gain a complete understanding of these unusual phenomena in these phosphorescent dyes, their highly emissive nature makes them attractive options for concurrent application in materials science (i.e. photovoltaics, photon upconversion).

The BODIPYs prepared in Chapter 3 exhibited unity PLQY ($\Phi_F = 1.0$) in the red region and remained emissive even in the NIR. Such was the case for the asymmetrically [b]-fused **3.7** product ($\lambda_{em} = 776$ nm) formed during the Sonogashira coupling of 3,5-halogenated BODIPY. 3,5-Piperidyl substituted BODIPY **3.10** was prepared and also displayed emission in the NIR ($\lambda_{em} = 773$ nm) but a much lower quantum yield ($\Phi_F = 0.12 \pm 0.06$) than its red-emitting counterparts, presumably lost due to the free-rotor effect of the *N*-pip moieties.

Overall, this thesis takes a look at how discrete structural modification within a given family of NIR dyes leads to observable changes in photophysical properties. Modifications applied to BODIPYs and porphyrins for potential enhancement of PLQY include linear benz[c]annulation, isotopic substitution and rigidifying the molecular structure of the dye via annulation of imide moieties. Deuteration showed some enhancement of PLQY in the porphyrin series, whose interesting deviation from Kasha/Vavilov's rule merits further photophysical study and the BODIPY series displayed a consistently brighter emission than published BODIPYs emitting at similar wavelengths, making them attractive NIR fluorophores for a number of applications.

- (1) Zems, Y.; Moiseev, A. G.; Perepichka, D. F. Convenient Synthesis of a Highly Soluble and Stable Phosphorescent Platinum Porphyrin Dye *Org. Lett.* **2013**, *15*, 5330.

Appendix

A1 Synthesis of Carboxylated Ar₄TBPs and their
Application to Molecular Tectonics

A2 Inducing Severe Distortion of the
Porphyrin Core via Quadruple *meso*, β -Fusion

Synthesis of Carboxylated Ar₄TBPs and their Application to Molecular Tectonics

This chapter describes preparation and characterization of two different peripherally carboxylated TBP ligands PtPh₄TBC₈P and H₂(*p*-CO₂HPh)₄TBIP. These materials were designed to be used as tectons in an effort to create extended crystalline, Ln(III)-based MOFs. Additionally, discrete Ln(III)-porphyrin structures would be prepared starting from appropriately end-capped Ln(II)hfac complexes. The photophysical properties of the extended and discrete materials will be examined in solution and solid-state to gain insight into the photosensitizing/luminescent properties of the porphyrin tecton in the context of metal-organic materials (MOMs).

A1.1 Introduction to Molecular Tectonics

Although crystallization is a common phenomenon, it is still not fully understood. Crystal engineers and materials scientists are still not able to fully and accurately predict the way a certain material will interact with itself or others in the solid-state. Numerous focused studies are lending insight into the trends and structure-property relationships of rational crystal design within specific systems, while application to generalized cases remains somewhat unpredictable.¹ The primary aspiration within the field of molecular tectonics² is the rational, bottom-up design of extended multidimensional networks from individual building blocks (tectons), relying on intermolecular recognition and self-assembly properties. Reversibility is of utmost importance when choosing to act on for specific application since irreversible intermolecular interactions will lead to deformed/faulty molecular networks without the possibility of self-correction. Of particular relevance to the molecular recognition properties of tectons are van der Waals, electrostatic, halogen-

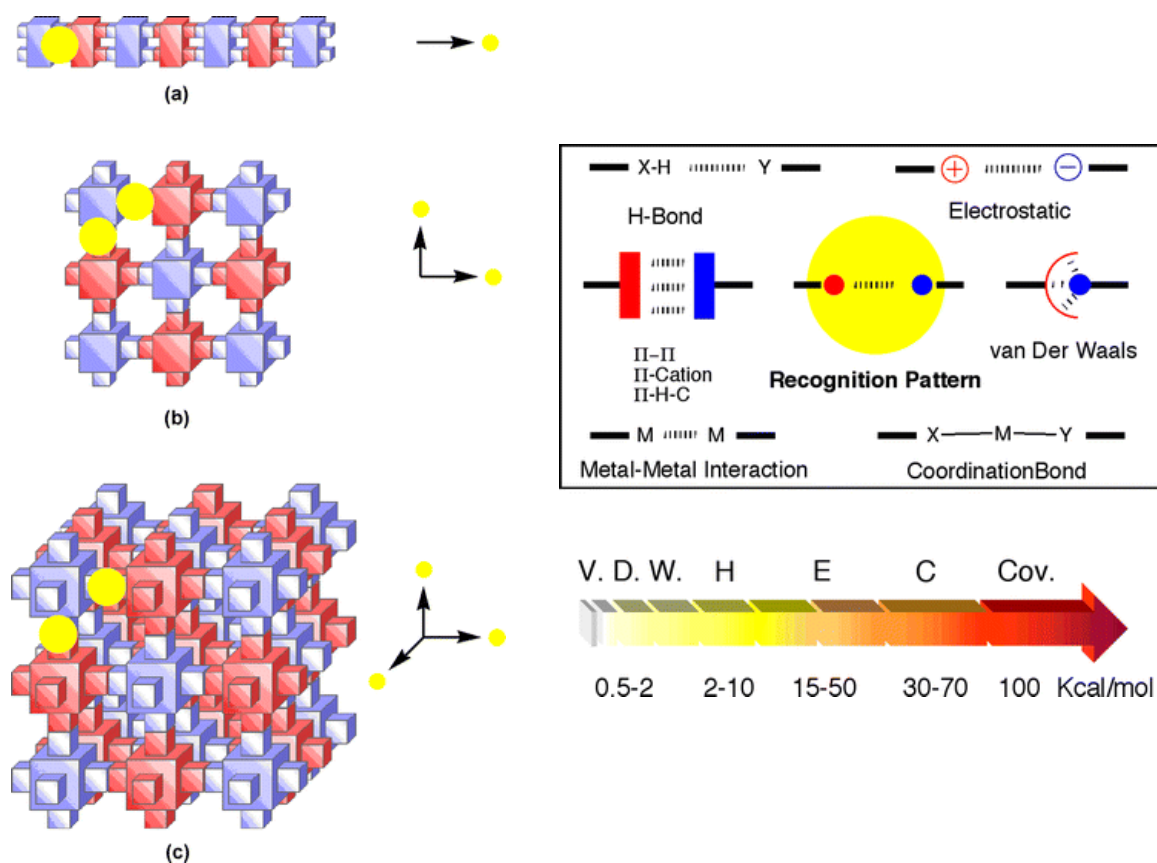


Figure A1.1 (Left) Schematic representation of 1-D (a), 2-D (b) and 3-D (c) networks formed upon molecular recognition processes between complementary tectons leading to assembling nodes (yellow circle). (Right) Toolbox of reversible intermolecular interactions and their energies. Reproduced from [1] with permission from The Royal Society of Chemistry.

halogen, π - π and hydrogen bonding interactions as well as and metal coordination (Figure A1.1). Permutations of these interactions and their combinations give rise to a variety of recognition patterns (Figure A1.2). In particular, aromatic carboxylates such as naphthalenedicarboxylate (NSC) ligands, have proven to be robust building blocks for extended MOM structures.

A1.1.1 Carboxylated Porphyrins as Tectons

Among the wide variety of tectons available, carboxylated porphyrins have proven themselves to be valuable additions to the chemist's toolbox. Their excellent chemical and

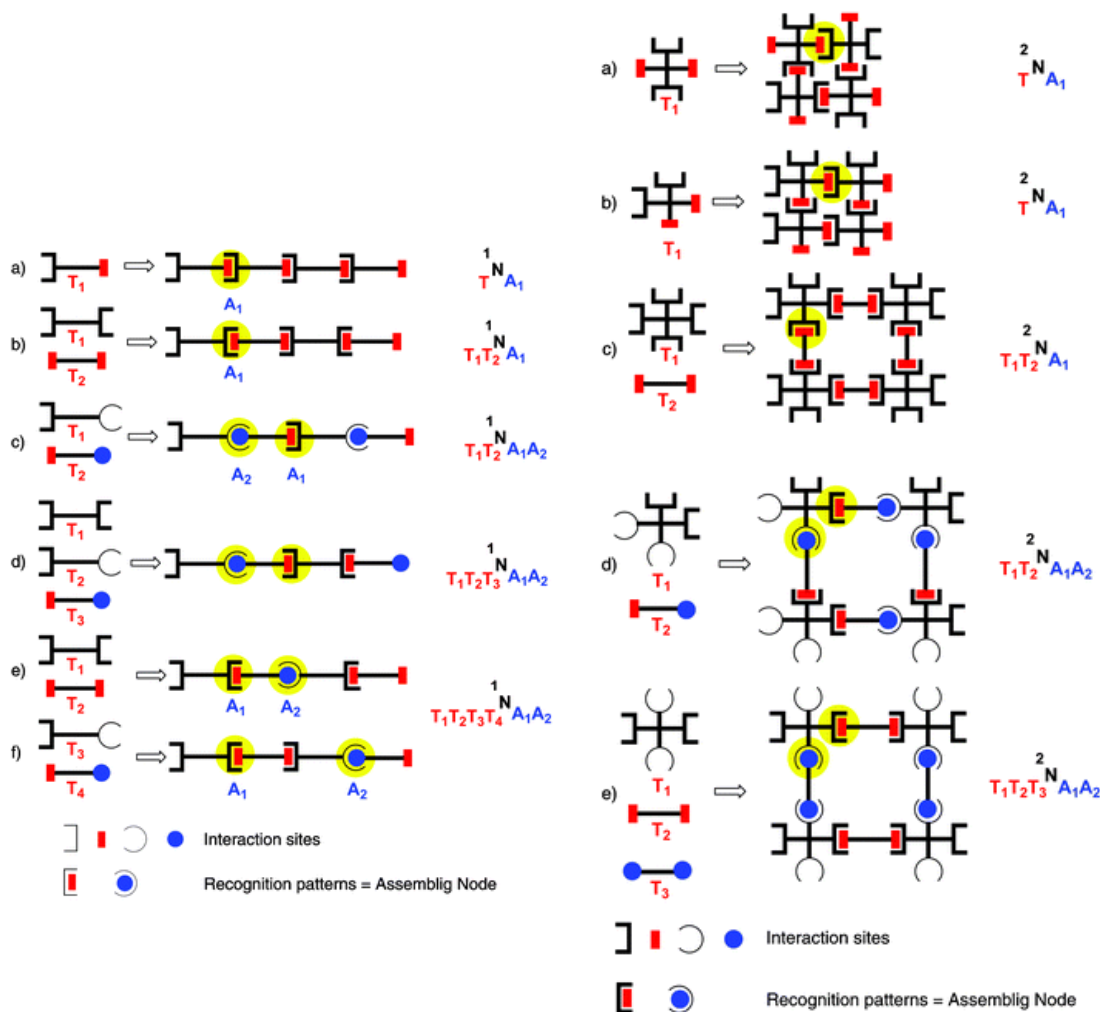


Figure A1.2 Non-exhaustive representation of 1D (left) and 2D (right) molecular networks based on self-assembly of complementary tectons (T_i and A_i represent tectons and assembling nodes, respectively). Reproduced with permission from [1] © 2013 Royal Society of Chemistry.

thermal stability, modular synthetic chemistry, rigid/planar shape and attractive optical properties make them desirable choices for a number of supramolecular applications, including guest adsorption/separation, catalysis (oxidative, Lewis acid, biomimetic^{13,14} and electrocatalysis), nano-thin MOF films and light harvesting. Of particular interest to materials scientists is the possibility of achieving panchromatic absorption through highly ordered metalloporphyrin frameworks for applications in photovoltaic devices and solar energy conversion. Carboxylated porphyrins have also been applied as an integral part of synthetic strategy to crystal engineering,^{22,23} formation of metal-metalloporphyrin frameworks (MMPFs), metal-organic polyhedron cages^{8,25,26} (MOPs), pillared MOFs²⁷ and post-synthetic metal exchange²⁸ within MOFs (Figure 3.3) including single-crystal to single-

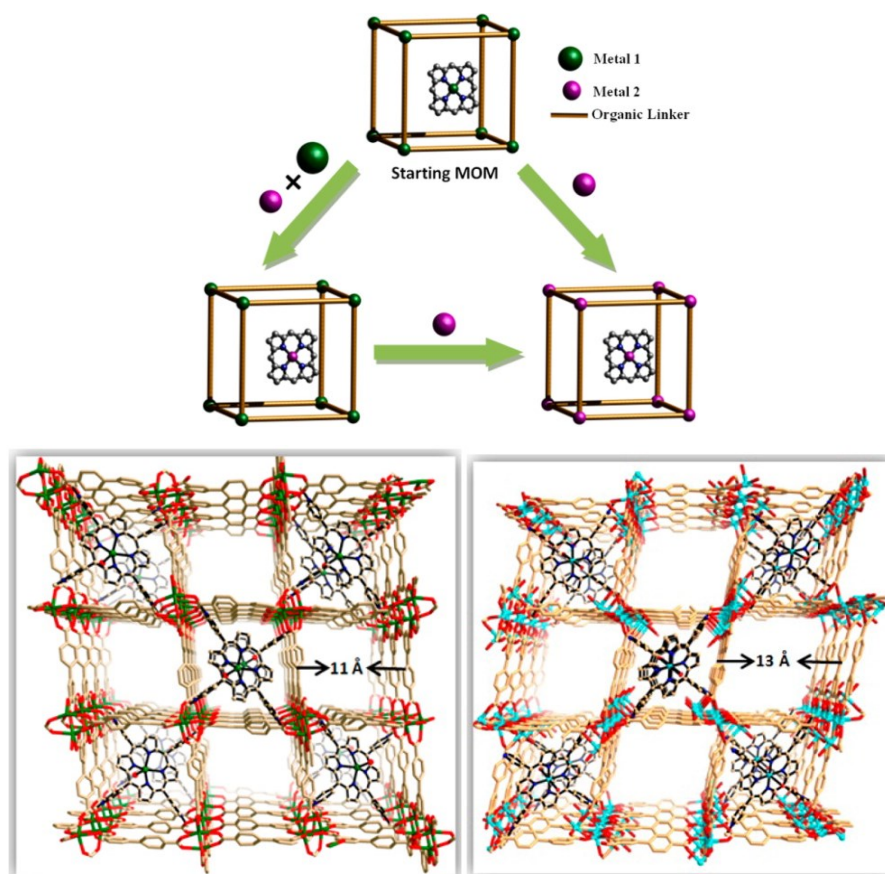


Figure A1.3 Post-synthetic metal exchange within metal-organic materials (MOMs). Reprinted with permission from [28] © 2017 American Chemical Society

crystal transformation. For example, reversible photochromism has been achieved in a carboxylated porphyrin-based single-crystal²⁹ MOF (Figure A1.4) while retaining single-crystallinity. A noteworthy counterpart to carboxylated porphyrins are *meso*-

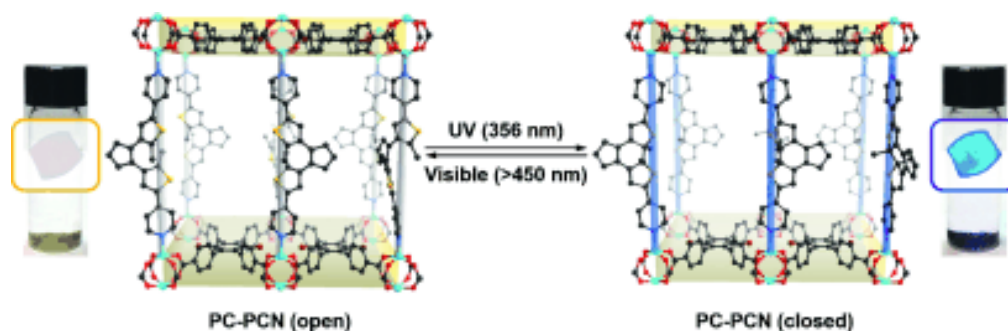


Figure A1.4 Reversible photochromic reaction in single-crystalline PC-PCN upon irradiation with UV-visible light. Reprinted with permission from [29] © 2017 Wiley & Sons

tetrapyrridylporphyrins, which have also been used in systematic assemblies³⁰ of similar porphyrinic networks.

A1.1.2 Lanthanide Complexes

Bright emission from lanthanides is usually achieved by sensitization with an organic chromophore in order to overcome the forbidden *f-f* transitions of Ln(III) cations. Carboxylated porphyrins ligands are prime candidates for such sensitization due to their well-matched excited-state energy levels, strong absorption in the UV and visible regions as well as universal coordination to nearly all Ln(III) cations. Ln(III)/porphyrin complexes deserve special mention due to their varied coordination modes (Figure A1.5) and storied history, evident from the number of publications dedicated to the synthesis and study of Ln porphyrin/phthalocyanine single-molecule complexes (*i.e.* double/triple-decker sandwiches). Comparatively fewer publications use Ln(III) and porphyrin tectons in tandem to generate extended, organized structures.³²⁻³⁴ An interesting example is efficient photosensitization of ¹O₂ by a Eu(III)/porphyrin³⁵ MOF.

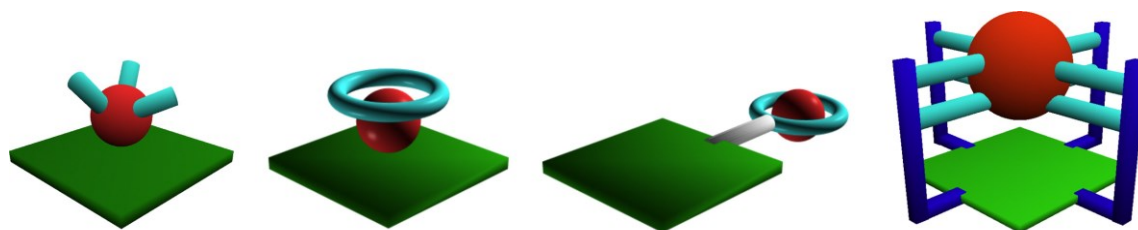


Figure A1.5 Different coordination modes for Ln/porphyrin complexes: (from left to right) core-coordinated (multi/mono-ligated) and peripheral mono/multi-coordination. Reprinted with permission from [31] © Elsevier 2017.

A1.2 Synthesis of π -Extended Carboxylated Porphyrins

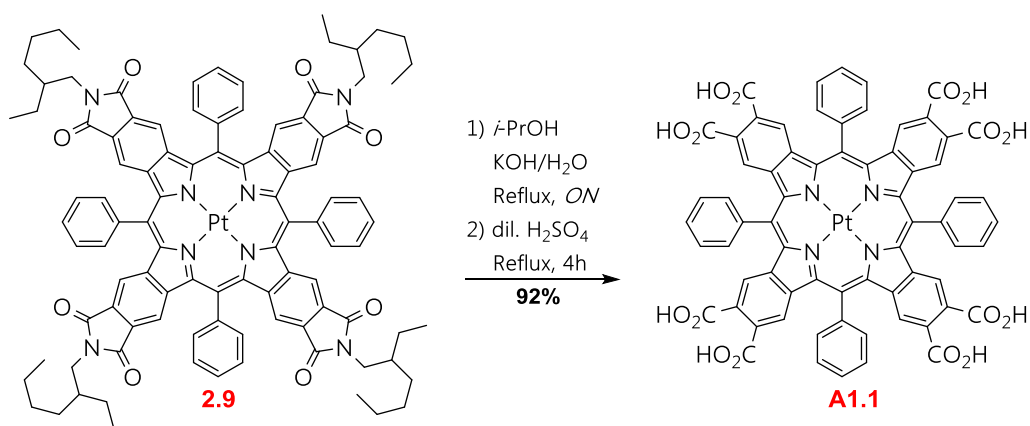
A1.2.1 Core-Carboxylated PtPh₄TBC₈P

During the large scale synthesis of PtPh₄TBIP (see Chapter 2), a large amount of carbonaceous tar was formed during the one pot metalation/aromatization that proved to be soluble only in refluxing benzonitrile. In order to remove the tar, the glassware was immersed in a base bath (*i*PrOH/KOH/H₂O) over several days. Upon returning to the base bath, it had unexpectedly acquired a vivid green colour which was thought to be due to be a platinum porphyrinoid species. After recovery from the caustic bath, it became apparent

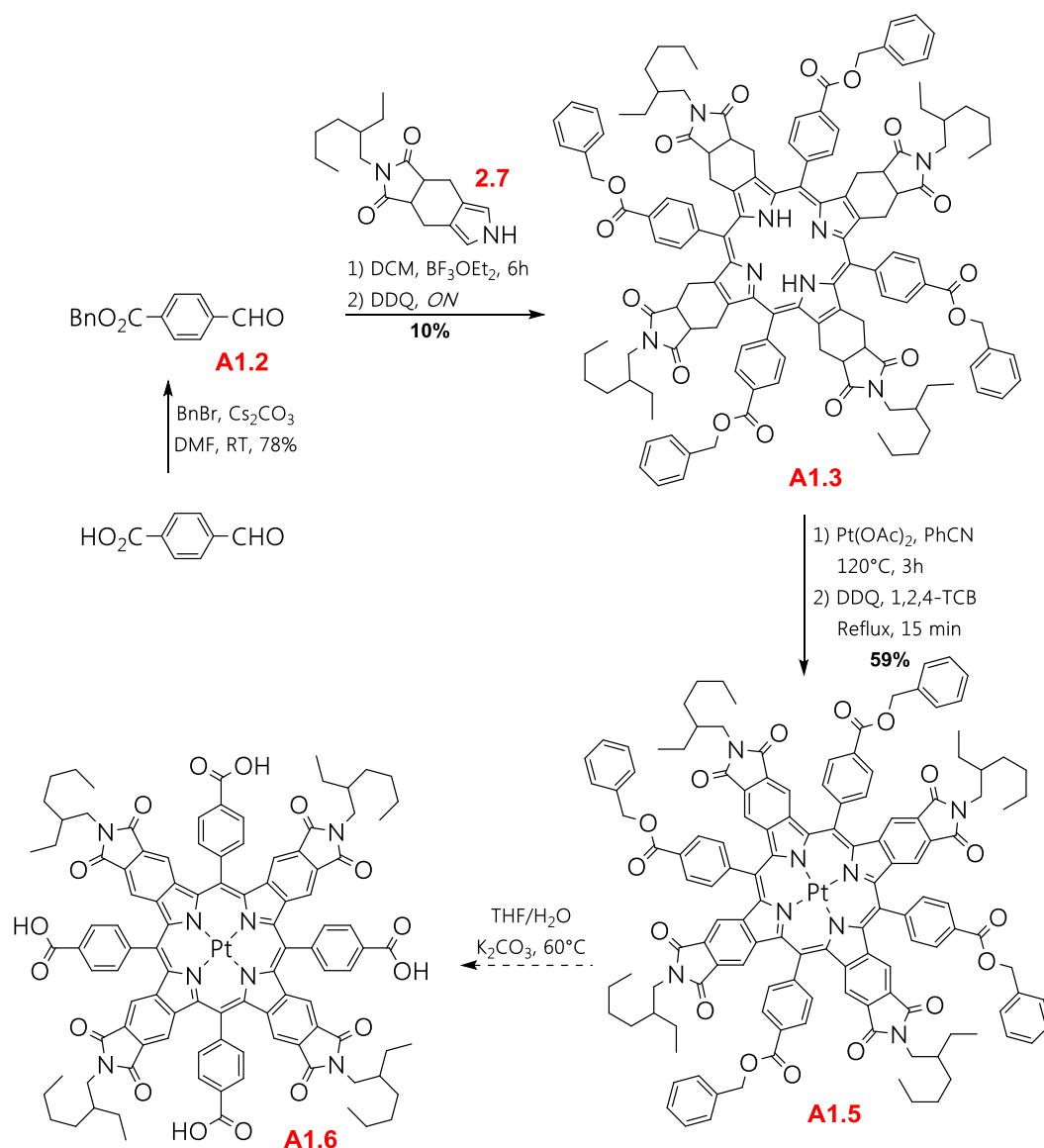
that the π -extended porphyrin had survived prolonged treatment with the base bath. This unresolved mixture of porphyrinoids did not retain the characteristics of high solubility in organic solvents (comparable to those observed for PtPh₄TBIP) and became readily soluble in water upon treatment with base. Additionally, the absorption spectrum for the porphyrin mixture revealed Soret/Q-band shape and maxima nearly identical to those of **2.9**. For these reasons, it was hypothesized that trapped dye in the insoluble tar leached into the base bath and hydrolyzed into a π -extended Pt (II) porphyrin species bearing multiple pre-carboxylated moieties (**A1.1**). Since the porphyrin mixture from the base bath proved difficult to purify, *de novo* sequential basic/acidic hydrolysis of clean PtPh₄TBIP yielded PtPh₄TBC₈P **A1.1** in excellent yield (Scheme 3.1). Recrystallization of **A1.1** from alcohols should be avoided in order to prevent unwanted esterification of the peripheral carboxylate moieties since traces of unwanted acid may remain.

A1.2.2 *meso*-Carboxylated H₂(4-CO₂HPh)₄TBIP

Since a vicinal arrangement of carboxylate moieties does not possess favourable geometry for coordination to Ln(III), an alternative to **A1.1** was thought up, where the carboxylate ligands were located on the peripheral *meso*-Ph rings. Having a single binding site in the same vicinity (instead of two in **A1.1**) as well as being located further away from the bulky core should decrease the likelihood of unwanted and non-ordered material formation. As it stands, one of the most widely adopted arrangements³⁶ of chelating ligands on porphyrins has been tetratopic aryl *p*-carboxylates. Typically, a short-chain alkyl ester protects the carboxylic group during porphyrin synthesis and is later deep protected with aqueous acid or base. After facile hydrolysis of imide **2.7** was observed in base, it was immediately



Scheme A1.1 Sequential basic and acidic hydrolysis of PtPh₄TBIP into PtPh₄TBC₈P **A1.1**.



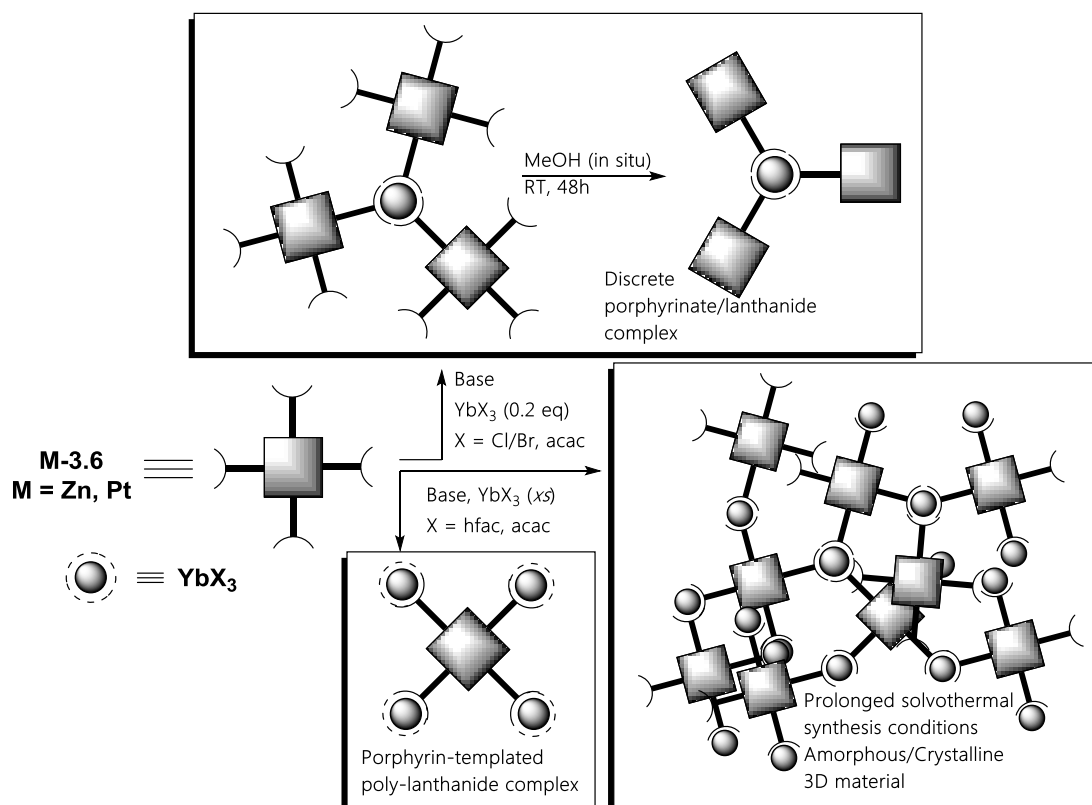
Scheme A1.2 Synthesis of tetratopic *p*-carboxylated $\text{H}_2(4\text{-CO}_2\text{HPh})_4\text{TBIP}$ **A1.6** starting from pyrrole **2.7**.

apparent that methodology relying on aqueous de-protection of an the ester moiety would not compatible with the imide starting material. Benzyl tetraester porphyrin **A1.3** was prepared under standard Lindsey conditions from aldehyde **A1.2** (prepared according to a previously published³⁷ procedure). The condensation is unfortunately low-yielding (10%), which is uncharacteristically compared to the similar published preparations (25-35%). Platinum insertion occurs with greater yield with platinum (II) acetate as opposed to platinum chloride, the latter seemingly causing decomposition of the macrocycle upon prolonged heating. Aromatization of the intermediate platinum porphyrin yields **A1.5** in modest yield (59%). De-protection of the benzyl esters with H_2/Pd produces insoluble

porphyrin-like material, possibly affecting the imide moieties and cleaving the alkyl chains. It was found that a water/tetrahydrofuran system along with a weak base (i.e. K_2CO_3) is able to cleave the benzyl esters at $60^\circ C$ while leaving the alkyl chains intact. However, a pure sample of **A1.6** was never completely characterized.

A1.3 Co-crystallization with Ln(III)

Two separate strategies are employed to generate new extended structures (Scheme 3.3). Exploratory co-crystallization by slow evaporation of **A1.6** with Ln(III) salts (Yb, Nd) at room temperature provided preliminary indication of interaction between the two



Scheme A1.3 Outline of general strategies for co-crystallization of Ln(III) with **A1.6**. species but not in a reproducible nor well-defined manner. Varying the counterion (halides, acetylacetonate, nitrates) does not seem to have an effect on solution properties or crystallization success rates.

A1.4 Conclusions

Octatopic (A1.1) and tetratopic (A1.6) porphyrins were prepared and are currently being characterized for their use in extended lanthanide-based MOMs. Pt(II) porphyrin A1.5 was prepared and its photophysical properties are currently being characterized. Preliminary crystallization with halide salts of Ln(III) has resulted in mixed results, indicating that the Ln(III) species interacts sporadically with the carboxylated tecton A1.6 but requires a change in crystallization conditions in order to achieve more extended coordination networks. It is possible that the saddle-shaped porphyrin core and abundant aliphatic side chains preclude required symmetry to drive crystallization.

A1.5 Experimental

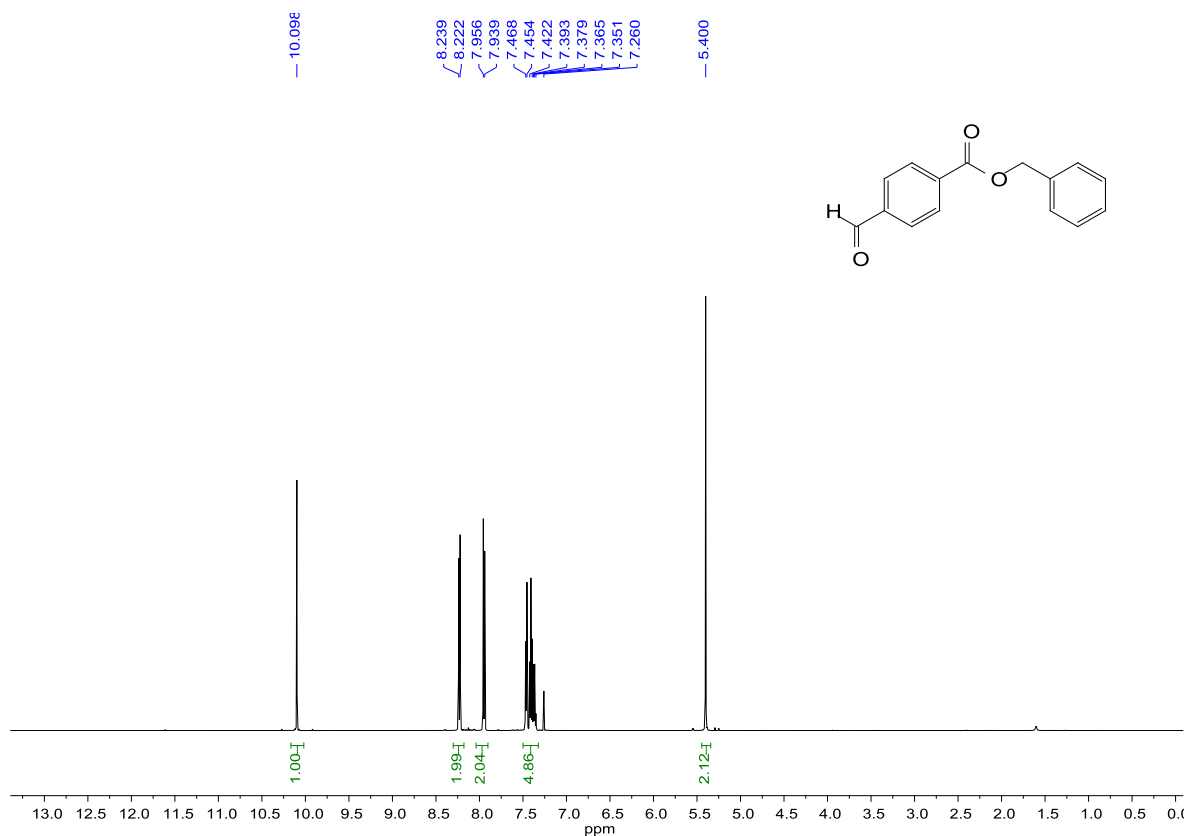
Platinum (II) acetate PtCl₂ (4.41 g, 19.5 mmol) and silver (II) acetate (6.84 g, 41 mmol) were added to a 250 mL round-bottom flask equipped with a magnetic stir bar. Glacial AcOH (150 mL) was added and a reflux condenser was attached to the flask. The headspace was flushed with N₂, the flask was covered with aluminium foil and the mixture was refluxed for 1 h. The flask was cooled to room temperature and stirred overnight in the dark. The precipitated AgCl was filtered off and the solvent was removed under reduced pressure. The residue was re-dissolved in dichloromethane (100 mL) and passed through a short pad of Celite (2") to remove residual metallic Pt and AgCl. Upon addition of Et₂O (200 mL), the dark blue solids that precipitated out of solution were filtered out yielding Pt(OAc)₂ as a dark blue powder (2.65 g, 43.4%).

Benzyl 4-formylbenzoate (A1.2) 4-Formylbenzoic acid (75.0 g, 0.333 mol) was added to a 1000 L round-bottom flask equipped with a magnetic stir bar and dissolved in dry dimethylformamide (500 mL) and anhydrous Cs₂CO₃ (114 g, 0.350 mol) was added. With vigorous magnetic stirring, benzyl bromide (58.2 g, 0.340 mol) was added in one portion. The mixture was vigorously stirred for 3 h at room temperature before pouring the contents of the flask into H₂O (5000 mL) and extracting with Et₂O (3 x 500 mL per 1500 mL H₂O). The combined organic fractions were concentrated down to 1200 mL and were washed with H₂O (500 x 3 mL), saturated sodium bicarbonate (500 mL) and brine (500 mL) followed by

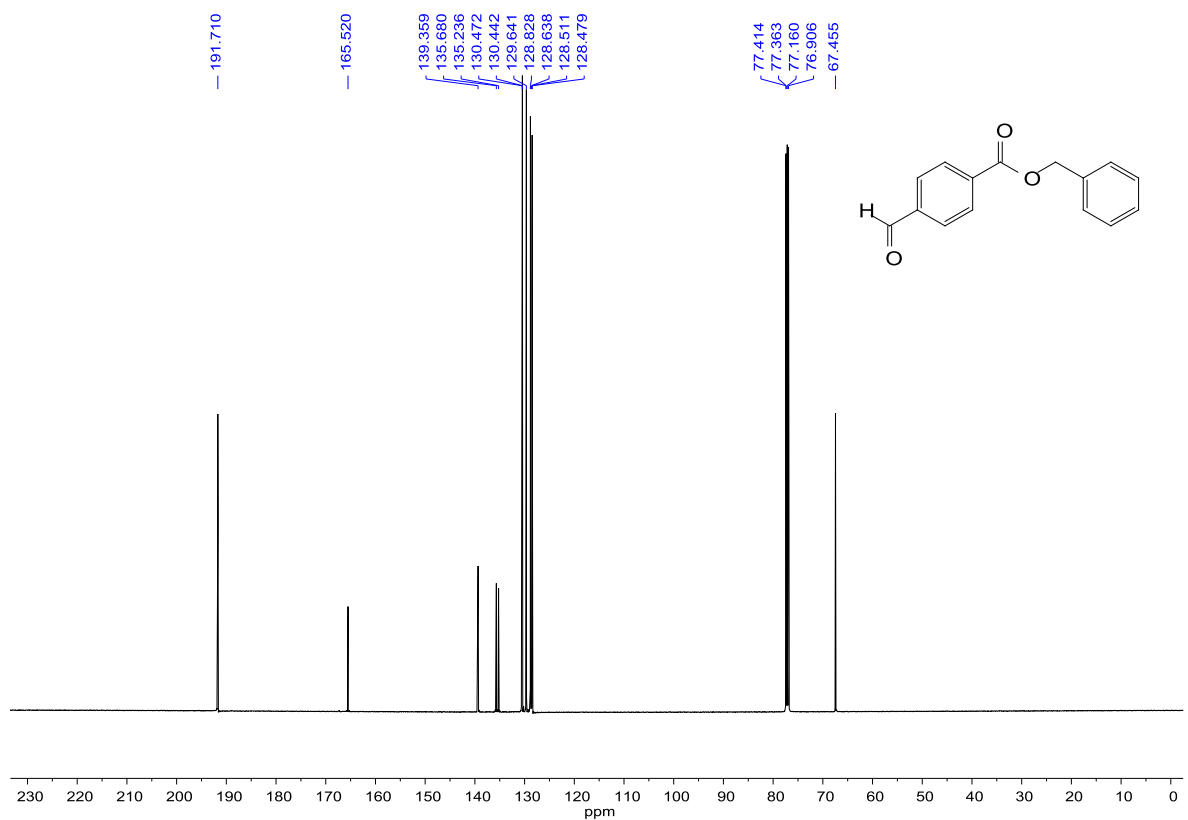
drying over MgSO₄ (20 g). The solvent was removed under reduced pressure, yielding a white solid which was distilled over as a clear oil (155 °C @ 63 μ) which crystallized upon standing overnight yielding **3.2** as an opaque crystalline solid (62.1 g, 78%). ¹H NMR (500 MHz, CDCl₃) δ 10.10 (s, 1H), 8.23 (d, *J* = 8.5 Hz, 2H), 7.95 (d, *J* = 8.5 Hz, 2H), 7.41 (m, 5H), 5.40 (s, 2H); ¹³C NMR (125 MHz, CDCl₃) δ 191.70, 165.52, 139.36, 135.68, 135.24, 130.47, 130.44, 129.64, 128.83, 128.64, 128.51, 128.48, 67.46. Spectral data matches published values.

Pt(4-(CO₂Bn)Ph)₄TBIP (A1.5) Pyrrole **2.7** (6.4 g, 24 mmol) and aldehyde **A1.2** (5.1 g, 24 mmol) were added to a 4500 mL boiling flask equipped with a magnetic stir bar. Dry dichloromethane (2400 mL) was added and sparged thoroughly with N₂ for 45 min over vigorous stirring. The flask was covered with aluminium foil and BF₃OEt₂ (0.75 mL) was added in one portion. The contents were stirred for 6 h before adding a booster aliquot of BF₃OEt₂ (0.3 mL) and after an additional 15 min of stirring, DDQ (5.9 g, 26 mmol) was added. The solution was stirred overnight in the dark before adding NEt₃ (3 mL) and removing the solvent under reduced pressure. The black residue was re-dissolved in PhMe and passed through a short pad of silica (6") (liquid-loading) with a PhMe/NEt₃ gradient mobile phase. The fast eluting fractions were collected and the solvent was removed under reduced pressure. The brown residue was re-dissolved in dichloromethane (500 mL) and washed vigorously with HCl (5%, 500 mL). The organic fraction was then washed with brine (500 mL) and dried over Na₂SO₄ (30 g). The solvent was concentrated down to ~25 mL and the solution was transferred to a tall-form 250 mL beaker. The solution was then very slowly layered with a large excess of hexanes/ Et₂O (1:1 v/v, up to the 200 mL mark on the beaker). The beaker was covered with a watch glass under a larger 1L beaker to minimize disturbances and left alone for several days. Once the layers were fully mixed, the contents were filtered and the solids were washed with cold hexanes/Et₂O (1:1, 2 x 100 mL). The free-base form of the porphyrin **A1.3** was obtained by washing with saturated Na₂CO₃ solution and isolated as deep purple crystals (1.16 g, 10.2%) by slow evaporation-induced crystallization out of a 1:1 v/v methanol/dichloromethane solution. Porphyrin **A1.3** (75 mg, 33.5 μmol) and Pt(OAc)₂ (15 mg, 50 μmol) were added to a 200 mL round-bottom flask equipped with a magnetic stir bar and dissolved in PhCN. After thorough degassing, the flask was covered with aluminium foil and brought to 120 °C. After stirring for 6 h, the flask was cooled to room temperature and the solvent was distilled under reduced pressure. The contents of the flask were re-dissolved in 1,2,4-TCB (80 mL) and DDQ (0.88 g, 390 μmol).

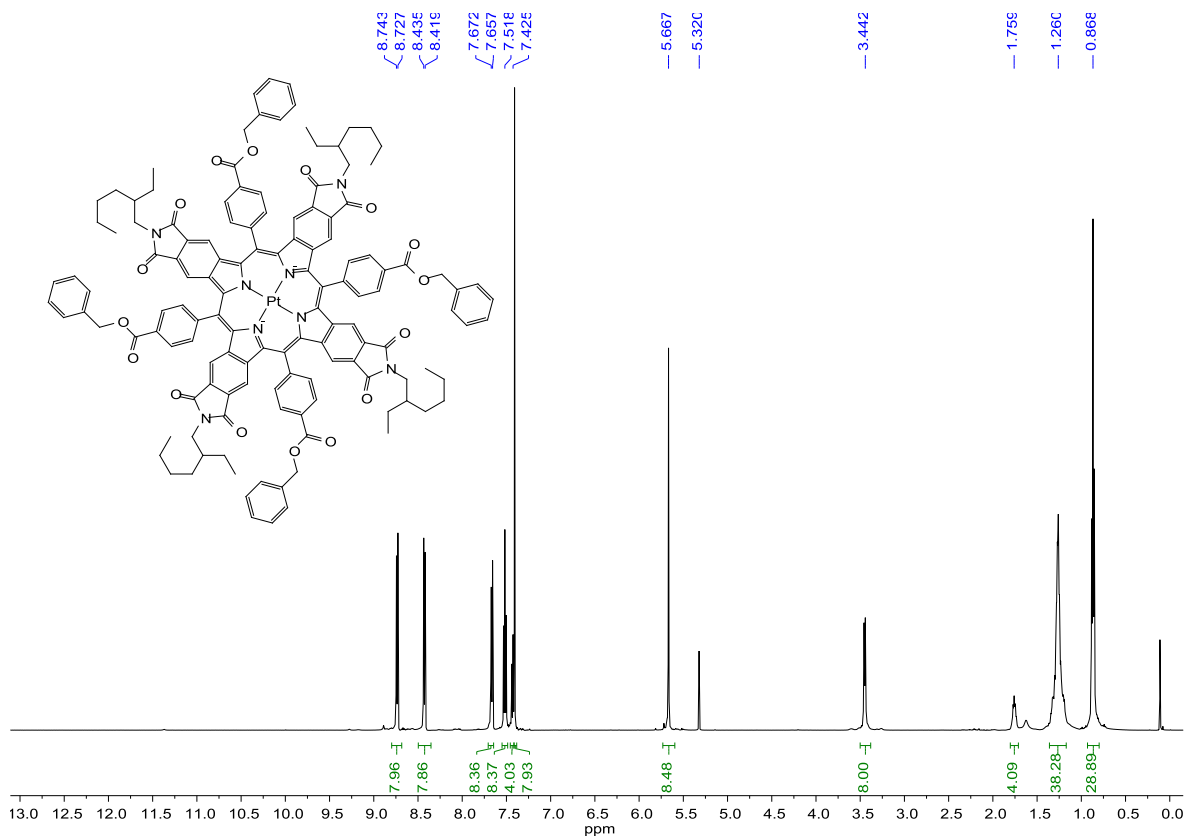
After degassing the solution once again, a reflux condenser was attached to the flask. The contents of the flask were slowly (30 °C/15 min.) brought to reflux and stirred at 200 °C for 1 h. The flask was equipped with a short-path distillation apparatus and the solvent was removed under reduced pressure, leaving behind a metallic green/red residue which was dissolved in dichloromethane (300 mL) and passed through a short pad of silica (2"). The bright green fraction was collected in the solvent was once removed. The residue was purified with column chromatography (PhMe/EtOAc) and recrystallized from dichloromethane/methanol to afford **A1.5** as purple/green solids with a metallic lustre (45 mg, 59%). ¹H NMR (500 MHz, CDCl₃) δ 8.73 (d, *J* = 8.0 Hz, 8H), 8.42 (d, *J* = 8.0 Hz, 8H), 7.66 (d, *J* = 7.5 Hz, 8H), 7.52 (t, *J* = 8.0 Hz, 8H), 7.42 (m, 4H), 7.41 (s, 8H), 5.67 (s, 8H), 3.44 (d, *J* = 7.0 Hz, 8H), 1.76 (m, 4H), 1.26 (m, 38H), 0.87 (m, 29H); ¹³C NMR (125 MHz, CDCl₃) δ 168.24, 166.34, 144.54, 141.06, 137.30, 136.70, 134.41, 132.79, 131.76, 129.78, 129.30, 128.83, 128.61, 120.73, 119.75, 67.91, 42.61, 38.93, 31.12, 29.17, 24.41, 23.53, 14.39, 10.74; HRMS APCI, *m/z* for C₁₃₂H₁₁₉O₁₆N₈Pt calcd 2266.83973, found 2266.83994.



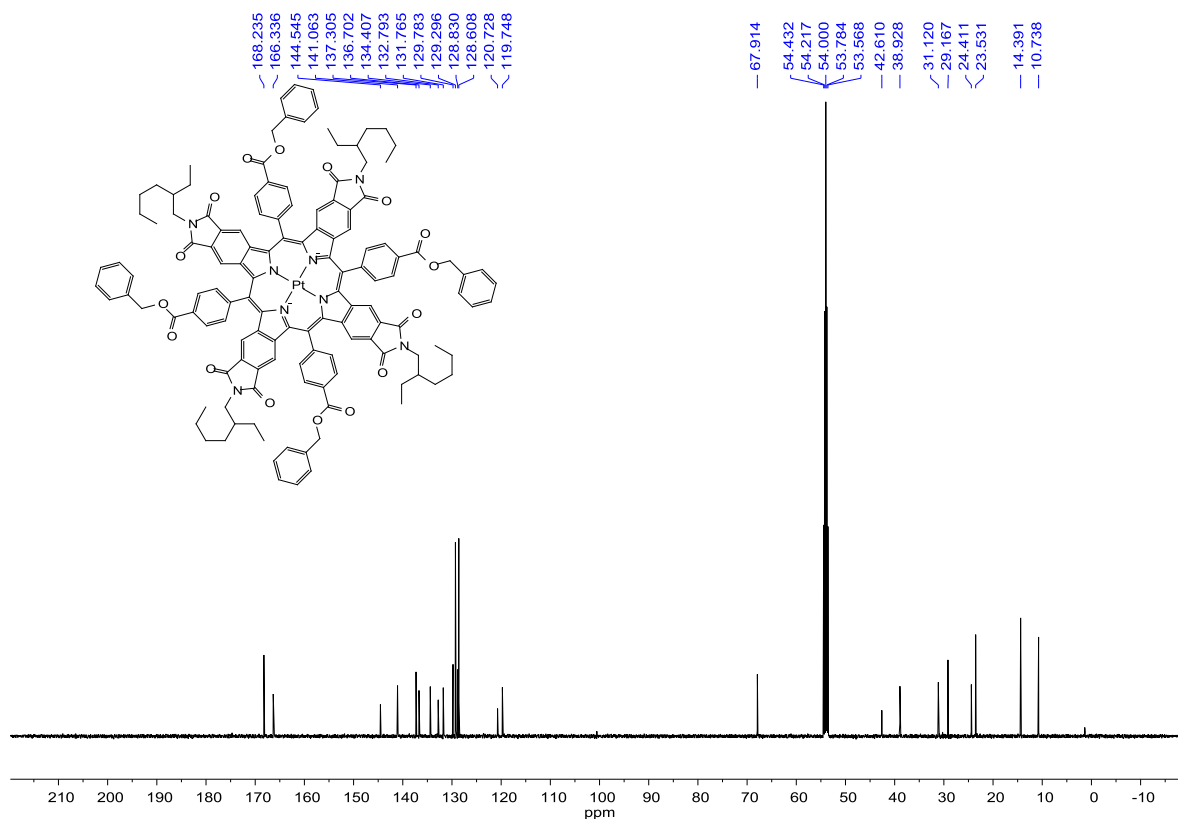
^1H NMR spectrum of **A1.2** in CDCl_3 .



^{13}C NMR spectrum of **A1.2** in CDCl_3 .

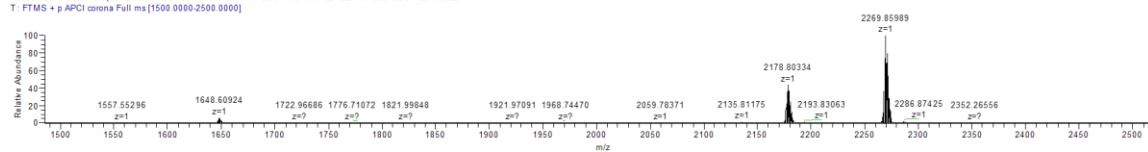


¹H NMR spectrum of A1.5 in CD₂Cl₂.

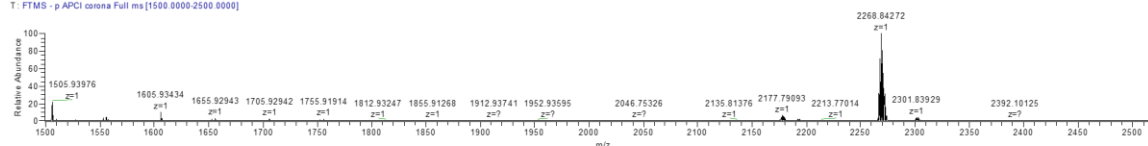


¹³C NMR spectrum of A1.5 in CD₂Cl₂.

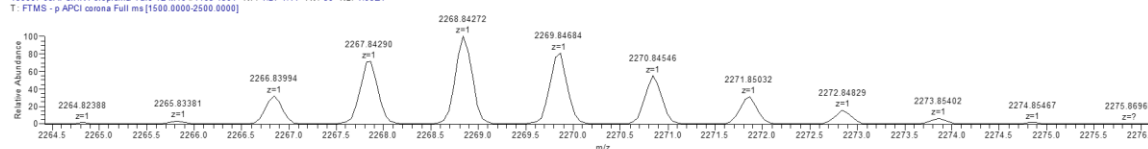
180807-03APCIHR-Perepichka-Yaro-YZ M10 #1386-1417 RT: 3.99-4.10 AV: 32 SB: 4.3 83-3.98 NL: 1.00E5
T: FTMS - p APCI corona Full ms [1500 0000-2500 0000]



180807-03APCIHR-Perepichka-Yaro-YZ M10 #1463-1501 RT: 4.27-4.41 AV: 39 NL: 4.08E4
T: FTMS - p APCI corona Full ms [1500 0000-2500 0000]



180807-03APCIHR-Perepichka-Yaro-YZ M10 #1463-1501 RT: 4.27-4.41 AV: 39 NL: 4.08E4
T: FTMS - p APCI corona Full ms [1500 0000-2500 0000]



m/z	Intensity	Relative	Resolution	Charge	Theo. Mass	Delta (ppm)	RDB equiv.	Composition
2266.83994	13149.3	100.00	11596.86	1.00	2266.83973	0.10	77.5	C ₁₃₂ H ₁₁₉ O ₁₆ N ₈ Pt

HRMS spectrum for **A1.5**.

A1.6 References

- (1) Hosseini, M. W. Reflection on molecular tectonics *CrystEngComm* **2004**, *6*, 318.
- (2) Mann, S. Molecular tectonics in biomineralization and biomimetic materials chemistry *Nature* **1993**, *365*, 499.
- (3) Hosseini, M. W. Molecular Tectonics: From Simple Tectons to Complex Molecular Networks *Acc. Chem. Res.* **2005**, *38*, 313.
- (4) Gangu, K. K.; Maddila, S.; Jonnalagadda, S. B. A review on synthesis, crystal structure and functionality of naphthalenedicarboxylate ligated metal-organic frameworks *Inorg. Chim. Acta* **2017**, *466*, 308.
- (5) Gao, W.-Y.; Zhang, Z.; Cash, L.; Wojtas, L.; Chen, Y.-S.; Ma, S. Two rare indium-based porous metal-metalloporphyrin frameworks exhibiting interesting CO₂ uptake *CrystEngComm* **2013**, *15*, 9320.
- (6) Wang, X.-S.; Chrzanowski, M.; Kim, C.; Gao, W.-Y.; Wojtas, L.; Chen, Y.-S.; Peter Zhang, X.; Ma, S. Quest for highly porous metal-metalloporphyrin framework based upon a custom-designed octatopic porphyrin ligand *Chem. Commun.* **2012**, *48*, 7173.
- (7) Choi, E.-Y.; Wray, C. A.; Hu, C.; Choe, W. Highly tunable metal-organic frameworks with open metal centers *CrystEngComm* **2009**, *11*, 553.
- (8) Morris, W.; Voloskiy, B.; Demir, S.; Gándara, F.; McGrier, P. L.; Furukawa, H.; Cascio, D.; Stoddart, J. F.; Yaghi, O. M. Synthesis, Structure, and Metalation of Two New Highly Porous Zirconium Metal–Organic Frameworks *Inorg. Chem.* **2012**, *51*, 6443.

- (9) Feng, D.; Jiang, H.-L.; Chen, Y.-P.; Gu, Z.-Y.; Wei, Z.; Zhou, H.-C. Metal–Organic Frameworks Based on Previously Unknown Zr₈/Hf₈ Cubic Clusters *Inorg. Chem.* **2013**, *52*, 12661.
- (10) Xie, M.-H.; Yang, X.-L.; He, Y.; Zhang, J.; Chen, B.; Wu, C.-D. Highly Efficient C≡H Oxidative Activation by a Porous Mn^{III}–Porphyrin Metal–Organic Framework under Mild Conditions *Chem. - Eur. J.* **2013**, *19*, 14316.
- (11) Gao, W.-Y.; Wojtas, L.; Ma, S. A porous metal-metalloporphyrin framework featuring high-density active sites for chemical fixation of CO₂ under ambient conditions *Chem. Commun.* **2014**, *50*, 5316.
- (12) Feng, D.; Chung, W.-C.; Wei, Z.; Gu, Z.-Y.; Jiang, H.-L.; Chen, Y.-P.; Darensbourg, D. J.; Zhou, H.-C. Construction of Ultrastable Porphyrin Zr Metal–Organic Frameworks through Linker Elimination *J. Am. Chem. Soc.* **2013**, *135*, 17105.
- (13) Feng, D.; Gu, Z.-Y.; Li, J.-R.; Jiang, H.-L.; Wei, Z.; Zhou, H.-C. Zirconium-Metalloporphyrin PCN-222: Mesoporous Metal–Organic Frameworks with Ultrahigh Stability as Biomimetic Catalysts *Angew. Chem. Int. Ed.* **2012**, *51*, 10307.
- (14) Chen, Y.; Hoang, T.; Ma, S. Biomimetic Catalysis of a Porous Iron-Based Metal–Metalloporphyrin Framework *Inorg. Chem.* **2012**, *51*, 12600.
- (15) Jahan, M.; Bao, Q.; Loh, K. P. Electrocatalytically Active Graphene–Porphyrin MOF Composite for Oxygen Reduction Reaction *J. Am. Chem. Soc.* **2012**, *134*, 6707.
- (16) Motoyama, S.; Makiura, R.; Sakata, O.; Kitagawa, H. Highly Crystalline Nanofilm by Layering of Porphyrin Metal–Organic Framework Sheets *J. Am. Chem. Soc.* **2011**, *133*, 5640.
- (17) Makiura, R.; Motoyama, S.; Umemura, Y.; Yamanaka, H.; Sakata, O.; Kitagawa, H. Surface nano-architecture of a metal–organic framework *Nat. Mater.* **2010**, *9*, 565.
- (18) Lee, C. Y.; Farha, O. K.; Hong, B. J.; Sarjeant, A. A.; Nguyen, S. T.; Hupp, J. T. Light-Harvesting Metal–Organic Frameworks (MOFs): Efficient Strut-to-Strut Energy Transfer in Bodipy and Porphyrin-Based MOFs *J. Am. Chem. Soc.* **2011**, *133*, 15858.
- (19) Son, H.-J.; Jin, S.; Patwardhan, S.; Wezenberg, S. J.; Jeong, N. C.; So, M.; Wilmer, C. E.; Sarjeant, A. A.; Schatz, G. C.; Snurr, R. Q.; Farha, O. K.; Wiederrecht, G. P.; Hupp, J. T. Light-Harvesting and Ultrafast Energy Migration in Porphyrin-Based Metal–Organic Frameworks *J. Am. Chem. Soc.* **2013**, *135*, 862.
- (20) Beletskaya, I.; Tyurin, V. S.; Tsivadze, A. Y.; Guillard, R.; Stern, C. Supramolecular Chemistry of Metalloporphyrins *Chem. Rev.* **2009**, *109*, 1659.
- (21) Drain, C. M.; Varotto, A.; Radivojevic, I. Self-Organized Porphyrinic Materials *Chem. Rev.* **2009**, *109*, 1630.
- (22) Desiraju, G. R. Crystal Engineering: A Holistic View *Angew. Chem. Int. Ed.* **2007**, *46*, 8342.
- (23) Moulton, B.; Zaworotko, M. J. From Molecules to Crystal Engineering: Supramolecular Isomerism and Polymorphism in Network Solids *Chem. Rev.* **2001**, *101*, 1629.
- (24) Gao, W.-Y.; Chrzanowski, M.; Ma, S. Metal-metalloporphyrin frameworks: a resurging class of functional materials *Chem. Soc. Rev.* **2014**, *43*, 5841.
- (25) Wang, X.-S.; Chrzanowski, M.; Gao, W.-Y.; Wojtas, L.; Chen, Y.-S.; Zaworotko, M. J.; Ma, S. Vertex-directed self-assembly of a high symmetry supermolecular building block using a custom-designed porphyrin *Chem. Sci.* **2012**, *3*, 2823.
- (26) Wang, X.-S.; Meng, L.; Cheng, Q.; Kim, C.; Wojtas, L.; Chrzanowski, M.; Chen, Y.-S.; Zhang, X. P.; Ma, S. Three-Dimensional Porous Metal–Metalloporphyrin Framework Consisting of Nanoscopic Polyhedral Cages *J. Am. Chem. Soc.* **2011**, *133*, 16322.
- (27) Choi, E.-Y.; Barron, P. M.; Novotny, R. W.; Son, H.-T.; Hu, C.; Choe, W. Pillared Porphyrin Homologous Series: Intergrowth in Metal–Organic Frameworks *Inorg. Chem.* **2009**, *48*, 426.

- (28) Burnett, B. J.; Barron, P. M.; Hu, C.; Choe, W. Stepwise Synthesis of Metal–Organic Frameworks: Replacement of Structural Organic Linkers *J. Am. Chem. Soc.* **2011**, *133*, 9984.
- (29) Park, J.; Feng, D.; Yuan, S.; Zhou, H.-C. Photochromic metal-organic frameworks: Reversible control of singlet oxygen generation *Angew. Chem., Int. Ed.* **2015**, *54*, 430.
- (30) Chung, H.; Barron, P. M.; Novotny, R. W.; Son, H.-T.; Hu, C.; Choe, W. Structural Variation in Porphyrin Pillared Homologous Series: Influence of Distinct Coordination Centers for Pillars on Framework Topology *Cryst. Growth Des.* **2009**, *9*, 3327.
- (31) Bulach, V.; Sguerra, F.; Hosseini, M. W. Porphyrin lanthanide complexes for NIR emission *Coord. Chem. Rev.* **2012**, *256*, 1468.
- (32) Zou, C.; Wu, C.-D. Functional porphyrinic metal-organic frameworks: crystal engineering and applications *Dalton T.* **2012**, *41*, 3879.
- (33) Goldberg, I. Crystal engineering of porphyrin framework solids *Chem. Commun.* **2005**, 1243.
- (34) Burnett, B. J.; Barron, P. M.; Choe, W. Recent advances in porphyrinic metal-organic frameworks: materials design, synthetic strategies, and emerging applications *CrystEngComm* **2012**, *14*, 3839.
- (35) Demel, J.; Kubat, P.; Millange, F.; Marrot, J.; Cisarova, I.; Lang, K. Lanthanide-Porphyrin Hybrids: from Layered Structures to Metal-Organic Frameworks with Photophysical Properties *Inorg. Chem.* **2013**, *52*, 2779.
- (36) Zha, Q.; Rui, X.; Wei, T.; Xie, Y. Recent advances in the design strategies for porphyrin-based coordination polymers *CrystEngComm* **2014**, *16*, 7371.
- (37) Basato, M.; Biffis, A.; Martinati, G.; Tubaro, C.; Venzo, A.; Ganis, P.; Benetollo, F. Reaction of platinum acetate with phosphines and molecular structure of trans-[Pt(OAc)₂(PPh₃)₂] *Inorg. Chim. Acta* **2003**, *355*, 399.
- (38) Riches, A. G.; Cablewski, T.; Glattauer, V.; Thissen, H.; Meagher, L. Scalable synthesis of an integrin-binding peptide mimetic for biomedical applications *Tetrahedron* **2012**, *68*, 9448.

Inducing Severe Distortion of the Porphyrin Core via Quadruple *meso*, β -Fusion

Whereas previous chapters described syntheses, properties and applications of materials synthesized from a specialty pyrrole precursor, this chapter explores the consequences of non-planarity in a novel symmetrically-fused porphyrin prepared from less exotic starting materials. The interest in this work was achieving DR-NIR porphyrinoids by putting to better use the aromatic moieties already present (*i.e.* the nearly-orthogonal *meso*-Ph rings). By forcing them into a co-planar arrangement with the pyrrole moieties, a more extended π -system and more soluble/less aggregating core could be achieved simultaneously. Calculations are used to gauge the extent of macrocyclic distortion, which in turn is used to rationalize the observed photophysical properties in solution for the tetra-fused porphyrin and its Pt complex. Applications of such materials fall under the purview of previous chapters (DR-NIR luminescent materials).

A2.1 Introduction to Fused Porphyrins

The origin and effects of non-planarity in porphyrin systems has always been a highly studied and debated facet of porphyrin science. In the context of biological systems^{1,2} (*i.e.* cytochromes, chlorophyll), macrocycle non-planarity is a major driving force for assembly of larger biological systems such as folded protein structures and photosynthetic chains. Under the umbrella of materials science, non-planarity greatly influences a material's photophysical properties, solubility/aggregation properties and in some cases, supramolecular π - π recognition. It is well-known to researchers within the field that non-planarity in a porphyrin macrocycle core results in bathochromic shifting of optical

properties.³ Senge and Kalisch have observed progressively red-shifted absorption bands in solution by systematically introducing β -ethyl substituents⁴ to tetraphenylporphyrin H₂TPP. Crystal structures support this observation by showing a stepwise increase in distortion of the macrocycle with increasing peripheral crowding in the series H₂TPP, H₂DETPP, H₂TETPP, H₂OHTPP and H₂OETPP. While the shift in optical properties is often considerable, distorted porphyrins tend to have lower PLQY than their planar counterparts. Porphyrins exhibiting out-of-plane distortion show an enhancement of non-radiative decay rates of the $^1(\pi,\pi^*)$ excited state and increased ISC rates arising from increased spin-orbit coupling of the nonplanar macrocycle.⁵

While many options are available to achieve redder emission in porphyrin compounds, exploiting non-planarity comes with the added benefit of making the dyes less prone to aggregation/more soluble. While there has been a lot of discourse and controversy⁶ as to the precise source of the red-shifting in nonplanar systems, it is now evident that *meso*-aryl substituents contribute to extension of the π -system by partially rotating out of their orthogonal orientation with the porphyrin core. In turn, the porphyrin core distorts (saddling, ruffling) somewhat to accommodate the steric bulk of the aryl moieties. Hence, the degree of actual distortion in the porphyrin macrocycle results from a balancing act between the in-plane π -conjugation of the aryl rings and retention of planarity/aromaticity of the porphyrin core. However, the functionalization of the *meso*-positions with freely-rotating aryl rings introduces additional degrees of freedom which can

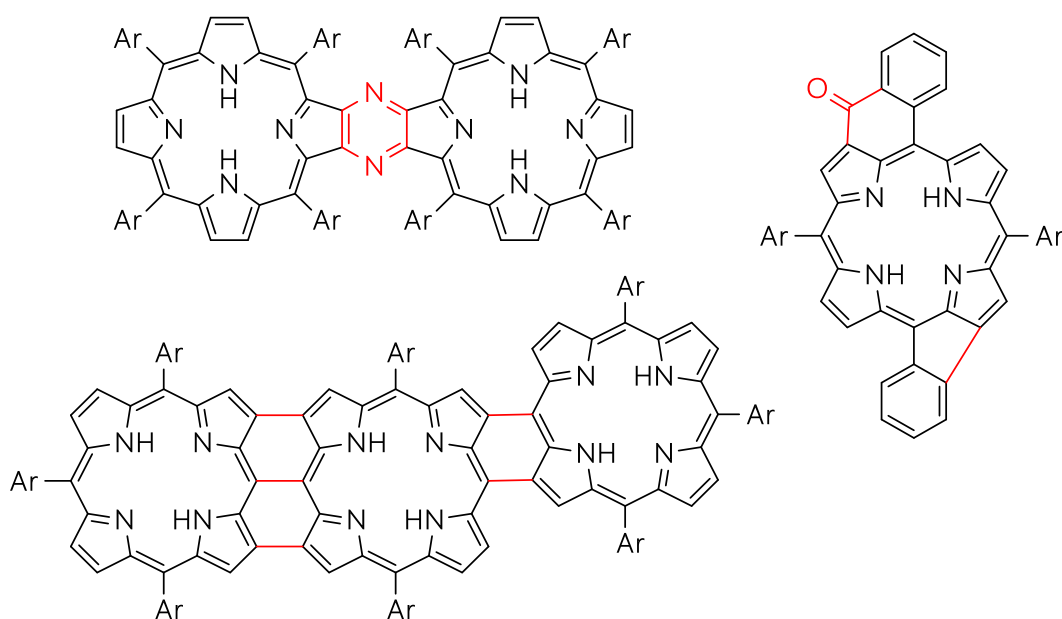


Figure A2.1 Representative examples of inter- and intramolecular meso/ β fusion patterns. Fusion sites are marked in red for clarity.

enhance non-radiative decay rates for $S_1 \rightarrow S_0$ transitions. What kind of properties could we see in porphyrin systems⁷ where the *meso*-aryl substituents are forcibly locked into a coplanar arrangement while retaining a fraction of their original non-planarity?

The most straightforward way to accomplish this would be through either intermolecular or intramolecular ring fusion (Figure A2.1⁸⁻¹⁰). Most synthetic methods¹¹ for exocyclic ring formation rely on metal-mediated (*meso*-(2-iodophenyl)/Pd¹², β -halopyrrole/Pd¹³, activated Zn¹⁴ and HgCl/Pd⁸) acid/base-catalyzed intramolecular cyclization¹⁵ or oxidative C-C coupling¹⁶ (FeCl₃, DDQ-Sc(OTf)₃). Less common methods include Diels-Alder and cycloaddition reactions as well as Bergman cyclization of diyne-functionalized porphyrins.¹⁷ Intermolecular cyclization has been widely employed to produce interesting NIR materials such as dimer/trimer porphyrin arrays, of which porphyrin tapes^{9,18} are a famous example. Possible fusion modes are divided between β,β -, *meso*, β - and *meso*,*meso*-fusion, demonstrated within one all-inclusive material in Figure A2.1. In addition to fusion modes, the type of linker used has a profound effect on the photophysical characteristics of the final materials. Anderson and co-workers¹⁰ compared the effects of different *meso*, β linkers in *para*-phenylene bridged porphyrin tapes. Cross-conjugated keto linkers extended fluorescence further into the NIR ($\lambda_{em} = 960$ nm, $\Phi_F = 0.013$) while non-conjugated CPh₂ linkers preserved NIR PLQY ($\lambda_{em} = 736$ nm, $\Phi_F = 0.10$) and resulted in a material with strikingly similar absorption behaviour to *meso-meso* ethynyl-bridged porphyrin dimers. In contrast to conventional porphyrin tapes (fully planar and severely aggregated) bearing *meso-meso* $\beta-\beta-\beta$ triple linkages, arch-tapes prepared by Osuka and co-workers containing non-conjugated methine linkers exhibited enhanced conformational flexibility and remarkably contorted structures.¹⁹ They possess significantly improved solubility while avoiding the severe aggregation issues plaguing this important class of materials. A recent report used the same *meso-meso* $\beta-\beta-\beta$ triple linkage in a novel bowl-shaped subporphyrin dimer²⁰ ($\lambda_{max} = 942$ nm). Recently, synthesis of 7,8-dehydropurpurin by Pd-catalysed [3+2] annulation of *meso*-bromoporphyrin with 1,4-diphenylbutadiyne was reported.²¹ Subsequent treatment with NBS produced highly fluorescent ($\Phi_F = 0.17$) β -to- β vinylene-bridged porphyrin dimers which exhibited panchromatic absorption spectra up to ~650 nm. Even beyond porphyrin tapes, completely fused tetrameric porphyrin sheets²² have been prepared. Intramolecular fusion however, has only recently come to the forefront of fused porphyrinoid research. Its simplest iteration is the incorporation of an olefin²³ or phenyl¹² moiety across the *meso*, β positions. While such compounds show enhanced absorption properties in the red, optical properties can be pushed to the limit²⁴ of the NIR

region like the quadruply azulene-fused porphyrin²⁵ that exhibits intense panchromatic absorption up to 1200 nm or the porphyrin *meso*, β -fused to four anthracenes²⁶ with $\lambda_{\max} = 1417$ ($\epsilon = 1.2 \times 10^5 \text{ M}^{-1} \text{ cm}^{-1}$). In the case of *N*-annulated perylene fused porphyrins, NIR photoluminescence can still be detected²⁷ at 800 nm ($\Phi_F = 0.056$) and 982 nm ($\Phi_F = 0.008$) which is impressive considering their porphyrin tape counterparts are essentially non-emissive at the same wavelengths. Novel fused porphyrinoids are also shedding light on the aromatic/anti-aromatic character of such systems as *meso*, β dibenzo[*a,g*]corannulene-fused¹⁶ thieno-bridged²⁸ porphyrins. Not surprisingly, complete

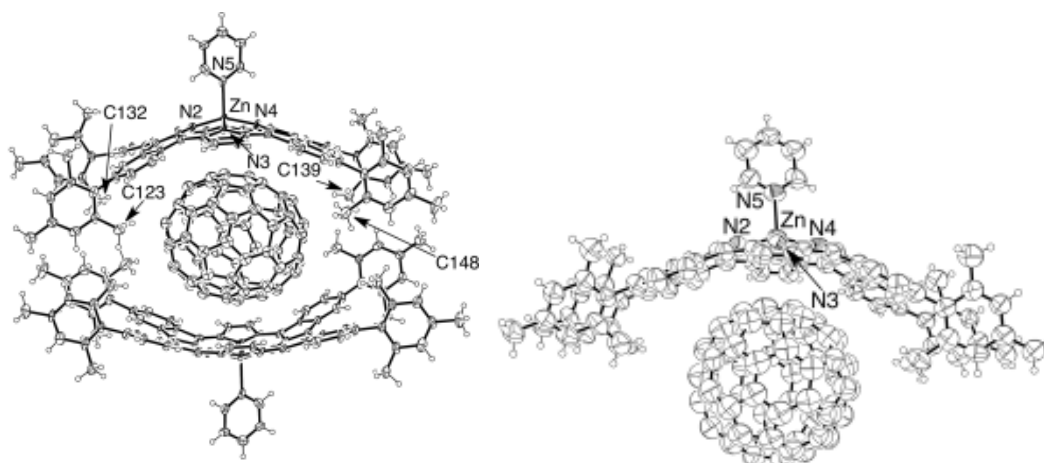


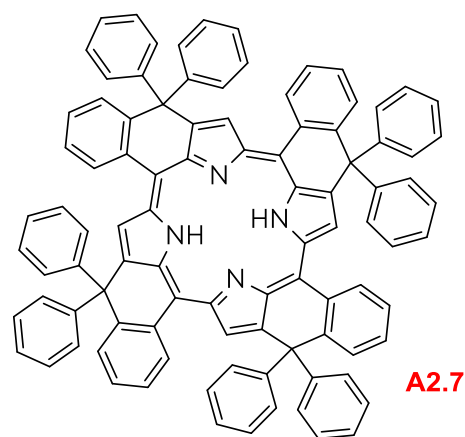
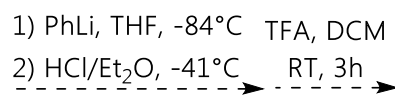
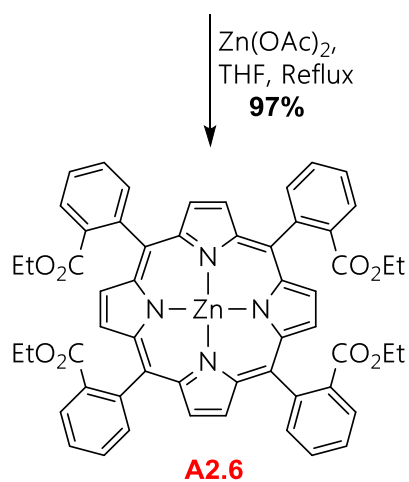
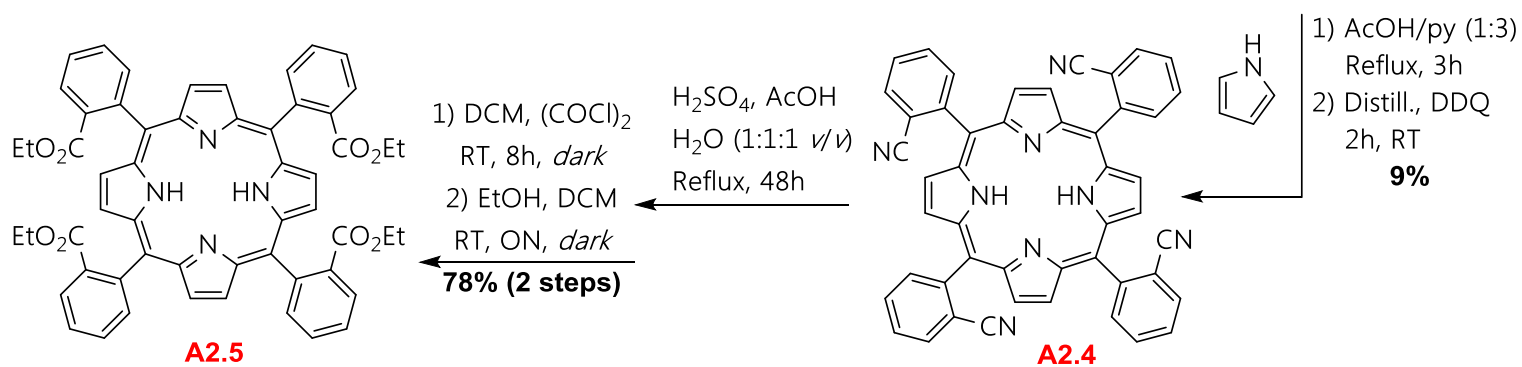
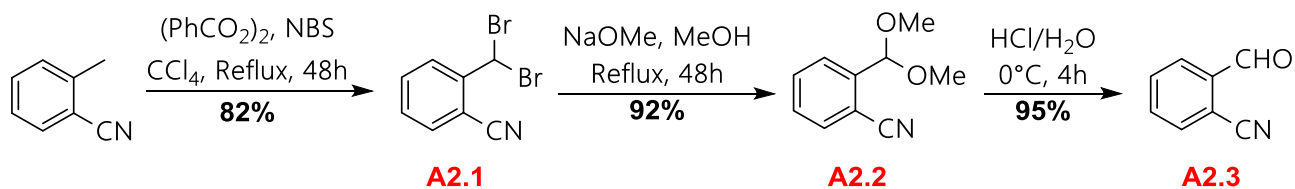
Figure A2.2 ORTEP rendering of bowl shaped (left) $(\text{ZnQFP-py})_2\text{C}_{70}$ and (right) ZnQFP-pyC_{70} crystal structures. Reprinted with permission from [29] © 2017 RSC.

meso, β -fusion results in extreme porphyrin core distortion. So much so that enough doming distortion was induced in the bowl-shaped quadruply-fused porphyrin (ZnQFP)^{29,30} to form stable and strongly-interacting complexes with C_{60} and C_{70} .

While direct C-C intramolecular aromatic coupling produces interesting materials such as indenoporphyrins³¹ (represented in Figure A2.1), these materials achieve redder optical properties mainly via extended π -conjugation as they tend to retain their relatively planar structures. The aim of this project was to synthesize a material that would achieve comparable photophysical performance with reduced self-aggregation in solution.

A2.2 Synthesis of Quadruply *meso*, β -fused Porphyrin

Since condensation of pyrrole and sterically hindered *o*-aldehydes is known to be a generally low-yielding³² reaction for porphyrin synthesis, large quantities of *o*-cyanobenzaldehyde were required for multi-gram preparation of the precursor porphyrin. Given its surprisingly



A2.1 Synthesis of quadruply CAr_2 meso, β -fused porphyrin **A2.7** starting from *o*-tolunitrile.

low commercial availability, it was prepared in three steps according to a literature procedure³³ from more readily available starting materials. Benzoyl peroxide-initiated radical bromination of *o*-tolunitrile with NBS in CCl₄ produced benzal bromide **A2.1** in large quantities (~200 g). It should be noted that even after rigorous purification, **A2.1** corrodes/rusts any nearby metal (including disposable needles) within days, even without direct contact. This material should be handled inside a fumehood and care should be taken to avoid cross contamination with surroundings as it is a potent skin and respiratory tract irritant. Treatment of **A2.1** with sodium methoxide in anhydrous methanol afforded acetal **A2.2** which was deprotected into *o*-cyanobenzaldehyde **A2.3** with aqueous HCl. Subsequent condensation with pyrrole under modified Adler-Longo conditions³⁴ (3:1 AcOH/pyr) and oxidation with DDQ after thorough removal of solvent generated H₂(*o*-CNPh)P **A2.4** in poor yield (9%) as a mixture of atropisomers. Hydrolysis of the cyano moieties in refluxing H₂SO₄/aqueous acetic acid, treatment of the resulting tetracarboxylic acid with an excess of oxalyl chloride produced the tetraacyl derivative which was used immediately without characterization. Overnight reaction of this intermediate with anhydrous ethanol in dichloromethane afforded tetraester **A2.5** in 84% yield (for 3 reactions). Metalation with Zn(OAc)₂ afforded precursor Zn (II) porphyrin **A2.6** as a mixture of atropisomers which was reacted with excess PhLi/tetrahydrofuran at -84 °C followed by workup with anhydrous ethereal HCl to generate the CPh₂OH carbinol intermediate (not shown in Scheme A2.1) It is important to use a metalloporphyrin for this reaction because alkyllithium reagents are known to effect substitution^{35,36} at the *meso*-position and in order to avoid generation of porphyrinylolithiums. The intermediate was used immediately in the subsequent low temperature TFA/dichloromethane condensation, spawning a mixture of closely-related porphyrinoid products. Chromatographic separation of side products was attempted on basic Al₂O₃ (Brockmann 1) and silica. Although separate fractions were collected, no unambiguous identification was made possible by HRMS and NMR spectroscopy.

A2.3 Physical and Electronic Properties

A2.3.1 Theoretical Calculations

An initial geometry optimization was performed at the B3LYP/6-31G(d) level of theory, followed by re-optimization with B3LYP/Def2SVPP. The results reveal an exceedingly distorted structure, characterized by a rotating propeller-like arrangement of the pyrrole

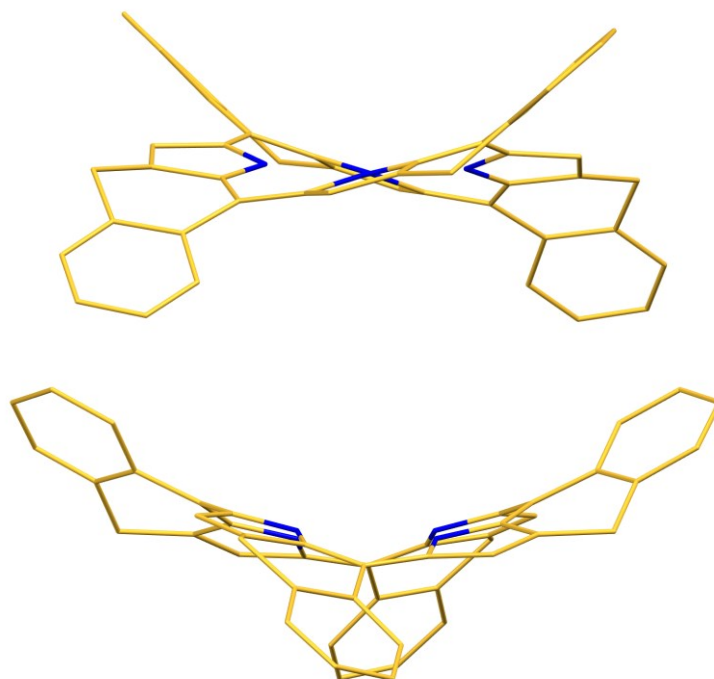


Figure A2.3 B3LYP/Def2SVPP calculated geometries for free-base **A2.7**. Hydrogens and methine Ph rings removed for clarity.

subunits (Figure A2.3). This pseudo-saddle shape can be described as a mix of twist/saddle distortions; analogous to a corkscrew. It is an unusual distortion, because straddling usually occurs along the axes bisecting opposing pyrroles; in this case, the pyrrole subunits are seemingly experiencing a lot of twisting while the brunt of the saddling is occurring along the *[b]* face of the pyrrole. In the calculated structure, the meso-Ph rings are only $\sim 22^\circ$ from complete co-planarity with the pyrrole subunits. Comparing that to the usual tetrakis-meso-arylated porphyrins ($\sim 70\text{--}75^\circ$ from co-planarity), a much larger contribution to the π -electron system would be expected to manifest in the photophysical properties, most likely with red-shifting and broadening optical maxima.

A2.4 Conclusions

To summarize, synthesis of a quadruply *meso*, β -fused porphyrin ($\text{H}_2\text{QFPh}_8\text{P}$) bridged by $-\text{CPh}_2$ linkers was attempted via acid-catalyzed condensation of a tetracarbinol intermediate. The resulting complex mixtures were not sufficiently purified to make an unambiguous identification of intended product **A2.7**. The predicted structure for free-base **A2.7**

undergoes severe distortion characterized by a mix of twisting and settling. The latter occurs almost exclusively^{35,37} along the pyrrolic axes; quantum mechanical calculations unexpectedly found that nearly all the saddling occurs along the *meso*-axes, resulting in a dual-bowl porphyrin shape delimited by multiple π -electron rich moieties. Such dualistic architecture could prove useful for supramolecular applications in molecular recognition/sensing or as a tecton for extended structures such as 1D columnar stacks and MOFs.

A2.5 Experimental

2-(Dibromomethyl)benzonitrile (A2.1) N-bromosuccinimide (455.5g, 2.55 mol) and benzoyl peroxide (20.7g, 0.085 mol) were added in succession to a solution of *o*-tolunitrile (100g, 0.85 mol) and CCl₄ (1000 mL) in a 3L round-bottom flask. The mixture was brought to reflux and stirred vigorously for 48h in the dark under argon atmosphere. The contents of the flask were brought to room temperature and filtered to removed succinimide and unreacted NBS. The solids were washed with Et₂O (300 mL x 3), the organic fractions were combined, washed with H₂O (5 x 500 mL) and dried over Na₂SO₄ (40 g). The solvent was removed under reduced pressure yielding a dark orange oil. Crystallization was induced by dissolving the oil in dichloromethane (200 mL) and adding hexanes (100 mL). The mixture was cooled (ice bath) for 30 min before filtering the yellow crystals and re-crystallizing twice from Et₂O/hexanes and once from PhMe/hexanes to yield benzal bromide **A2.1** as transparent, inch-long crystals (191.7g, 82%) after drying under vacuum. *Note:* **A2.1** causes severe skin and respiratory irritation, even after indirect contact. Disposable metal needles used during purification were rusted shut without direct contact with **A2.1**. Exercise caution with this material and do not handle outside fumehood. ¹H NMR (300 MHz, CDCl₃) δ 8.03 (d, *J* = 8 Hz, 1H), 7.70 (t, *J* = 7.6 Hz, 1H), 7.62 (t, *J* = 7.6 Hz, 1H), 7.45 (t, *J* = 7.6 Hz, 1H); ¹³C NMR (75 MHz, CD₂Cl₂) δ 144.38, 133.92, 132.46, 130.23, 129.99, 116.02, 108.61, 35.88.

2-(Dimethoxymethyl)benzonitrile (A2.2) Sodium methoxide (62.0 g, 1.148 mol) was dissolved in dry methanol (400 mL) in a 1L round-bottom flask. The solution was brought to reflux over magnetic stirring while a solution of benzal bromide **A2.1** (154 g, 0.560 mol) in dry methanol (300 mL) was added dropwise over 1h. The solution was refluxed for 2 days and subsequently cooled to room temperature. The solvent was removed under reduced

pressure to yield a yellow oil which was fractionally distilled under reduced pressure (104 microns, 71 °C), affording acetal **A2.2** as a light yellow oil (91.1 g, 91.8%) which crystallized partially upon standing overnight into 1-2 cm long transparent rectangular crystals (M.P. = 78-79 °C, see Figure 5.5). The acetal was used in its entirety for the next reaction without further manipulation.

2-Formylbenzonitrile (A2.3) Acetal **A2.2** (91.0 g, 0.513 mol) was added to a 1L round-bottom flask equipped with a magnetic stir bar. Deionized H₂O (300 mL) was added to the flask before immersing it into an ice/water slurry. Taking care to keep temperature of the mixture between 0-2 °C, HCl (35%, 200 mL) was added dropwise over 2 h with vigorous stirring. Upon complete addition, stirring was resumed for another 6 h at 0 °C before pouring the contents of the flask onto dichloromethane (500 mL). The aqueous layer was extracted with dichloromethane (3 x 200 mL) and the combined organic fractions were washed with H₂O (500 mL) followed by brine (500 mL). The organic layer was dried over Na₂SO₄ (25g) and the solvent was removed under reduced pressure to yield off-white solids. The crude solids were recrystallized (see note below) from dichloromethane/MTBE and dried under vacuum overnight to yield **A2.3** as white glassy (1-2 inch) needles (63.8 g, 94.8%). *Note:* Needle growth easily disturbed; vibration/movement of the crystallization vessel immediately induces precipitation of cotton-like pads of amorphous string. The crystalline needle form can be obtained by keeping the solution slightly below boiling point (30 °C)

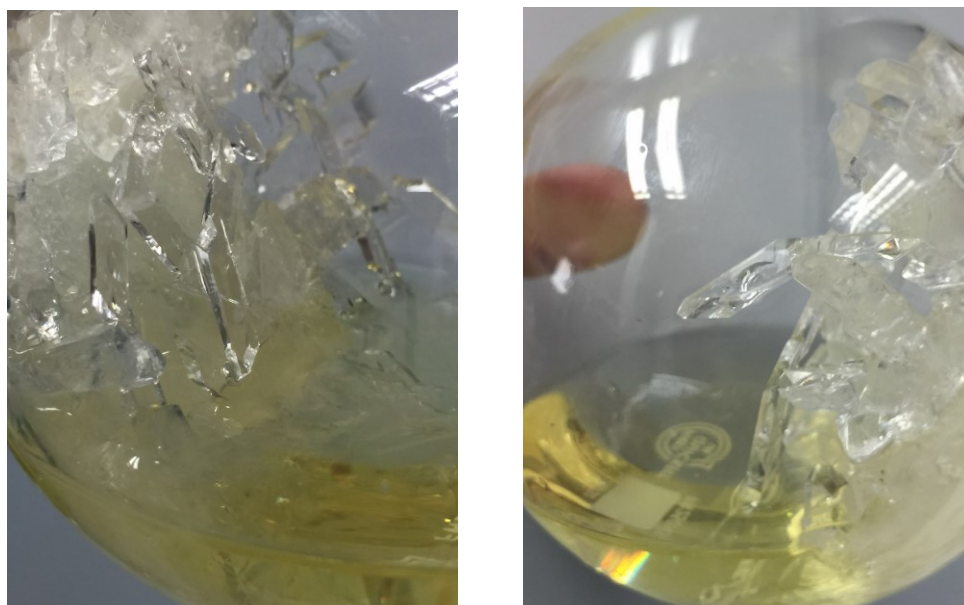


Figure A2.5 Partial crystallization out of freshly distilled **A2.2**.

during crystal growth. ^1H NMR (500 MHz, CDCl_3) δ 10.33 (s, 1H), 8.03 (d, $J = 8$ Hz, 1H), 7.79 (m, 3H); ^{13}C NMR (125 MHz, CD_2Cl_2) δ 188.66, 136.86, 134.35, 134.22, 133.34, 129.80, 116.09, 113.82.

2,2',2'',2'''-(Porphyrin-5,10,15,20-tetrayl)tetrabenzonitrile (A2.4)

Note: pyrrole was freshly distilled from NaH before use. Glacial AcOH (1250 mL) and 2-formylbenzonitrile **A2.3** (39.16 g, 0.299 mol) were added to a 4L boiling flask equipped with a magnetic stir bar. Subsequent addition of pyridine (315 mL) dissolved the remaining aldehyde and the flask was loosely wrapped in a sheet of aluminium foil to prevent heat losses and shield the solution from ambient light. A reflux condenser was fitted to the top of the flask and the solution was brought to reflux (115-120 °C). Freshly distilled pyrrole (20.06 g, 0.299 mol) was diluted with glacial AcOH (20 mL) and loaded into a 50 mL pressure-equalizing dropping funnel fitted to the top of the reflux condenser. The pyrrole solution was added dropwise over 30 min with subsequent rinsing of the dropping funnel with AcOH (2 x 20 mL). The solution was kept at reflux for 90 min and subsequently cooled to room temperature. The solvent was distilled off under reduced pressure and PhMe was used (3 x 300 mL) to solvent chase any remaining acetic acid/pyridine via azeotrope (~20% with toluene at 110 °C) before re-dissolving/suspending the remaining solids in dichloromethane (1000 mL) and passing the solution through a pad of silica (6" length, 2" ID). The atropisomers of **A2.4** and associated chlorins were eluted with dichloromethane/ Et_2O (3:1) as a dark ruby fraction. A large amount of black insoluble polymer was left sitting on top of the silica pad, which was discarded. After complete removal of the solvent, the solids were once again re-dissolved in dry dichloromethane (1000 mL) and DDQ (7.00g, 30.8 mmol) was added in one portion and the solution was stirred overnight in the dark under N_2 atmosphere. The solution was washed with Na_2SO_3 (10%, 2 x 1000 mL), K_2CO_3 (1000 mL) and brine (500 mL) before drying the combined organic fractions over Na_2SO_4 (50 g). The crude solids obtained after removal of solvent were purified via column chromatography (dichloromethane/ NEt_3) and recrystallization from 1:1 dichloromethane /hexanes to afford $\text{H}_2(o\text{-CNPh})_4\text{PA2.4}$ presenting as bright purple solids (4.81 g, 9.1%). Note: **A2.4** exists as a mixture of atropisomers^{34,38} ($\alpha,\beta,\alpha,\beta$ -



Figure A2.6 TLC (dichloromethane/tetrahydrofuran/ NEt_3) of crude solids showing red atropisomers and blue/green chlorins.

A2.4, α,β,β,β -**A2.4**, $\alpha,\alpha,\beta,\beta$ -**A2.4** and $\alpha,\alpha,\alpha,\alpha$ -**A2.4**). Within a stationary frame of reference, an upward-facing CN group is denoted by α , while β indicates a downward-facing CN group. All elute as one continuous band except $\alpha,\alpha,\alpha,\alpha$ -**A2.4** which has a lower RF due to omnidirectional orientation of the CN moieties (making it more polar and distorted). This atropisomer is significantly more insoluble than all others. Hot tetrahydrofuran or CHCl_3 is needed for complete dissolution. Therefore, if recrystallization of the mixed material, there will always be quantities of insoluble $\alpha,\alpha,\alpha,\alpha$ -**A2.4** which could be filtered out for separate recrystallization. Similarly, a solution of the mixed material in deuterated solvent should be passed through cotton or glass wool in order to avoid gritty solids in the NMR tube. ^1H NMR (500 MHz, CD_2Cl_2) δ 8.77 (br s, 8H), 8.45 (d, $J = 8$ Hz, 3H), 8.36 (d, $J = 8$ Hz, 1H), 8.12 (d, $J = 8$ Hz, 4H), 8.03 (t, $J = 8$ Hz, 4H), 7.95 (t, $J = 8$ Hz, 4H), -2.74 (s, 2H); ^{13}C NMR (125 MHz, CD_2Cl_2) δ 145.51, 135.61, 132.32, 131.66, 129.64, 118.50, 117.94, 116.99.

Tetraethyl 2,2',2'',2'''-(porphyrin-5,10,15,20-tetrayl)tetrabenzoate (A2.5) $\text{H}_2(o\text{-CNPh})_4\text{P}$ **A2.4** (1.87g, 2.62 mmol) was added to a 500 mL round-bottom flask equipped with a magnetic stir bar and a reflux condenser. A pre-mixed 1:1:1 solution of $\text{H}_2\text{SO}_4/\text{H}_2\text{O}/\text{AcOH}$ was added to the flask, immediately producing a dark but vivid green colour. The headspace was flushed with N_2 gas and the contents were refluxed for 48h with adequate stirring. The flask was brought back to room temperature, TFA (3 mL) was added and to the contents were poured onto cold H_2O (900 mL), which was extracted with EtOAc (4 x 400 mL). The combined organic fractions were washed with brine (600 mL), dried over Na_2SO_4 (40 g) and the solvent removed under reduced pressure to leave behind greenish-blue solids which were used in the subsequent step without further purification. After drying under vacuum (100 microns) for 2 h, a magnetic stir bar was added and the solids were re-dissolved in dry dichloromethane (300 mL). Oxalyl chloride (30 mL, xs) was added and the solution was stirred under N_2 atmosphere for 8 h. The solvent and excess oxalyl chloride were distilled away under reduced pressure to once again leave behind green solids. After re-dissolving in dry dichloromethane (300 mL), anhydrous EtOH (60 mL) was added to the flask and the mixture was allowed to stir overnight in the dark. Removal of the solvent followed by dissolution in dichloromethane (500 mL), washing with H_2O (600 mL), saturated NaHCO_3 (600 mL), drying over Na_2SO_4 (30 g) and removal of solvent under reduced pressure afforded crude $\text{H}_2(o\text{-(CO}_2\text{Et)Ph})_4\text{P}$ **A2.5** as brownish-purple solids. Recrystallization by slow evaporation over several days from a 1:1 dichloromethane/hexanes solution refined **5.5** into dark purple crystalline powder (1.83 g, 78%).

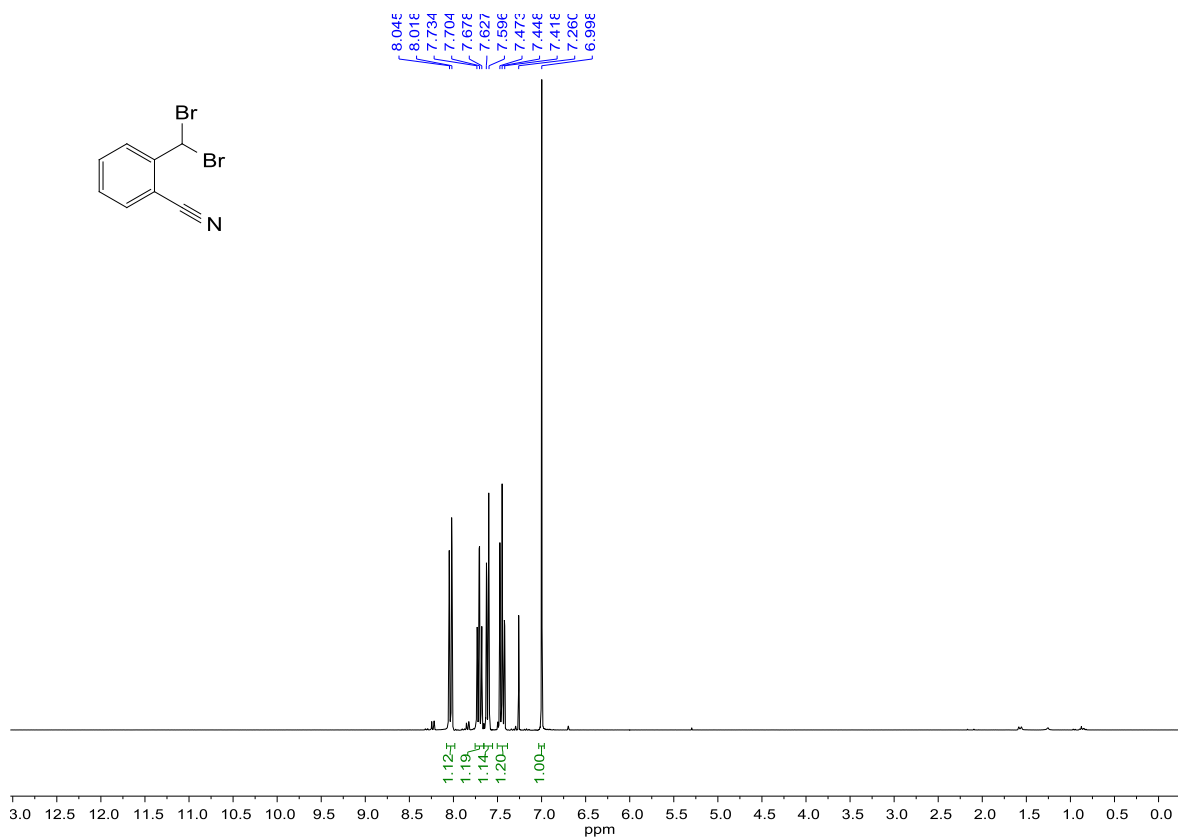
Zinc (II) Tetraethyl 2,2',2'',2'''-(porphyrin-5,10,15,20-tetrayl)tetrabenzoate (A2.6) $\text{H}_2\text{O}-(\text{CO}_2\text{Et})\text{Ph}_4\text{P}$ **5.5** (1.80 g, 2.03 mmol) was dissolved in tetrahydrofuran (200 mL) and added to a 500 mL Erlenmeyer flask equipped with a magnetic stir bar. Zinc (II) acetate dihydrate (5 g, 23 mmol) was added to the flask and the heterogeneous mixture was refluxed for 15 min. The solvent was removed under reduced pressure, the crude pink solids were redissolved in dichloromethane (200 mL) and passed through a short pad of silica (2" length, 2" ID). Recrystallization from dichloromethane/hexanes afforded **A2.6** as bright pink/purple crystals (1.92 g, 1.99 mmol).

A2.6 References

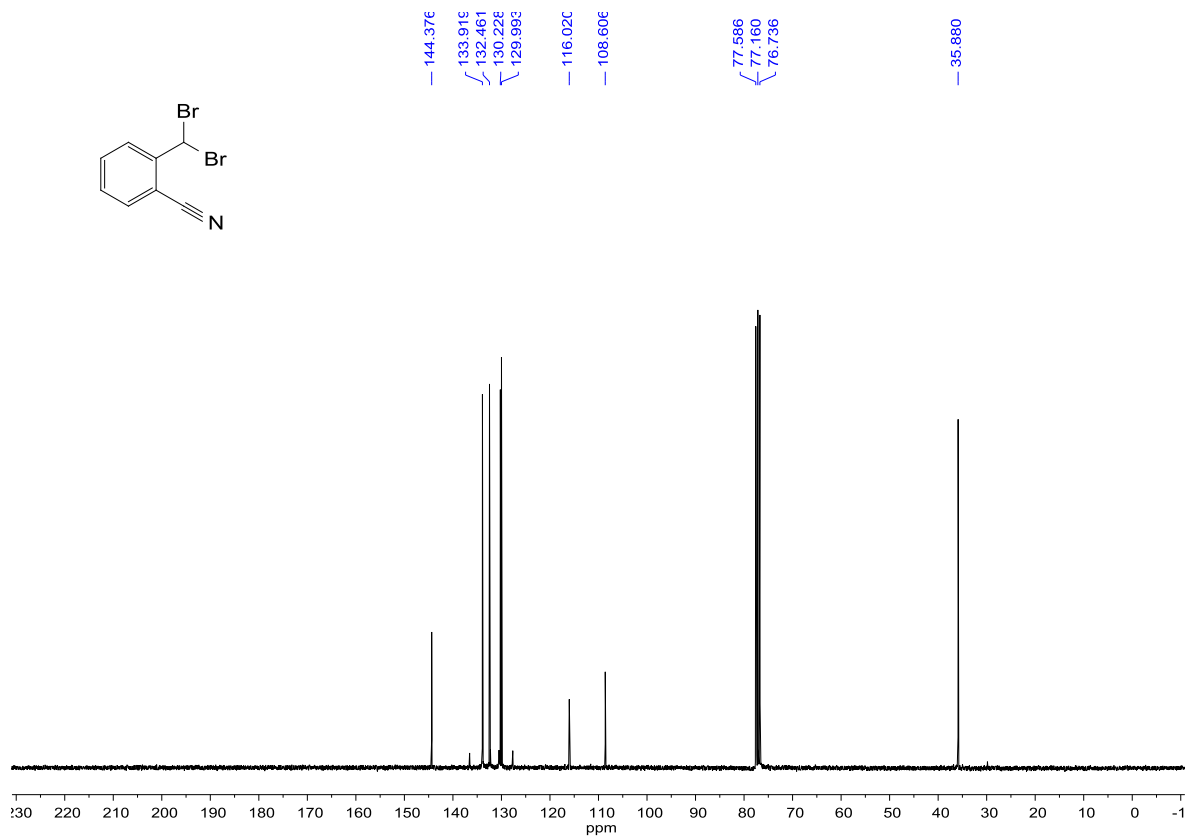
- (1) Shelnut, J. A.; Song, X.-Z.; Ma, J.-G.; Jia, S.-L.; Jentzen, W.; Medforth, C. J.; Medforth, C. J. Nonplanar porphyrins and their significance in proteins *Chem. Soc. Rev.* **1998**, *27*, 31.
- (2) Jentzen, W.; Ma, J.-G.; Shelnut, J. A. Conservation of the conformation of the porphyrin macrocycle in hemoproteins *Biophys. J.* **1998**, *74*, 753.
- (3) Finikova, O. S.; Cheprakov, A. V.; Carroll, P. J.; Dalosto, S.; Vinogradov, S. A. Influence of Nonplanarity and Extended Conjugation on Porphyrin Basicity *Inorg. Chem.* **2002**, *41*, 6944.
- (4) Senge, M. O.; Kalisch, W. W. Synthesis and Structural Characterization of Nonplanar Tetraphenylporphyrins and Their Metal Complexes with Graded Degrees of β -Ethyl Substitution *Inorg. Chem.* **1997**, *36*, 6103.
- (5) Gentemann, S.; Medforth, C. J.; Forsyth, T. P.; Nurco, D. J.; Smith, K. M.; Fajer, J.; Holten, D. Photophysical Properties of Conformationally Distorted Metal-Free Porphyrins. Investigation into the Deactivation Mechanisms of the Lowest Excited Singlet State *J. Am. Chem. Soc.* **1994**, *116*, 7363.
- (6) Ryeng, H.; Ghosh, A. Do Nonplanar Distortions of Porphyrins Bring about Strongly Red-Shifted Electronic Spectra? Controversy, Consensus, New Developments, and Relevance to Chelatases *J. Am. Chem. Soc.* **2002**, *124*, 8099.
- (7) Mori, H.; Tanaka, T.; Osuka, A. Fused porphyrinoids as promising near-infrared absorbing dyes *J. Mater. Chem. C* **2013**, *1*, 2500.
- (8) Smith, K. M.; Lee, S. H.; Vicente, M. G. H. Porphyrins with β, β' -fused five-membered rings *J. Porphyr. Phthalocya.* **2005**, *9*, 769.
- (9) Tsuda, A.; Osuka, A. Fully Conjugated Porphyrin Tapes with Electronic Absorption Bands That Reach into Infrared *Science* **2001**, *293*, 79.
- (10) Pawlicki, M.; Morisue, M.; Davis, N. K. S.; McLean, D. G.; Haley, J. E.; Beuerman, E.; Drobizhev, M.; Rebane, A.; Thompson, A. L.; Pascu, S. I.; Accorsi, G.; Armaroli, N.; Anderson, H. L. Engineering conjugation in para-phenylene-bridged porphyrin tapes *Chem. Sci.* **2012**, *3*, 1541.
- (11) Fox, S.; Boyle, R. W. Synthetic routes to porphyrins bearing fused rings *Tetrahedron* **2006**, *62*, 10039.
- (12) Fox, S.; Boyle, R. W. First examples of intramolecular Pd(0) catalysed couplings on ortho-iodinated meso-phenyl porphyrins *Chem. Commun.* **2004**, 1322.

- (13) Shen, D.-M.; Liu, C.; Chen, Q.-Y. A General and Efficient Palladium-Catalyzed Intramolecular Cyclization Reaction of β -Brominated Porphyrins *J. Org. Chem.* **2006**, *71*, 6508.
- (14) Shen, D.-M.; Liu, C.; Chen, Q.-Y. A novel and facile Zn-mediated intramolecular five-membered cyclization of β -tetraarylporphyrin radicals from β -bromotetraarylporphyrins *Chem. Commun.* **2005**, 4982.
- (15) Callot, H. J.; Schaeffer, E.; Cromer, R.; Metz, F. Unexpected routes to naphthoporphyrin derivatives *Tetrahedron* **1990**, *46*, 5253.
- (16) Ota, K.; Tanaka, T.; Osuka, A. meso- β Dibenzo[a,g]corannulene-Fused Porphyrins *Org. Lett.* **2014**, *16*, 2974.
- (17) Nath, M.; Pink, M.; Zaleski, J. M. Controlling Both Ground- and Excited-State Thermal Barriers to Bergman Cyclization with Alkyne Termini Substitution *J. Am. Chem. Soc.* **2005**, *127*, 478.
- (18) Tsuda, A.; Furuta, H.; Osuka, A. Syntheses, Structural Characterizations, and Optical and Electrochemical Properties of Directly Fused Diporphyrins *J. Am. Chem. Soc.* **2001**, *123*, 10304.
- (19) Fukui, N.; Kim, T.; Kim, D.; Osuka, A. Porphyrin Arch-Tapes: Synthesis, Contorted Structures, and Full Conjugation *J. Am. Chem. Soc.* **2017**, *139*, 9075.
- (20) Okuda, Y.; Fukui, N.; Kim, J.; Kim, T.; Jiang, H.-W.; Copley, G.; Kitano, M.; Kim, D.; Osuka, A. A meso-meso β - β Triply Linked Subporphyrin Dimer *Angew. Chem.* **2017**, *129*, 12485.
- (21) Fukui, N.; Yorimitsu, H.; Lim, J. M.; Kim, D.; Osuka, A. Synthesis of 7,8-Dehydropurpurin Dimers and Their Conversion into Conformationally Constrained β -to- β Vinylene-Bridged Porphyrin Dimers *Angew. Chem., Int. Ed.* **2014**, *53*, 4395.
- (22) Nakamura, Y.; Aratani, N.; Shinokubo, H.; Takagi, A.; Kawai, T.; Matsumoto, T.; Yoon, Z. S.; Kim, D. Y.; Ahn, T. K.; Kim, D.; Muranaka, A.; Kobayashi, N.; Osuka, A. A Directly Fused Tetrameric Porphyrin Sheet and Its Anomalous Electronic Properties That Arise from the Planar Cyclooctatetraene Core *J. Am. Chem. Soc.* **2006**, *128*, 4119.
- (23) Sahoo, A. K.; Mori, S.; Shinokubo, H.; Osuka, A. Facile Peripheral Functionalization of Porphyrins by Pd-Catalyzed [3+2] Annulation with Alkynes *Angew. Chem., Int. Ed.* **2006**, *45*, 7972.
- (24) Gill, H. S.; Harmjanz, M.; Santamaria, J.; Finger, I.; Scott, M. J. Facile oxidative rearrangement of dispiro-porphodimethenes to nonplanar and sheetlike porphyrins with intense absorptions in the near-IR region *Angew. Chem., Int. Ed.* **2004**, *43*, 485.
- (25) Kurotobi, K.; Kim, K. S.; Noh, S. B.; Kim, D.; Osuka, A. A quadruply azulene-fused porphyrin with intense near-IR absorption and a large two-photon absorption cross section *Angew. Chem., Int. Ed.* **2006**, *45*, 3944.
- (26) Davis, N. K. S.; Thompson, A. L.; Anderson, H. L. A Porphyrin Fused to Four Anthracenes *J. Am. Chem. Soc.* **2011**, *133*, 30.
- (27) Jiao, C.; Huang, K.-W.; Guan, Z.; Xu, Q.-H.; Wu, J. N-Annulated Perylene Fused Porphyrins with Enhanced Near-IR Absorption and Emission *Org. Lett.* **2010**, *12*, 4046.
- (28) Mitsushige, Y.; Yamaguchi, S.; Lee, B. S.; Sung, Y. M.; Kuhri, S.; Schierl, C. A.; Guldi, D. M.; Kim, D.; Matsuo, Y. Synthesis of Thieno-Bridged Porphyrins: Changing the Antiaromatic Contribution by the Direction of the Thiophene Ring *J. Am. Chem. Soc.* **2012**, *134*, 16540.
- (29) Saegusa, Y.; Ishizuka, T.; Kojima, T.; Mori, S.; Kawano, M.; Kojima, T. Supramolecular Interaction of Fullerenes with a Curved π -Surface of a Monomeric Quadruply Ring-Fused Porphyrin *Chem. - Eur. J.* **2015**, *21*, 5302.
- (30) Saegusa, Y.; Ishizuka, T.; Komamura, K.; Shimizu, S.; Kotani, H.; Kobayashi, N.; Kojima, T. Ring-fused porphyrins: extension of π -conjugation significantly affects the

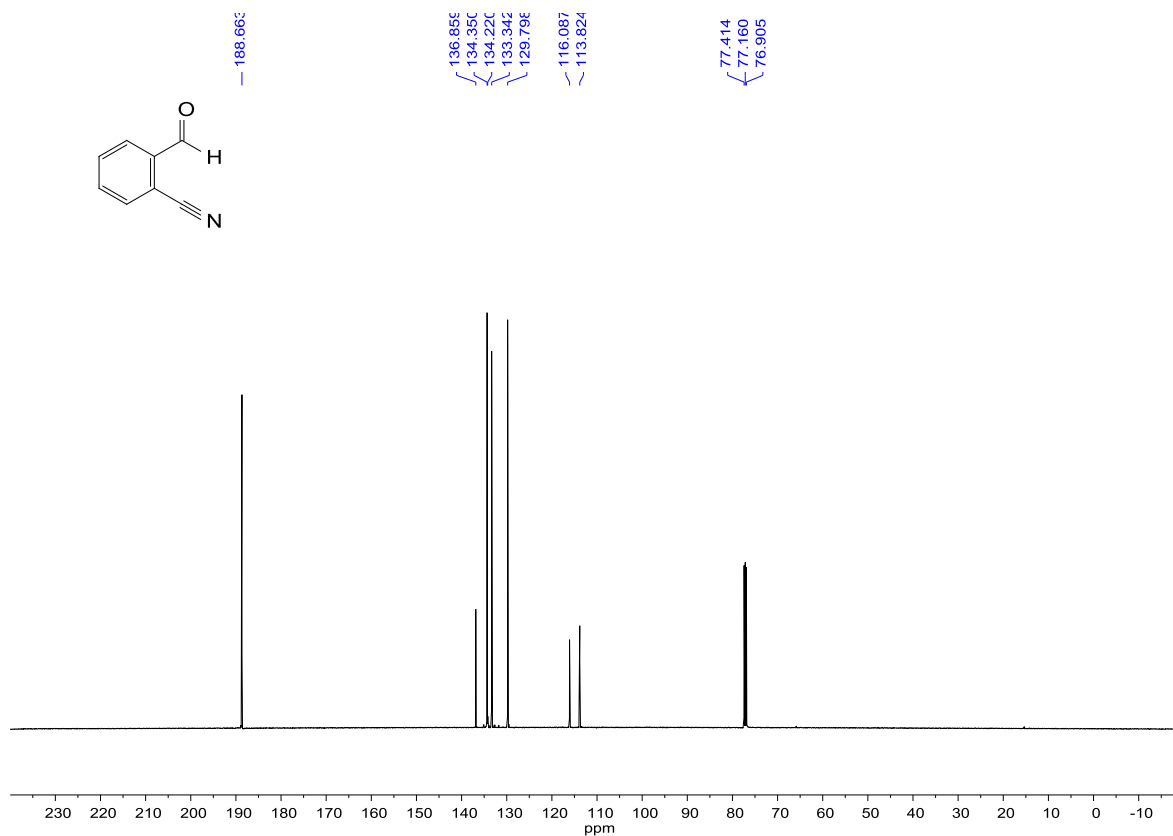
- aromaticity and optical properties of the porphyrin π -systems and the Lewis acidity of the central metal ions *Phys. Chem. Chem. Phys.* **2015**, *17*, 15001.
- (31) Lash, T. D.; Smith, B. E.; Melquist, M. J.; Godfrey, B. A. Synthesis of Indenoporphyrins, Highly Modified Porphyrins with Reduced Diatropic Characteristics *J. Org. Chem.* **2011**, *76*, 5335.
- (32) Lindsey, J. S.; Wagner, R. W. Investigation of the synthesis of ortho-substituted tetraphenylporphyrins *J. Org. Chem.* **1989**, *54*, 828.
- (33) Sun, C.; Xu, B. A Tandem Elimination-Cyclization-Suzuki Approach: Efficient One-Pot Synthesis of Functionalized (Z)-3-(Arylmethylene)isoindolin-1-ones *J. Org. Chem.* **2008**, *73*, 7361.
- (34) Leondiadis, L.; Momenteau, M. 5,10,15,20-Tetrakis($\alpha,\alpha,\alpha,\alpha$ -o-(N-tert-butyl-carbamoyl)phenyl)porphyrin: synthesis and redox properties of zinc(II) and copper(II) complexes *J. Org. Chem.* **1989**, *54*, 6135.
- (35) Senge, M. O.; Bischoff, I. Regioselective synthesis of conformationally designed porphyrins with mixed meso-substituent types and distortion modes *Eur. J. Org. Chem.* **2001**, 1735.
- (36) Kalisch, W. W.; Senge, M. O. Facile meso functionalization of porphyrins by nucleophilic substitution with organolithium reagents *Angew. Chem., Int. Ed.* **1998**, *37*, 1107.
- (37) Wertsching, A. K.; Koch, A. S.; DiMugno, S. G. On the Negligible Impact of Ruffling on the Electronic Spectra of Porphine, Tetramethylporphyrin, and Perfluoroalkylporphyrins *J. Am. Chem. Soc.* **2001**, *123*, 3932.
- (38) Hatano, K.; Anzai, K.; Kubo, T.; Tamai, S. Synthesis and kinetic investigation of the atropisomerization of meso-tetra(2-cyanophenyl)porphine *Bull. Chem. Soc. Jpn.* **1981**, *54*, 3518.



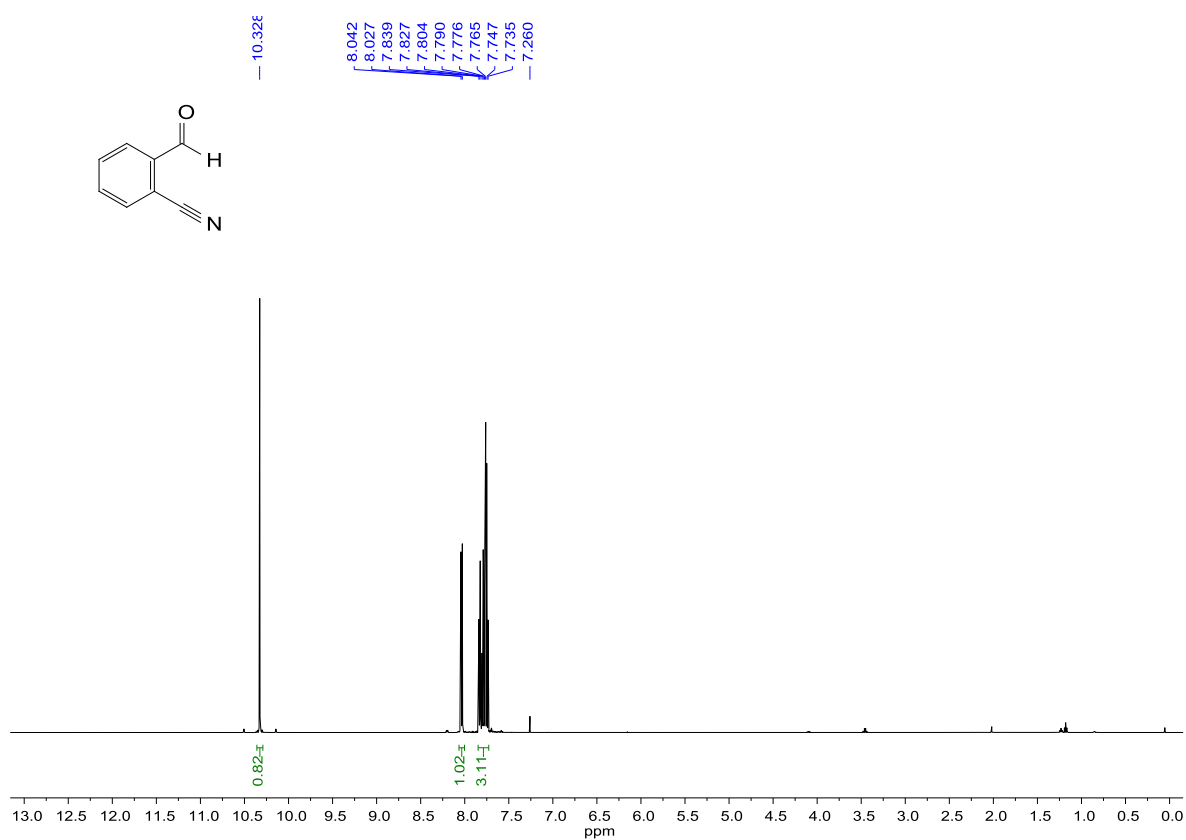
¹H NMR spectrum of A2.1 in CDCl₃.



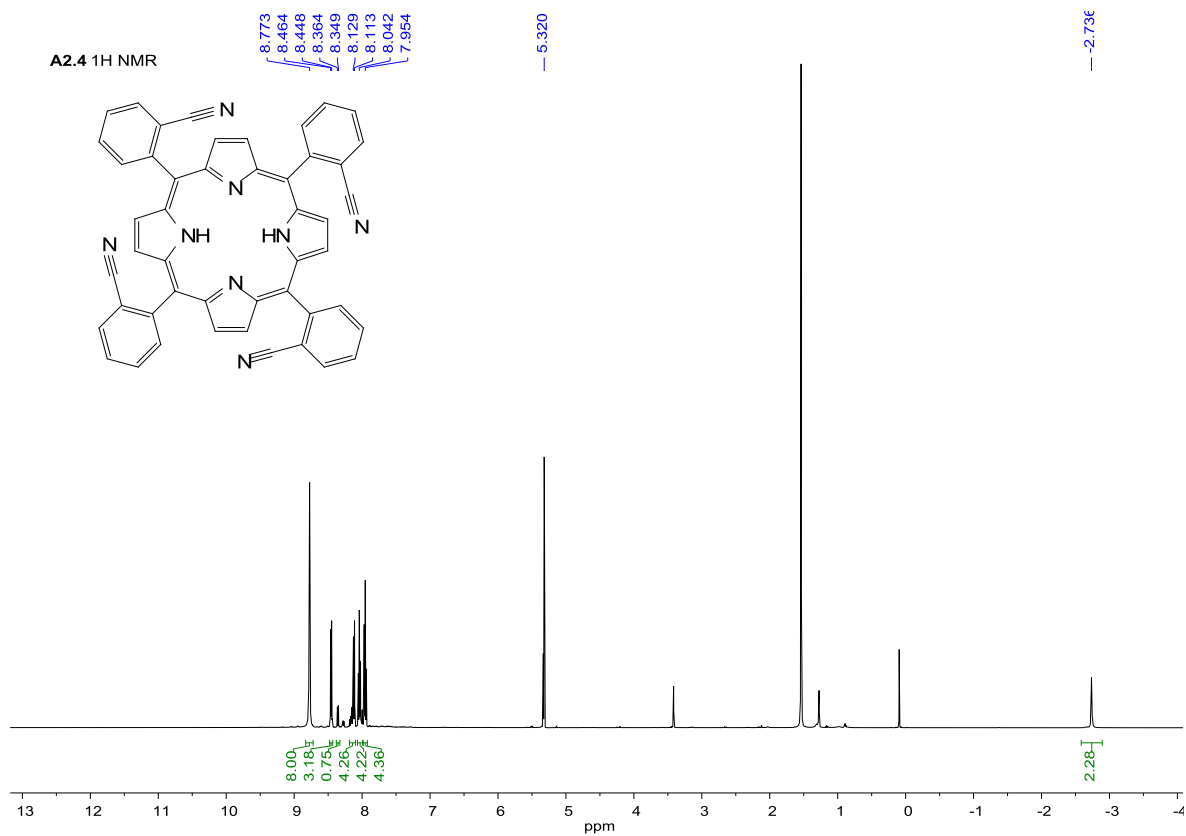
¹³C NMR spectrum of A2.1 in CDCl₃.



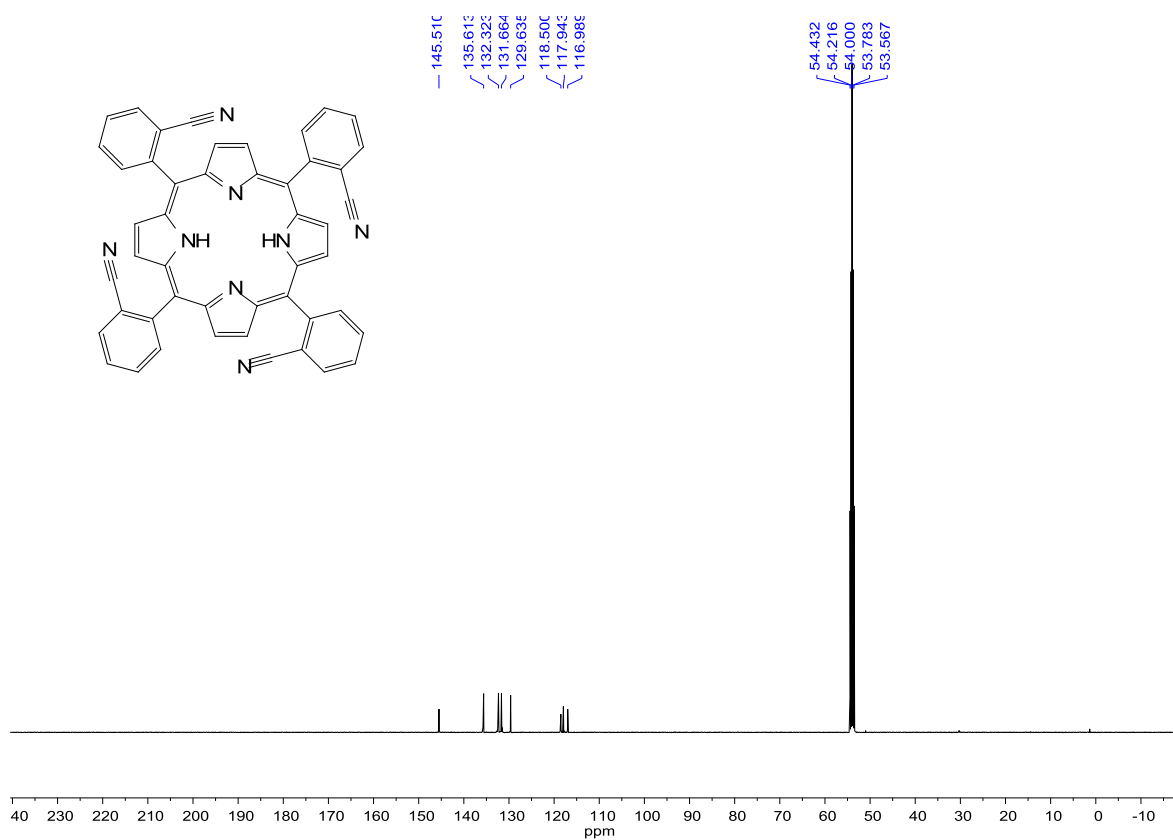
¹³C NMR spectrum of A2.3 in CD₂Cl₂.



¹H NMR spectrum of A2.3 in CDCl₃.



^1H NMR spectrum of **A2.4** in CD_2Cl_2 .



^{13}C NMR spectrum of **A2.4** in CD_2Cl_2

